Gasification of Biomass

An Investigation of Key Challenges to Advance Acceptance of the Technology

Le, Chien Dinh

Award date:
2012

Awarding institution:
University of Bath

PhD Thesis

GASIFICATION OF BIOMASS: AN INVESTIGATION OF KEY CHALLENGES TO ADVANCE ACCEPTANCE OF THE TECHNOLOGY

CHIEN DINH LE

MPhil/PhD Registration started on: 1st October 2009

Supervisor: Prof. Stan Kolaczkowski

Department of Chemical Engineering
University of Bath

April 2012

GASIFICATION OF BIOMASS: AN INVESTIGATION OF KEY CHALLENGES TO ADVANCE ACCEPTANCE OF THE TECHNOLOGY

Chien Dinh Le

A thesis submitted for the degree of Doctor of Philosophy

University of Bath

Department of Chemical Engineering

April 2012

COPYRIGHT

Table of Contents

List of Tables

List of Figures

Acknowledgement

First, I would like to express my sincere gratitude to my supervisor Prof. Stan Kolaczkowski, for his support and guidance throughout this programme of research, and for his help in giving me the opportunity to participate in the 2010 BIOTEN conference.

I am grateful for the support received from Refgas Ltd and Green Sky Systems Ltd, who are developing biomass-to-energy processes, and also for the support from the Vietnam Ministry of Education & Training, in the form of a research studentship.

Special thanks are due to Dr. Serpil Awdry for showing me Matlab, Aspen Plus and giving me opportunities to participate in teaching to improve my skills and knowledge in this area.

I also would like to express my love and my gratitude to my wife Anh Thi Ngoc Nguyen, and my little sons Binh Nguyen Dinh Le and Hai Nguyen Dinh Le, for their support and patience during the time I have spent working in this programme of research.

Further I would like to thank my parents Ly Dinh Le and Xiem Thi Do, my parents-in-law, Thanh Trung Nguyen and Hanh Thi Pham, and my siblings for encouraging me to continue studying.

Thanks go also to David McClymont, Firas Al Badran, Przemek Jodlowski and my other friends in our research group, for all of their assistance throughout the project.

Finally, thanks to technical staff including Robert Brain, Fernando Acosta, John Bishop, and Richard Bull for their help in the laboratory, and to all the other staff of the Chemical Engineering Department of the University of Bath.

Abstract

Although the general principles of biomass gasification are broadly understood, at a larger scale of operation (e.g. > 200 kg/h) there is a lack of confidence in the translation of the basic scientific concepts into a financially viable operation that satisfies regulatory requirements. Looking in particular at the operation of a down-draft type of gasifier, a number of challenges were identified and studied in greater detail.

Gasification experiments were performed on wood and straw pellets in a small scale, 21 mm i.d. quartz-tube reactor. These provided useful insight into what was occurring inside the gasifier, and the complexity and roles of the various reaction zones. In order to perform on-line gas analysis measurements in real time, a method was developed which enabled a quadrupole mass spectrometer (QMS) to be used. This was tested in a laboratory environment, and then used on a commercial pilot-plant gasifier (150 to 250 kg/h). This enabled the composition of the gas to be monitored while the plant was started up, and then operated at various levels of gas flow through the plant. In general the concentrations measured during a stable operation were as follows: CO = 16.0 vol.%, H_2 = 11.9 vol.%, CO_2 = 15.8 vol.%, N_2 = 54.1 vol.%, CH_4 = 1.9 vol.%, O_2 = 0.3 vol.%. Measurements of O_2 concentrations in the gas stream on start-up provide useful information on conditions when a flammable atmosphere could exist in the lines/vessels.

To help with the development of suitable gas clean-up strategies, the presence of two key sulphur species, H_2S and carbonyl sulphide (COS), was studied in more detail. Experimental measurements were taken on the laboratory reactor (e.g. H_2S = 286 ppmv, COS = 28 ppmv for gasification of refuse-derived fuel (RDF) pellets), and the commercial pilot-scale gasifier (e.g. H_2S = 332 ppmv, COS = 12 ppmv). This data was also compared with theoretical thermodynamic predictions.

The steam gasification of char was also studied in a laboratory 9.5 mm i.d. reactor, and kinetic expressions were determined for RDF-derived char. It was shown that high concentrations of H_2 (20 vol.%) and CO (15 vol.%) can be achieved, and the temperature at which reactions were initiated was > 700 ºC, and significant at 900 ºC. Interestingly, the RDF-derived char (at carbon conversion from 10 to 70 %) appears to be more reactive than other biochars reported in the literature. However, at high conversion (> 50 %), its apparent reactivity decreases with carbon conversion, behaving in a similar manner to coal chars.

Key words: Gasification, biomass, char, QMS, clean-up, analysis, kinetics, quartz-tube.

Nomenclature

Latin Letters

a_i	Activity of species i	
A	Pre-exponential factor	1/bar^n.s
$C_{i(j)}$	Ratio of partial pressure of species i at spectrum m/z(j) to that of component i at the main spectrum, used for the QMS methods	
d_C	Diameter of unreacted core in char particle	μm
d_q	Diameter of char particle	μm
$\overline{d}_q$	Mean char particle diameter	μm
$(\Delta d_q)_i$	Char particle size interval *i*	μm
D	Initial diameter of char particle before reaction	μm
E	Activation energy	kJ/mol
ER	Equivalence ratio	
f_i	Mass flow rate of species i	g/min, or kg/h
f_{air}^0	Stoichiometric air flow	kg/h
f_{air}	Air flow fed into the gasifier	kg/h
$\hat{f}_{iv}$	Fugacity of species i in the mixture	Pa
f_{iv}^o	Fugacity of species i in the standard state	Pa
F_{gas}	Total molar flow of producer gas	mol/h
F_i	Molar flow rate of species i	mol/min, or mol/h
ΔG_R^o	Standard free energy change due to reaction	J/mol
h	Number of time intervals in the flowchart of simulation programme for char gasification	
ΔH_R^o	Standard enthalpy change due to reaction	J/mol
k	Specific (or apparent) reaction rate coefficient	1/bar^n.s
k_C	Reaction rate coefficient (Shrinking-Core model)	mol/bar^n. μm^2.s
k_C	Reaction rate coefficient (Uniform-Reaction model)	1/bar^n.s
K_a	Thermodynamic equilibrium constant	
L_{pellet}	Length of RDF pellets	mm

m/z	Mass-to-charge ratio	
m_i	Mass fraction of char particle in size interval i	
M_i	Molar mass of species i	g/mol
n	Reaction order	
N_C	Number of moles of carbon in char particle	
	at reaction time t	mol
N_0	Initial number of moles of carbon in char particle	mol
p_i	Partial pressure of species i	Pa, or bar
P	Pressure	Pa, or bar
P_{H2O}	Partial pressure of steam	bar
P_i	Corrected partial pressure of species i,	
	used for the QMS methods	Torr
$P_{m/z(j)}$	Raw partial pressure,	
	recorded by the QMS at spectrum m/z(j)	Torr
q	Differential frequency mass (or fixed carbon content)	
	distribution of char particle size	1/μm
q_i	Differential frequency mass (or fixed carbon	
	content) fraction of size interval i	1/μm
Q	Volumetric flow of producer gas, Chapter 8	m^3/h
Q	Cumulative frequency mass (or fixed carbon content)	
	distribution of char particle size, Chapter 7	
Q_i	cumulative frequency mass (or fixed carbon content)	
	fraction of particles smaller than size $(d_q)_i$	
Q_{std}	Standard volume flow of producer gas	m^3/h
r	Specific (or apparent) reactivity of char in gasification	1/s
r_C	Reaction rate in char gasification (Shrinking-Core)	$mol/\mu m^2.s$
r_C	Reaction rate in char gasification (Reaction-Uniform)	1/s
R_g	Universal gas constant	8.314 J.mol/K
RS_i	Relative sensitivity of species i,	
	used for the QMS methods	
S_C	Available surface of unreacted core in char particle	μm^2
t	Time	s, min, or h
Δt	Time interval	s

T	Temperature	K
V_o	Molar volume of any ideal gas at 25 ^oC and 101.325 kPa	24.47 m^3/kmol
w	Char sample weight at any reaction time t	g
w_0	Initial char sample weight	g
w_{ash}	Ash content measured after gasification reaction of char	g
x_i	Volume fraction of species i, used for the QMS methods	
X	Carbon conversion at any reaction time t	%
y_i	Mole fraction of species i	

Greek Symbols

ε	Change in moles to achieve equilibrium	mol
ϕ_i	Fugacity coefficient of species i	
η_{HG}	Hot gas efficiency	%
η_{CG}	Cold gas efficiency	%
ρ	Molar density of carbon in char particle	mol/μm
π	Constant pi ~ 3.14	

Abbreviations

1D	One Dimensional
2D	Two Dimensional
3D	Three Dimentional
AAEM	Alkali and Alkaline Earth Metallic
AGR	Acid Gas Removal
AMU	Atomic Mass Unit
BFB	Bubbling Fluidised Bed
BTG	Biomass Technology Group
CC	Combined Cycle
CFB	Circulating Fluidised Bed
CFD	Computational Fluid Dynamic
CHP	Combined Heat and Power
COS	Carbonyl Sulphide
DEA	Diethanolamine
DeNOx	Decomposition/Destruction of Nitrogen Oxides

DIPA	Di-isopropanolamine
DME	Dimethyl Ether
EF	Entrained Flow
ELVs	Emission Limit Values
EP	Electrostatic Precipitators
ER	Equivalence Ratio
FCC	Fluidized Catalytic Cracking
FICFB	Fast Internal Circulation Fluidised Bed
FT	Fischer-Tropsch
GC	Gas Chromatography
HCs	Hydrocarbons
HESS	High Efficiency Water Scrubber
HGD	Hot Gas Desulphurization
HHV	Higher Heating Value
HV	Heating Value
IC	Internal Combustion
IGCC	Integrated Gasification Combined Cycle
I-TEQ	International Toxic Equivalency
LAN	Local Area Network
LFL	Lower Flammability Limit
LHV	Lower Heating Value
MDEA	Methyldiethanolamine
MEA	Monoethanolamine
MS	Mass Spectrometer
MSW	Municipal Solid Waste
NOx	Nitrogen Oxides
NTP	Normal Temperature and Pressure (25 ^{o}C and 101.325 kPa)
NREL	National Renewable Energy Laboratory
PC	Personal Computer
PPB	Parts Per Billion
PPM	Parts Per Million
PSA	Pressure Swing Adsorption
QIC	Quartz Inlet Capillary
QMS	Quadrupole Mass Spectrometer

RC	Radio Communication
RDF	Refuse-Derived Fuel
RF	Radio Frequency
RS	Relative Sensitivity
T/C	Thermocouple
TCD	Thermal Conductivity Detector
TGA	Thermo Gravimetric Apparatus
SEM	Secondary Electron Multiplier
SNG	Synthetic Natural Gas
SOFC	Solid Oxide Fuel Cell
SRU	Claus Sulfur Recovery Unit
UFL	Upper Flammability Limit
UHV	Ultra High Vacuum
WID	Waste Incineration Directive

A Note on Units

For the most part of this thesis, the SI system of units has been used. The SI base units are as follows, with abbreviations given in brackets.

Length	metre (m)
Time	second (s)
Mass	kilogram (kg)
Amount of substance	mole (mol)
Temperature	kelvin (K)

Some derived quantities are given below. Not all of these terms are accepted SI terms, but all are frequently encountered.

Energy	1 joule (J) ≡ 1 kg.m^2/s^2
Power	1 watt (W) ≡ 1 J/s
Pressure	1 bar (bar) ≡ 10^5 Pa ≡ 750.06 Torr
Temperature	kelvin (K) ≡ Celsius (^{o}C) + 273.15
Volume	1 litre (L) ≡ 10^{-3} m^3
Length	1 metre (m) ≡ 10^{-3} mm ≡ 10^{-6} μm ≡ 10^{-9} nm
Mass	1 kilogram (kg) ≡ 1000 grams (g)

CHAPTER 1

Introduction

1.1 BACKGROUND

As oil and natural gas resources are decreasing, and they are also finite, it is becoming more important to make more use of renewable sources of biomass as a feedstock for the supply of energy and chemicals in the future.

In a text book on Gasification (Higman and Burgt, 2008, p. 75), the term “biomass” is considered to cover a very broad range of materials, that offer themselves as fuels, or raw materials, and have in common the fact that they are all derived from recently living organisms. This definition excludes traditional fossil fuels, since although they also derived from plant (coal) or animal (oil and gas) life, it has taken millions of years to convert them into their current form. There is also a degree of overlap between materials that may be classified as waste, or biomass.

One way of converting biomass into useful gaseous products is *via* a process known as gasification, which is a thermal conversion process (see Figure 1.1). In this type of process, the intention is to convert solid biofuels into gaseous products, which in turn are more valuable than the original feedstock (Hofbauer and Knoef, 2005, p. 115; Basu, 2010, p. 19). Knoef (2005, p. 13) states that the biomass gasification process consists of a number of steps:

- Thermal decomposition to gas, condensable vapours and char (pyrolysis).
- Subsequent thermal cracking of vapours to gas and char.
- Gasification of char by steam or carbon dioxide.
- Partial oxidation of combustible gas, vapours and char.

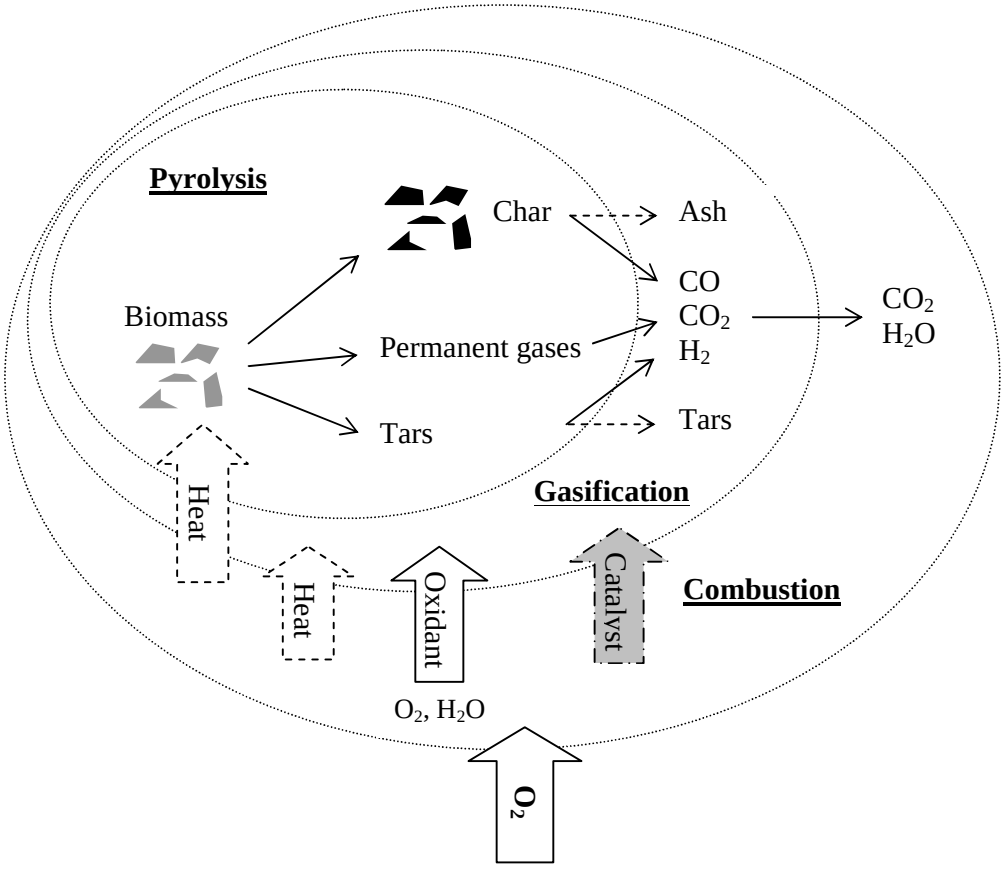

Figure 1.1 Schematic presentation of gasification as one of the thermal conversion processes, adapted from BTG (2002) as presented in Knoef (2005, p. 13).

1.1.1 Reactions

Biomass gasification is defined as incomplete combustion of biomass to produce combustible gases consisting of carbon monoxide (CO), hydrogen (H_2) and traces of methane (CH_4). During the process of gasification of biomass, the principal chemical reactions may involve species such as carbon, carbon monoxide, carbon dioxide, hydrogen, water (or steam) and methane. The main reactions may be represented (Higman and Burgt, 2008, pp. 12-13) as:

Combustion reactions:

$$C + \tfrac{1}{2} O_2 \rightarrow CO \qquad -111 \text{ kJ/mol} \qquad (1.1)$$

$$CO + \tfrac{1}{2} O_2 \rightarrow CO_2 \qquad -283 \text{ kJ/mol} \qquad (1.2)$$

$$H_2 + \tfrac{1}{2} O_2 \rightarrow H_2O \qquad -242 \text{ kJ/mol} \qquad (1.3)$$

The Boudouard reaction:

$$C + CO_2 \leftrightarrow 2CO \qquad +172 \text{ kJ/mol} \qquad (1.4)$$

The water gas reaction:

$$C + H_2O \leftrightarrow CO + H_2 \qquad +131 \text{ kJ/mol} \qquad (1.5)$$

The methane reaction:

$$C + 2H_2 \leftrightarrow CH_4 \qquad -75 \text{ kJ/mol} \qquad (1.6)$$

The water gas shift reaction:

$$CO + H_2O \leftrightarrow CO_2 + H_2 \qquad -41 \text{ kJ/mol} \qquad (1.7)$$

According to Boerrigter and Rauch (2005, pp. 215-222), gasification is seen as a key conversion technology in many processes that produce energy, fuels, and/or products from biomass. Rather than just burning the biomass to produce energy, there are a number of important advantages in the selection of a gasification pathway, for example (adapted from Reed and Guar (2000) as represented in Knoef (2005, p. 1)):

- The gas produced may be transported in pipelines.
- Gasification is easier to control and is capable of continuous operation.
- The volumetric flow of the gas produced is less than the flow of flue gas from an incineration process, so it should be easier to clean-up the gas from a gasifier.
- The combustion of the resulting gas stream results in a cleaner combustion process, as many of the impurities have been removed from the gas before it is burned.
- The combustion of the gas produced is more efficient than trying to burn a solid feed stream of biomass.
- The gas produced could be used as a fuel in internal combustion (IC) engines or gas turbines, and these can achieve higher overall efficiencies (fuel to electricity) than fuel to steam and then electricity.
- The gas, in particular syngas, can be used for chemical synthesis e.g. fertilizers and transportation fuels.

More commercial attractions of biomass gasification can be found in Basu (2010, pp. 19-21).

In a gasification process, air is used to support the partial combustion reactions that generate the heat for the gasification process, then a producer gas is formed. This generally consists (e.g. De Bari *et al.*, 1999) of: CO (18 to 21 vol.%), H_2 (10 to 16 vol.%), O_2 (1.5 to 2.5 vol.%), CH_4 (1 to 3 vol.%), and N_2 (40 to 54 vol.%), together with traces of hydrocarbons and contaminants which include volatile ash, organic condensable compounds (tar), inorganic constituents such as HCN, NH_3, H_2S, and COS. These contaminants are normally incompatible with the way in which the gas is used; therefore, gas cleaning is required (Iversen and Gobel, 2005, pp. 189-191). Depending on the design of the gasifier and the type of biomass used as a source of fuel, the concentration of contaminants varies (Boerrigter and Rauch, 2005, p. 225). However, these often need to be reduced to low levels, depending very much on the planned end-use of the system. An example of the level of gas clean-up required for different applications is illustrated in Table 1.1.

Table 1.1. Indicative specifications of product gas for different applications, adapted from Iversen and Gobel (2005, p. 190).

Application	Tar (mg/Nm^3)	Particles (mg/Nm^3)	Alkalis (mg/Nm^3)	Ammonia (mg/Nm^3)	Chloride (mg/Nm^3)	Sulphur (H_2S, COS) (mg/Nm^3)
Gas engine[1)]	< 50	< 50	< 1	< 50	< 10	< 100
Gas turbine[2)]		< 30	<0.25			
Syngas / Methanol[3)]	<0.1	<0.02	Below ppmv level			
Fuel cell[4)]	<1		Below ppmv level			

1) If an engine exhaust catalyst is used, some specifications are stricter on levels of sulphur, chloride, alkalis and heavy metals.
2) Turbines are not sensitive to tar because gas temperature is usually high and tars are in vapour form. Alkalis (Na, K, P) are critical compounds for erosion.
3) Specifications are very strict for the shift plant.
4) Specifications are very strict.

If the gas is used as a fuel in a gas boiler, then the specification would depend on the allowable emission limits from the stack. In addition, restrictions may apply on levels of chloride and/or sulphur compounds if their levels may lead to corrosion/fouling problems (Iversen and Gobel, 2005, p. 190).

1.1.2 Gasification Processes

The composition of the gas generated is very dependent on the type of gasification process, gasification agent and the gasification temperature (Boerrigter and Rauch, 2005), see Figure 1.2. The gas produced may be classified as product gas (producer gas) or bio-syngas (syngas). In general, producer gas is formed at temperatures less than 1000 ºC, and syngas is formed at temperatures higher than 1200 ºC. Syngas has a higher content of CO and H_2 than producer gas. The producer gas can be converted into syngas by thermal cracking or reforming (CO and H_2 content is increased).

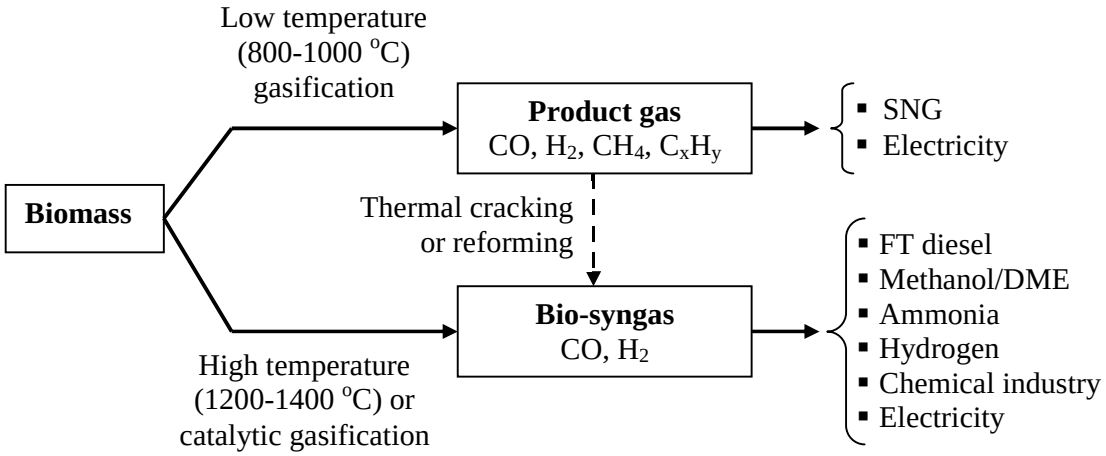

Figure 1.2 Difference between 'bio-syngas' and 'product gas' and their typical applications, adapted from Boerrigter and Rauch (2005, p. 212).

Producer gas is suitable for power generation, whereas syngas could be used as a feedstock in Fischer-Tropsch synthesis, ammonia and hydrogen production, and in other processes such as olefin hydroformylation and mixed alcohol synthesis.

1.2 MOTIVATION FOR PRESENT WORK

In this thesis, the production of a producer gas in a down-draft gasifier, which is then cleaned and used in a gas engine to produce electricity and heat, is of special interest.

Typically, in a down-draft gasifier the, biomass is fed from the top, while the oxidant (air) comes from the nozzles on the sides, see Figure 1.3. The gas moves downward in the same direction as the fuel, and leaves at the bottom of the reactor. Char and/or ash are also removed from the bottom.

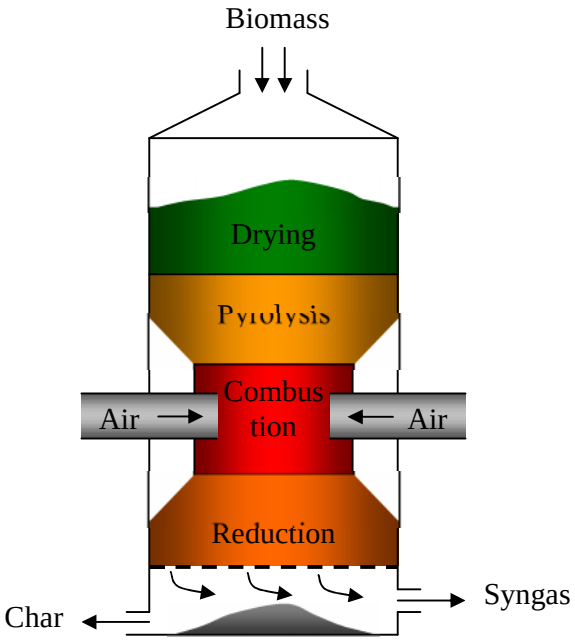

Figure 1.3 Typical schematic of a down-draft gasifier, adapted from Olofsson (2005) as presented in Knoef (2005, p. 24).

The motivation for the work arises from the recognition (Kolaczkowski *et al.*, 2011) that although the general principles of biomass gasification are broadly understood, unfortunately at a larger scale of operation (e.g > 0.5 MW_e), there is still a lack of confidence in the translation of the basic scientific concepts into a financially viable operation that satisfies current regulatory requirements.

Although in the literature (e.g. Knoef, 2005; Wang *et al.*, 2004), descriptions are provided of many different types of gas clean-up devices (e.g. cyclones, solid bed filters, bag filters,

scrubbers, rotating particle separators, tar crackers, electrostatic precipitators (EP)), cost effective solutions still need to be selected and developed. Barriers to progress remain from:

(a) the need to develop cost effective solutions for the removal of contaminants, and
(b) the need to develop robust gasification technology that can be scaled from e.g. 50 kW_e to 500 kW_e and then up to 2MW_e and higher scale.
[Note: where the subscript 'e' on 'kW_e' or 'MW_e' refers to an electrical rating.]

1.3 STRUCTURE OF THESIS

The link between these different activities, and the value of the work done, is summarized in Figure 1.4.

Chapter 2 starts with a brief literature review of biomass gasification processes, which sets the scene for the work that follows.

In **Chapter 3** the development of a small-scale quartz-tube down-draft gasifier is described. This enables visual observations to be made, and experiments are performed with wood and straw pellets. Interesting observations are made about the movement of the combustion zone and the role of a secondary charcoal bed in the gasification process, and gas composition is measured with a GC.

Then in **Chapter 4**, gas analysis techniques are developed further and a method is developed which makes use of a quadrupole mass spectrometer (QMS), which enables on-line measurements to be performed.

The presence of sulphur compounds (e.g. H_2S and COS) in the producer gas stream is considered in **Chapter 5**. This includes a theoretical consideration of thermodynamic equilibrium, and then measurements are also performed on the gas produced from the gasification of wood pellets, straw pellets and refuse-derived fuel (RDF) pellets.

In **Chapter 6** experiments are performed on the steam gasification of char obtained from actual pilot-plants that have used (a) wood pellets as fuel, and (b) RDF pellets as a fuel.

These are interesting results, as experiments are performed on actual char samples (rather than model compounds), and the gas is analyzed with the QMS. This then leads to further work in **Chapter 7**, where kinetic experiments are performed on the gasification of char with steam. The char used is from a pilot-plant that was gasifying RDF pellets.

Finally, an opportunity arises, to take the QMS onto a pilot-plant, and to use the techniques developed in this thesis, to perform some on-line gas measurements. These are performed with waste-wood as the feedstock into the gasifier, while the plant is started-up, and run at different gas flow rates. The results are discussed in **Chapter 8**.

Then in **Chapter 9**, conclusions and recommendations for further work are presented.

In the appendices, useful information is provided, which includes the MATLAB programmes.

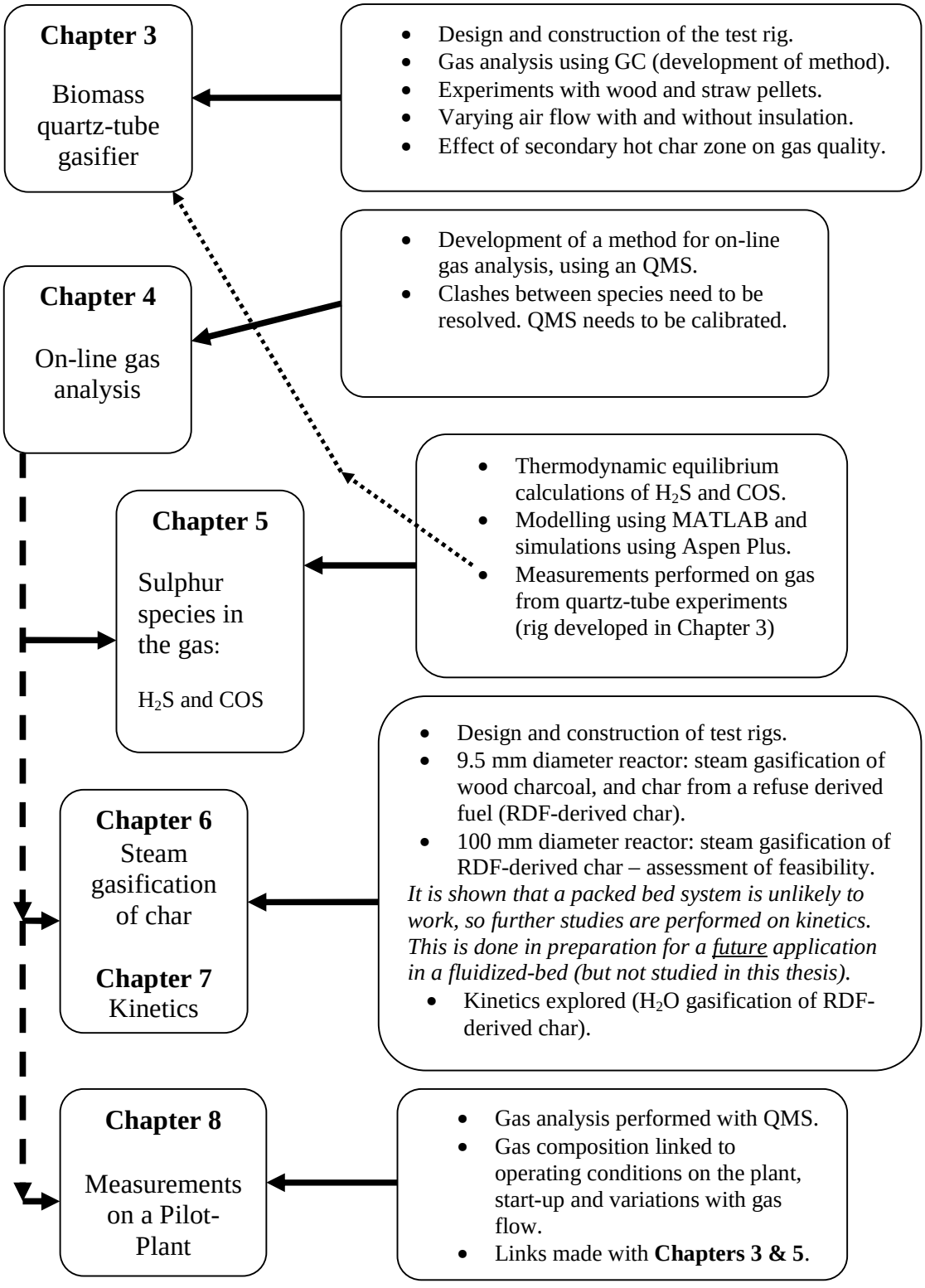

Figure 1.4 Links between the activities in this thesis.

REFERENCES

Basu, P. (2010). Biomass Gasification and Pyrolysis. Elsevier Inc.

Boerrigter, H. and Rauch, R. (2005). Syngas production and utilization. In Handbook Biomass Gasification, Knoef H.A.M (Ed), pp. 211-230.

De Bari, I., Barisano, D., Cardinale, M., Matera, D., Nanna, F. and Viggiano, D. (1999). Air Gasification of Biomass in a Downdraft Fixed Bed: A Comparative Study of the Inorganic and Organic Products Distribution. Energy and Fuels, Vol. 14, pp. 889-898.

Higman, C. and Burgt, M.V.D. (2008). Gasification. Second edition, Elsevier.

Hofbauer, H. and Knoef, H. (2005). Success stories on biomass gasification. Handbook Biomass Gasification, Knoef H.A.M (Ed), pp. 115-161.

Iversen, H. L. and Gobel, B. (2005). Update on gas cleaning technologies. Handbook Biomass Gasification. Knoef H.A.M (Ed), pp. 189-210.

Knoef, H.A.M., edited, (2005). Handbook Biomass Gasification. BTG biomass technology group.

Kolaczkowski, S., Le, C.D. and Jodlowski, P. (2011). Gasification of wood pellets in an experimental quartz tube gasifier – How visual 1D experiments can aid 3D design considerations. In Proceedings of the bioten conference on biomass and biofuels 2010, Bridgwater, A.V. (Ed), CPL Press UK, pp. 720-732.

Wang L. K., Pereira N. C. and Hung Y-T., edited, (2004). Air Pollution Control Engineering. Handbook of Environmental Engineering, Vol. 1, Humana Press Inc, Totowa, New Jersey.

CHAPTER 2

Literature Review

In this chapter, a literature review is provided, which illustrates how the technology has developed, and then highlights some of the key challenges which remain to be resolved before gasification can be more rapidly adopted at a commercial scale.

2.1 BIOMASS GASIFICATION

Based on information in the literature, there are various designs, and some of these will be briefly described.

2.1.1 Biomass Gasifiers

Different designs have been investigated for more than a century, and these are well described in many published sources (e.g. Knoef, 2005); Higman and Burgt, 2008; Rezaiyan and Cheremisinoff, 2005; and Basu, 2010). In Figure 2.1, a simplified schematic is provided to illustrate heat flow inside a fixed-bed gasifier. The heat requirements for drying, pyrolysis and the reduction processes can be provided:

- either, directly by partial combustion of the fuel, called autothermal gasification,
- or, by indirect or external heat sources, called allothermal gasification.

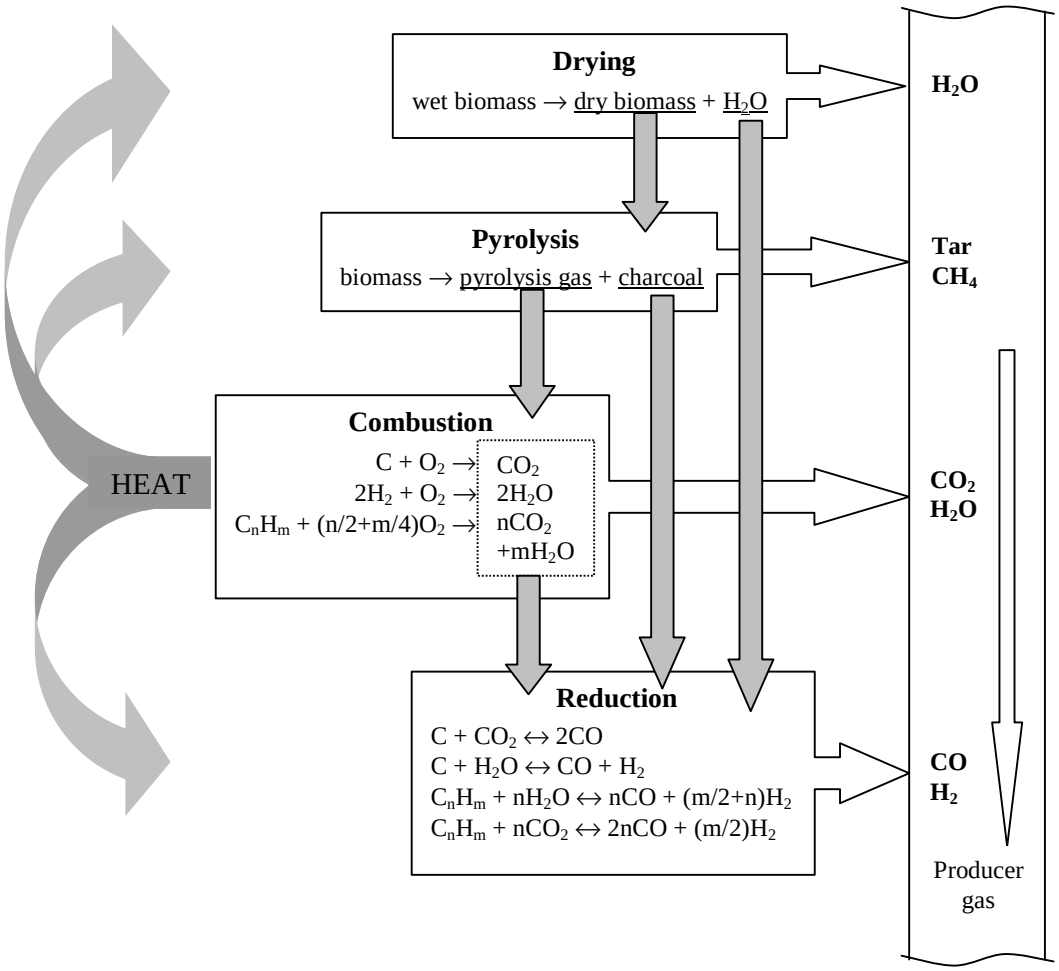

Figure 2.1 Heat flow and chemical reactions in down-draft gasification processes, adapted from Knoef (2005, p. 23).

As described in Knoef (2005, p. 22), in broad terms there are three main types of gasifier, namely: a fixed-bed gasifier, a fluidized-bed gasifier, and an entrained-flow gasfier.

Fixed-bed Gasifier: The fixed-bed (sometimes called moving bed) system consists of three different designs: down-draft gasifier, up-draft gasifier and a cross-draft gasifier, see Figure 2.2. In a fixed-bed gasifier, the bed of biomass moves slowly in a downward direction under the influence of gravity, as it is gasified by:

- a counter-current gasifying agent (e.g. air and/or steam) stream in an **up-draft gasifier**,
- or, by a co-current gasifying agent in a **down-draft gasifier**,
- or, by a horizontal flow of gasifying agent in a **cross-draft gasifier**.

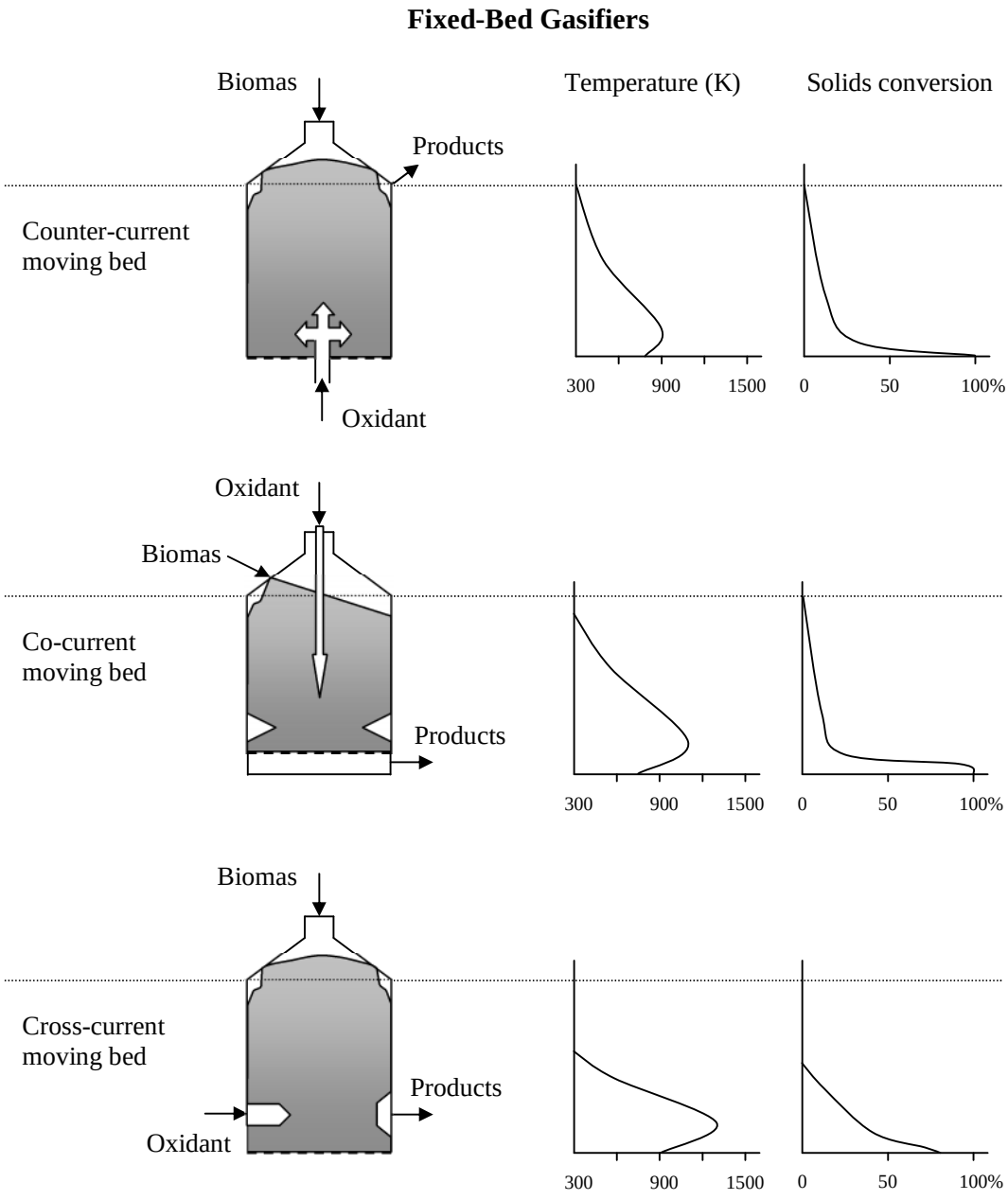

Figure 2.2 Characteristics of different gasifier configurations (wood as a feedstock), adapted from a schematic in Knoef (2005, p. 26).

Table 2.1. Some characteristics of fixed-bed gasifers, adapted from Knoef (2005, p. 26).

	Down-draft	**Up-draft**
Fuel (wood)		
- moist. cont. (wt.% in wet basis)	12 (max. 25)	43 (max. 60)
- ash content (wt.% in dry basis)	0.5 (max. 6)	1.4 (max. 25)
- size (mm)	20 – 100	5 – 100
Gas exit temp. (^{o}C)	700	200 – 400
Tars (g/Nm^3)	0.015 – 0.5	30 – 150
Sensitivity to load fluctuations	Sensitive	Not sensitive
Turn down ratio	3 - 4	5 – 10
η_{HG} full load (%) [1)]	85 – 90	90 – 95
η_{CG} full load (%) [2)]	65 – 75	40 – 60
Producer gas LHV (MJ/Nm^3) [3)]	4.5 – 5.0	5.0 – 6.0

1) η_{HG} Hot gas efficiency, taking into account the heat contained in the gas. To be applied for heat applications

2) η_{CG} Cold gas efficiency. The gas will be cooled after leaving the gasifier to ambient temperature. To be applied for engine (and power) applications

3) LHV Lower Heating Value

Based on explanations in Knoef (2005, pp. 23-24), each type of fixed-bed gasifier has its own advantages, together with its drawbacks. For example, in an up-draft gasifier the gas has a relatively high tar content, whereas in a down-draft gasifier more of the tar that is produced in the pyrolysis zone is in turn combusted in the oxidation zone, leading to a gas with a lower tar content. Despite the presence of different designs, a fixed-bed gasifier producing a tar-free producer gas still does not exist (e.g. Basu, 2010, pp. 109-112; Knoef, 2005, pp. 27-28). The main reason why a tar-free gas is seldom reached is that the high temperature zone is never completely uniform, and so slippage occurs. There are also other drawbacks with fixed-bed gasifiers, such as fuel blockage, scale-up limitations, etc, that also need to be considered.

Fluidized-bed Gasfier: This type of design is extremely good at mixing the fuel particles with the gasifying agent, and promoting both heat and mass transfer. Fluidized-bed gasifiers have been used in large-scale gasification processes. For example, in a review by Basu (2010, pp. 168-169):

- fixed-bed gasifiers were used for smaller units (10 kW_T to 10 MW_T),
- fluidized-bed gasifiers were more appropriate for intermediate units (5 MW_T to 100 MW_T),
- while entrained-flow reactors were used for large capacity units (>50 MW_T).

[Note: where the subscript 'T' on 'MW_T', refers to a thermal rating.]

As described in Knoef (2005, p. 29):

> Fluidized-bed gasification was originally developed for large-scale coal gasification, and then it was applied to biomass gasification to overcome some of the operational problems with fixed-bed gasifiers, like:
>
> - fuels having high ash content,
> - bridging & channelling,
> - hot spots,
> - scale-up limitations, and
> - not being suitable for small particles in the feed, because of plugging and increased pressure drop.

However, there are still some drawbacks with fluidized-bed gasifiers such as low carbon conversion, ash slagging and complex feeding system. Knoef (2005, p. 30) listed some drawbacks of fluidized-bed gasifiers:

- high tar and dust content of the produced gas;
- high producer gas temperatures containing alkali metals in the vapour state;
- incomplete carbon burn out;
- complex operation because of the need to control the supply of both air and solid fuel; and
- the need for power consumption to compress the gas stream.

Entrained-flow Gasifier: This type of design is considered to be most successful and widely used for large-scale gasification of coal, petroleum coke, and refinery residues. According to Higman and Burgt (2008, p. 93): these gasifiers operate with feed and blast in co-current flow. They stated that the residence time in these processes is short (a few seconds). The feed is ground to a size of 100 μm or less to promote mass transfer, and allow the particles to transport in the gas. Due to the short residence time, high temperatures are required to ensure a good conversion; therefore, all entrained-flow gasifiers operate in the slagging range. The high-temperature operation creates a high oxygen demand for this type of process.

Although entrained-flow gasifiers have an advantage of easily destroying tar, their suitability in biomass gasification is questionable. The main reason is that molten biomass ash is highly aggressive, which greatly shortens the life of the gasifier's refractory lining (Basu, 2010, p. 163). Table 2.2 shows the operating conditions of down-draft, up-draft, bubbling fluidized-bed (BFB), circulating fluidized-bed (CFB) and entrained-flow (EF) gasifiers.

Table 2.2. Operating conditions of fixed-bed, fluidized-bed and entrained-flow gasifiers, adapted from BTG (2002) as presented in Knoef (2005, p. 32).

	Down-draft	**Up-draft**	**BFB**	**CFB**	**EF**
T, ^{o}C	700 to 1200	700 to 900	< 900	< 900	~1450
Tars	Low	High	Moderate	Moderate	Very low
Control	Easy	Very easy	Moderate	Moderate	Complex
Scale (MW_T)	< 5	< 20	10 to 100	20 to ??	>100
Feedstock	Very critical	Critical	Less critical	Less critical	Only fines

2.1.2 Producer Gas Composition from Gasifiers

The composition of the gas produced depends mainly on the characteristics of feedstock and the design of the gasifier. Typically, the gas will consist of:

- H_2, CO, N_2, CO_2, O_2, CH_4, and other hydrocarbons,
- sulphur compounds (H_2S/COS), nitrogen compounds (NH_3/HCN), chloride compounds (HCl),
- tars and particulates, and
- volatile inorganics.

Design of the gasifier and its operating conditions also have a strong effect on the gas composition. For example, at a low gasification temperature (e.g. <1000 ^{o}C), the gas in general contains higher levels of hydrocarbons, than the gas from a process operating at higher temperatures (e.g. >1200 ^{o}C). Then if the biomass is directly heated by the partial oxidation of the fuel with air, the gas (producer gas) contains a high level of nitrogen, whereas if it is heated indirectly (or by an oxygen enriched stream), a low level of nitrogen is found in the gas (syngas).

Examples of indirect gasification processes, where the heat is transferred by inert material, are the Fast Internal Circulation Fluidised Bed (FICFB) process developed by the Vienna University of Technology, the SilvaGas process based on the Batelle development, and the MILENA gasifier developed at the Energy research Centre of the Netherlands. Typical gas compositions for these three processes are presented in Table 2.3.

Table 2.3. Typical gas compositions of three indirect gasification processes (wood as fuel), adapted from Boerrigter and Rauch (2006, p. 13).

Gas component, dry basis		**FICFB (Güssing)**	**SilvaGas**	**MILENA (ECN)**
Hydrogen	vol.%	30-45	20-22	15-20
Carbon monoxide	vol.%	20-30	41-44	40-43
Carbon dioxide	vol.%	15-25	11-14	10-12
Methane	vol.%	8-12	12-16	15-17
C_2^+ hydrocarbons	vol.%	1-3	4-6	5-6
Benzene	vol.%		1	1
Nitrogen	vol.%	1-3	2-10	1-4
Ammonia	ppmv	500-1000		500-1000
H_2S	ppmv	20-120		40-100
Tar	g/Nm^3	0.5-1.5	40	40
Particles	g/Nm^3	10-20		

As described in Boerrigter and Rauch (2006, p. 14), bio-syngas is produced by high-temperature (>1200 °C) gasification. In principal, the (oxygen-blown) down-draft and the entrained-flow gasification processes are suitable for this. However, the down-draft fixed-

bed gasifiers are limited in scale, and they require a well-defined fuel, making them not fuel-flexible. Therefore, the preferred process to produce bio-syngas is entrained-flow gasification. There are two different types of entrained-flow (EF) gasifiers:

- slagging, for ash-containing feedstock (e.g. biomass), and
- non-slagging, for essentially ash-free feedstock.

Table 2.4 shows typical bio-syngas compositions produced by slagging EF gasification. Product gas compositions are also included in this table for comparison. The effect of the gasification temperatures on the yield of the hydrogen and carbon monoxide is also very clear.

Table 2.4 Typical bio-syngas compositions of entrained-flow (EF) gasification of woody biomass (7 wt.% moisture) compared to product gas compositions from a direct circulating fluidized-bed (CFB) gasifier at 850 °C and various conditions, adapted from Boerrigter and Rauch (2006, p. 14).

Gasification process:		**CFB**	**CFB**	**CFB**	**EF**	**EF**
Pressure (bar):		**1**	**1**	**20**	**1**	**20**
Gasification agent:		**Air**	**O_2/steam**	**O_2/steam**	**O_2**	**O_2**
Hydrogen	vol.%	14	32	19	33	27
Carbon monoxide	vol.%	21	27	20	53	53
Carbon dioxide	vol.%	14	29	40(*)	13	19(*)
Methane	vol.%	5	8	15	0	0
C_2^+ hydrocarbons	vol.%	2	3	5	0	0
Benzene (i.e. C_6H_y)	vol.%	0.4	1	1	0	0
Nitrogen	vol.%	44	0	0	0	0
Tar (wet gas)	g/Nm^3	8	8	11	0	0
H_2O	vol.%$_{wet}$	11	28	30	19	22
LHV (dry gas)	MJ/Nm^3	7.7	12.4	14.9	10.3	9.6

(*) In pressurized gasification carbon dioxide is used for inertisation of the feed to prevent nitrogen dilution of the gas.

2.2 END-USE APPLICATIONS OF PRODUCER GAS AND LIMITATIONS FOR FLUE GAS

2.2.1 End-use Applications of Producer Gas

According to Iversen and Gobel (2005, pp. 189-191): for biomass gasification to be successful, it is important that the gasifier, the gas cleaning system and the end-use application are designed as an integrated unit. This is a very important statement, as the 'end-use application', or emissions from the plant, often determine the requirement of gas quality. Kilns, or co-fired systems do not usually require much gas clean-up, while others such as gas engines, or gas turbines are more demanding. In Table 2.5 examples are provided of applications which can use syngas (bio-syngas), or producer gas (product gas).

Table 2.5 Applications for the use of bio-syngas and product gas, adapted from Boerrigter and Rauch (2005, p. 222).

Heat	Product gas
Power – Combined cycle	Product gas
Power – CHP gas engine	Product gas, low tar content
Power– CHP fuel cell (SOFC)	Product gas, low hydrocarbon & organic content
SNG	Product gas, nitrogen-free, high methane
Liquid fuel synthesis	Bio-syngas, nitrogen-free
Chemical synthesis	Bio-syngas, nitrogen-free
Hydrogen production	Bio-syngas, nitrogen-free
Ammonia production	Bio-syngas, containing nitrogen

In general, producer gas is favoured for power production, as it costs less to produce (than syngas), whereas syngas is generally preferred (low nitrogen content) as a feedstock for chemical conversion to other high valuable products.

Producer Gas: Boerrigter and Rauch (2005, pp. 222-223) provide an extensive discussion of the use of producer gas from which the following information has been obtained:

(a) For heat production by direct firing of the gas, there are in principle no technical specifications for the main gas composition. To reduce corrosion problems the chloride content should not be too high.

(b) The gas must be combustible (i.e. with a lower heating value of >5 MJ/Nm^3).

(c) Limitations on dust content of the gas may apply, depending on the type of boiler and the burner. Emission limits can usually be met with standard and commercially available flue gas cleaning systems.

(d) For power production in a combined cycle (CC), there is only the requirement of a gas free of dust and volatile metals (i.e. potassium and sodium). A pressurised feed gas is required; therefore, the product gas must be generated by pressurised gasification. If gasification occurs at atmospheric pressure, intermediate product gas compression is an option; however, to allow compression to typical CC pressure (15 to 40 bar) the gas must be completely clean, making this route much less attractive.

(e) Supply of gas into a gas engine requires a dust-free gas with a tar dewpoint below the engine inlet temperature to prevent tar condensation and fouling, i.e. typically, up to 2 g/Nm^3 of tars and a few vol.% of benzene and toluene may be present in the gas.

(f) The use of fuel cells for power generation is in theory an attractive proposition. However, the gas specifications are much stricter, and sulphur must be almost completely removed to avoid poisoning of the fuel cell. In addition, the aliphatic and aromatic hydrocarbons and tars must be not too high to prevent soot formation and coking, although a nitrogen-free gas is not required.

Syngas: The maximum levels of impurities in syngas depend very much on the end-use application. However, in catalytic synthesis processes, catalysts are in general very sensitive to small amounts of impurities. Tables 2.6 and 2.7 present levels for different applications.

Table 2.6 Purification level of main bio-syngas impurities, adapted from Boerrigter *et al*. (2003) as represented in Boerrigter and Rauch (2005, p. 224).

Impurity	Removal level
Sum of sulphur compounds (H_2S + COS + CS_2)	< 1 ppmv
Sum of nitrogen compounds (NH_3 + HCN)	< 1 ppmv
HCl + HBr + HF	< 10 ppbv
Alkaline metals	< 10 ppbv
Solids (soot, dust, ash)	Essentially completely
Organic compounds (hydrocarbons, tars)	Below dewpoint(*)

Table 2.7 Overview of main gas composition (vol.%) specifications for selected applications, adapted from Boerrigter and Rauch (2005, p. 224).

Synthesis	H_2 for refinery	Ammonia	Methanol	Fischer-Tropsch	Oxo alcohols
H_2	> 98	75	71	60	60
CO	< 10-50 ppmv	CO + CO_2 <20 ppmv	19	30	40
CO_2	< 10-50 ppmv		4-8		
N_2		25			
Inert	N_2, Ar, CH_4 balance	Ar, CH_4 as low as possible	N_2, Ar, CH_4 as low as possible	CO_2, N_2, Ar, CH_4 low	
H_2/N_2		~3			
H_2/CO				0.6-2	1-1.5
$H_2/(2\times CO+3\times CO_2)$			1.3-1.4		
Process temperature (^oC)		350-550	300-400	200-350	85-200
Process pressure (bar)	>50	100-250	50-300	25-60	15-350

2.2.2 Limitations for Flue Gas

When a gas is produced, that is then burned in some form of power plant, it is important to consider the impact of any impurities in the gas on emissions from that plant, or on the catalytic systems (e.g. CO and hydrocarbon oxidation catalysts, or DeNOx catalysts) that are used to control final emissions into the atmosphere. In general, these must follow the regulations in the country/local area where the plant is built.

For example, in a gasification process that is using waste as a fuel, according to the Department of the Environment, Food and Affairs in Enland (2008), Directive 2000/76/EC on the incineration of waste (WID) has to be followed.

The tables and notes below summarise the Emission Limit Values (ELVs) that must be achieved in WID. It should be noted that the reference conditions in the following tables are: temperature 273 K, pressure 101.3 kPa, 11 % oxygen (3 % oxygen if burning waste oils), dry gas. The tables and notes are adapted from Department of the Environment, Food and Affairs in England (2008).

Table 2.8 Daily average emission limit values for incinerators (WID).

Total dust	10 mg/m^3
Gaseous and vaporous organic substances, expressed as total organic carbon	10 mg/m^3
Hydrogen chloride (HCl)	10 mg/m^3
Hydrogen fluoride (HF)	1 mg/m^3
Sulphur dioxide (SO_2)	50 mg/m^3
Nitrogen monoxide (NO) and nitrogen dioxide (NO_2), expressed as nitrogen dioxide for existing incineration plants with a nominal capacity exceeding 6 tonnes per hour or new incineration plants	200 mg/m^3 (*)
Nitric oxide (NO) and nitrogen dioxide (NO_2), expressed as nitrogen dioxide for existing incineration plants with a nominal capacity of 6 tonnes per hour or less	400 mg/m^3 (*)

(*) Until 1 January 2007, an emission limit value for NO_x does not apply to plants only incinerating hazardous waste.

Table 2.9 Half-hourly average emission limit values for incinerators (WID).

	(100 %) A	**(97 %) B**
Total dust	30 mg/m^3	10 mg/m^3
Gaseous and vaporous organic substances, expressed as total organic carbon	20 mg/m^3	10 mg/m^3
Hydrogen chloride (HCl)	60 mg/m^3	10 mg/m^3
Hydrogen fluoride (HF)	4 mg/m^3	2 mg/m^3
Sulphur dioxide (SO_2)	200 mg/m^3	50 mg/m^3
Nitrogen monoxide (NO) and nitrogen dioxide (NO_2), expressed as nitrogen dioxide for existing incineration plants with a nominal capacity exceeding 6 tonnes per hour or new incineration plants	400 mg/m^3 (*)	200 mg/m^3 (*)

(*) Until 1 January 2007 and without prejudice to relevant Community legislation the emission limit value for NO_x does not apply to plants only incinerating hazardous waste.

Table 2.10 shows average values over the sample period of a minimum of 30 minutes and a maximum of 8 hours. These average values cover also gaseous and the vapour forms of the relevant heavy metal emissions as well as their compounds.

Table 2.10 Average values for heavy metal emissions (WID).

Cadmium and its compounds, expressed as cadmium (Cd)	total 0.05 mg/m^3	total 0.1 mg/m^3 (*)
Thallium and its compounds, expressed as thallium (Tl)		
Mercury and its compounds, expressed as mercury (Hg)	0.05 mg/m^3	0.1 mg/m^3 (*)
Antimony and its compounds, expressed as antimony (Sb)	total 0.5 mg/m^3	total 1 mg/m^3
Arsenic and its compounds, expressed as arsenic (As)		
Lead and its compounds, expressed as lead (Pb)		
Chromium and its compounds, expressed as chromium (Cr)		
Cobalt and its compounds, expressed as cobalt (Co)		
Copper and its compounds, expressed as copper (Cu)		
Manganese and its compounds, expressed as manganese (Mn)		
Nickel and its compounds, expressed as nickel (Ni)		
Vanadium and its compounds, expressed as vanadium (V)		

(*) Until 1 January 2007 average values for existing plants for which the permit to operate has been granted before 31 December 1996, and which incinerate hazardous waste only.

The WID requires dioxins to be reported using the I-TEQ (International Toxic Equivalency) Toxicity reporting convention to assess compliance against an emission limit of 0.1ng I-TEQ/Nm^3.

The following emission limit values for carbon monoxide (CO) must not be exceeded (excluding the start-up and shut-down phase):

- 50 milligrams/m^3 of combustion gas determined as daily average value;
- 150 milligrams/m^3 of combustion gas of at least 95 % of all measurements determined as 10-minute average values or 100 mg/m^3 of combustion gas of all measurements determined as half-hourly average values taken in any 24-hour period.

Exemptions may be authorized by the regulators for plants using fluidized-bed technology, provided that the permit foresees an emission limit value for carbon monoxide (CO) of not more than 100 mg/m^3 as an hourly average value.

Preliminary conclusion: From this consideration of WID limits, then for heat and power production, the applicable emission regulations for heat/power plants are likely to be very important in deciding on the specification to which the gas has to be cleaned prior to end-use. Also, the technical needs of catalyst systems for the clean-up of residual CO, hydrocarbon and NOx emissions from the plant may also impose strict requirements on the contaminants present in the gas that is used as the fuel in the power plant. For example, a sulphur contaminant in the fuel, e.g. H_2S, COS, when it is burnt in the power plant, will be converted into SO_2. This will then appear as an emission from the plant, and depending on its concentration, could also act as a catalyst poison.

2.3 GAS CLEAN-UP OVERVIEW

From the explanations in the previous sections, it is clear that the gas from a gasifier needs to be cleaned, to match the requirements of the process. In this section, an overview is provided of gas clean-up options, and areas for further work to be explored in this thesis are considered in more detail.

In the sections below, the gas clean-up technologies will be described, which are often used in combination with one another to achieve the desired overall reduction in contaminants.

2.3.1 Particle Removal

There are a various ways in which particulate matter may be reduced, and these devices are often positioned in the dirty hot gas steam from the gasifier to trap the carry-over of char particles and other particulate matter.

Cyclones: According to Wang *et al.* (2004, p. 98), cyclones are relatively inexpensive and easy to construct, require little maintenance, and can, in principle, work at high temperatures and pressures. Cyclones should not be used to trap sticky particles, or solids with a high moisture content, as caking and clogging may occur. If a cyclone is designed properly, particles >10 μm can be collected (with good efficiency). For smaller particles, the efficiency drops considerably.

For particles > 5 μm (diameter), it is possible to remove more than 90 % of the bulky particles (Iversen and Gobel, 2005, p. 192). To achieve high removal efficiencies, a number of cyclones may be placed in series. The main advantages of cyclones are their simplicity and their ability to operate at higher temperatures.

Fabric filtration: Small-diameter particles in the range 0.5 to 100 μm can be effectively removed in a fabric filtration system (Iversen and Gobel, 2005, p. 192). While this is especially effective in removing dry particles, it is less suitable for sticky or moist contaminants. Fabric filters are not suitable for applications at high temperatures, and at low temperatures, tars in the dirty gas will start to condense and would clog such filters.

Electrostatic Precipitator (EP): Electrostatic precipitation is defined as the use of electrostatic forces to remove charged solid particles or liquid droplets from gas streams in which the particles or droplets are carried in suspension (Wang *et al.*, 2004, p. 153). In an EP, the particles can be removed in a wet or dry form. In a dry EP, the particles are removed periodically by some form of mechanical action. This can be done at temperatures of about 500 ^{o}C, whereas in a wet EP, a thin film of flowing water is used to remove the

particles and these operate at temperatures of about 65 ^{o}C (Iversen and Gobel, 2005, p. 194).

Wet scrubbers: According to Iversen and Gobel (2005, p. 194): wet scrubbers use liquids, normally water at a temperature below 100 ^{o}C. Other kinds of scrubbing liquids have been developed to operate at higher temperatures. In a wet scrubber, particulate matter can be collected by collision with droplets of the scrubber liquid. Subsequently, the droplet of liquid is removed from the gas by coalescence, and finally by a demister.

In addition, wet scrubbers can be used to absorb other contaminants that may be present in the dirty gas stream, and this is discussed further in the sections that follow.

2.3.2 Tar Removal

As explained in Torres *et al.* (2007):

(a) Tars are a complex mixture of secondary and tertiary products (mostly aromatics) from the thermal decomposition or partial-oxidation of organic material.

(b) The primary products of organic decomposition during biomass gasification (or pyrolysis) are oxygen rich compounds such as alcohols, aldehydes, ketones, carboxylic acids, phenols and furans.

(c) At temperatures > 500 ^{o}C, the primary products decompose further into secondary products that comprise of aromatics of one ring (benzene, toluene, phenols, and benzaldehydes), two rings (naphthalenes, benzofurans) and three rings (phenanthrenes) with very small concentrations of compounds with more than three rings.

(d) Gasification in the range of 700–900 ^{o}C produces polyaromatic compounds with 4 rings (pyrene, fluoranthene) and traces of five ring compounds (perylene).

Iversen and Gobel (2005, p. 195) emphasize that tar removal is of great importance: (a) when the product gas is cooled prior to use, (b) when the product gas is compressed prior to use, and (c) when used in mechanical systems such as combustion engines or gas turbines. Tars can cause many problems in downstream operations when they condense (e.g. blocking gas coolers, filter elements and engine suction channels). However, their

levels may be reduced significantly by a variety of methods, e.g. physical, thermal conversion and catalytic conversion. Tar conversion to other gaseous fuel species is the generally preferred option, so that the heating value of the tars is retained in the enhanced gas stream. In some cases, the concentration of CO and H_2 may even be higher due to the conversion process. Figure 2.3 shows different routes to convert or eliminate tar.

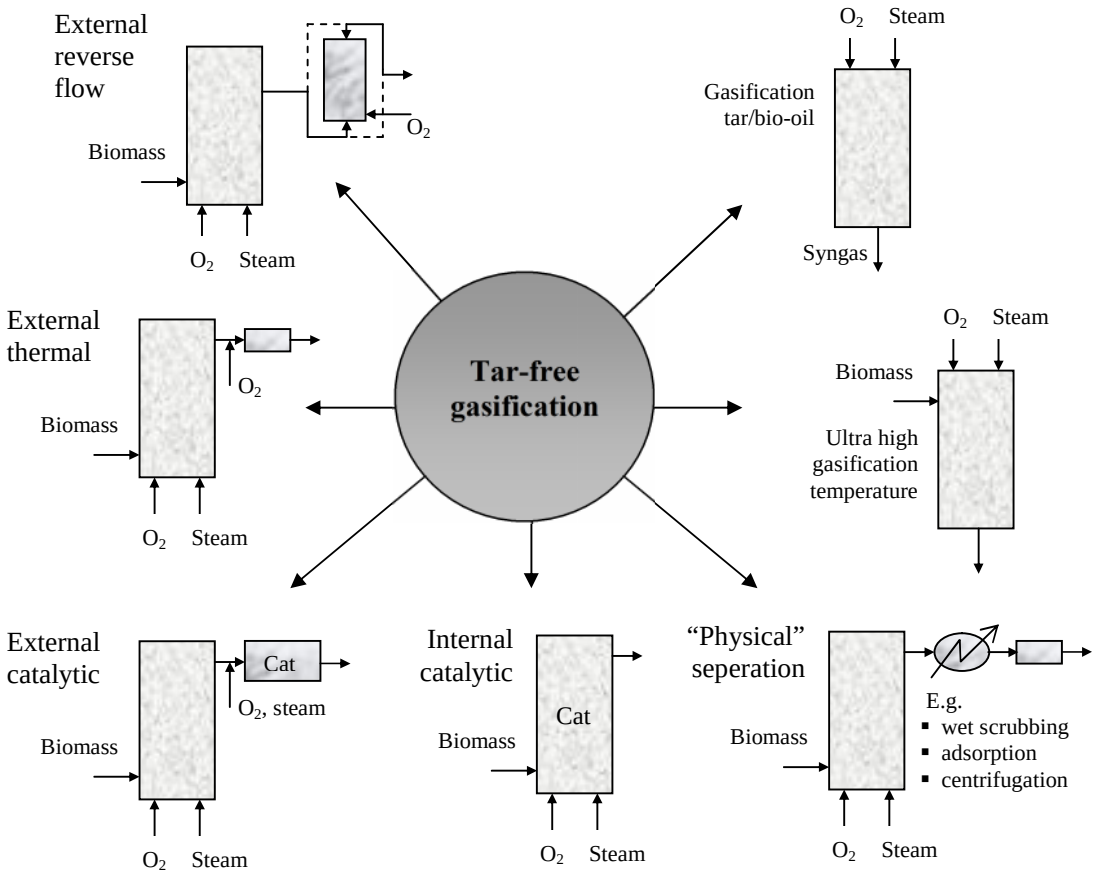

Figure 2.3 Different tar conversion or elimination concepts, adapted from BTG (2002) as shown in Iversen and Gobel (2005, p. 195).

2.3.2.1 Physical Removal of Tars

Physical removal methods have their own benefits as they are inexpensive and uncomplicated in design. However, the use of these methods results in a reduction in the calorific content of the dirty gas. There is also a tar disposal problem that needs to be addressed, and if a water quench system is used to condense/trap the tars, there may also a water usage and water clean-up issues to be considered.

Iversen and Gobel (2005, p. 195-197): provide a good summary of physical removal methods, stating that wet scrubbers are the most common method of physical removal, quoting examples of their use in the Gussing plant in Austria. They describe tars as hydrophobic so only aerosols are removed; thus, the use of lipophilic liquids in scrubbing fluids can improve gas phase tar removed. Wet electrostatic precipitators can be used to remove aerosol tars with efficiency of up to 99 %, and it is reported that this has been successfully applied to a down-draft gasifier in Wiener Neustadt. Barrier Filters are another option but are not generally suitable due to difficulties of cleaning. However, one such system is in place at the Gussing plant in Austria, where a pre-coated fabric filter is used to remove particles and some tar. It is reported that packed bed filters have also been used in small-scale gasifiers.

2.3.2.2 Thermal Conversion of Tars

This is achieved by raising the temperature of the gas to a point at which thermal cracking occurs of the tars. Temperatures for thermal cracking (and reforming of tars) depend on the nature of the tars, and there is great inconsistency in the literature of an appropriate temperature, although a common conclusion is that temperatures exceeding 1100ºC are required (Donnot *et al.*, 1985). Disadvantages of this method include:

- High operating costs and a possible reduction in the heating value of the stream (Brandt *et al.*, 2000).
- At very high temperatures soot is produced, which means that additional gas cleaning is necessary (Kandassamy *et al.*, 2003).
- When operating at high temperatures, heat losses also become more significant.

2.3.2.3 Catalytic Conversion of Tars

As described in Torres *et al*. (2007): Catalysts have been used inside a gasifier and also in secondary catalytic reactors to promote tar conversion reactions. Sometimes, an additional oxidant (O_2), or steam is injected into the secondary catalytic bed. Tars can be cracked or hydrocracked into light hydrocarbons, or converted into CO and H_2 through the so-called steam and dry reforming reactions. This is illustrated in the following equations using toluene to represent the tars in the dirty gas stream.

Steam reforming reactions:

$$C_7H_8 + 7H_2O \rightarrow 7CO + 11H_2 \quad (2.1)$$

$$C_7H_8 + 14H_2O \rightarrow 7CO_2 + 18H_2 \quad (2.2)$$

Dry reforming reactions:

$$C_7H_8 + 7CO_2 \rightarrow 14CO + 4H_2 \quad (2.3)$$

$$C_7H_8 + 11CO_2 \rightarrow 18CO + 4\ H_2O \quad (2.4)$$

Hydrocracking:

$$C_7H_8 + 10H_2 \rightarrow 7CH_4 \quad (2.5)$$

If the tar is hydrocracked all the way to methane (reaction (2.5)) then this is desirable, but if it is used for synthesis of methanol or ammonia then it is undesirable. A common byproduct in all of these catalytic processes is carbonaceous materials deposited on the catalyst as a result of:

Cracking: $C_7H_8 \rightarrow 7C + 4H_2$ (2.6)

Boudouard reaction: $2CO \rightarrow CO_2 + C$ (2.7)

The water gas shift reaction: $CO + H_2O \rightarrow H_2 + CO_2$ (2.8)

can also occur, increasing the concentration of H_2 at the expense of CO.

Catalysts for tar conversion:

Although acid catalysts such as FCC catalysts or zeolites could be used, they are unsuitable due to their rapid elutriation and coke build up (Torres *et al.*, 2007). Therefore, basic catalysts tend to be considered for this application.

Torres *et al.* (2007) reported that the catalytic properties of mixtures of CaO and MgO exhibit a high potential for hot gas cleaning of tars.

According to Bain *et al.* (2005), calcined dolomites are the most widely used non-metallic catalysts for tar conversion in biomass gasification processes. They are described as relatively inexpensive and disposable; however, they quickly undergo attrition in fluidized-bed reactors. Tar-conversion efficiency was claimed to be high when calcined dolomites were used at high temperatures (900 °C) with steam. However, their catalytic activity is very sensitive to the level of CO_2. In order for these materials to retain high catalytic activity, the CO_2 partial pressure in the reactor cannot be greater than the equilibrium decomposition pressure of dolomite (Torres *et al.*, 2007).

Olivine, another naturally occurring mineral, has also demonstrated tar-conversion activity similar to that of calcined dolomite. Olivine has been shown to resist attrition better than calcined dolomite and has been applied as a primary catalyst to reduce the output tar levels from fluidized-bed biomass gasifiers (Bain *et al.*, 2005). However, both reforming activity (especially for applications where conversion of lower hydrocarbons is desired) and their catalytic stability were lower than calcined dolomite (Zhao *et al*., 2009).

Nickel catalysts (commonly used for steam reforming of methane/naphtha and hydrogenation reactions) have been widely tested as secondary catalysts for the removal of tars from biomass gasifiers (Torres *et al.*, 2007). However, there are two main limitations in their application:

(a) Commercial Ni catalysts are usually designed for use in fixed-bed applications, and are therefore not robust enough to be used in a fluidized-bed application. So they are more likely to be used as fixed-bed catalysts in a secondary catalytic bed (to increase tar conversion).

(b) Ni catalysts are known to quickly deactivate in biomass gasifier conditions, which leads to limited catalyst lifetimes (Li *et al.*, 2009).

According to Torres *et al.* (2007), monoliths have also been considered as catalyst supports for tar cracking. Monoliths are ceramic blocks containing parallel straight channels, and they have a thin layer of catalytically active material deposited on the walls. The open structure offers a low pressure drop, and it is easier to process gases containing particulate matter. Monoliths are well established as catalytic converters in the automotive industry, and as support structures for DeNOx catalysts.

In the literature there are many examples of other catalysts that have been studied, for example:

- Li *et al.* (2009) have used Ni/Mayenite ($Ni/Ca_{12}Al_{14}O_{33}$), which showed an excellent carbon and H_2S resistance property.
- Zirconia has been used, but because its activity is relatively low (compared with nickel catalysts), it has instead been used as a support for nickel catalysts (to prevent Ni-associative deactivation problems). In studies, improved stability and reduced effects of sulphur poisoning have been shown (e.g. Ma and Baron, 2008; Sutton *et al.*, 2001; Sutton *et al.*, 2002; and Siangchin, 2004).
- In Torres *et al.* (2007), other catalysts are also listed.

An additional consideration when looking at catalysts for the purpose of tar removal is their effectiveness at reducing the level of ammonia, and this has been considered in Simell (1996).

2.3.3 Removal of Nitrogen Compounds

Removal of the nitrogen compounds, mostly ammonia, from the product gas is really necessary due to the fact that ammonia is converted to NO_x when the gas is burned.

As described in Torres *et al.* (2007), during the gasification process, nitrogen in the biomass feed ends up as ammonia (NH_3) and N_2, with lower concentrations of hydrogen cyanide (HCN), isocyanic acid (HNCO), and oxides of nitrogen (NO_x). The concentration of these species could vary from a few hundred ppmv to 2 vol.%, depending on the nitrogen content of the biomass, gasification temperature and other process variables. Nitrogen containing species are undesirable because they can poison catalysts, or serve as precursors for NO_x in downstream burners, gas engines, or gas turbines.

Cleaning the product gas from ammonia can be performed in two different ways:

(a) Wet scrubbing for ammonia removal: Wet scrubbing is a well-developed technology and ammonia may be removed with other contaminants, in a scrubbing system using dilute acid (HCl solution, pH =1) as a scrubbing liquor (Wang *et al.*, 2004, pp. 198-204).

(b) Catalytic destruction of ammonia: It is possible using similar catalysts as those used for the catalytic destruction of tar. Two catalytic routes have been proposed (e.g. Torres *et al.*, 2007) for the removal of NH_3 from coal or biomass gasification products, namely decomposition and selective oxidation:

$$2NH_3 \rightarrow N_2 + 3H_2 \quad (2.9)$$

$$4NH_3 + 3O_2 \rightarrow 2N_2 + 6H_2O \quad (2.10)$$

Decomposition of ammonia to N_2 and H_2 is highly desirable because such a reaction does not introduce any additional contaminants into the fuel gas stream. In the literature (e.g. Torres *et al.*, 2007) the use of calcined dolomite, nickel and iron catalysts, is mentioned; however, high temperatures (> 850 ^oC) are required.

2.3.4 Removal of Sulphur Compounds

Sulphur compounds (e.g. H_2S, COS, SO_2) which are present in the dirty gas stream need to be significantly reduced/removed.

According to Higman and Burgt (2008, pp. 328-352), a wide range of processes could be used, for example:

- Absorption (physical or chemical) in a liquid solvent with a subsequent desorption step.
- Adsorption (again physical and chemical) onto a mass of solid particles.
- Diffusion through a permeable or semi-permeable membrane.
- Chemical conversion, generally on a catalyst, often as a preparatory step to one of the above three methods.

In general sulphur removal process operate 'cold' – that is, at ambient temperatures or lower (chemical adsorption of trace H_2S on zinc oxide is the prominent exception), Higman and Burgt (2008, p. 329). The loss of overall efficiency in IGCC and fuel cell (SOFC) applications, which is associated with gas cooling between gasifier and the end-use systems, has generated considerable interest in the development of hot desulphurization processes. Hence, in the sections that follow, hot and cold approaches are considered.

2.3.4.1 Cold Desulphurization Approaches

Traditional wet scrubbers (with solvent recovery): The dirty gas is scrubbed with a liquid, which selectively removes a range of components (e.g. H_2S) from the gas. The laden solvent is then regenerated, releasing the absorbed components, and the solvent is recirculated back to the absorber. The washing or absorption process takes place in a column or a scrubber, which is usually fitted with (structured or unstructured) packing or trays.

The absorption characteristics of a solvent depend either on simple physical absorption, or on a chemical bond with the solvent itself. Klinkenbijl *et al.* (1999) showed three basic types of liquid absorption processes:

Physical absorption processes*:* these use a solvent that physically absorbs CO_2, H_2S and organic sulphur components. Examples are the Purisol and Selexol (more information could be found in Higman and Burgt (2008, pp. 335-338)) processes. Physical solvents can be applied advantageously when the partial pressure of the contaminants is high, the treated gas specification is moderate, and large volumes of gas have to be purified. However, physical solvents can also absorb significant quantities of hydrocarbons (tars), which could be a disadvantage.

Chemical absorption processes: chemicals have been used to absorb H_2S, CO_2 and to some extent COS. Organic sulphur components do not chemically react with the solvent. Common examples are amine processes, using aqueous solutions of alkanol amines such as MEA (monoethanolamine), DEA (diethanolamine), MDEA (methyldiethanolamine), DIPA (di-isopropanolamine) and Flexsorb, and carbonate processes such as the Benfield process (see Higman and Burgt (2008, p. 332-334) for more information). Chemical solvents are specifically suitable when contaminants at relatively low partial pressure have to be removed to very low concentrations. However, such chemical solvents will not remove mercaptans down to low levels (due to their low solubility). Due to the chemical reaction between the solvent and CO_2 and H_2S, the regeneration energy requirements are normally higher than for a physical solvent.

Mixed solvents: are a mixture of a chemical and a physical solvent. The most widely known process is the Shell Sulfinol Process (see Higman and Burgt (2008, p. 338)), which applies a mixture of sulfolane (tetrahydro thiophene dioxide), water and DIPA or MDEA, Sulfinol-D and Sulfinol-M, respectively. An advantage of the Sulfinol process is its claim to simultaneously remove organic sulphur compounds and COS, which are not normally removed in pure chemical solvents. Another commercial, Flexsorb SE process, also combines sulfolane and an amine, and is in many ways similar to the Shell Sulfinol Process.

An example of an acid gas removal scheme using MDEA is shown in Figure 2.4. In large-scale processes, sulphur is recovered. For example, above about 15 t/day of sulphur, the common choice is the two-stage Claus process, which typically achieves 95 % sulphur recovery (Klinkenbijl *et al.*, 1999).

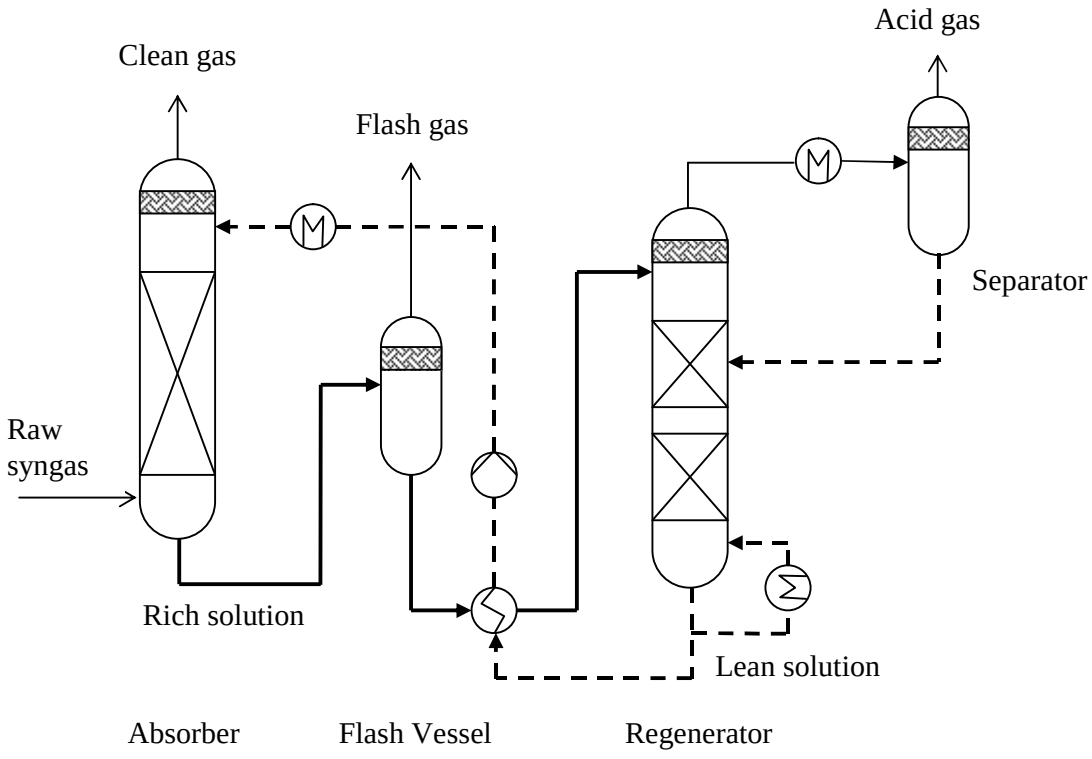

Figure 2.4 Example of an MDEA flowsheet with a single flash stage, adapted from Higman and Burgt (2008, p. 334).

However, in the absorption process, as CO_2 absorption from the dirty gas also occurs, this then acts as an inert gas in the Claus unit, increasing the size of the unit and reducing the sulphur recovery efficiency. Klinkenbijl *et al.* (1999) concluded that in situations where the

molar ratio of H_2S:CO_2 in the feed gas is < 0.2, the acid gas exiting the acid gas removal plant will be difficult to process in a straight through Claus unit, so CO_2 must be removed from acid gas before it is fed into the Claus unit, or another solvent which is selective for removing H_2S in the gas removal plant should be used.

Innovative wet scrubbers: As described in the literature (e.g. Wang *et al.*, 2004, pp. 282-284; Higman and Burgt, 2008, pp. 339-340), other methods for H_2S removal involve the use of oxidative washes or liquid redox systems. They differ from other types of absorption systems in which H_2S in the acid gas is oxidized directly to elemental sulphur in the absorption stage. The solvents in such oxidative washes absorb essentially the H_2S, but not CO_2 or COS to any extent. This makes them suitable for applications where H_2S must be removed from a stream containing large quantities of CO_2, even if the H_2S partial pressure is low. In such a system, very high H_2S removal efficiencies (99+ %) can be achieved, and they have high turndown capabilities (Wang *et al.*, 2004, pp. 283-284).

Wet scrubbing systems using inorganic chemicals: These tend to be used in smaller applications, where it is uneconomical to recover the sulphur. If NH_3, HCl and H_2S levels need to be reduced, then a three-stage scrubbing system could be used in which, in the:

- 1^{st} scrubber, HCl, NH_3 and metals are mainly removed, using dilute acid (HCl solution, pH =1) as a scrubbing liquor (Wang *et al.*, 2004, p. 270),
- 2^{nd} scrubber, 80 % of H_2S is removed, and
- 3^{rd} scrubber, most of the remaining H_2S is removed.

A typical scrubbing liquor for H_2S removal (in the 2^{nd} scrubber) is a solution of 0.1 % caustic + 0.3 % NaOCl sodium hypochlorite, with pH control between 9.0 to 9.5, at 80 ºF (26 ºC) and atmospheric pressure (Wang *et al.*, 2004, p. 269). In the 3^{rd} scrubber, H_2S can be oxidized by an oxidizing agent such as H_2O_2 or sodium hypochlorite (additional information is provided in Appendix 1).

Challenges of COS removal: It is recognized in the literature that if COS is present in the dirty gas, it is more difficult to remove. For example, in Astarita *et al.* (1983, p. 252), when the removal of sulphur compounds from synthesis gas was discussed, COS was considered to be a lot more difficult to remove than H_2S. If a gas contains a relatively high

concentration of COS, then it may be viable to install a hydrolysis step (e.g. Boerrigter and Rauch, 2005, p. 227):

$$COS + H_2O \leftrightarrow H_2S + CO_2 \qquad -30 \text{ kJ/kmol} \qquad (2.11)$$

This converts the COS into H_2S, which can then be more readily removed in the gas scrubbing system. In the literature, there are various methods and catalysts, which it is claimed could be used (e.g. Wakker *et al.*, 1993; Zhao *et al.*, 2010; Sasaoka, 1995; and Williams *et al.* (1999)).

2.3.4.2 Hot Desulphurization Approaches

As described in Park *et al.* (2005), Hot Gas Desulphurization (HGD) processes are being developed to remove sulphur at high temperatures from coal-derived fuel gas. HGD is a relatively new technology, which has the advantage of high thermal efficiency over the conventional wet desulphurization processes. High levels of H_2S (~ 10,000 ppmv) in the dirty gas can be reduced to several tens of ppmv. Over the last two decades, development of HGD technologies has focused on the use of regenerable sorbents, mainly metal oxides (Flexgas Project, 2009). The characteristics of a selection of metal oxide sorbent materials are listed in Table 2.11.

Table 2.11 Characteristics of metal oxide sorbent materials, based on a table in Flexgas Project (2009).

Sorbent material	Sulphidation temperature, ^oC	Regeneration temperature, ^oC	Sorbent utilization, %	H_2S outlet concentration, ppmv
Tin oxide	350-500	400-500	85	<100
Copper oxide	350-550	650	70	<20
Manganese oxide	350-870	900	50	<10
Iron oxide	360-500	500-650	25-45	<100
Zinc oxide	480-540	500-700	50-70	<1
Zinc ferrite	450-600	600	20-80	<20
Zinc titanate	450-750	600-750	40-60	<10
Copper chromite	650-850	750	40-80	<10
Cerium oxide	750-1000	600	90	<100

As described in Torres *et al.* (2007), reusable metal oxide (MO_x) can be used:

$$MO_x + xH_2S \rightarrow MS_x + xH_2O \quad (2.12)$$

The sulfided sorbent can be regenerated *via*:

$$MS_x + 3x/2\ O_2 \rightarrow MO_x + xSO_2 \quad (2.13)$$

Zhang *et al.* (2004) used the old technology of disposable calcium oxide-based sorbents (such as calcined limestone and calcined dolomites) in combination with a nickel catalyst in an attempt to simultaneously remove H_2S and tars from a biomass gasifier. The experimental system consisted of a guard bed of dolomite stone in series with a tar-cracking reactor containing a metallic catalyst. The guard bed was designed to: (a) capture fine particulates and steam; (b) reform the heavy tar; and (c) absorb H_2S. However, when using the dolomite guard bed (at 650^{o}C) and the nickel catalyst reactor (at 740 to 820^{o}C), the authors observed significant breakthrough of H_2S through the dolomite guard bed.

A significant problem with the simultaneous or sequential removal of NH_3 and H_2S in a gasification process is that the sulphur may poison the catalysts used for NH_3 decomposition. Materials with bi-functional (catalytic/sorbent) properties may provide a solution to this challenge. This led Jun *et al.* (2003) to study the problem, and they found that the addition of cobalt and nickel promoters to Zn-Ti sorbents allowed both the decomposition of NH_3, as well as H_2S absorption. High NH_3 decomposition activity was retained by the Co-modified sorbent even in the presence of H_2S. According to Gangwal and Portzer (1998), the Research Triangle Institute developed a proprietary of mixed metal oxide materials with dual catalytic-sorbent properties that can remove NH_3 and H_2S from a simulated coal gasifier gas.

2.4 CHAR FROM THE GASIFIER

When biomass is gasified, a quantity of char is produced, which consists of carbon and ash. This char could be:

- burned to produce heat and power,
- gasified to produce a gas,
- activated for adsorption, or
- used as a soil additive, and a possible carbon sequestration agent (e.g. Boateng, 2007, and Brewer *et al*., 2009).

The way in which the char can be used depends on its physical and chemical characteristics, and these are not well understood. Based on information in the literature, and discussions with companies working on pilot-scale gasification technology (at the 50 kW_e to 2 MW_e scale), there is great interest in converting the char produced into a gas, which could be mixed/used with the gas produced from the gasifier rather than off-site disposal. According to Chaudhari *et al.* (2003), the char is highly reactive and can be gasified with agents such as CO_2, O_2 and H_2O to make gaseous fuels.

2.5 CONCLUSIONS THAT IMPACT ON WORK IN THIS THESIS

Based on this literature review, and discussions with companies that are trying to develop commercial processes at the small to medium scale (50 kW_e to 2 MW_e), the commercial reality still remains a challenge. Despite the vast amount of information in the literature on the use of different types of gas clean-up devices, and information on the performance and construction of a wide variety of small and large scale demonstration gasification plants, cost effective solutions still need to be identified and developed in order to make commercial progress. Some of the more major barriers to progress arise from:

(a) the need to develop cost effective solutions for the removal of contaminants from the dirty gas before it is used as a fuel (and then resulting emissions into the atmosphere), and

(b) the need to develop robust gasification technology that can be viable at the small scale of operation (50 to 100 kW_e), and that can also be scaled from e.g. 250 kW_e to a 2 MW_e scale and higher.

Based on this review, it was decided to explore further in this thesis the following themes:

2.5.1 Need to Understand COS Levels

Looking at gas clean-up before the gas engine, the removal of SO_2 and H_2S is considered to be relatively easy (e.g. by scrubbing); however, the removal of COS is a more complex situation.

Decision 1: To help with the development of suitable gas clean-up strategies, the presence of COS species will be considered in more detail in this thesis.

2.5.2 Need to Understand the Down-draft Gasification Process

Because of the high peak temperatures (e.g. 1000 to 1200 ºC) in a down-draft gasifier, experiments and pilot-plant trials are generally performed in steel vessels, and it is very difficult to see what is actually happening in the hot zone, and below, where the gas is separated from the hot char.

Decision 2: To develop a better level of understanding of the down-draft gasification process, experiments will be performed in a small quartz-tube laboratory gasifier (visual observation and gas analysis).

2.5.3 Need to Understand the Gas Composition

In order to explore possible gas clean-up options, and to know how changes in operating conditions affect the quality of the gas produced, it is important to know the composition of the gas from the gasifier. Although composition data can be obtained from measurements on the plant, data of this type is not easy to obtain for a variety of reasons, which include the cost of performing such an analysis. As the design of the gasifier evolves, the performance changes and hence gas composition also changes. The composition of the sulphur in the biomass feeding can vary, and so too will the sulphur species in the gas. Finally, when information is available, it is often considered proprietary.

Decision 3: To perform some measurements of gas composition on a pilot-scale gasifier.

Decision 4: To perform some measurements of gas composition using wood and straw pellets, and also to consider a Refuse Derived Fuel (RDF).

2.5.4 Conversion of Char to Gas

This aspect remains of interest to companies that are developing 50 kW_e to 2 MW_e gasification processes, and there is great interest in converting the char produced into a gas, which could be mixed and used with the gas produced from the gasifier (rather than off-site disposal)

Decision 5: To investigate in more detail the gasification of char with steam.

2.5.5 Conversion of Tars to Gas, and Removal of Tars from Gas

Although this remains a very big challenge in the development of 50 kW_e to 2 MW_e gasification processes, this was not explored further in this thesis, and is recommended for further work.

REFERENCES

Astarita, G., Savage, D.W. and Bisio, A. (1983). Gas Treating with chemical solvents. John Wiley & Sons.

Bain, R.L., Dayton, D.C., Carpenter, D.L., Czernik, S.R., Feik, C.J., French, R.J, Magrini-Bair, K.A. and Phillips, S.D. (2005). Evaluation of Catalyst Deactivation during Catalytic Steam Reforming of Biomass-Derived Syngas. Ind. Eng. Chem. Res., Vol. 44, pp. 7945-7956.

Basu, P. (2010). Biomass Gasification and Pyrolysis. Elsevier Inc.

Boerrigter, H. and Rauch, R. (2005). Syngas production and utilization. In Handbook Biomass Gasification, Knoef H.A.M (Ed), pp. 211-230.

Boerrigter, H. and Rauch, R. (2006). Review of applications of gases from biomass gasification. Energy research centre of the Netherland, report No. ECN-RX-06-066.

Boateng, A. A. (2007). Characterization and thermal conversion of charcoal derived from fluidized-bed fast pyrolysis oil production of switchgrass. Ind. Eng. Chem. Res., Vol. 46, No. 26, pp. 8857-8862.

Brandt, P., Larsen, E. and Henriksen, U. (2000). High tar reduction in a two-stage gasifier. Energy & Fuel, Vol. 14, pp. 816-819.

Brewer, C. E., Rohr, K.S., Satrio, J.A. and Brown, R.C. (2009). Characterization of biochar from fast pyrolysis and gasification systems. Enviromental Progress & Systainable Energy, Vol. 28, No. 3, pp. 386-396.

Chaudhari, S. T., Dalai, A.K. and Bakhshi, N.N. (2003). Production of Hydrogen and/or Syngas (H_2 + CO) via steam gasification of biomass-derived chars. Energy and Fuel, Vol. 17, No. 4, pp. 1062-1067.

Department of the Environment, Food and Rural Affairs in Enland (2008). Environmental Permitting Guidance on the Incineration of Waste, Crown.

Directive 7000/76/EC of the European Parliament and of the Council of 4 December 2000 on the incineration of waste, Official Journal of the European Communities.

Donnot, A., Reningovolo, J., Magne, P. and Deglise, X. (1985). Flash Pyrolysis of Tar from the Pyrolysis of Pine Bark. Journal of Analytical and Applied Pyrolysis, Vol. 8, pp. 401-414.

Fagan, M. (2009). Sodium Hypochlorite vs. Hydrogen Peroxide. H_2O_2 Update. Volume 2, H2O2.com. Available from: http://www.h2o2.com/h2o2update/volume2/hypochlorite.html [Accessed 21 December 2009].

Flexgas Project (2009). Optimisation of experimental conditions for Ex-Bed Desulphurisation. Report DL6.6.
Available from: http://www.flexgas.cnr.it/Deliverables/DL6_6.pdf [Accessed 25 December 2009].

Gangwal, S.K. and Portzer, J.W. (1998). Simultaneous removal of H_2S and NH_3 from coal gas. The final report in work performed under contract No. DE-AC21-92MC29001, United States Government. Available from: http://www.fischer-tropsch.org/DOE/DOE_reports/Gangwal/29011/29011_2/29011_2_finrpt/29011_2_finrpt.pdf [Accessed 11 October 2010].

Higman, C. and Burgt, M.V.D (2008). Gasification. Second edition, Elsevier.

Iversen, H. L. and Gobel, B. (2005). Update on gas cleaning technologies. Handbook Biomass Gasification. Knoef H.A.M (Ed), pp. 189-210.

Jun, H.K., Jung, S.Y., Lee, T.J, Ryu, C.K. and Kim, J.C. (2003). Decomposition of NH_3 over Zn-Ti-based desulfurization sorbent promoted with cobalt and nickel. Catalysis Today, Vol. 87, pp. 3–10.

Kandassamy, K., Natarajan, E. and Renganarayanan, S. (2003). Producer gas cleaning techniques. 17th International Fluidized Bed Combustion Conference , Jacksonville, Florida, USA, pp. 29-36.

Klinkenbijl, J.M., Dilon, M.L. and Heyman, E.C. (1999). Gas Pre-Treatment and their Impact on Liquefaction Processes. GPA, Nashville.

Knoef, H.A.M., edited, (2005). Handbook Biomass Gasification. BTG biomass technology group.

Li, C., Hirabayashi, D. and Suzuki, K. (2009). Development of new nickel based catalyst for biomass tar steam reforming producing H_2-rich syngas. Fuel Processing Technology, Vol. 90, pp. 790-796.

Ma, L. and Baron, G.V. (2008). Mixed zirconia-alumina supports for Ni/MgO based catalytic filters for biomass fuel gas cleaning. Powder Technology, Vol. 180, pp. 21-29.

Park, N.K., Lee, J.D., Lee, T.J., Ryu, S.O. and Chang, C.H. (2005). The preparation of a high surface area metal oxide prepared by a matrix-assisted method for hot gas desulphurization. Fuel, Vol. 84, pp. 2165–2171.

Rezaiyan, J. and Cheremisinoff, N.P. (2005). Gasification Technologies: A primer for engineers and scientists. Taylor & Francis, LLC.

Sasaoka, E. (1995). Catalytic Activity of ZnS Formed from Desulfurization Sorbent ZnO for Conversion of COS to H_2S. Ind. Eng. Chem. Res., Vol. 34, pp. 1102-1106.

Siangchin, C. (2004). CH_4/CO_2 Reforming over Ni-ZrO_2/Al_2O_3 Catalyst for Synthesis Gas Production. The Joint International Conference on Sustainable Energy and Environment (SEE), Hua Hin, Thailand.

Simell, P., Kurkela, E., Stahlberg, P. and Hepola, J. (1996). Catalytic hot gas cleaning of gasification gas. Catalysis Today, Vol. 27, pp. 55-62.

Sutton, D., Kelleher, B. and Ross, J.R.H. (2001). Review of literature on catalysts for biomass. Fuel Processing Technology, Vol. 73, pp. 155-173.

Sutton, D., Parle, S.M. and Ross, J.R.H. (2002). The CO_2 reforming of the hydrocarbons present in a model gas stream over selected catalysts. Fuel Processing Technology, Vol. 75, pp. 45-53.

Torres, W., Pansare, S.S. and Goodwin, J.G. (2007). Hot Gas Removal of Tars, Ammonia, and Hydrogen Sulfide from Biomass Gasification Gas. Catalysis Reviews, Vol. 49, pp. 407-456.

Wakker, J.P., Gerritsen, A.W. and Moulijn, J.A. (1993). High temperature H_2S and COS removal with MnO and FeO on γ-Al_2O_3 acceptors. Ind. Eng. Chem. Res., Vol. 32, pp. 139-149.

Wang L. K., Pereira N. C. and Hung Y-T., edited, (2004). Air Pollution Control Engineering. Handbook of Environmental Engineering, Vol. 1, Humana Press Inc, Totowa, New Jersey.

Williams, P., Young, N.C., West, J., Rhodes, C. and Hutchings, G.J. (1999). Carbonyl sulphide hydrolysis using alumina catalysts. Catalysis Today, Vol. 49, pp. 99-104.

Zhang, R., Brown, R.C., Suby, A. and Cummer, K. (2004). Catalytic destruction of tar in biomass derived producer gas. Energy Convers. Mgmt., Vol. 45, pp. 995–1014.

Zhao, Z., Lakshminarayanan, N., Kuhn, J.N., Naber, A.S, Felix, L.G., Slimane, R.B. Choi, C.W. and Ozkan, U.S. (2009). Optimization of thermally impregnated Ni–olivine catalysts for tar removal. Applied Catalysts A: General 363, pp. 64-72.

Zhao, H., Zhang, D., Wang, F., Wu, T. and Gao, J. (2010). Removal of Carbonyl Sulfide from Syngas Using a Novel Mixed-Oxide Sorbent. Energy Sources, Part A: Recovery, Utilization, and Environmental Effects, Vol. 32, pp. 759-768.

CHAPTER 3

Gasification of Wood Pellets in a Quartz-tube Gasifier

In this chapter, to increase the level of understanding of some of the processes that occur in a biomass gasifier, an experimental system was designed, in which a visual section enabled observations of the gasification process to be made at a well controlled location. This was seen as a key requirement, as in many experimental and pilot-scale studies this visual aspect was missing, and in private discussions with a few investigators (from two different companies), this led to many questions about what was actually going on inside the unit, as this was not adequately explained in the literature that they had read.

It is pleasing to report that much of the work described in this chapter has recently been published in Kolaczkowski *et al.* (2011)[*].

The paper was also presented in a poster presentation at the 2010 BIOTEN conference by the author of this thesis.

The quartz-tube apparatus was available at the start of the project, but had to be adapted, rebuilt in a new laboratory, and improved – all of that was done by the author of this thesis. A co-author in the paper, Jodlowski, was a visiting PhD student (Jagiellonian University, Krakow, Poland), and his main contribution was with the commissioning of the Gas Chromatograph (GC). He also assisted with some of the experiments.

[*] Kolaczkowski, S., Le, C.D. and Jodlowski, P. (2011). Gasification of wood pellets in an experimental quartz tube gasifier – How visual 1D experiments can aid 3D design considerations. In Proceedings of the bioten conference on biomass and biofuels 2010, Bridgwater, A.V. (Ed), CPL Press UK, pp. 720-732.

3.1 INTRODUCTION

Discussions on the choice of technology to convert biomass into energy feature in a number of publications (e.g. Bridgwater *et al.*, 2002; Bridgwater, 2003), where the relative merits of pyrolysis, gasification and combustion are compared. In Chapter 1, it was stated that the process of gasification, in a down-draft gasifier, was of special interest in this thesis.

3.1.1 Example of Zones in a Down-draft Gasifier

Dogru *et al.* (2002): Their experimental 5 kWe gasifier consisted of four distinct regions:

- Drying (70 to 100 ºC): height approximately 100 mm.
- Pyrolysis (350 to 500 ºC): height approximately 170 mm.
- Oxidation (1000 to 1200 ºC): height approximately 120 mm.
- Reduction zones (gases leave this zone between 200 to 300 ºC).

In that particular design of test gasifier, there was clearly an axial temperature profile in the gasifier, and the regions as indicated in the paper had a significant depth. Biomass consumption rates varied from 1.73 to 5.4 kg/h (optimum was 4.02 kg/h), and the diameter of the drying zone was 305 mm which tapered through the pyrolysis zone, reaching a diameter of 450 mm in the oxidation zone. This was then reduced to a throat diameter above the reduction zone of 135 mm.

Sheth and Babu (2009): In their work, four zones were also identified. The biomass consumption rates varied from 1 to 3.6 kg/h. The diameter of the pyrolysis zone was 310 mm, and of the reduction zone was 150 mm. The experiments were performed at equivalence ratios that varied from 0.167 to 0.355, and these affected the temperatures in the respective zones. For example:

- Drying.
- Pyrolysis (260 to 550 ºC): height depends on biomass loading.
- Oxidation (900 to 1050 ºC): height approximately 53 mm.
- Reduction zones: height approximately 100 mm.

The highest temperatures in the pyrolysis and oxidation zones corresponded to an equivalence ratio of 0.205.

Even by looking at these last two studies, it is clear that although there are similarities in the design, there are big differences in the internal geometry and aspect ratios for a fixed flow of biomass, and the reported height of the various zones.

3.1.2 Equivalence Ratio

In a down-draft gasifier, air is added at an approximate equivalence ratio of 0.25, and in simple terms this means that 25 % of the volume of air to achieve complete combustion is added to sustain the oxidation reactions. This then provides the energy required in the drying, pyrolysis, and reduction zones. At an equivalence ratio of about 0.25, this in general coincides with the region where the highest energy density of the gas is obtained (Knoef, 2005, p. 17). This clearly provides a useful indication of the air to fuel ratio at which a gasifier should be operated. However, in Sheth and Babu (2009), a comparison is presented of three studies and it was shown that the optimum equivalence ratio was:

0.205 in their study (furniture wood waste),

0.276 in Dogru *et al.* (2002) using hazelnut shell, and

0.388 in Zainal *et al.* (2002) using furniture wood with charcoal.

This provides a clear indication that optimum conditions depend on the composition of the biomass, and design and operation of the gasifier. Hsi *et al.* (2008) also investigated the performance of a bed operating with wooden cubes, and they describe the importance of keeping the air fuel ratio as low as possible, but not so low that it fails to be self sustainable. Likewise, if the flow is too high, the gasification reactions would decrease and combustion reactions would increase, and this would lead to a dilution of the producer gas formed.

3.1.3 Physical Shape of the Different Zones

Much of the literature on gasifiers, and including descriptions in Earp (1988), Evans (1992), Milligan (1994), Knoef (2005, p. 24), Sheth and Babu (2009) and Dogru *et al.* (2002), tends to provide explanations in which the results are portrayed looking at the bed

from a one-dimensional (1D) perspective. As described in the literature review in Tinaut *et al.* (2008), this is also evident in many modelling studies, and occasionally 2D models are encountered. However, in reality, the situation is far more complex. For example, the way in which the air is added will result in oxidation regions that correspond to the direction and shape of the expanding air jets, and this in turn will impact on the movement of the bed as biomass and char are consumed. A true representation of such a bed would require a three-dimensional (3D) consideration, and this would add complexity. This consideration is something that stimulated the work in this thesis, which tries to understand what is happening from a 1D perspective, which would help to interpret the 3D situation.

3.1.4 Design of Experiment

To help answer the questions raised, it was essential that the experimental gasifier had a visual section. Also, a decision was taken to keep the diameter of the test gasifier small, so that the associated experimental apparatus did not become too bulky, hampering progress. So the decision was made to work with a 21 mm i.d. quartz-tube, providing the key requirement of enabling visual observations to be made. In working with a small diameter gasifier, it was accepted right from the start that a compromise was being made on geometric aspects, but scale-down or scale-up was never the intention in this experimental unit. This decision turned out to be fortuitous, as it enabled a study to be made of the reacting zones where a 1D representation was closer to conditions in this experimental reactor, and this facilitated the explanation of phenomena occurring to match observations and measurements when a 3D environment exists.

3.2 EXPERIMENTAL SETUP

3.2.1 Experimental Apparatus

The apparatus is illustrated in Figure 3.1 and consisted of the following key features:

(a) The gasification experiments were performed in a 21 mm i.d. quartz-tube (wall thickness 1 mm), that was approximately 1 m long.

(b) At the top of the tube was a rubber bung, which provided some explosion relief. Through the bung, air was introduced into the reactor.

(c) The bottom of the quartz tube sat on a machined grove in a stainless steel bracket, and this was sealed with a gasket sealant (premium copper silicone). At the base of this bracket a stainless tube was welded, and this bracket acted as the glass to metal joint.

(d) The base of the tube was positioned in a cylindrical, electrically heated furnace, whose temperature could be adjusted.

(e) In general, only the top section of the quartz tube (above the furnace) was filled with biomass pellets. The lower half contained an inert stainless steel support (to support the biomass), or it contained charcoal.

(f) The flow of air was measured with a rotameter, which had been calibrated. The air supply pressure at the top of the quartz tube was about 0.1 bar (g).

(g) From the base of the test section, the gas flowed through a cooler, and condensate was trapped in the first plastic vessel (see Figure 3.2). The gas then passed through a cooling coil, where more of the liquid condensed. The gas was passed through a glass wool filter, and then discharged into the vent from the fume cupboard.

(h) A clear safety screen was positioned in front of the quartz tube, and the entire apparatus was mounted inside a walk-in fume cupboard.

(i) After the glass wool filter, samples of gas were drawn from the exhaust line, and the composition of the dry gas was analysed using gas chromatography.

Start-up: To initiate the reactions inside the quartz tube, the external surface of the quartz tube was heated at a specific location with a blow torch, as illustrated in Figure 3.1(b). Air was then added and oxidation reactions were initiated inside the tube. The external flame was then extinguished. The vigour, position, and height of the red-hot zone inside the quartz tube could be observed, and the composition of the resulting gas was also measured.

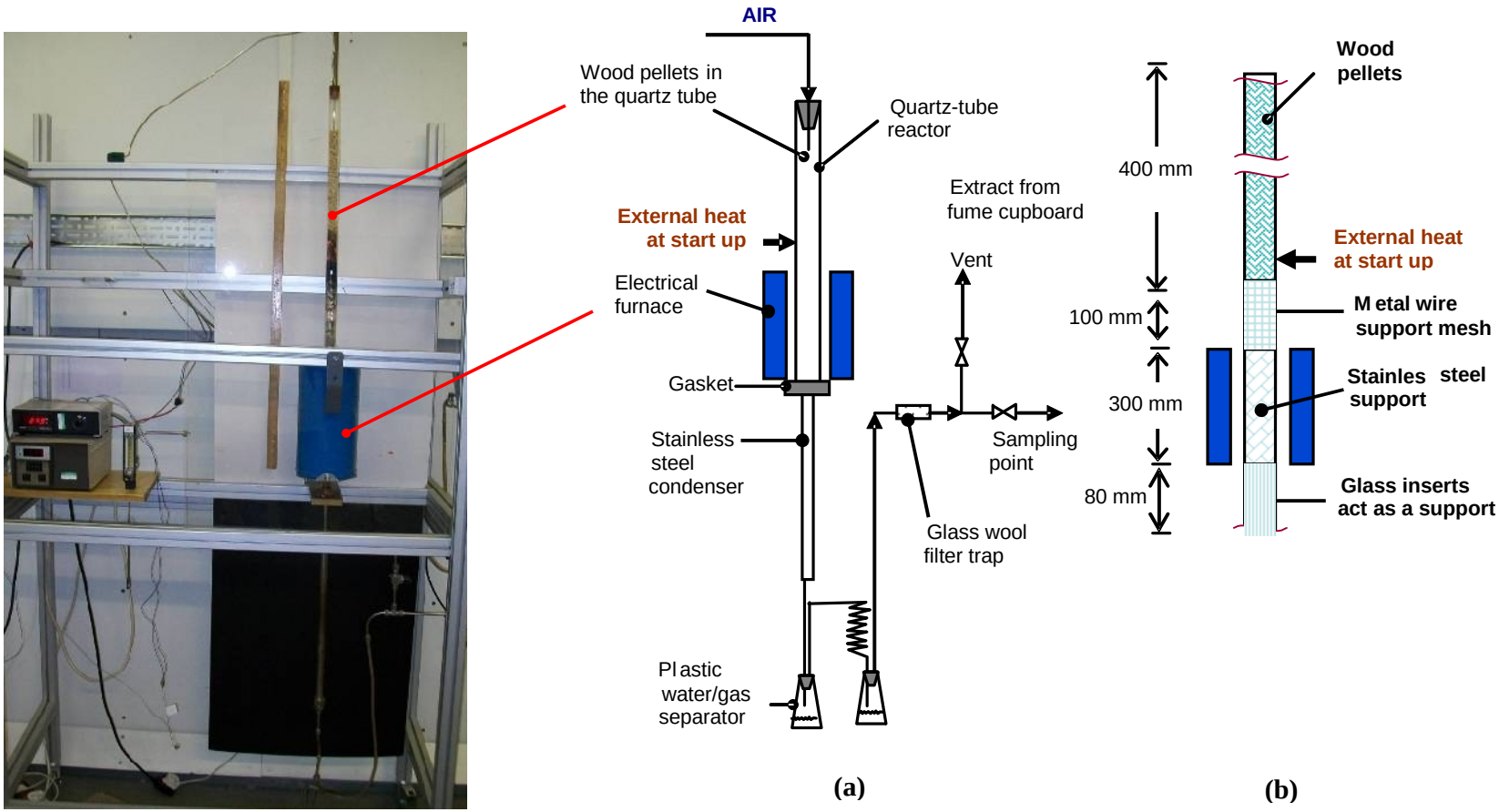

Figure 3.1. Quartz-tube gasification apparatus (a) outline schematic, (b) magnified view of the tube loaded for one of the experiments.

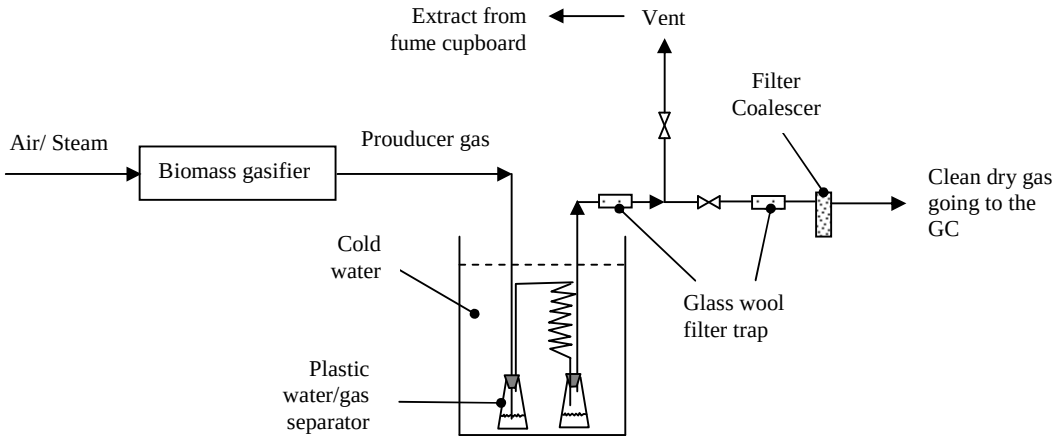

Figure 3.2 Outline schematic of gas clean-up prior to analysis.

3.2.2 Gas Analysis with GC

As illustrated in Figure 3.2, when samples of gas were withdrawn from the exhaust line, they were passed through another glass wool filter and a filter coalescer before going to the gas chromatograph (GC). This system of filters helped to remove the majority of tars and particulates in the gas stream, so as not to damage the analytical equipment.

The GC used was a Chrompack CP9001, fitted with one pre-column and one molecular sieve column (connected in series), and a thermal conductivity detector (TCD). The GC was calibrated using calibration gas mixtures with argon as the carrier gas. The specifications of the columns are presented in Table 3.1.

Table 3.1 Specifications of the columns used in the GC.

	Pre-column	**Molecular sieve column**
Manufacturer	Chrompack	Alltech Associates, Inc.
Part number	84211	57732
Packing	Hayesep T + Hayesep Q	Molecular sieve 13X
Mesh size	80-100	80-100
Column outside diameter	1/8 inch (3.2 mm)	1/8 inch (3.2 mm)
Column length	0.5 m	6 feet (1.83 m)

As CO_2 could be absorbed in the molecular sieve, it was necessary to separate it from the other gases in the pre-column. The columns were connected *via* a pair of multi-port valves, allowing the injection of a known volume of sample gas and allowing the detector to be connected to either column. These valves were controlled by a computer inside the GC, which could switch them on in a timed sequence. A PC running Chrompark Maestro version 2.4 received the signals from the GC to perform the necessary integration and analysis. The following description of possible configurations of this GC is mainly based on explanations in Shirley (2005) who used this GC for a different project.

(a) **Gas Chromatograph Configuration:** Two alternative carrier gases (helium and argon) could be fed at pressure of 4 bar(g) to a two-way valve that allowed the required gas to be selected. That gas was then passed through a moisture filter before entering the GC. Helium could be used to detect CO, CO_2, O_2, N_2 and CH_4. However, hydrogen cannot be measured accurately using helium carrier gas, as the two gases have a very similar thermal conductivity. As a result, argon was used as the carrier gas to detect hydrogen and other gases in the gas sample. The other gases also show up on the argon chromatograms, but the response is much smaller, so the errors are higher.

The flow of gas through the GC was controlled by two multi-port valves, Valve 1 and Valve 2. Figures 3.3 to 3.6, illustrate the possible flow sequences, for different settings of the two valves.

The pre-column separates the CO_2 from the other gases in the sample to make sure that it does not enter the molecular sieve column, where it would be adsorbed. After the other gases have passed into the molecular sieve, it is isolated and the output of the pre-column is switched to the detector for measuring CO_2 content. The hydrogen passes through both columns very quickly and emerges through the detector before the other gases pass into the molecular sieve. The molecular sieve column is re-connected after the CO_2 has passed through the detector and all of the remaining gases are sent to the detector.

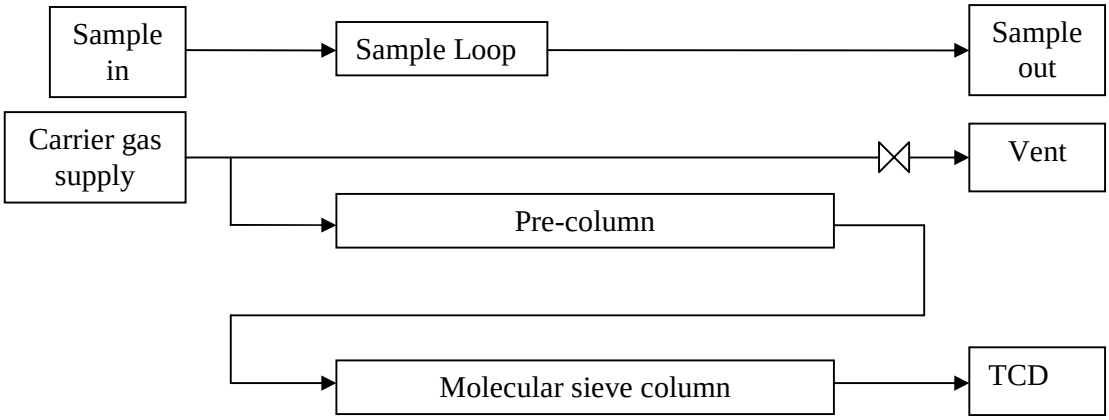

Figure 3.3 Flow sequence with Valves 1 and 2 in Position 1 (initial and final condition), adapted from Shirley (2005).

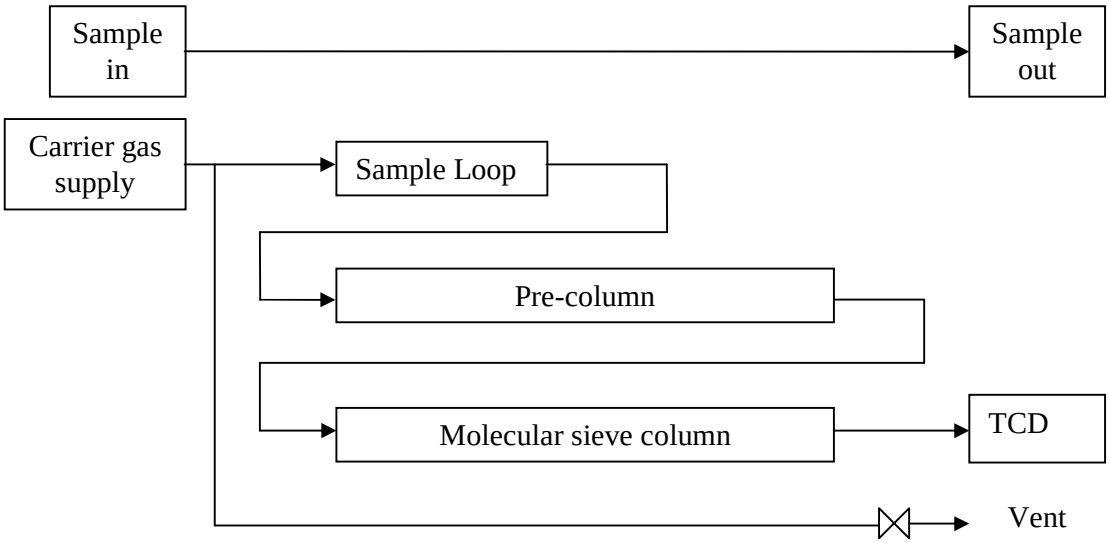

Figure 3.4 Flow sequence with Valve 1 in Position 2, and Valve 2 in Position 1, adapted from Shirley (2005).

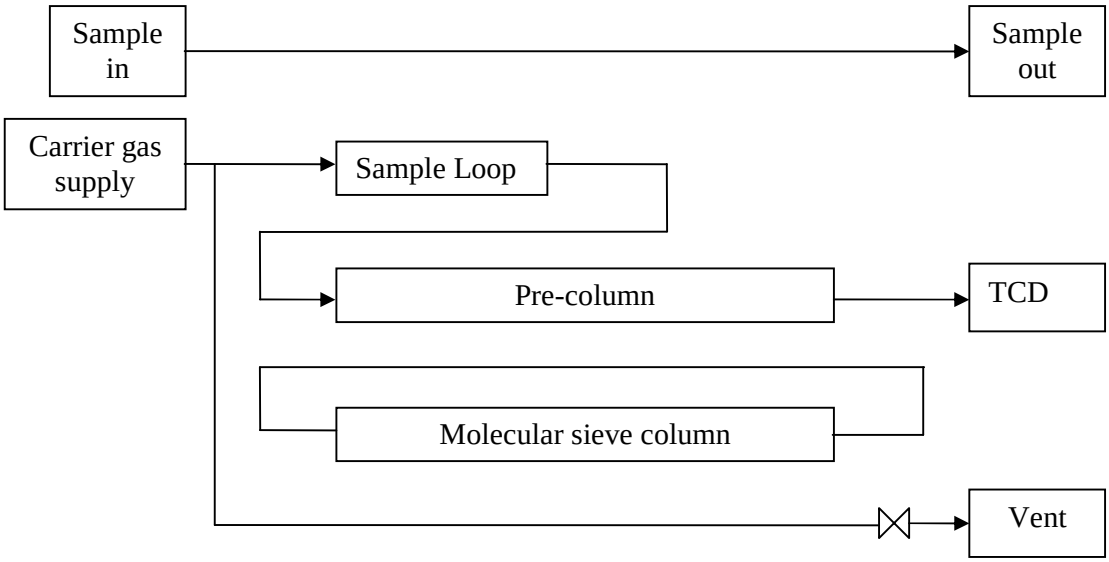

Figure 3.5 Flow sequence with Valves 1 and 2 in Position 2, adapted from Shirley (2005).

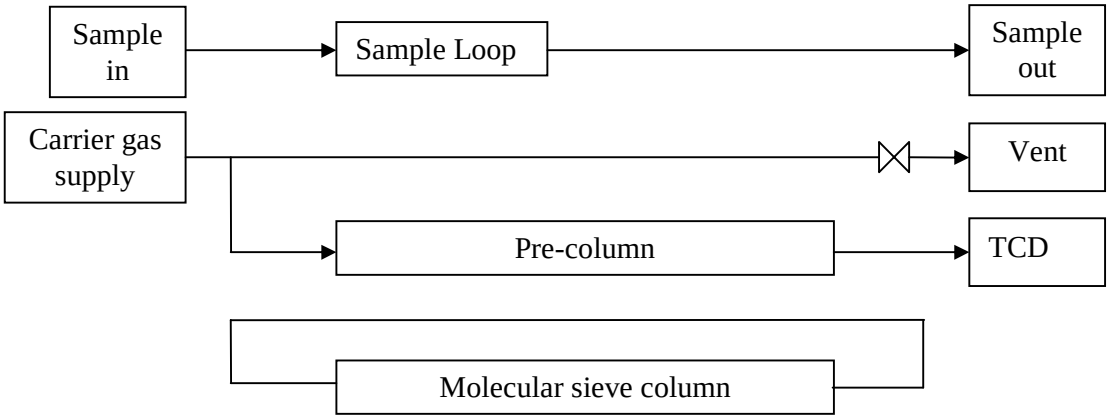

Figure 3.6 Flow sequence with Valve 1 in Position 1 and Valve 2 in Position 2, adapted from Shirley (2005).

(b) Detection of methane: Unfortunately, the use of a pre-column causes an undesirable side-effect, as it not only separates CO_2 from other gases, but also CH_4. This means that the CH_4 enters the molecular sieve after the remaining components. However, the CH_4 then passes through the molecular sieve faster than CO, leading to the possibility of the peaks for CO and CH_4 being overlapped and poorly separated (see Figure 3.7). If either peak is very large, the two peaks join together, the smaller one forming a shoulder on the larger one.

One way to deal with this difficulty is to isolate the molecular sieve column before CH_4 has entered it. The CH_4 would then emerge first, before the CO_2. However, due to an unresolved problem with Valve 2, there is always a large peak on the chromatogram as the valve is switched over that makes it impossible to take accurate CH_4 readings using this technique.

(c) Moisture in GC columns: Over time, the author of this thesis noted that the columns started to become contaminated with trace levels of water from the gas. This resulted in a slight and gradual movement of the position of the peaks of all the gases. Most interestingly, the peaks for CO and CH_4 became separated from one another – which was beneficial (see Figure 3.8). However, this trend also finally led to the movement of the O_2 and N_2 peaks towards the large 'noise peak'. Therefore, it was necessary to regenerate the columns. This was done by placing the columns in an oven (at 150 ^{o}C - the maximum temperature for the pre-column), with carrier gas flowing through the columns for 3 days.

(d) Control of GC Valves: The computer built into the GC was programmed to alter the valve settings at specific times. Initially, both valves were set to Position 1 so that the sample gas entering the GC would flow through the sample loop, carrier gas would back-flush the pre-column, and more carrier gas would flow through the molecular sieve column to the detector. After the sample loop was charged with sample gas, the program was started. The program is outlined in Table 3.2.

The specific timings were adjusted to suit the flow rate of carrier gas through the system. Argon flowed at a slower rate than helium, necessitating a longer delay between each step of the program.

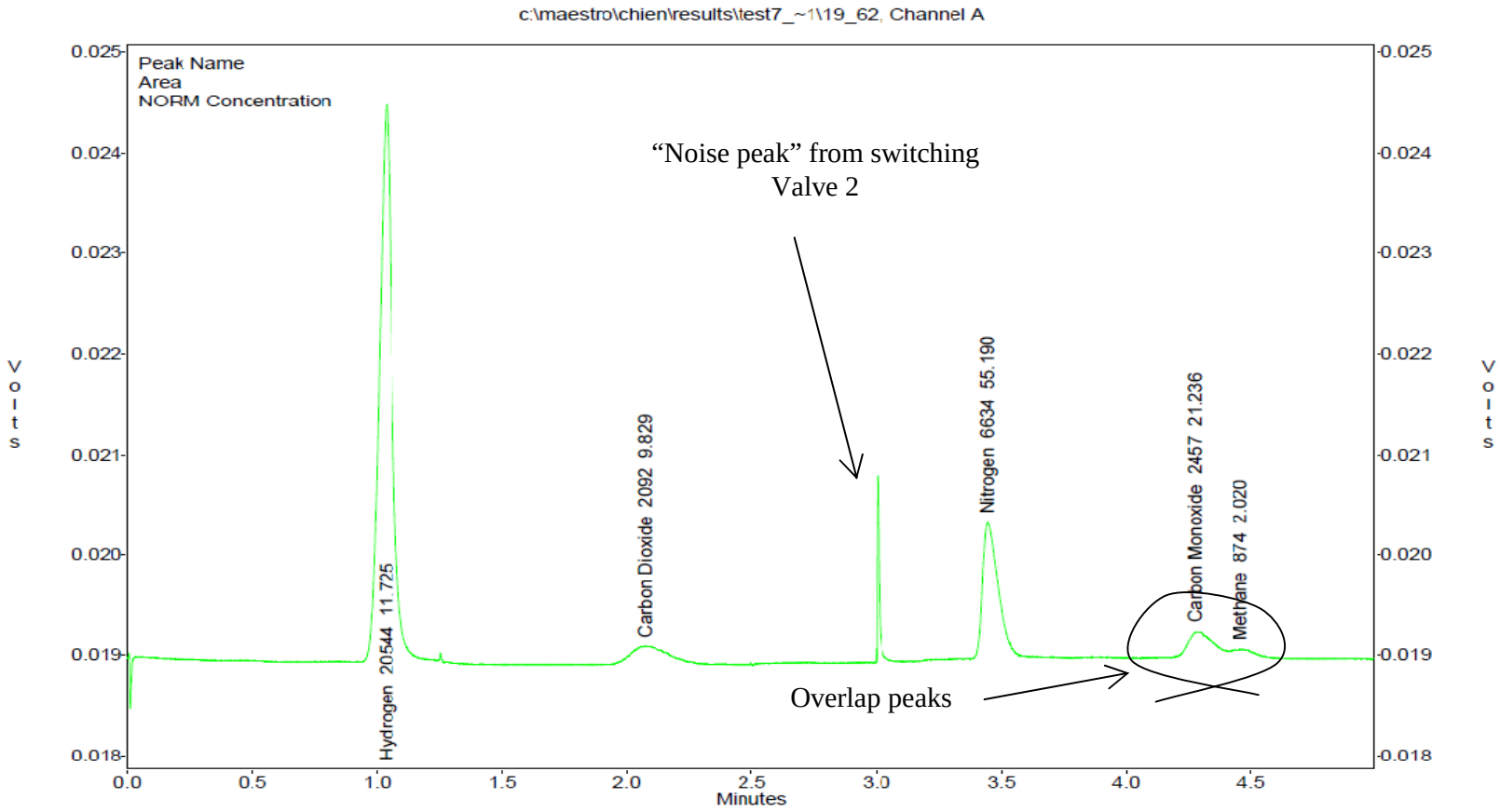

Figure 3.7 An example of a gas chromatogram of a producer gas sample, showing the 'noise peak' and the overlap peaks of CO and CH_4.

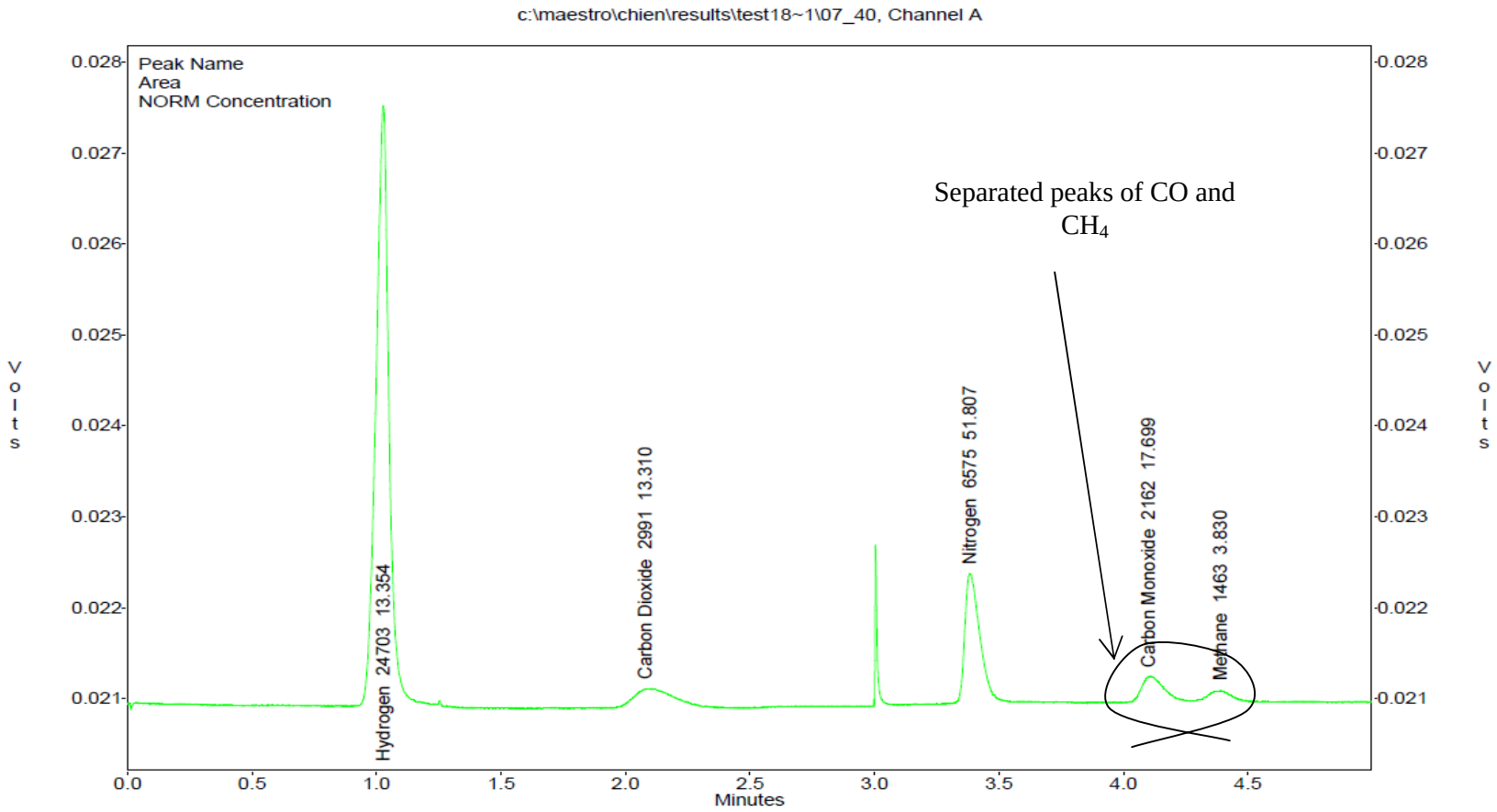

Figure 3.8 An example of a gas chromatogram of a producer gas sample, showing the movement of peaks as the column becomes contaminated with water.

Table 3.2 Valve control sequence for the GC.

Start	Valve 1 to Position 2	Connect sample loop to pre-column and carrier gas flow to sample loop to inject sample
After all gases apart from CO_2 have passed into mol sieve and H_2 has passed through detector	Valve 2 to Position 2	Connect pre-column output to detector and insolate mol sieve, preventing CO_2 from entering mol sieve
After CO_2 has passed out of pre-column	Valve 1 to Position 1	Set pre-column and sample loop back to initial condition
After CO_2 has passed through the detector	Valve 2 to Position 1	Re-connect mol sieve to detector and carrier gas supply in order to feed remaining components to the detector and set system back to initial state.

(e) Recording and Analysing Signal Data: Signals from the GC were sent by serial connection to a PC running Chrompack Maestro version 2.4. This software records the data in a chromatogram and can perform integration and multi-level calibration operations on the data. Maestro does not perform statistical analyses or estimate data errors. After completion of the experiments, the calibration was performed manually in order to gain a better understanding of the precision of the results.

Gas Chromatograph Calibration: It is necessary to know for each component what quantity is represented by the area under the corresponding peak on the chromatogram. The peaks represent a certain quantity of material, rather than a proportion. However, the total volume of the sample gas present is always the same (the volume of the sample loop) and the pressure is always the same. Therefore, the peaks can be calibrated for a molar percentage, or fraction, of each component present in the sample.

For calibration with argon (as the carrier gas), 7 different gas standards and one calibration gas mixture were run through the GC to ascertain the response to methane, carbon monoxide, carbon dioxide, oxygen and nitrogen:

1. 50 % Methane in argon from cylinder.
2. Pure carbon monoxide from cylinder.
3. Pure carbon dioxide from cylinder.

4. Air from cylinder.
5. Pure nitrogen from cylinder.
6. Pure oxygen from cylinder.
7. Pure hydrogen from cylinder.
8. Calibration gas mixture consists (vol.%) of: 13.63 hydrogen; 17.75 carbon monoxide; 12.32 carbon dioxide; 2.52 oxygen; 0.99 methane; 0.2 propane; 0.2 propene; 0.2 acetylene; 0.2 ethylene; 0.49 ethane; and balanced nitrogen.

Calibration was carried out every week that the GC was used, prior to running that week's samples through the GC.

To check the repeatability of measurements with the GC, a bag-sample of gas was taken during a steam gasification of char experiment (discussed further in Chapter 6). To this bag a quantity of air was added from a gas cylinder, so that O_2 was also present. Then the gas was injected into the column 10 times, and the results are presented in Figure 3.9. From these the average gas composition was: H_2 = 28.68 (± 0.56) vol.%; CO_2 = 7.60 (± 0.50) vol.%; O_2 = 7.51 (± 0.35) vol.%; N_2 = 48.01 (± 0.73) vol.%; CO = 7.79 (± 0.82) vol.%; and CH_4 = 0.56 (± 0.09) vol.%.

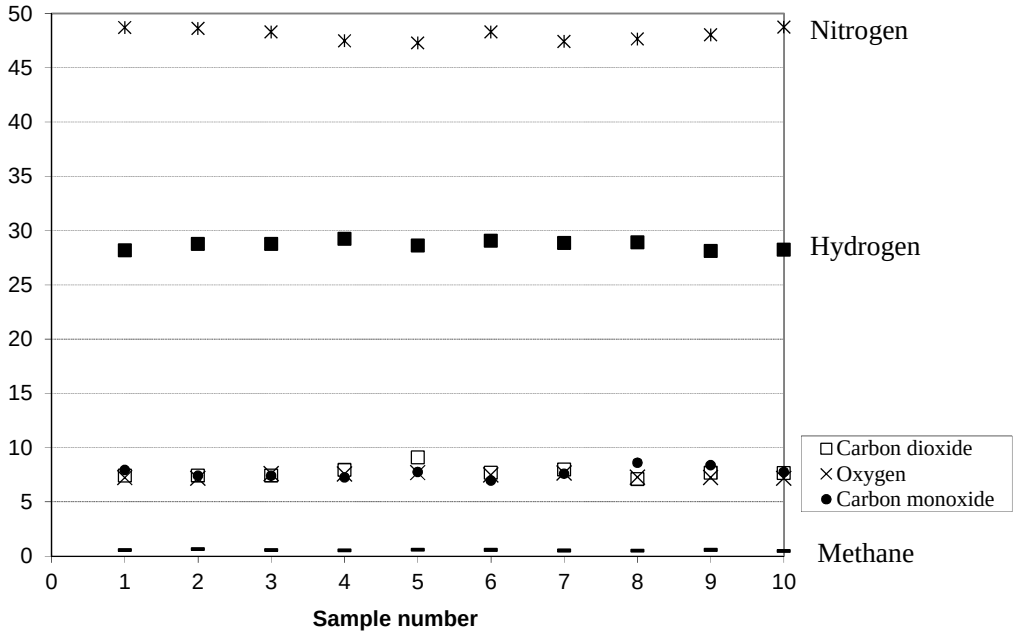

Figure 3.9 Example of a repeatability test using the GC for gas analysis.

Having established a method in which the GC could be used for the quantitative analysis of this complex gas mixture, it was then used in the experiments that follow.

3.3 RESULTS AND DISCUSSION

3.3.1 Properties of the Wood Pellets Used

Commercially produced wood pellets were used in these experiments, and their key properties are summarised in Table 3.3, and a picture of the sample used is presented in Figure 3.10.

Table 3.3 Properties of the wood pellets (as measured) with proximate analysis.

All pellets are cylindrical in shape (supplied by Treenergy Ltd, Monmouth)	Absolute density (kg/m^3)	Bulk density (kg/m^3)
Wet pellets: 5 mm diameter x 17.3 mm	1170	510
Dried pellets:	1000	502
Pellets reduced to char: 3.9 mm diameter x 9.9 mm	670	365

Moisture	Volatiles	Fixed carbon	Ash
7.4 wt.%	72.6 wt.%	18.8 wt.%	1.3 wt.%

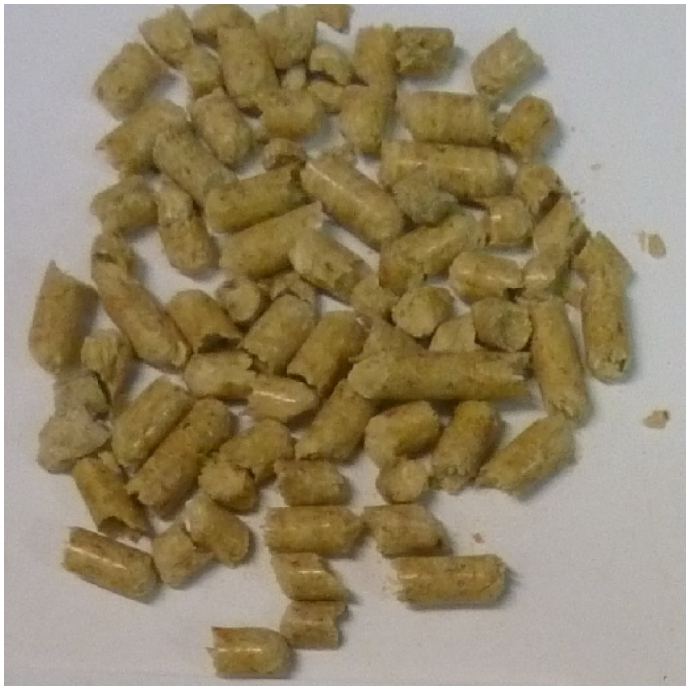

Figure 3.10 Photograph of the wood pellets used in the experiments.

3.3.2 Gasification at Wood Pellets (Air Flow Varied)

Experiments were performed with the tube filled with wood pellets (5 mm diameter, and 13 mm long), to a depth of about 400 mm. These were slightly shorter than the pellets described in Table 3.3. The biomass was supported on a stainless steel support, and the furnace was set at a temperature of 750 ºC.

The results of the first set of experiments, in which reactions were initiated in the middle of the biomass zone, and without any insulation around the quartz tube, are presented in Figure 3.11. From these results, the following observations are made:

Gas composition:

(a) There is a significant amount of scatter in the data – probably caused by the unstable nature of the reactions that are taking place in the hot zone.

(b) The concentrations of CO and H_2 are small due to the fact that without any insulation around the quartz tube, a significant amount of heat was lost from the hot zone (mainly by radiation). Hence, this affected the composition of the gas produced, and this gas was not combustible.

(c) As the air flow is increased, there is a slight increase in the concentrations of CO and H_2, while the concentrations of CH_4 and CO_2 decrease. This is because with an increase of the air flow, more heat would be generated in the combustion zone, enhancing endothermic reactions, which produce more CO and H_2, in the gasification zone. However, when air flow reaches a certain point where the combustion becomes dominant, more CO_2 would be generated, leading to a decrease in the concentration of CO and H_2 in the gas produced.

(d) A comparison of the gas composition produced from experiments with and without insulation around the quartz tube will be discussed in more detail in Section 3.3.3, where the role of the insulation layer on the quality of the gas will be considered.

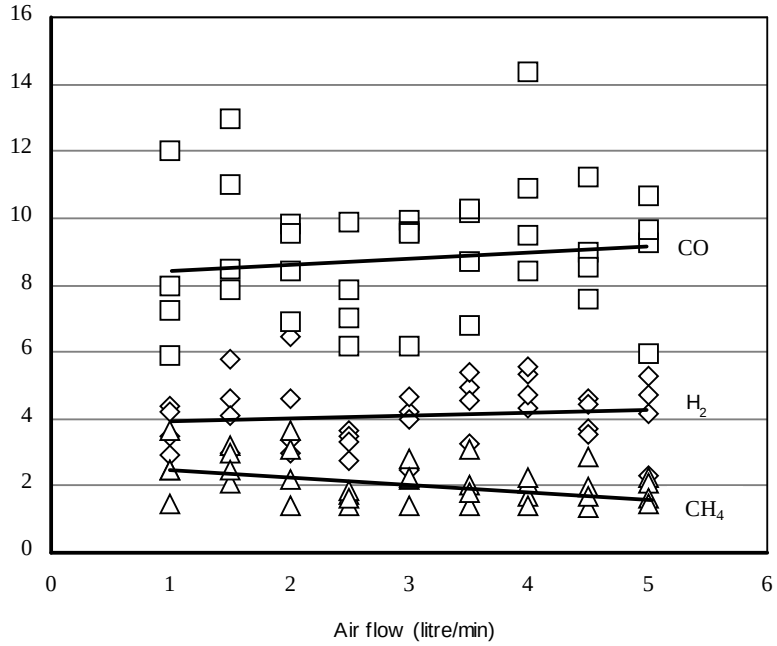

(a)

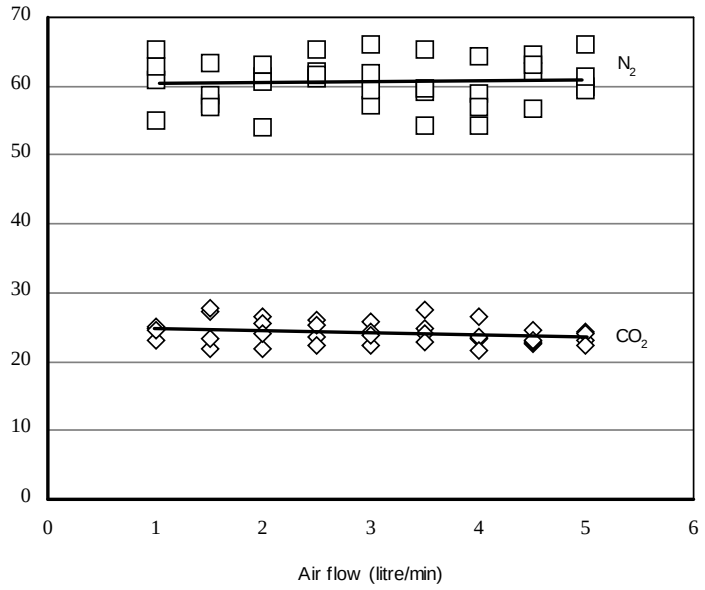

(b)

Figure 3.11 Experiments with wood pellets, showing dry gas compositions as a function of the air flow: (a) CO, H_2 and CH_4; (b) N_2 and CO_2.

Movement of hot zone: Because a quartz-tube was used, this enabled a visual observation to be made of the movement of the hot combustion zone, and this shows some very interesting features which are summarized in Figure 3.12.

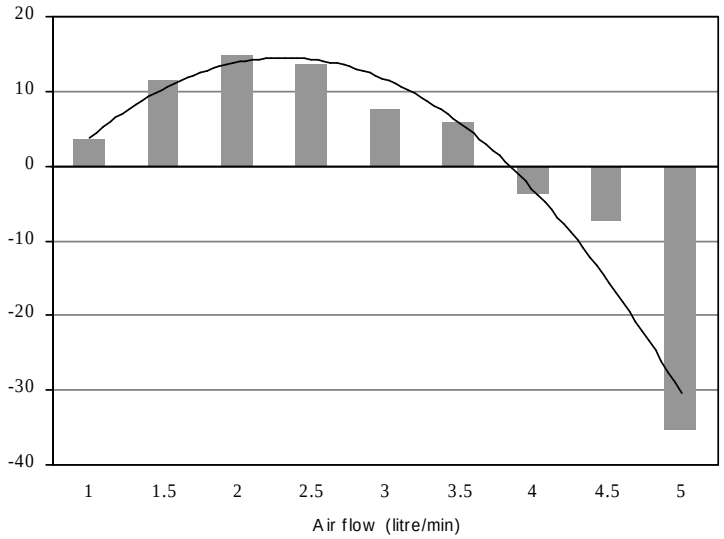

Figure 3.12 The movement of combustion zone as a function of air flow (experiment lasted about 30 min and the movement was measured over a 10 min period).

Air flow 1 to 3.5 litre/min: in this region the hot zone moved upwards, as illustrated in the photograph of the quart-tube in Figure 3.13(a). As the hot zone moved, the pellets were reduced in size and had the appearance of char.

Air flow of 4 litre/min: the hot zone started to move downwards, see Figure 3.13(b). As it moved, it consumed the char, turning it to ash.

Air flow 5 litre/min: the hot zone moved downwards in a rapid manner.

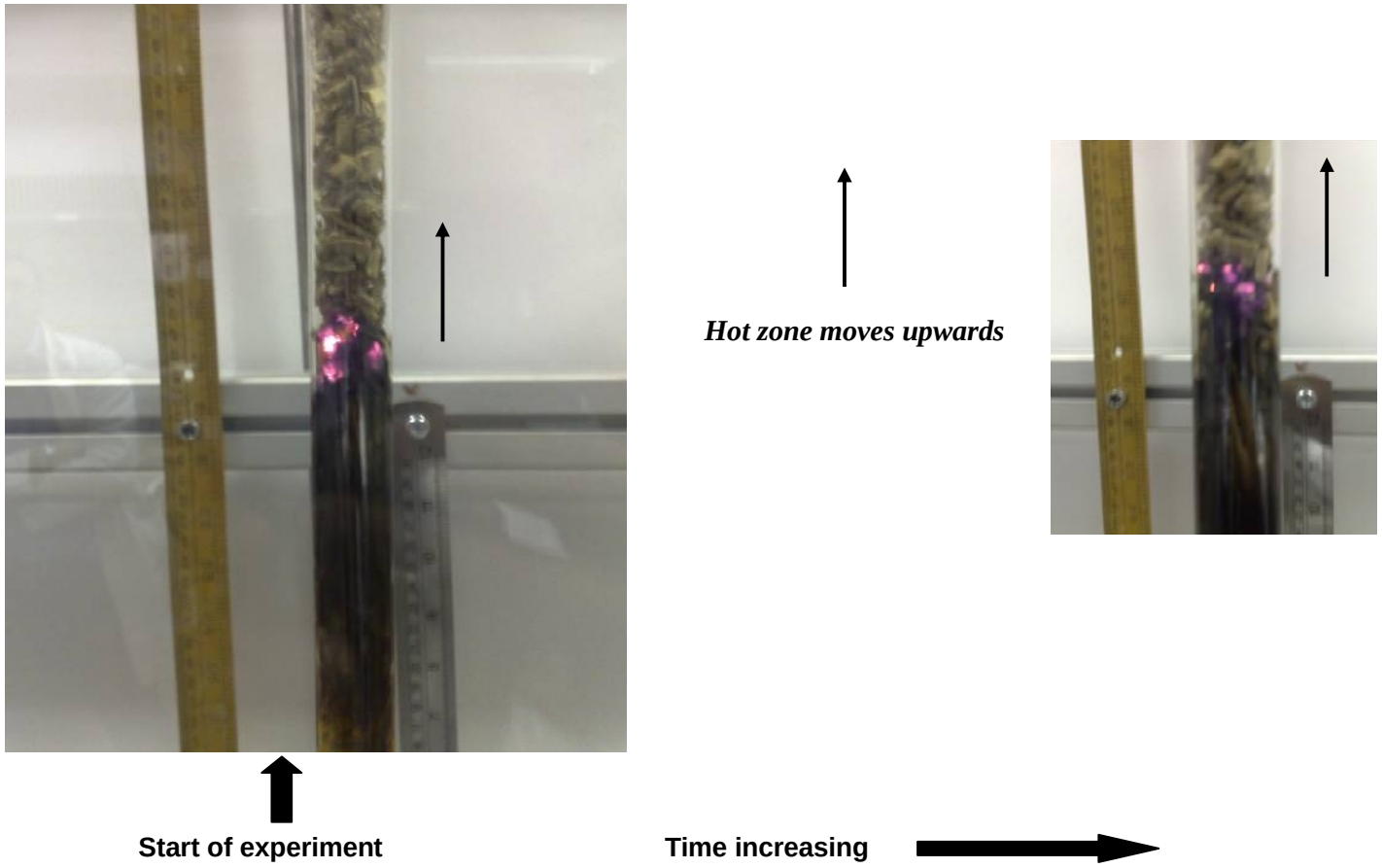

Figure 3.13(a) Hot combustion zone moving upwards.

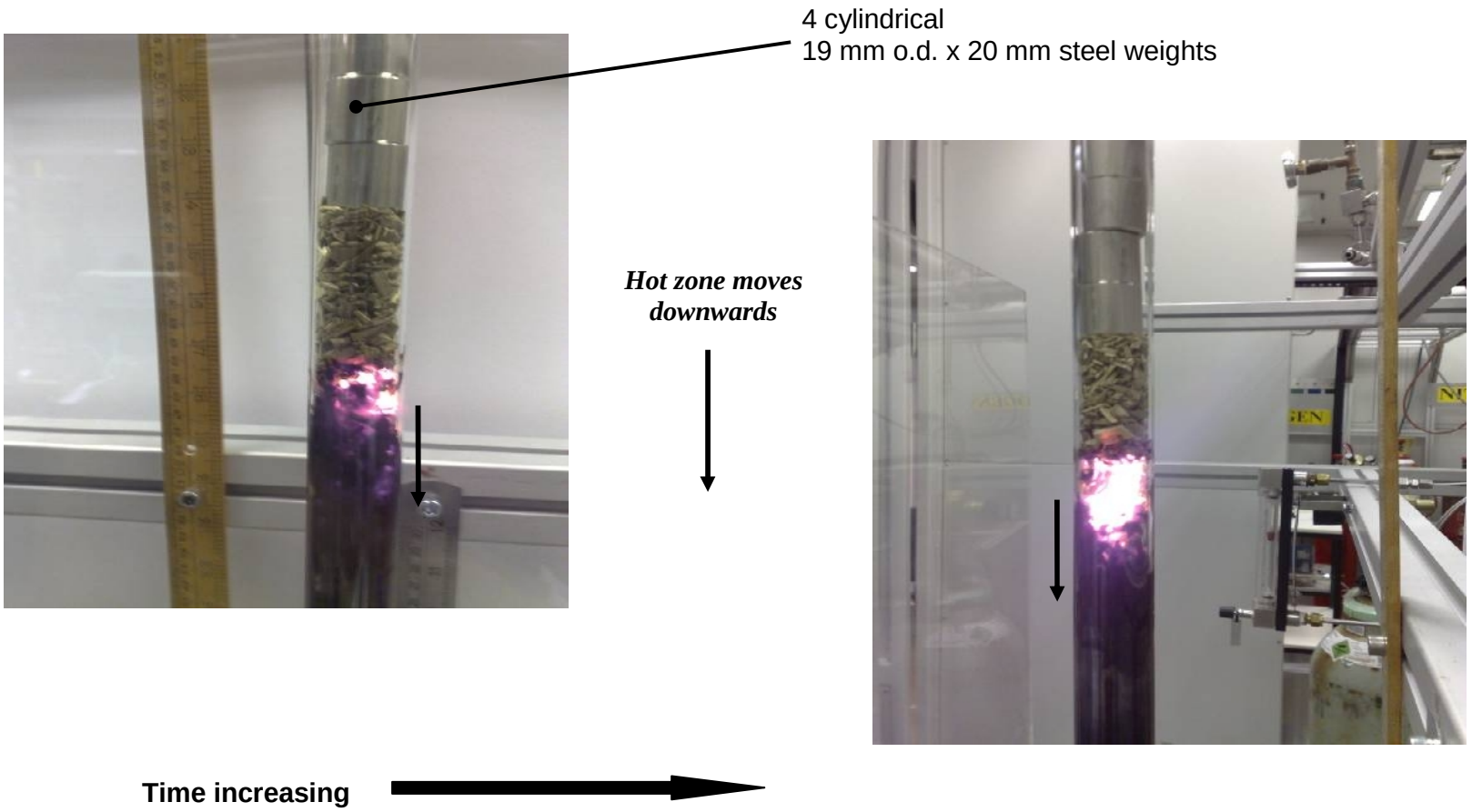

Figure 3.13(b) Hot combustion zone moving downwards.

In work by Hsi *et al.* (2008), the movement of the combustion zone in the direction of the point of air supply was described in a down-draft experimental gasifier (200 mm i.d. and 1000 mm height). An igniter was located 130 mm above the grate and the air inlet was 530 mm above the grate. On ignition of the bed, the flame front was found to propagate upwards to the location of the air inlets. This is consistent with the findings in Figure 3.12, where at relatively low air flows the combustion zone moves in the direction of the air supply. However, at very high flows, the direction changes – this aspect was not recognized in Hsi *et al.* (2008).

In other studies, both Earp (1988) and Evans (1992) used a transparent quartz reactor (50mm i.d.) in attempts to measure the heights of reaction zones in an open-core (stratified) down-draft gasifier. Earp (1988) employed pine and ramin (nominal size: 2.6-6.35 mm), whereas Evans (1992) used a variety of feed stocks (e.g. wooden beads and chips of different sizes) with the average feed rate of 1.27 kg/h. They both found that the movement of the flames (combustion zone) varied with the mode of operation, depending on the relative rates of char production by pyrolysis and char consumption by gasification. There were three modes, namely:

- Stable operation: there was no net production of char in the gasifier, leading to a stationary combustion zone observed;
- Char consumption (gasification) dominant operation: there was a net consumption of char in the gasifier, making a downward movement of the combustion zone;
- Pyrolysis dominant operation: there was a net production of char in the gasifier, resulting in an upward movement of the combustion zone.

Both authors concluded that the mode of operation is altered by varying the air to feed ratio in the gasifier. They explained the rise of the combustion zone as a result of greater heat loss in the pyrolysis dominant mode due to the increase of the char bed height. This led to less energy passed on to the gasification zone, and hence less char conversion (e.g. Evans, 1992, pp. 235-238). Therefore, they both found that during pyrolysis dominant operation, there was a higher air requirement (or higher air to feed ratio) compared with stable operation.

However, using the same experimental apparatus, Milligan (1994) proved that the mode of operation did not depend on the air to feed ratio, but on the superficial gas velocity within the gasifier. In other words, it relied on the air feeding flow rate. Milligan (1994, p. 114) used wood chips (nominal size: 4.75-12.7 mm) with a feed rate of up to approximately 2.2 kg/h, and showed that even greater heat loss was experienced in the pyrolysis dominant mode, the sum of energy lost and the sensible heat of the products was approximately constant at 28 % for all operation modes, see Figure 3.14.

By calculating the pyrolysis and gasification propagation velocities for stable, pyrolysis dominant and gasification dominant operation, Milligan (1994, p. 115) showed that the rate of char production by pyrolysis was approximately the same for stable (96.7 cm/h) and pyrolysis dominant operation (99.7 cm/h), but was very much reduced for gasification dominant operation (37.2 cm/h). The rate of char consumption by gasification increased from pyrolysis to stable, to gasification dominant operation. Therefore, a rising combustion zone was a result of decreased char gasification, while a falling combustion zone was a result of decreased char production by pyrolysis and increased char consumption by gasification.

Milligan (1994, p. 116) finally concluded that during the gasification dominant operation, the decrease in velocity of pyrolysis propagation might be explained by the forced convection of heat away from the combustion zone as the air flow into the gasifier was increased, leading to a convective cooling effect in the pyrolysis zone. He added that as the flame was pulled downwards further into the gasification zone, the heat flow into this zone was enhanced (i.e. forced convection), resulting in an increase in the rate of char gasification. Hence, the rate of char gasification became increasingly dominant when the superficial velocity of gases through the reactor was increased (due to the increase of the air flow into the reactor).

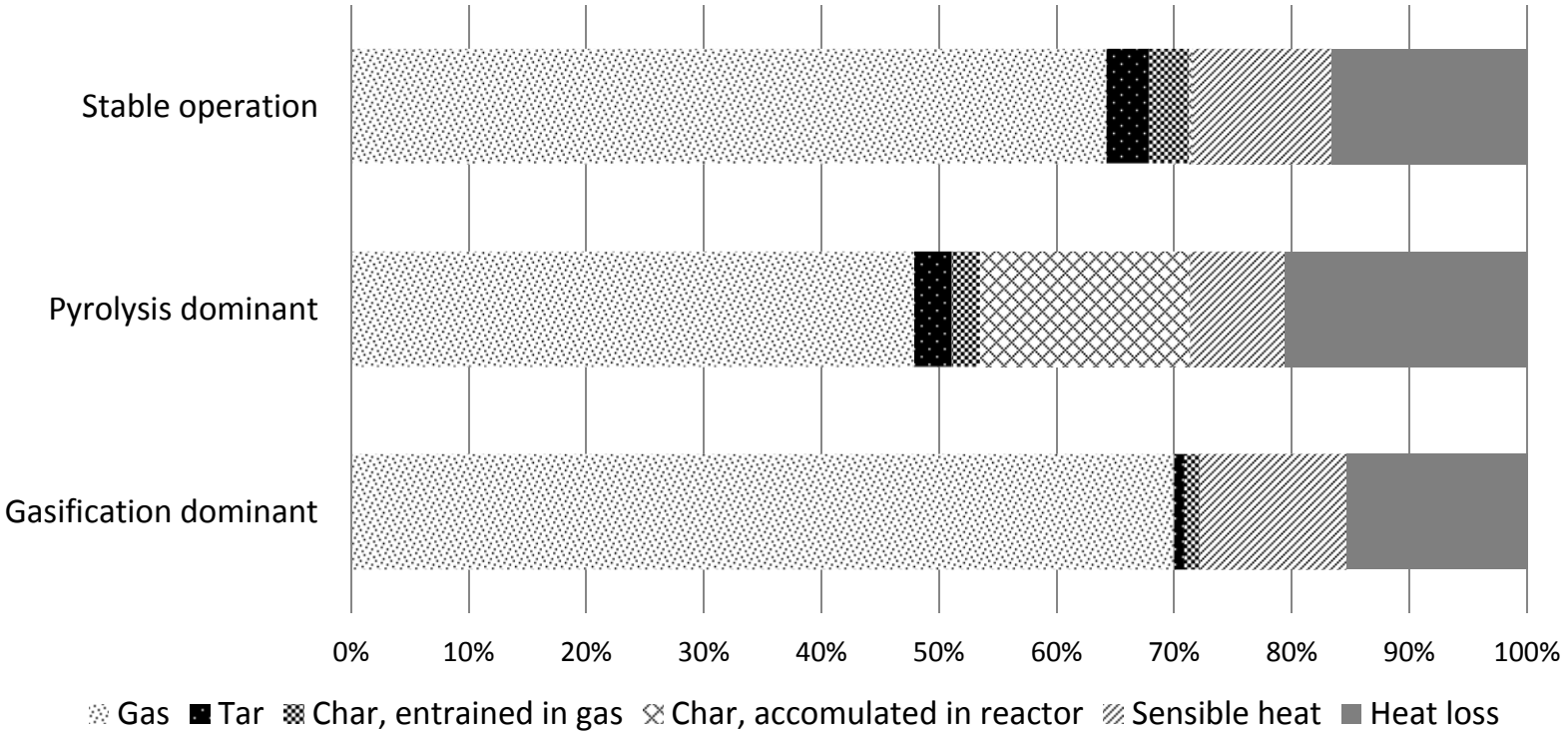

Figure 3.14 Energy output distribution of the open-core gasifier operating in stable, pyrolysis and gasification dominant modes, adapted from Milligan (1994, p. 113).

The findings of Milligan (1994) are almost consistent with results gained in this study. For example, during what was as a stable operation, the movement of the combustion zone was -2.81 cm/h, at 49.5 litre/min of air feed (Milligan, 1994, p. 300). If this air flow was scaled-down to the 21 mm i.d. quartz-tube, this would correspond to an air flow of 3.9 litre/min. From Figure 3.12, at an air flow of 4.0 litre/min, this would suggest a movement of the hot zone of -3.6 cm/h, which provides a close match.

Nevertheless, all three authors (Earp, 1988; Evans, 1992; and Milligan, 1994) did not report the variation in the height of the combustion zone, which was discovered in this work, varying with either the air feed rate or the superficial gas velocity.

Height of hot zone: It was also interesting to observe that as the air flow was increased, the height of the hot zone also increased, see Figures 3.15, and this can also be seen in the photographs in Figures 3.13(a) and 3.13(b).

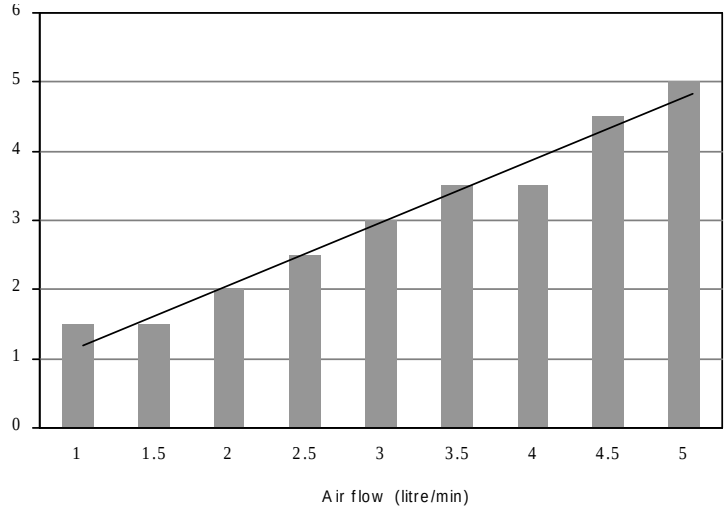

Figure 3.15 The height of the red hot zone as a function of air flow.

From Figure 3.15, an indication is obtained of the height of the red-hot zone. For the range of conditions tested, this appears to vary with air flow in a linear manner. This zone is also relatively short, and this can be supported by interpreting some of the results in Tinaut *et al.* (2008). They studied an inverted fixed bed down-draft gasifier (50 mm i.d.), in which the bed was ignited at the top, and air was supplied upwards from the base. This resulted in the hot zone moving downwards. Thermocouples were positioned at 30 mm intervals, and one of the temperature plots (with air flow 12 litre/min) provides a clue as to the length of

the hot zone, which would be about 30 mm. If their air flow was scaled-down to the 21 mm i.d. quartz-tube, this would correspond to an air flow of 2.1 litre/min. From Figure 3.15, this would suggest a hot zone of 20 mm, which, considering that the quartz tube is not insulated, provides a close match.

Superficial gas velocity: What is also interesting to note, is how the superficial velocity may vary in these experiments. As an illustration, at a fixed air flow of 3 litre/min, the superficial velocity of air was calculated at a range of temperatures, and is illustrated in Figure 3.16. Then in Figure 3.17, the superficial velocity is calculated at a fixed temperature of 500 ºC, and over a range of air flowrates.

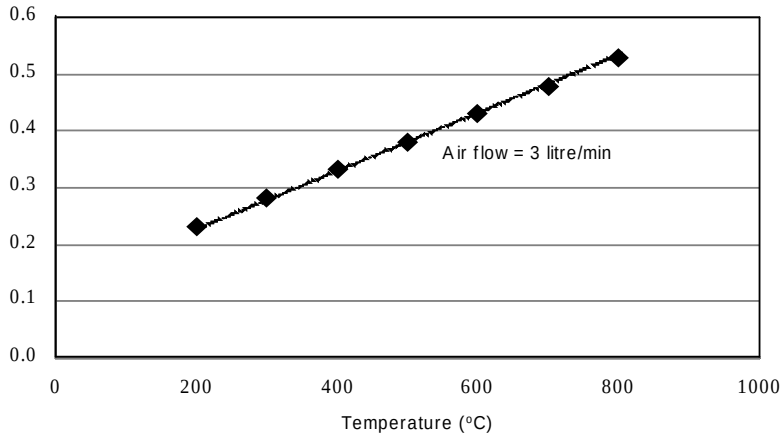

Figure 3.16 Superficial air velocity as a function of temperature at an air flow of 3 litre/min.

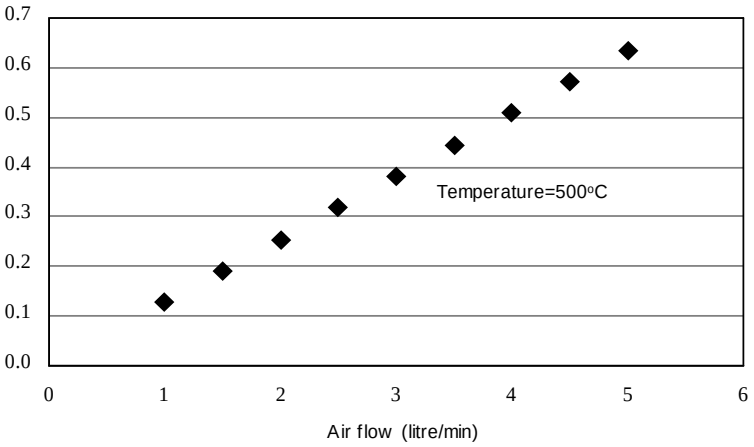

Figure 3.17 Superficial air velocity as a function of air flow at a temperature of 500 °C.

Possible 3D shape of the hot-zone in a commercial gasifier: From the experimental observations made so far, the following picture has been formed of what this hot zone may look like in a larger-scale commercial down-draft gasifier.

As air is supplied *via* nozzles (around the perimeter of the throat in the gasifier), the direction and shape of the expanding air jets will depend on a number of factors e.g.:

- the obstacles it encounters (size and shape of the biomass particles),
- voidage in the bed,
- movement of the bed,
- local pressure drop and influence of temperature variations on gas velocity.

As the air jet expands, its local gas velocity will vary, and conditions may exist where the hot combustion zone may move down (away from the jet), or upwards to it. A schematic illustrating what could be taking place is presented in Figure 3.18.

This type of consideration is not often encountered in explanations in the literature where for example in Earp (1988), Evans (1992), Milligan (1994), Knoef (2005), Sheth and Babu, (2009), Dogru *et al.* (2002), and Tinaut *et al*., (2008), discussions are in general limited to a 1D representation of this complex system.

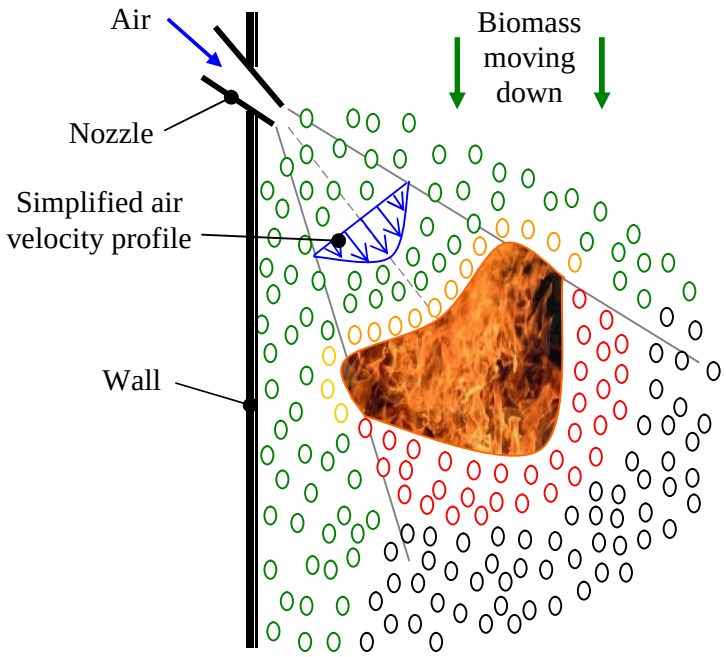

Side view of one air nozzle in the combustion zone

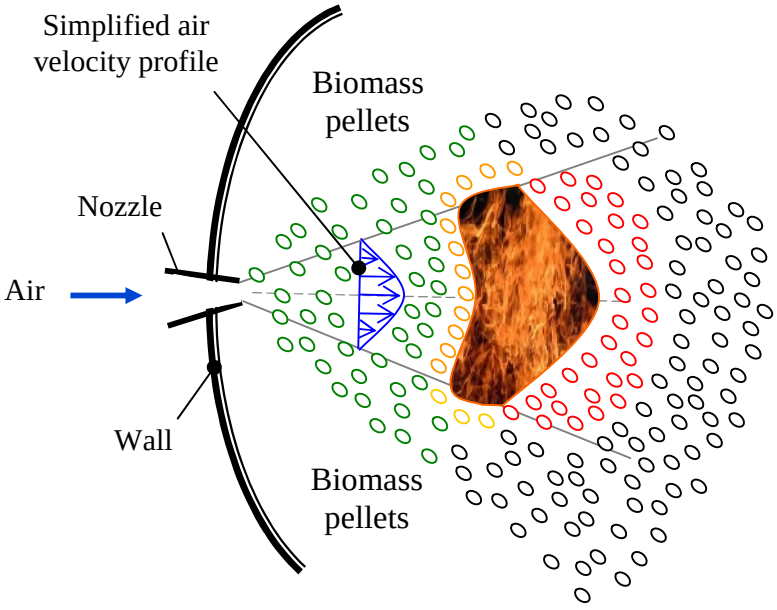

Plan view of one air nozzle in the combustion zone

(O: fresh biomass pellets; O: red hot char particles; O: char particles)

Figure 3.18 Representation of what might be taking place in the oxidation zone in a down-draft gasifier.

3.3.3 Gasification of Wood Pellets (Air Flow Varied) – <u>with Thermal Insulation</u>

From the experiments with the quart-tube, it was clear that without any thermal insulation around the quart-tube, a significant amount of heat was lost from the hot zone (mainly by radiation), and this in turn would have affected the extent of any neighbouring pyrolysis reactions, and hence affected the composition of the gas. Consequently, concentrations of H_2 and CO in the gas stream were small, see Figure 3.11(a). The gas produced was also very sticky, smoky and not combustible.

To enhance the quality of the gas produced, in the next set of experiments, a layer of thermal insulation was placed around the hot zone in the quartz-tube (see Figure 3.19).

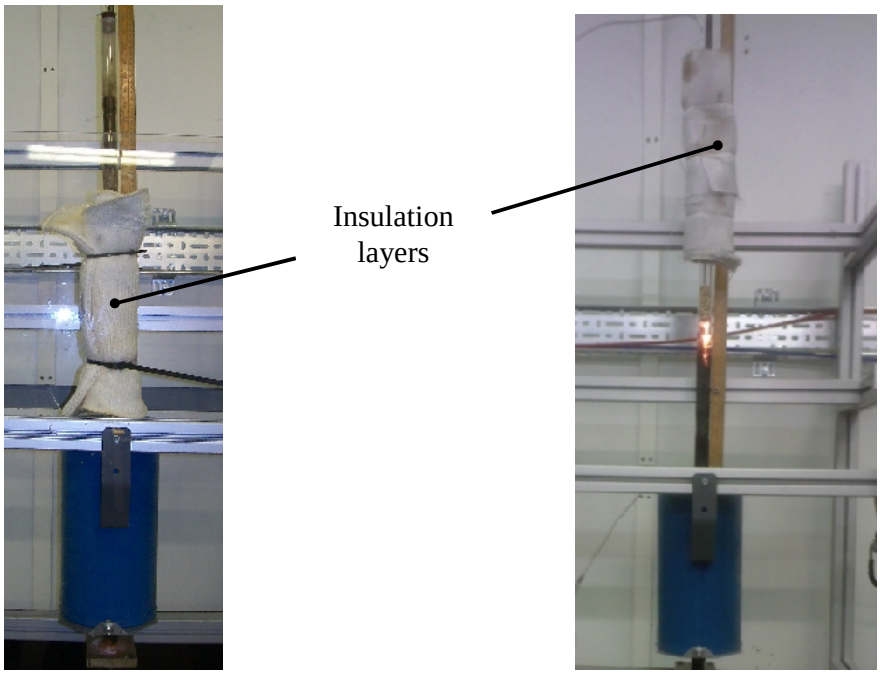

Figure 3.19 Illustrating the layer of insulation around the quartz-tube.

Gas composition:

The results of these experiments are presented in Figure 3.20. With insulation, a clearer trend can be observed, and there is less scatter in the data. In general, CO and H_2 levels increase with air flow. This may be due to the fact that with insulation, the temperatures in reaction zones are more uniform and stable. In addition, less heat is lost into surroundings

with insulation, resulting in more heat provided for the endothermic reactions that occur in the reduction zone, which in turn generate more CO and H_2.

During some of these experiments, the insulation was lifted briefly and the height of the red hot zone was a lot deeper. For example, at an air flow of 3 litre/min the zone was 5 cm in comparison with 3 cm (without insulation). This extension of the hot zone resulted from an extension of the gasification zone in the bed, as the heat losses were reduced. Therefore, there was a big improvement in the quality of the gas produced from the gasifier, where the concentrations of H_2 and CO were much higher, and the gas stream produced also looked cleaner (less sticky and smoky).

This improvement was due to the high and uniform temperature in the combustion zone, providing enough energy for endothermic reactions in the pyrolysis and reduction zones. At high temperature, more char was gasified to generate combustible gases such as H_2 and CO. In addition, tar was also cracked when it went through the high temperature area.

Evans (1992, p. 248) estimated the heat loss as a percentage of the energy input from quartz open-core down-draft gaisifier experiments. He found that the heat losses from the gasifier were reduced by insulation from 39 % to 16 % of the wood input to the gasifier.

Milligan (1994, p. 137) reported a reduction of 50 % tar content of the producer gas, when a comparison of the experiments with and without insulation was performed. It was believed that in the insulated reactor higher temperatures promote tar cracking, leading to a reduction in tar content.

Figures 3.21 and 3.22 present the chromatographs of the gas stream produced from gasification of wood pellets at 3 litre/min, without and with insulation, respectively.

During the course of an experiment, a thermocouple was inserted between the outside surface of the quartz-tube, and the insulation that surrounded the tube. This provided a good indication of the temperature inside the quartz-tube at that location. As the hot zone approached the location of the thermocouple, the temperature rose, and its maximum value was recorded. From a number of experiments, the temperature of this hot zone was in the region of 912 to 1046 ºC, and it was found to occasionally peak at 1084 ºC.

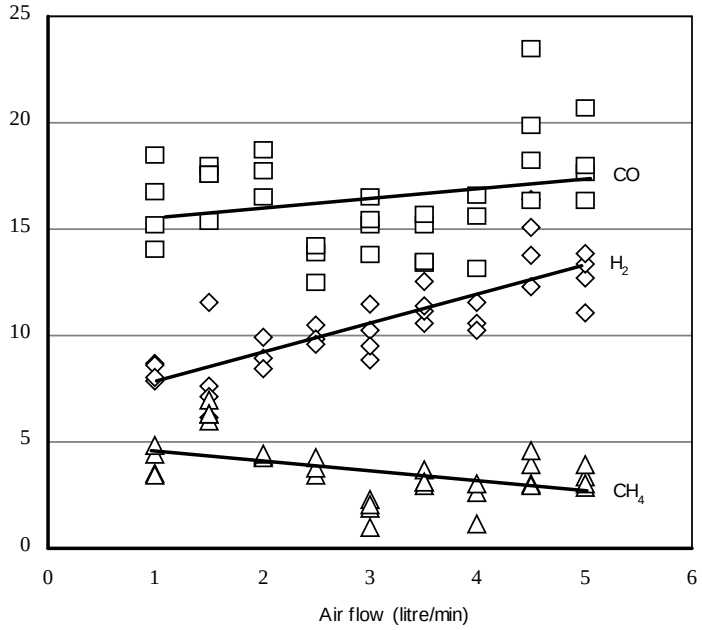

(a)

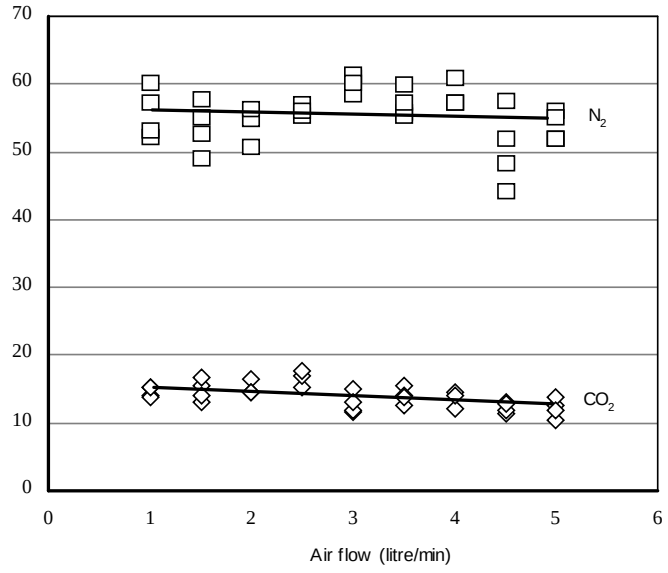

(b)

Figure 3.20 Experiments with wood pellets (with thermal insulation around the hot-zone), showing dry gas compositions as a function of the air flow: (a) CO, H_2 and CH_4; (b) N_2 and CO_2.

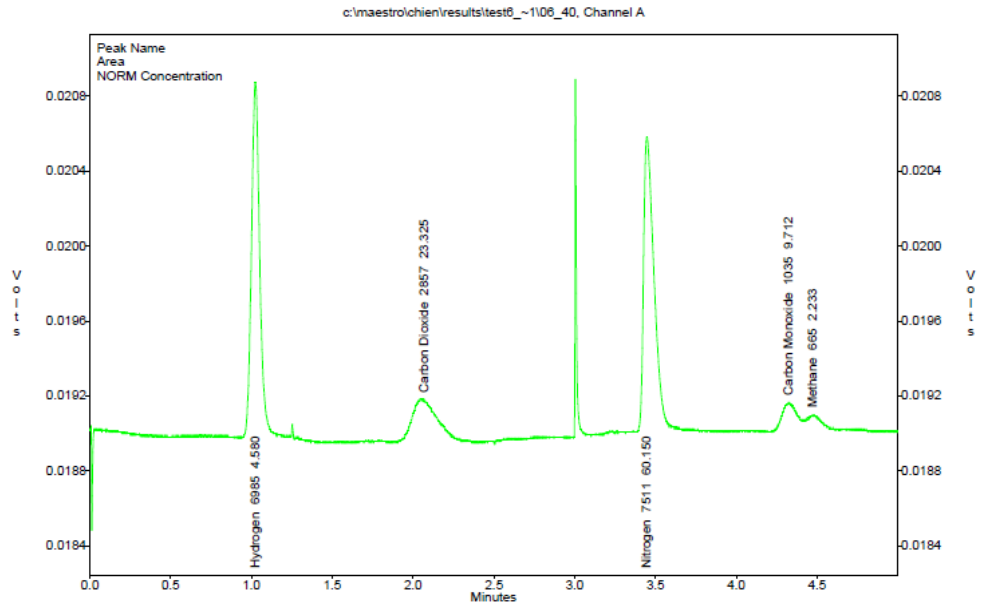

Figure 3.21 Chromatograph of the gas produced from gasification of wood pellets at 3 litre/min, **without any insulation**.

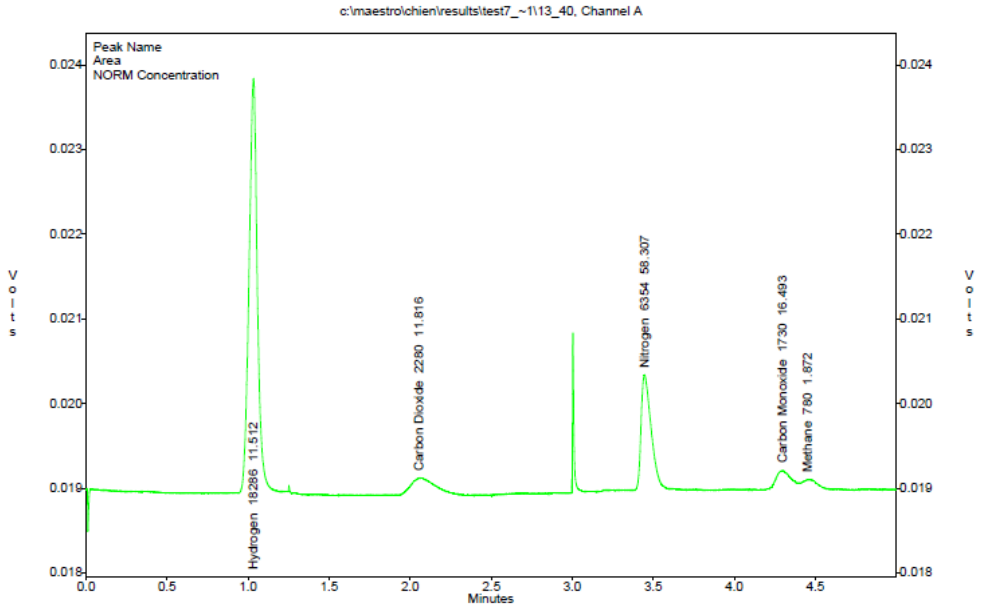

Figure 3.22 Chromatograph of the gas produced from gasification of wood pellets at 3 litre/min, **with insulation.**

Experiments with smaller pellets: To explore how small variations in pellet length might affect the results, a few experiments were performed in which the length of the wood pellets was reduced from 13 mm to 5 mm. The experiments were then performed at a fixed air flow of 3 litre/min, and also at 5 litre/min: the results are presented in Table 3.4. From these, it is clear that as the size of the pellet was decreased, slightly higher concentrations of CO and H_2 were achieved (up to approximately a 4 % improvement).

Table 3.4 Dry gas composition as pellet size is reduced.

Cylindrical wood pellets	**Wood pellet size (diameter × length), mm**			
	5 × 13	**5 × 5**	**5 × 13**	**5 × 5**
	3 litre/min of air flow		5 litre/min of air flow	
CO	15.2	15.4	18.1	18.6
H_2	10.1	10.1	12.7	13.3
CH_4	1.8	3.2	3.3	2.8
CO_2	12.9	12.9	12.2	10.5
N_2	60.0	58.4	53.7	54.8

Repeatability: As a check on repeatability, at an air flow of 3 litre/min and with 5 mm diameter x 13 mm long pellets, the experiments were repeated three times, and it was found that the average gas composition was: CO = 14.87 (±0.32) vol.%; H_2 = 10.17 (±0.16) vol.%; and CH_4 = 2.15 (±0.25) vol.%.

Wood to char to ash: Because of the way in which the wood pellets are made, their length was found to vary. Also, during the gasification process, at high temperatures, they fracture into small pieces and shrink as the char is formed, see Figure 3.23. Finally, depending on the experimental conditions:

- either a collection of char particles remains in the bed, or
- the char may be converted to ash, see Figure 3.23(c).

(a)

(b)

(c)

Figure 3.23 Photos of (a) wood pellets, (b) char produced from the wood pellets, and (c) ash from the char.

3.3.4 Gasification of Wood Pellets – with Thermal Insulation and a Hot Secondary Char Zone

In a down-draft gasifier, it was discussed earlier in Section 1.1.1 that energy was necessary to support the following endothermic reactions, which take place in the reduction zone:

$$C + CO_2 \leftrightarrow 2CO \qquad + 172 \text{ kJ/mol} \qquad (1.4)$$

$$C + H_2O \leftrightarrow CO + H_2 \qquad + 131 \text{ kJ/mol} \qquad (1.5)$$

These reactions are expected to occur at high temperature (600 to 900^0C) in the reduction zone of a down-draft gasifier, and it is claimed that they produce more of the H_2 and CO, and help to improve the quality of the producer gas stream (Basu, 2010, p. 132; Knoef, 2005, p. 23; Higman and Burgt, 2008, p. 12; Sheth and Babu, 2009).

Information on the possible height of this reduction zone, does vary in the literature. For example:

> **120 mm** in Dogru *et al.* (2002), for an experimental 5 kW_e down-draft gasifier.
>
> **100 mm** in Sheth and Babu (2009).
>
> Then, as specified by the Food and Agriculture Organization of the United Nations (1986) the height of the reduction zone should be **more than 200 mm**, and the average height of this region for down-draft gasifiers reviewed was **320mm**.

Therefore, to explore the role that this reduction zone may have, wood pellet (13 mm long) gasification experiments were performed with an additional bed of wood charcoal placed at the base of the quartz-tube, inside the furnace section, see Figure 3.24.

Experiments with the extra wood charcoal bed (reduction zone) were performed at an air flow of 3 litre/min. This charcoal layer was 300 mm deep and was heated up to between 600 and 900^oC to stimulate the reduction zone in a down-draft gasifier. Before the charcoal was used in these experiments, it was heated in a stream of N_2 (at 800 ºC, for 3 h) to remove any volatile species.

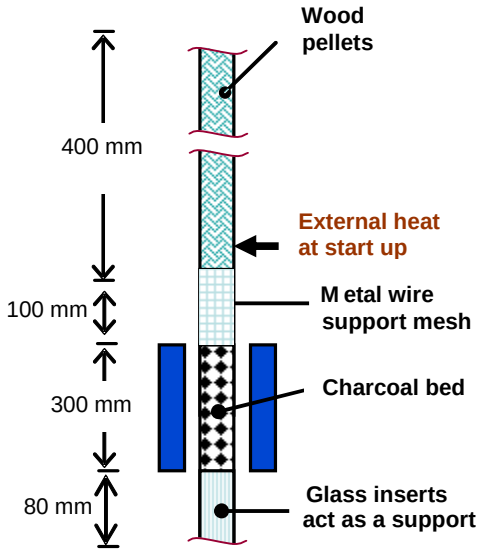

Figure 3.24 Schematic illustrating quart-tube gasifier with a wood charcoal bed at the base of the tube.

The results of the experiments are presented in Table 3.5, and it is clear that slightly higher concentrations of CO and H_2 were achieved when the gas flowed through the charcoal bed. In addition, their concentration increased slightly with temperature. From a visual observation of the colour of the gas produced, it also looked cleaner (less smoky).

By reviewing literature, Milligan (1994, p. 41) suggested that a temperature of 700^{o}C was required for tar cracking. Below this temperature, the rate of gasification also became insignificant. Therefore, there was an "inert" char bed, where the tar would not be cracked to any great extent. However, the inert char bed was believed to play a role by adsorbing a limited amount of tar from the gas stream, thereby providing a beneficial effect.

Table 3.5 Comparison of dry gas compositions with and without a hot secondary charcoal zone (air flow = 3 litre/min, with insulated hot zone).

Cylindrical wood pellets	Without charcoal			With charcoal		
	600 ºC	750 ºC	900 ºC	600 ºC	750 ºC	900 ºC
CO	15.8	15.1	16.7	16.5	16.1	17.5
H_2	9.5	10.3	10.3	10.6	12.0	13.4
CH_4	2.0	2.0	3.5	2.9	3.1	3.0
CO_2	14.5	12.9	12.9	14.5	12.9	13.0
N_2	58.2	59.7	56.6	55.5	55.9	53.1

What is interesting about these experiments is that as a result of passing through the 300 mm layer of hot charcoal, although the concentrations of CO and H_2 have increased slightly, their increase in concentration is relatively low. This implies that at the conditions tested, these reduction reactions are not as significant as claimed in the literature. This was also despite the maintenance of high temperatures in this zone with the aid of an external heat source (i.e. furnace). In the commercial application, the endothermic reactions would consume energy and lower the temperature of the gas.

This leads to a number of important questions about what is actually happening at the base of the gasifier in the so called 'reduction zone', which was three times longer than the 100 mm zone described in Sheth and Babu (2009).

In studies performed by Earp (1988), Evans (1992) and Milligan (1994), they also found that increasing the height of the char bed had a minimal influence on producer gas quality, and only a slight improvement in gas heating value. However, in all cases, the increasing energy content of the gas produced with char bed height might be due to variation in operation parameters (e.g. air feeding flow rate, air to feed ratio, feed size). For example, Evans (1992, p. 242) reported that increasing the char bed height in an open-core down-draft gasifier, due to slightly reduction of air requirement of the gasification process, led to a slight increase of H_2 and CO content in the producer gas.

The gas compositions from the quartz-tube experiments were also compared with the results from measurements on a small 40 kg/h pilot-scale gasifier (operated by a company outside of the University), which was fed with the same type of wood pellets. What is very interesting to see is that a similar range of values in gas composition was obtained as for the quartz-tube, when it was operating at high air flowrates. The results of 3 tests on the pilot-plant are illustrated in Table 3.6.

Table 3.6 Gas measurements on a pilot-scale down-draft gasifier[1] (using wood pellets at 40 kg/h).

	Calibration gas [2] (vol.%)	**No 1[3] (vol.%)**	**No 2[3] (vol.%)**	**No 3[3] (vol.%)**
Hydrogen	13.63	11.83	12.00	13.53
Hydrocarbons:				
CH_4 methane	0.99	3.05	3.05	2.59
C_2H_4 ethylene	0.2	0.84	0.81	0.66
C_3H_8 propane	0.2			
C_3H_6 propene	0.2	0.32 C_3s	0.29	0.17
C_2H_6 ethane	0.49	0.15	0.15	0.10
C_2H_2 acetylene	0.2	0.16	0.16	0.12
Carbon monoxide	17.75	24.01	24.04	26.44
Carbon dioxide	12.32	11.74	11.27	9.22
Oxygen	2.52	-	0.16	0.20
Nitrogen	51.5	47.90	48.07	46.97
			88.74	89.55
Sub total =	100.0	100.0	100.0	100.0

Notes:

(1) These measurements were made by a company that was developing a 40 kg/h wood pellet gasifier.

(2) Gas analysis was performed with a GC, which had been calibrated with the calibration gas specified.

(3) The results have been normalized (to ensure 100 % for the total volume).

3.3.5 Gasification of Straw Pellets – with Thermal Insulation (Air Flow 3 litre/min)

At an air flow of 3 litre/min, a short comparative study was performed, to asses how straw pellets would behave in comparison with wood pellets. Physical properties of the pellets are provided in Table 3.7, and a photograph is supplied in Figure 3.25.

Table 3.7 Properties of the straw pellets (as measured) with proximate analysis.

All pellets are cylindrical in shape (supplied by Agripellets Ltd, Evesham)	Absolute density (kg/m^3)	Bulk density (kg/m^3)
Wet pellets: 6.1 mm diameter x 16.4 mm	1232	538
Dried pellets	1064	479
Pellets reduced to char: 4.4 mm diameter x 13 mm	670	365

Moisture	Volatiles	Fixed carbon	Ash
10.9 wt.%	65.9 wt.%	21.7 wt.%	1.4 wt.%

Figure 3.25 Photograph of the straw pellets used in the experiments.

The results of some of these experiments are illustrated in Table 3.8.

Table 3.8 Comparison of dry gas compositions between wood and straw pellets without a hot secondary charcoal zone (air flow = 3 litre/min, with insulated hot zone, furnace at 750 ºC).

Cylindrical	Wood pellets (vol.%)	Straw pellets (vol.%)
CO	15.1	14.7
H_2	10.3	12.6
CH_4	2.0	2.0
CO_2	12.9	14.2
N_2	59.7	56.5

In general there was not a big difference, although the CO content of the gas was slightly lower, and the hydrogen content was slightly higher. The transition of the pellet from its manufactured form, to char and then ash, is illustrated in Figure 3.26.

(a)

(b)

(c)

Figure 3.26 Photos of (a) straw pellets, (b) char produced from the straw pellets, and (c) ash from the char.

3.4 EXPERIENCE GAINED FROM THE GASIFICATION EXPERIMENT

In this section, a number of important practical aspects are discussed, which also have links and implications on the performance of a pilot-scale gasifier.

3.4.1 Risk of Tube Fracture

The 21 mm i.d quartz-tube lost heat quickly, so it was covered with an insulating sleeve (which was briefly lifted for visual observations). This in turn, under certain operating conditions, led to very high temperatures in the hot zone (e.g. 1084 ^{o}C), and thermal stresses led to tube fracture. Care needs to be taken to ensure that in the event of the glass tube shattering, operatives would not be injured. This means that such high temperatures may also exist at local points in a pilot-scale gasifier – this aspect had not been fully appreciated by the two companies who remained in contact with this research project.

3.4.2 Biomass Sticking on Walls

As the reactions proceed in the hot zone, and biomass is consumed, there should be a general downward movement of biomass in the tube. However, because of tarry material that is produced, this may coat the walls of the tube, the biomass may stick to the walls and not fall downwards into the void that has been created. Some form of vibration on the walls of the glass tube can help to keep the biomass moving. In any development of this experimental concept, it may be better to have a device inside the tube to keep the biomass moving downwards. These problems also exist in pilot-scale gasifiers, where 'bridging' can occur between neighbouring particles, and the biomass may also adhere to the walls of the gasifier.

3.4.3 Slagging

If very high temperatures are reached, then the ash may melt and cause a slag to form which restricts the performance of the experimental tube. In that case, the experiment was stopped, the equipment had to cool down, and then the slag was removed. These problems also exist in pilot-scale gasifiers, and the melting point of the ash depends on the chemical composition of the biomass fed into the gasifier.

3.4.4 Tar Formation

This was formed during the gasification experiments, and was very visible in the lines and filters, see Figure 3.27. To prevent an excessive build-up of pressure in the lines, they had to be cleaned frequently.

These problems also exist in pilot-scale gasifiers. However, attempts to remove the tar by cooling and water scrubbing, creates a waste water effluent stream, high in phenols.

(a)

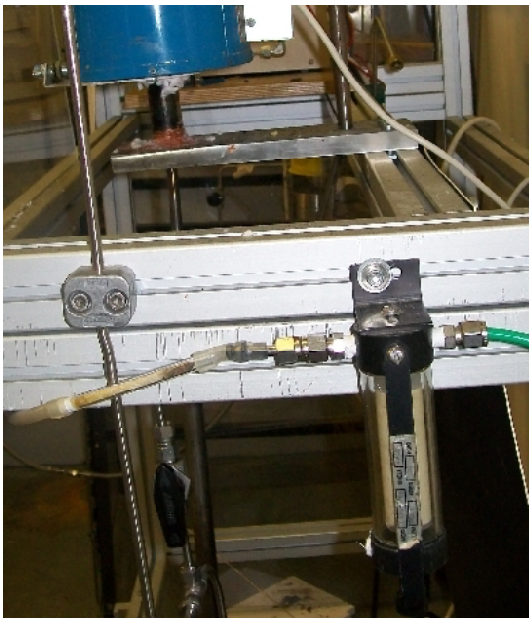

(b)

Figure 3.27 Examples of tar deposition (a) at the bottom of the quartz-tube, and (b) visible on the surface of the plastic lines and filters.

3.4.5 Condensate Formation

As the gas was cooled at the end of the quartz-tube, condensate was collected, and this contained mainly water and hydrocarbons (see Figure 3.28). Some of the hydrocarbons formed a tarry layer, while others discoloured the water and formed an emulsion. These condensates looked dirty and smelt. These problems also exist in pilot-scale gasifiers, and the treatment of the waste water formed involves a number of steps, and is seen to be a costly activity.

According to Knoef (2005, pp. 196-197), it may be possible to (a) avoid condensate being formed by keeping the temperature above the dew point up to the point of gas use, (b) cleaning the condensate, or (c) scrubbing with oil and subsequent recycling of the tar back into the gasifer.

Figure 3.28 Condensates collected from condensers at the bottom.

3.4.6 Gas Quality

Depending on the operating conditions, the quality of the gas varied. This will also occur in the pilot-scale gasifier. Although gas analysis is an expensive activity, it is essential if the links between cause and effect are to be properly understood on a pilot-plant.

3.4.7 Char Formation

During the experiments in the quartz-tube, char was formed (see Figure 3.29) which remained in the gasification tube. This char contains carbon, which could be reacted with H_2O and CO_2 to produce useful gas. However, in the experimental set-up, once the hot zone has moved and left the char, it cools and remains in the tube (until it is physically removed).

In a pilot-scale gasifier, char is also formed and withdrawn from the base of the gasifier. The appearance of such char was very similar to that observed in the quartz-tube gasifier, and it contained 25.57 wt.% volatiles, 71.03 wt.% fixed carbon, and 3.4 wt.% ash in dry

basis. If such biomass-to-energy processes are to become viable, then more of the carbon in this char needs to be converted into useful gas.

Figure 3.29 Example of char (from wood pellets) at the end of a gasification experiment.

3.5 CONCLUDING REMARKS

(a) At the start of the experimental work, it was accepted that this small 21 mm i.d. quartz-tube gasifier was not a scaled-down version of an operational gasifier. Nevertheless, this experimental apparatus has provided some very useful insights into the processes occurring inside the gasifier on issues, such as:

- gas composition and variations with air flow,
- direction of movement of the hot zone, peak temperatures in this zone, and depth of the hot zone,
- formation of char, and
- the role that carbon may play in the reduction zone.

(b) Measurements with the GC provided reliable data; however, there is a significant time-lag between the taking of the sample and obtaining results from such an analysis. This then led to the development of a method provided in Chapter 4, where a Quadrupole Mass Spectrometer (QMS) is used for on-line measurements. The QMS is then used in the chapters that follow.

(c) Depending on the air flowrate, the hot zone may move upwards or downwards, and this has important implications for the way in which these zones can be visualized in a full-scale gasifier.

(d) When the gases were passed through a fixed bed of hot charcoal, the improvement in CO and H_2 concentrations still raised some unanswered questions about the effectiveness of this zone in a full-scale gasifier. The way in which this zone is portrayed in 1D format is too simplistic. Also, the char produced needs to be more effectively utilized on-site to generate more useful gas. This leads to further work on that topic in Chapters 6 and 7.

(e) When the gas composition was measured in the quartz-tube experimental reactor, and then compared with data from a 40 kg/h pilot-scale, similar values were obtained. This provides confidence in the use of the smaller visual apparatus for exploratory trials. This leads to further work, and the results of on-site measurements on a 250 kg/h pilot-plant are described in Chapter 8.

(f) Finally, it is interesting to consider the question that was often asked by visiting industrialists about the comparison between benefits of producing more H_2 and those of CO in the producer gas. This depends on the way the fuel is used. If the fuel is used in an engine, then as the heat of combustion of CO is 283 kJ/mol, and that of hydrogen is 242 kJ/mol (lower heating value), then a decrease, for example of 1 vol.% in hydrogen if it is matched by an increase in 1 vol.% of CO, would be preferred. This assumes that the heating potential by condensing the water vapour formed is not included, and in many practical applications it would not be, as the exhaust gases need to be discharged at a temperature > 150 ºC up a chimney stack.

REFERENCES

Basu, P. (2010). Biomass Gasification and Pyrolysis. Elsevier Inc.

Bridgwater, A. V. (2003). Renewable fules and chemicals by thermal processing of biomass. Chemical Engineering Journal, Vol. 91, pp. 87 – 102.

Bridgwater, A.V., Toft , A.J. and Brammer, J.G. (2002). A techno-economic comparison of power production by biomass fast pyrolysis with gasification and combustion. Renewable and Sustainable Energy Reviews, Vol. 6, pp. 181 – 248.

Dogru, M., Howarth, C.R., Akay, G., Keskinler, B. and Malik, A.A. (2002). Gasification of hazelnut shells in a downdraft gasifier. Energy, Vol. 27, pp. 415 - 427.

Earp, D.M. (1988). Gasification of biomass in a downdraft reactor. PhD thesis, the University of Aston, Birmingham, United Kingdom.

Evans, G.D. (1992). Development and operation of an open-core downdraft gasifier system. PhD thesis, the University of Aston, Birmingham, United Kingdom.

Food and Agriculture Organization of the United Nations (1986). Wood as Engine Fuel. FAO Forestry Paper 72.

Higman, C. and Burgt, M.V.D. (2008). Gasification. Second edition, Elsevier.

Hsi, C.L., Wang T.Y., Tsai C.H., Chang C.Y., Liu C.H., Chang Y.C. and Kuo J.T. (2008). Characteristics of an air-blown fixed-bed downdraft biomass gasifier. Energy & Fuels, Vol. 22, pp. 4196 - 4205.

Knoef, H.A.M., edited, (2005). Handbook Biomass Gasification. BTG biomass technology group.

Kolaczkowski, S., Le, C.D. and Jodlowski, P. (2011). Gasification of wood pellets in an experimental quartz tube gasifier – How visual 1D experiments can aid 3D design considerations. In Proceedings of the bioten conference on biomass and biofuels 2010, Bridgwater, A.V. (Ed), CPL Press UK, pp. 720-732.

Milligan, J.B. (1994). Downdraft gasification of biomass. PhD thesis, the University of Aston, Birmingham, United Kingdom.

Shelth, P.N. and Babu, B.V. (2009). Experimental studies on producer gas generation from wood waste in a downdraft biomass gasifier. Bioresource Technology, Vol. 100, pp. 3127 - 3133.

Sirley, A. (2005). A transient steam reforming process to produce hydrogen from methane for use in fuel cells. PhD thesis, the University of Bath, Bath, United Kingdom.

Tinaut, F.V., Melgar, A., Perez, J.F. and Horrillo, A. (2008). Effect of biomass particle size and superficial velocity on the gasification process in a downdraft fixed bed gasifier. An experimental and modelling study. Fuel Processing Technology, Vol. 89, pp. 1076 – 1089.

Zainal, Z.A., Rifau, A., Quadir, G.A. and Seetharamu, K.N. (2002). Experimental investigations of a downdraft biomass gasifier. Biomass and Bioenergy, Vol. 23, pp. 283 - 289.

CHAPTER 4

Gas Analysis with a Quadrupole Mass Spectrometer

Before the Quadrupole Mass Spectrometer (QMS) could be used for the measurement of the composition of various gas streams in this thesis, a method had to be developed to calibrate the instrument and to interpret the raw data obtained from the QMS. This was not a trivial task, as the gas mixture was complex, there were clashes in the signals from some of the species (e.g. N_2 with CO), and the magnitude of the concentration of the species also varied.

So after attending an initial 3 day training course (by Hiden Analytical Limited), it took another 8 months to resolve problems that arose during equipment commissioning, and then to develop the methodology described in this chapter.

As the QMS methodology was being developed, other activities were also progressed in parallel, for example:

- the GC was being used for gas analysis, and
- the experimental equipment was being constructed and commissioned for the charcoal/char steam gasification experiments (described in Chapter 6).

This provided an opportunity to compare the results from the QMS with the GC, and also to use a relatively clean gas (from the gasification of wood charcoal with steam) for the first trials of the QMS.

4.1 INTRODUCTION

Although, it is fairly obvious that on-line gas analysis would be beneficial to monitor the quality of the gas produced from a gasification process, there is relatively little published on that topic that is specific to the analysis of ‘producer gas’ (high nitrogen content). Examples include work done by Karellas end Karl (2007), where the producer gas stream

from a fluidized-bed gasifier was analyzed on-line by means of laser spectroscopy; however, only the concentrations of the main constituents (H_2, CH_4, CO, CO_2, H_2O) and some heavier hydrocarbons were reported. In Karlegärd *et al.* (1995), the use of a quadrupole mass spectrometer (QMS) for on-line analysis of gas (from gasification process) was reported. Nevertheless, this method was limited due to its complexity, and it was only tested for a very narrow range of concentrations of species in the gas (N_2: 48.0 – 50.8 vol.%; H_2: 13.4 – 14.2 vol.%; CO: 18.6 – 19.6 vol.%; CO_2: 12.7 – 13.5 vol.%; CH_4: 4.01 – 4.25 vol.%; O_2: 0.47 – 0.5 vol.%).

Although the QMS is already used in many industries, its use for the analysis of fuel gas streams is not so widespread (Karlegärd *et al.*, 1995; Cook *et al.*, 1999). In addition, despite being a well-established technique, there are still some technical difficulties in using it for on-line analysis of multi-component gas mixtures. For example, Turner *et al.* (2004) reported that the accuracy of measurements using a QMS was questionable due to the non-linearity and instability of this method. Quadrupole mass spectrometry separates the species by using the difference in mass-to-charge ratio (m/z) of ionized atoms or molecules; therefore, overlapping fragments at similar m/z values can make identification of species problematic.

4.2 GASIFICATION EXPERIMENTAL SETUP

In this chapter, the emphasis is placed on how the QMS was used, and more information on the purpose and design of the steam gasification of wood charcoal experiments is provided in Chapter 6.

The apparatus which was used for gas analysis, is illustrated in Figure 4.1. The gas flowed from the experimental gasifier through a cooler, and then any condensate was trapped in the first plastic vessel. The gas then passed through a cooling coil, where more of the liquid was condensed. It then flowed through a glass wool filter, and was finally discharged into the vent from the fume cupboard. Samples of gas were drawn from the exhaust line, and passed through another glass wool filter and a filter coalescer, before going to a gas chromatograph (GC) and a QMS for analysis. So as not to damage the analytical equipment, this system of filters helped to remove the majority of tars and particulates in the gas stream.

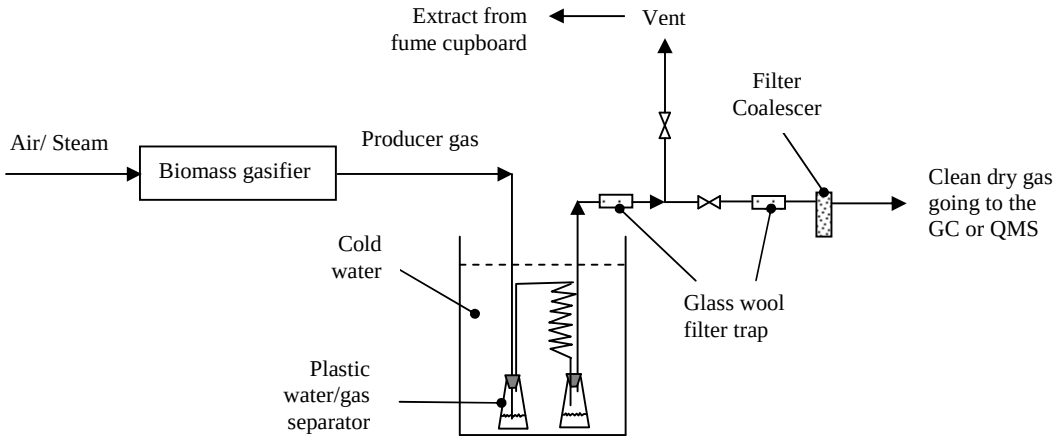

Figure 4.1 Outline schematic of the gasification experiment, focusing on gas analysis.

4.3 THE QUADRUPOLE MASS SPECTROMETER

Quadrupole mass spectrometry separates the species by using the difference in mass-to-charge ratio (m/z) of ionized atoms or molecules. Therefore, it is very useful to quantify atoms or molecules, and to determine chemical and structural information about molecules. Each molecule has its own distinctive fragmentation patterns that help to identify its structure. Further information can be found in the literature (e.g. Watson and Sparkman, 2007, pp. 53-177). In this study, a standard Hiden HPR-20 Quadrupole Mass Spectrometer was used, making use of Hiden's MASsoft software. This enabled data to be reviewed, and it had export facilities that were compatible with the Windows™ operating systems.

In the subsections that follow, the information that is presented has been obtained from various manuals and brochures on the QMS system from Hiden Analytical Limited.

4.3.1 Quadrupole Mass Spectrometer Specifications (Hiden Analytical Limited, 2004)

Gases and vapours are sampled continuously from atmospheric or near-atmospheric pressure *via* a flexible, heated Quartz Inert Capillary (QIC) inlet (see Figure 4.2 (b)).

(a) Hiden HPR-20 Quadrupole Mass Spectrometer

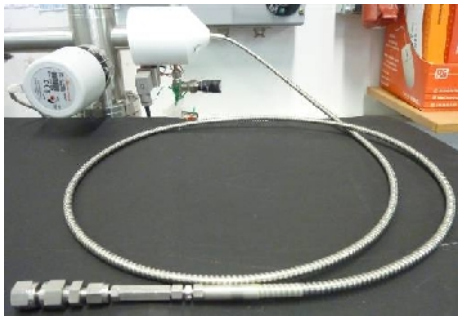

(b) Heated Quartz Inlet Capillary (QIC) line

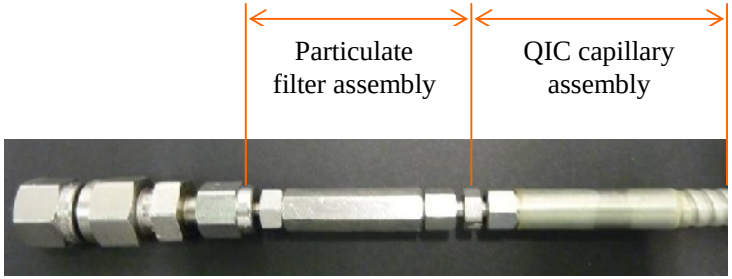

(c) Magnified picture of the tip of the QIC line

Figure 4.2 Pictures of the Hiden HPR-20 Quadrupole Mass Spectrometer used in this thesis.

The QIC inlet responds to changes in gas composition in less than 300 milliseconds and multiple gases can be measured simultaneously as a function of time and/or temperature. Gas concentrations may be tracked over a wide dynamic range (percent to ppb levels) at sampling rates of more than 50 data points per second.

The entire gas analysis package operates under the control of Hiden's versatile MASsoft software providing extensive data handling, review and export facilities that are compatible with Windows™ operating systems.

More detailed information on the QMS is provided in Table 4.1.

Table 4.1 Specifications of the Quadrupole Mass Spectrometer Hiden HPR-20 (Hiden Analytical Limited, 2004).

Specifications	Description
Sample pressure	100 mbar to 2 bar (options to 30 bar)
Sensitivity	100 ppb with standard single filter quadrupole 5 ppb with optional triple filter quadrupole
Mass range	200 amu (300, 500, 1000 amu options)
Detector	Dual Faraday/ Electron Multiplier
Ion source	Detect inlet twin filament electron impact ion source
Soft ionisation	0-150 eV in 0.1eV increments
Inlet type	2 metre, heated quartz inert capillary
Capillary temperature	Up to 200^{o}C
Gas consumption rate	20ml/min with options down to 1ml/min
Response	<300 msec
Acquisition rate	50 mass channels/sec
Library	72 species library with cracking patterns
External inputs	x2 (0-10 V) user configurable
Acquisition control	Extensive range of analogue (e.g. start/stop/pause) and digital I/O
Operating system	Windows^{TM} NT/98/2000/XP
Communications	RS232/Ethernet

4.3.2 Quadrupole Mass Spectrometer Configurations (Hiden Analytical Limited, 2004)

The configuration of HPR-20 *QIC* systems varies depending on the exact specification. Figure 4.3 shows a typical basic HPR-20 *QIC* system with the main system components labelled.

The complete HPR-20 *QIC* Benchtop Gas Analysis System comprises:

- HPR-20 *QIC* ultra high vacuum (UHV) housing with:
  - Conflate flange type ports for turbo pump, Probe, Penning gauge and inlet
- Vacuum pumping system comprising:
  - 60 litre per second turbomolecular pump with controller
  - Rotary backing pump
  - Automatic vent valve with vent delay
  - Cold cathode (Penning) gauge providing protection interlock
- QIC capillary inlet with:
  - 2 metre heated capillary with heater supply, operating up to 200^{o}C
  - Replaceable inert quartz capillary liner
  - Direct ionisation source inlet with replaceable platinum orifice leak
  - Variable bypass control valve and rotary bypass pump
  - Inlet particulate filter with replaceable element
- Quadrupole mass spectrometer comprising:
  - Quadrupole probe with:
    - 200 amu mass range capability
    - Dual Faraday / Electron Multiplier detectors
  - RF (Radio Frequency) Head with:
    - RF generator and pre-amplifier electronics
  - RC (Radio Communication) Interface unit with:
    - Microcomputer controlled data acquisition system
    - Power supply electronics
    - Variable supplies for Probe lenses
    - RS232, RS422 and Ethernet LAN serial communications interfaces
- MASsoft PC software including:
  - Full suite of data display modes
  - Quantitative analysis software with percentage, PPM and PPB data output
  - Comprehensive data export facilities
- Serial communications cables and mains supply cables
- Comprehensive set of manuals and spares kit

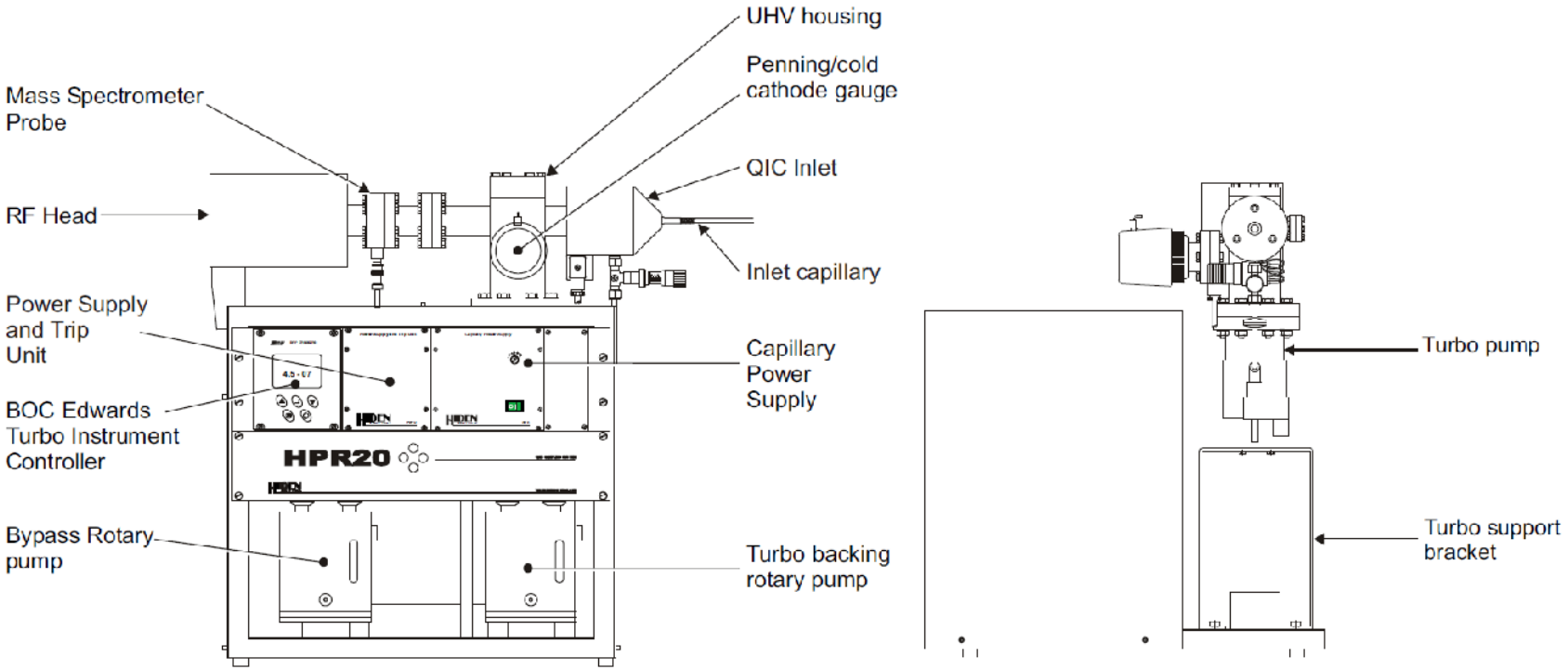

Figure 4.3 Typical HPR-20 QIC Benchtop Gas Analysis system (Hiden Analytical Limited, 2004).

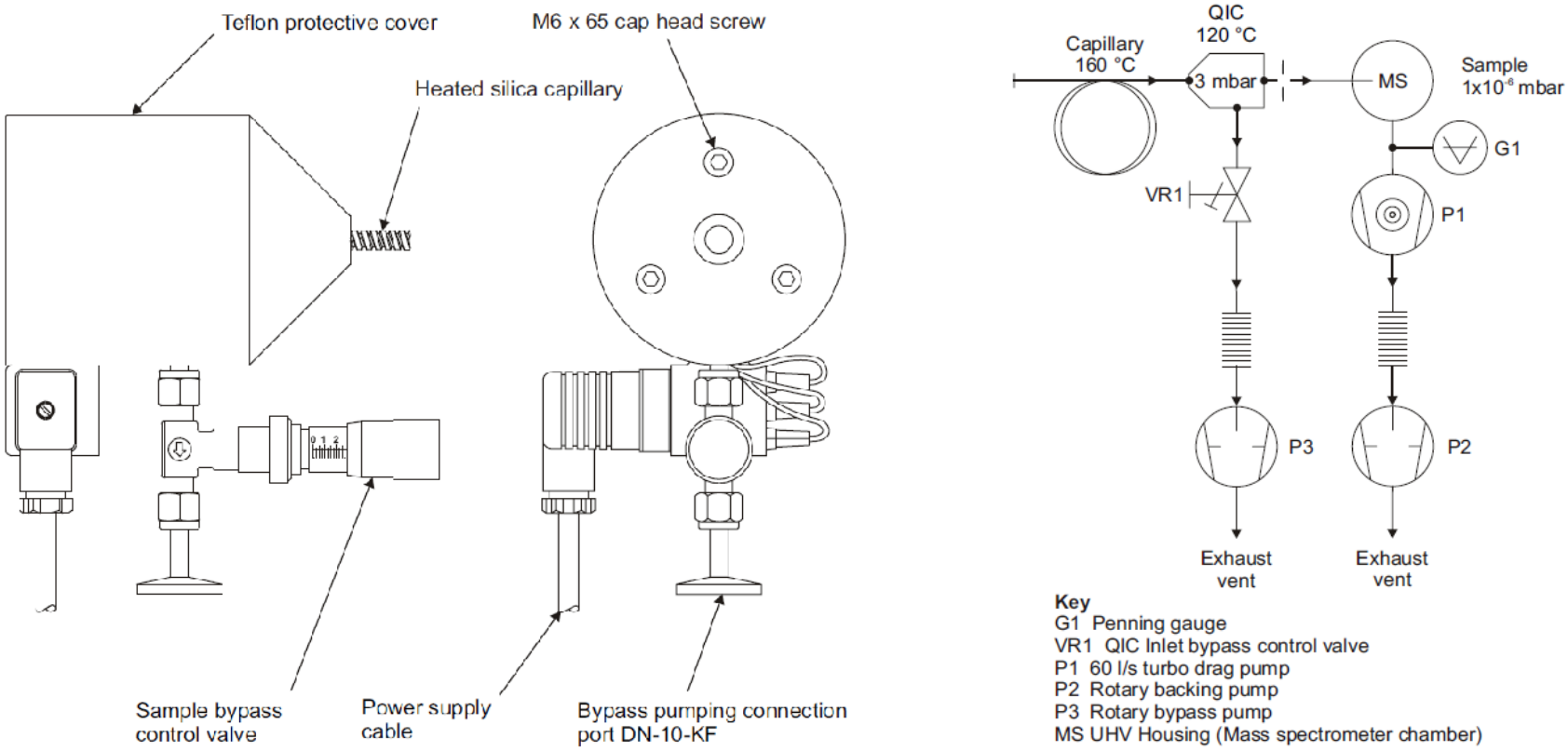

Figure 4.4 QIC-molecular leak inlet flange end (a), and vacuum schematic (b) (Hiden Analytical Limited, 2004).

The Hiden QIC (Quartz Inert Capillary) Fast Sampling Capillary Inlet is shown in Figure 4.4. According to Hiden Analytical Limited (1998), the following key features relating to gas sample flow are highlighted:

a) The QIC provides a dynamic method of sampling reactive or condensable gases and vapours by a mass spectrometer. The inlet employs two pressure reduction stages to reduce sample pressure to an acceptably low level for the operation of the mass spectrometer ion source.

b) In the first stage, sample gas is drawn down the silica capillary by the action of the sample bypass pumping line. The sample gas exits the capillary at low pressure and high velocity. This flow impinges on a platinum orifice which provides the second stage pressure reduction directly into the mass spectrometer ion source.

c) The distance from the capillary exit to the orifice, and from the orifice to the ion source, is very short, typically 4 mm and 12 mm respectively. This provides maximum free transmission of sample gas directly to the ion source with minimum surface interaction or memory effects.

d) Condensation of vapours, or adsorption of active sample gas species, is minimised by continuous heating of the inlet capillary, orifice and sample bypass regions. The silica capillary is resistively heated by passing an electric current through the stainless steel capillary sheath which surrounds its entire length. The capillary electrical connections are configured to ensure that the sampling end connection remains at ground potential.

e) The orifice and sample bypass regions are heated by an integral cartridge heater. A bimetallic disk-type thermal cut out provides over-temperature protection to these regions. The capillary and cartridge heater current is controlled by a Capillary Temperature Controller.

4.4 SETTING THE OPERATING PARAMETERS ON THE QMS

Before a methodology can be developed, the operating parameters for the QMS need to be set. The resolution and sensitivity of the QMS depends on these conditions. After calibration, any changes in these parameters will result in adverse effects on the repeatability of the QMS (Turner *et al.*, 2004).

4.4.1 Detector Selection: Either a Faraday cup, or an Electron multiplier (SEM detector) may be selected depending on the concentrations of the species in the gas. To detect a trace level of gas, a SEM detector with a detectable pressure range from 1×10^{-7} to 1×10^{-13} torr would be selected, whereas, the Faraday detector would be suitable for a gas with a detectable pressure range from 1×10^{-5} to 1×10^{-10} torr (Hiden Analytical Limited, 2010).

In preliminary experiments, it was found that the selection of a suitable detector (or a combination of both SEM and Faraday) for a particular gas mixture affects not only the sensitivities, but also the measuring time. If the SEM detector is selected, it is necessary to calibrate the voltage applied for it to give an equivalent signal to that of the Faraday detector. This voltage value changes slightly depending on the mass number and helps to increase the sensitivity when measuring trace levels of gases.

4.4.2 Electron Emission: This allows the QMS to maximize sensitivity for a particular gas. The value of this parameter is selected for a particular gas mixture by using a calibration facility in MASsoft, in which the highest concentration of gas in the mixture should give approximately 1×10^{-5} torr (Hiden Analytical Limited, 2010). This comes from the fact that above this value, the signal becomes non-linear, leading to inaccurate results.

4.4.3 Electron Energy: This is normally set at 70eV (Hiden Analytical Limited, 2010), and this will singly and doubly ionize most species. However, to avoid 2^{nd} ionization (producing a signal at ½ mass) electron energy can be adjusted to optimize the signal without double ionization.

4.4.4 Measuring Time: For on-line analysis, measuring time is important and depends on a number of operating parameters such as: the detector used, acquisition range, dwell and settle times. It was found that reducing both the dwell and settle times, and narrowing the acquisition range, helped to increase the number of measurements per minute. However, these values need to be optimized to avoid an undue reduction in accuracy.

4.4.5 Operating Pressure: During experiments, it was noticed that any change in the base pressure (the vacuum operating pressure), after correct calibration, had a strong negative effect on the accuracy of the measurement. This is consistent with findings in Turner *et al.* (2004). Thus, during an experiment, this operating pressure must be carefully monitored and adjusted (by using the sample by-pass control valve).

4.4.6 General Operating Procedure: This is an important factor, and was also found to affect the accuracy of the measurements (also discussed in Turner *et al.* (2004)). In this thesis, both the Faraday and the SEM detectors were used to analyze gas mixtures containing: N_2, CO, H_2, CO_2, CH_4, and trace gases of O_2, H_2S and COS. The values of SEM detector's voltage, electron emission, electron energy were optimized and set at 910V, 250uA and 70V, respectively. The analysis frequency was up to 10 samples per minute, which was adequate for many of the applications studied in this thesis.

The QMS was started-up and left running for at least two days to obtain ultimate base pressure and stability prior to measurement. Then, the filaments were also switched on and left running for 24 hours (to warm-up) prior to measurement. A final base pressure of 1.6×10^{-6} torr was achieved.

4.5 DEVELOPMENT OF THE 'METHODOLOGY' WITH THE QMS

4.5.1 Challenges

Turner *et al.* (2004) reported that mathematical methods are important to provide both qualitative and quantitative information from mass spectra. Basically, these methods are based on the assumption that the measured spectrum is linear for each pure component (Patnaik, 2004, pp. 10.24-10.26; Hoffmann and Stroobant, 2007, pp. 264-265). However, if the sample was a complex mixture, then considerable errors were noted (Karlegärd *et al.*,

1995; Turner *et al.*, 2004; Hoffmann and Stroobant, 2007, pp. 265-266). In attempts to solve this problem, some other methods have been developed (Cook *et al.*, 1999; Hoffmann and Stroobant, 2007, pp. 260-270), in which normalization methods are frequently employed.

When using a QMS to measure a real gas mixture, it is often difficult to separate some of the species in the mixture due to spectral interference and the extensive fragmentation of the ions produced (Hoffmann and Stroobant, 2007, pp. 71-72). This is particularly the case for organic species, which, because of their characteristics, have complex cracking patterns. In theory, this problem may be solved by the selection of non-interfering peaks. However, in practice, this is not always easy to do, and may be very difficult.

The gas stream to be analyzed may consist of H_2, CO, N_2, O_2, CO_2, CH_4, H_2O, C_2 & C_3 hydrocarbons, argon, longer chain hydrocarbons such as tars, and other contaminants such as sulphur and nitrogen compounds. In this study, a method was developed to measure the concentrations of the main gases (H_2, CO, N_2, CO_2, CH_4) and the trace gases (O_2, H_2S and COS) in a dry gas stream. In this case, three gases consisting of N_2, CO and CO_2 exhibit similar cracking patterns in the mass spectra. This can be problematic to even the experienced 'mass-spectrometerist'. Karlegärd *et al.*, (1995) also reported that the quantification of N_2 and CO in gas mixtures (biomass gasification) was a problem for QMS analysis. According to Cook *et al.* (1999): "in normal operation, a QMS does not have sufficient resolution to distinguish 'isobars' (ions of different elemental composition but the same nominal mass; e.g., CO at 27.99491 Da and N_2 at 28.006 Da both have nominal mass '28')."

An example of such a complex scheme, for a sample taken in this thesis of producer gas, is shown in Figure 4.5.

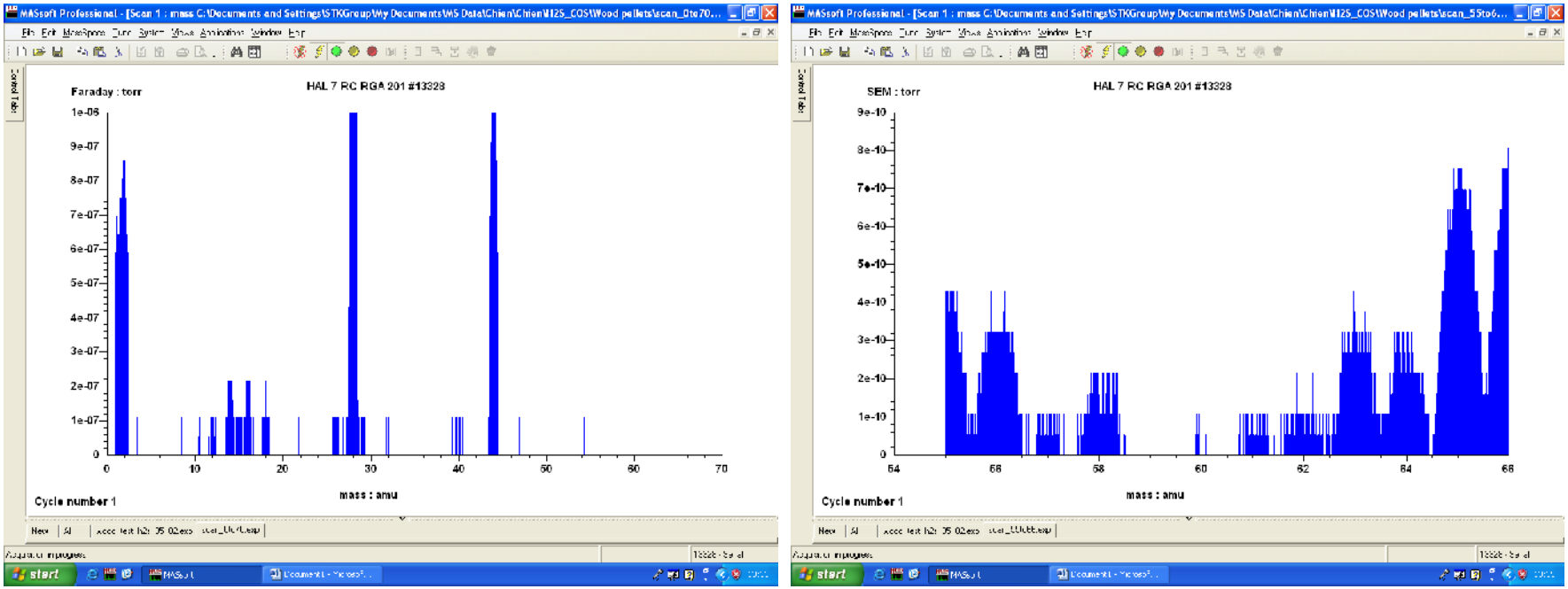

Figure 4.5 Example of a raw QMS profile for a sample of producer gas.

In order to construct a method for on-line gas analysis (with the QMS), it is best to deal with as few mass fragments as possible. This helps to reduce the complexity of the method, leading to a reduction in the measuring time of each measurement, thereby increasing the analysis frequency. However, for a complex gas mixture, the use of more fragments could improve the accuracy of measurements. For example, Karlegärd *et al.* (1995) encountered difficulties when trying to analyze the gas produced (gasification of biofuel) when they selected mass fragments of m/z(12), m/z(14), m/z(28) and m/z(44) to separate N_2, CO and CO_2. In their work, they used the method (called the external method) that attempted to determine absolute analyte concentrations from absolute signal intensities. In other words, they considered that the measured intensities were proportional to the concentration. This method, according to Cook *et al.* (1999) and Hoffmann and Stroobant (2007, pp. 264-266), is considered not to provide good measurement repeatability, due to the difficulty of precisely controlling operating parameters such as electron emission from the hot filament.

Therefore, in this thesis, in aiming to improve the speed and the accuracy of the analysis method, fewer mass fragments would be used. Normalizing to the total ion current (estimated by summing the peaks) is selected to build the method. This method (called the internal standard) is based on a comparison of the intensities of the signal, corresponding to the product that has to be quantified, with the signal of a reference compound.

4.5.2 Building the Method (Methodology)

In order to quantify the individual components in the gas mixtures (from the experiments), the following steps were taken:

- All molecular ions / significant peaks had to be identified.
- The peaks corresponding to known components in the mixture had to be identified.
- The remaining peaks had to be assigned, noting: the general appearance of the spectrum and checking for peak clusters (from isotope patterns and low-mass neutral fragment loss).
- The results had to be compared with reference spectra on the database (Patnaik, 2004, pp. 10.13-10.23).

A number of spectra were selected to create the mathematical method for quantification. Table 4.2 shows the mass fragments used in that analysis.

Table 4.2 Gas analysis matrix used for the QMS in this thesis.

Component	Mass							
	2	14	15	28	32	34	44	60
H_2	x							
CH_4		x	x					
CO_2				x			x	
N_2		x		x				
CO		x		x				
O_2					x	x		
H_2S					x	x		
COS								x

Note: Analysis of the H_2S and COS species, is developed further in the following chapter in this thesis.

Presented as the most intensive signal (the main peak) compared to the others (the minor peaks), the ion-molecule fragment of a species is often chosen. However, for CH_4, because there is an overlap with oxygen at the value of m/z(16), the minor peak of CH_4 at m/z(15) was selected. From the information presented in Table 4.2, the partial pressures of H_2, CH_4 and CO_2 were derived at peaks corresponding to values of m/z(2), m/z(15) and m/z(44), respectively.

For H_2, CH_4, and CO_2, the values of raw data do not need to be corrected. Therefore:

$$\begin{cases} P_{H_2} = P_{m/z(2)} \\ P_{CH_4} = P_{m/z(15)} \\ P_{CO_2} = P_{m/z(44)} \end{cases} \tag{4.1}$$

where: P_i and $P_{m/z(j)}$ are the corrected partial pressure of component i and the raw partial pressure recorded by the QMS at peak m/z(j), respectively.

For N_2 and CO, because there are overlaps with some of the species:

- the partial pressure of N_2 was derived from the m/z(14) N_2 minor peak, which was corrected for CH_4 and CO overlaps, while
- that of CO was derived from the m/z(28) peak, corrected for N_2 and CO_2 overlaps.

The following equations were applied to separate N_2 and CO. They were put into the calculation loops of the mathematical method.

The partial pressure of N_2, after being corrected for CH_4 and CO overlaps:

$$P_{N_2} = P_{m/z(14)} - P_{CH_4} \frac{C_{CH_4(14)}}{C_{CH_4(15)}} - P_{CO} \times C_{CO(14)} \tag{4.2}$$

The partial pressure of CO, after being corrected for N_2 and CO_2 overlaps:

$$P_{CO} = P_{m/z(28)} - P_{N_2} \times \frac{1}{C_{N_2(14)}} - P_{CO_2} \times C_{CO_2(28)} \tag{4.3}$$

where: $C_{i(j)}$ is the ratio of partial pressure of component i at peak m/z(j) to that of component i at the main peak (the highest peak of component i), and can be collected from the software's library. However, these ratios change, depending on the operating parameters. Thus, in this thesis, they were calculated by calibration at operating conditions.

For the species, H_2S and COS, very careful checks were performed to avoid spectral interference with other species (e.g. main gases, tars, and other contaminants). Thus, the non-interfering peak of m/z(60) was chosen for COS, whereas H_2S partial pressure was derived from the m/z(34) peak, corrected for O_2 overlap. Similarly, partial pressure of O_2 was derived from the m/z(32) peak, corrected for H_2S overlap.

The partial pressure of COS:

$$P_{COS} = P_{m/z(60)} \tag{4.4}$$

The partial pressure of H_2S, after being corrected for O_2 overlap:

$$P_{H_2S} = P_{m/z(34)} - P_{O_2} \times C_{O_2(34)} \tag{4.5}$$

The partial pressure of O_2, after being corrected for H_2S overlap:

$$P_{O_2} = P_{m/z(32)} - P_{H_2S} \times C_{H_2S(32)} \tag{4.6}$$

Finally, the concentrations of the species were calculated from:

$$x_i = \frac{\left(P_i / RS_i\right)}{\sum_i \left(P_i / RS_i\right)} \tag{4.7}$$

where: x_i and RS_i are the calculated concentration and relative sensitivity (RS value) of component i, respectively.

4.5.3 Calibration

To quantify the gases in a mixture, it is necessary to calibrate the Relative Sensitivity (RS) values. RS is a factor which takes into account the sensitivity of different species dependent on the efficiency of the quadrupole. It is best to determine these for the specific QMS used, at its particular set of operating conditions. The calibration requires a known gas mixture, and the highest concentration of gas is assigned a sensitivity of 1 (in this study, N_2 was selected and became the reference gas).

$$RS_i = \frac{P_i}{P_{N_2}} \times \frac{x_{N_2}}{x_i} \tag{4.8}$$

where: x_{N_2} and x_i are the known concentrations of reference gas N_2 and component i, respectively.

The gas mixture used to test the GC (see Section 3.2.2), was then used to calibrate the QMS, for the main components in the gas. For the trace gases, the RS values of H_2S and COS with N_2 as the reference gas were calculated by calibration with 2000 ppm H_2S in N_2, and 200 ppm COS in N_2.

4.6 COMPOSITION OF THE PRODUCER GAS – STEAM GASIFICATION OF WOOD CHARCOAL

To check the reliability of the developed QMS method in this thesis, experiments were performed on the steam gasification of wood charcoal, and the results from the QMS were then compared with measurements on the GC.

Experimental conditions were as follows:

- molar ratio H_2O:N_2 was 2:1 (nitrogen gas was fed with the water, and this helped to create a more complex gas mixture which would represent producer gas),
- the N_2 flow = 0.1 litre/min (NTP),
- the H_2O flow = 0.148 g/min, and
- the reactor tube (i.d. = 9.5 mm) packed with wood charcoal (particles 4 mm in diameter, depth = 330 mm).

The gasification experiments were then performed at conditions during which the temperature of the furnace (hence gasification temperature) was gradually increased over time. This generated a wide range in gas compositions over time, to test the method. Gas samples were also taken at 5½ min intervals for comparative analysis on the GC.

The results of such an experiment over a 45 min period are illustrated in Figure 4.6, where the change in composition of the following key 6 species was monitored: N_2, H_2, CO, CO_2, O_2 and CH_4.

The data from the QMS is presented as a continuous curve (because measurements are frequent), and the data from the GC is in the form of discrete data points. From these results it is clear that:

- a good match was obtained between the QMS and GC,
- as the gas composition was measured over a wide range of concentrations (which arose as a result of the experiment), the match between the QMS and GC remained very good. For example:

- For N_2 in the range of 21 to 100 vol.%, it was within ± 2.1 %.
- For H_2 in the range of 0 to 44 vol.%, it was within ± 2.7 %.
- For CO in the range of 1.2 to 29 vol.%, it was within ± 3.7 %.
- For CO_2 in the range of 2 to 14 vol.%, it was within ±2.1 %.
- For CH_4 in the range of 0.45 to 1 vol.%, it was within ±12.7 %.

Big differences only occurred at low concentrations of CO, CO_2, and CH_4.

In general, these results were most satisfying, as the methodology was shown to work and produce good results.

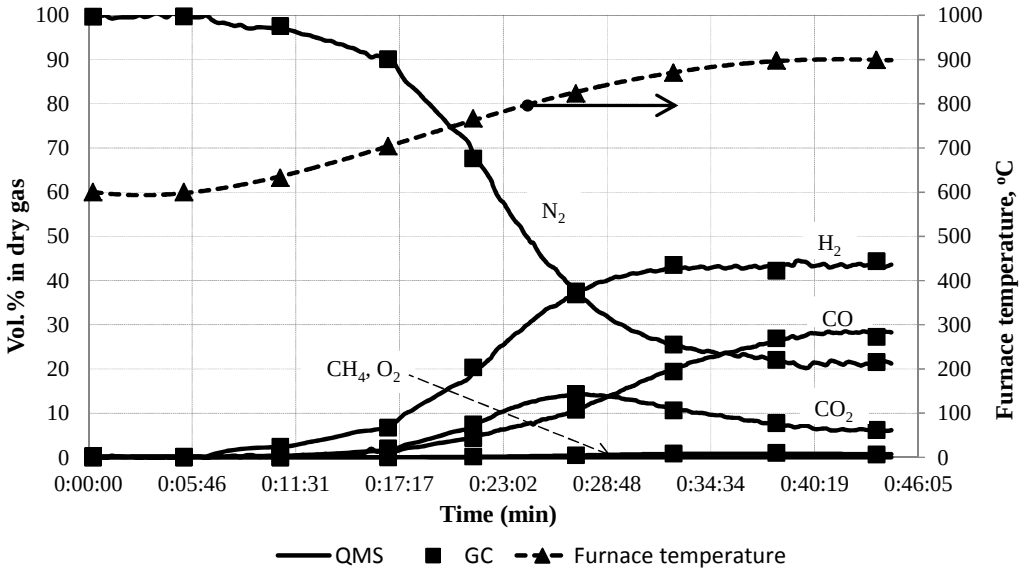

Figure 4.6 Comparison between QMS and GC measurements (data points correspond to GC measurements).

To check on the accuracy of the method for O_2 detection, a quick test was run using an air cylinder. This was tested in 'as supplied form', and it was also diluted by 50 % with nitrogen (using rotameters). The results obtained were close to the expectation. For example, for air it was about 23 vol.%, slightly higher than the real number (21 vol.%). For air diluted by 50 % with nitrogen, it was about 11 vol.%, which was close to the expected number (10.5 vol.%). Therefore, together with the fact that the QMS was calibrated at 7.5 vol.% of O_2, and the method showed no O_2, as expected, in the gas stream produced from steam gasification of wood charcoal (see Figure 4.6), it may be concluded that the method is good enough to quantify O_2 in the range of 0 to 21 vol.%.

Repeatability check: To check the repeatability of measurements with the QMS, a bag-sample of gas was taken during an experiment (steam gasification of char). To this bag a quantity of air was added from a gas cylinder, so that O_2 was also present. The gas was then connected to the QMS sampling line. The repeatability was checked over a 10-minute period, during which it was found that the average composition of the species was:

N_2 = 38.56 (± 0.29) vol.%,

CO = 12.9 (± 0.09) vol.%,

H_2 = 33.65 (± 0.32) vol.%,

CO_2 = 9.31 (± 0.04) vol.%,

O_2 = 5.02 (± 0.01) vol.%, and

CH_4 = 0.56 (± 0.0) vol.%.

Repeatability is also illustrated in Figure 4.7, showing measurements taken with the QMS on the same gas mixture over a 13-minute test period.

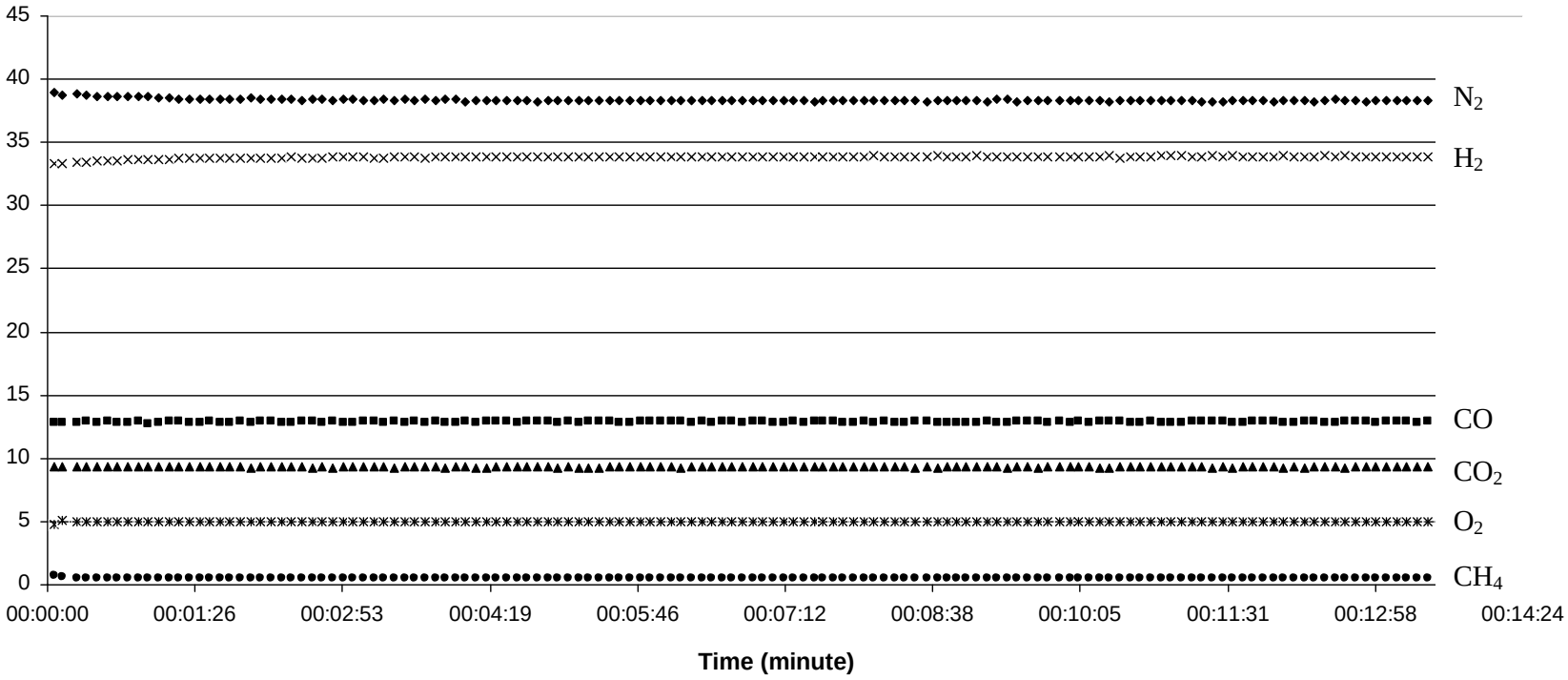

Figure 4.7 A repeatability test of gas analysis with the QMS.

4.7 CONCLUDING REMARKS

(a) Recognizing the difficulty of using the QMS to analyze in a quantitative manner complex mixture of gases, a method has been successfully developed (also listed in Appendix 2). This was tested by measuring the gas composition from the steam gasification of wood charcoal. A good match was obtained between the results from the QMS and the GC. These measurements were also close over a wide range of gas concentrations (N_2: 21 to 100 vol.%; H_2: 0 to 44 vol.%; CO: 1.2 to 29 vol.%; CO_2: 2 to 14 vol.%; CH_4: 0.45 to 1 vol.%; and O_2: 0 to 21 vol.%).

(b) In comparison with the use of the GC, the on-line measurement technique with the QMS provides quick results (almost in real time). This provides a great opportunity to follow transient experiments.

(c) It was shown that an acceptable level of repeatability was attainable with the QMS, and it was stable over a number of months, without needing to be re-calibrated.

(d) Operating parameters set on the QMS had a strong effect on the resolution and sensitivity. Therefore, it is important to optimize them for a particular gas mixture prior to developing a method to interpret the raw data obtained.

(e) It is important to emphasize that dirty gas streams must be cleaned of contaminants which could condense or form deposits in the QMS capillary lines. Otherwise, the inlet filter (used to protect the capillary sampling line) may become blocked. Also, if contaminants condense inside the capillary line, these will start to cause measurement errors, and then the base pressure may also change during the set of measurements.

(f) Finally, the method that has been developed for the QMS works well, and in the chapters that follow, this technique will be used, and it will also be enhanced to measure more complex species in the gas.

REFERENCES

Cook, K.D., Bennett, K.H. and Haddix, M.L. (1999). On-line Mass Spectrometry : A Faster Route to Process Monitoring and Control. Ind. Eng. Chem. Res., Vol. 38, pp. 1192-1204.

Hoffmann, E.D. and Stroobant, V. (2007). Mass Spectrometry principles and applications. 3rd edition, John Wiley & Sons Ltd.

Hiden Analytical Limited (2010). Training Materials, provided by Hiden Analytical Limited in the training course in the University of Bath, Bath, United Kingdom.

Hiden Analytical Limited (2004). HPR-20 QIC gas analysis system manual. Document Number: HA-085-092.

Hiden Analytical Limited (1998). QIC fast sampling capillary inlet user manual. Document Number: HA-085-027.

Karellas, S. and Karl, J. (2007). Analysis of the product gas from biomass gasification by means of laser spectroscopy. Optics and Lasers in Engineering, Vol. 45, pp. 935-946.

Karlegärd, Å., Götz, A., and Bjerle, I. (1995). On-Line mass spectrometer analysis of gasification gas. Chemical Engineering & Technology, Vol. 18, Issue 3, pp. 183-192.

Patnaik, P. (2004). Dean's Analytical Chemistry Handbook. 2nd edition, McGRAW-HILL.

Tuner, P., Taylor, S., Clarke, E., Harwood, C., Cooke, K. and Frampton, H. (2004). Calibration effects during natural gas analysis using a quadrupole mass spectrometer. Trends in Analytical Chemistry, Vol. 23, No. 4, pp. 281-287

Watson, J.T. and Sparkman, O.D. (2007). Introduction to Mass Spectrometry. 4th edition, John Wiley & Sons Ltd.

CHAPTER 5

Consideration of the Presence of H_2S and COS in the Producer Gas Stream and Implication on the Gas Clean-Up Technology: Calculation and Measurement

Following on from the discussion in Chapter 2 (Section 2.3.4), the removal of SO_2 and H_2S from the dirty producer gas was considered to be relatively easy (e.g. by scrubbing); however, the removal of COS is more difficult. As a reminder, any residual sulphur compounds in the gas:

(a) may act as catalyst poisons and affect the performance of the catalysts used to clean-up the emissions in the exhaust gas (after the gas engine), or

(b) when burnt in the gas engine, are likely be converted to oxides of sulphur, which could exceed the WID limits in the exhaust gas emissions from the plant.

Therefore, to help with the development of a suitable gas clean-up strategy, the presence of COS species is considered in more detail in this chapter, under the following themes:

- Theoretical thermodynamic equilibrium calculations: based on published information on gas composition from a gasifier, a theoretical study was performed to identify the possible ratio between H_2S and COS species.

- Experimental gasification in the quartz-tube reactor: measurements were taken when wood, straw and RDF pellets were gasified, and the ratio of H_2S and COS species was quantified. This also necessitated an extension to the methodology in the way the QMS was used.

The work on the theoretical equilibrium calculations was recently published in Kolaczkowski *et al.* (2011)[*].

The paper was also presented in a poster presentation at the 2010 BIOTEN conference by the author of this thesis. The co-author Dr Awdry is a co-supervisor of this PhD thesis.

5.1 INTRODUCTION

In a down-draft air biomass gasifier, the fuel to air equivalence ratio is about 0.25 (Knoef (2005, p. 17). This means that only 25 % of the stoichiometric requirement of air (to achieve complete combustion) is provided. The reactions between hydrogen and sulphur compounds are likely to lead to the formation of H_2S, and the oxidation reactions could lead to the formation of SO_2. However, other reactions can also lead to the formation of lower quantities of COS. For example, based on information in the literature, Higman & Burgt (2008, p. 209) highlight the importance of the following reversible reaction:

$$H_2S + CO \leftrightarrow H_2 + COS \qquad (5.1)$$

Depending on the source of RDF, its sulphur content will vary. As an example, based on information from one supplier (Kolaczkowski, 2009a), sulphur levels can vary from 0.12 to 0.17 wt.%, yet can even be as low as 0.09 wt.%, or peak as high as 0.3 wt.%. These variations have huge implications for the design of the subsequent gas clean-up processes, especially as the final emission limits on the plant must conform to the Waste Incineration Directive (2000/76/EC), otherwise known as WID limits.

If the producer gas is then used as fuel in a gas engine to produce combined heat and power (CHP), it could be argued that it is preferable to reduce the sulphur content of the fuel before the gas engine, rather than trying to remove it after the gas engine (although a

---

[*] Kolaczkowski, S., Le, C.D. and Awdry, S. (2011). Equilibrium reactions(s) involving H_2S and COS species – consideration of thermodynamics and implications on the biomass gasification process. In Proceedings of the bioten conference on biomass and biofuels 2010, Bridgwater, A.V. (Ed), CPL Press UK, pp. 733-744.

combination of the two is possible). Clean-up before the gas engine requires the removal of H_2S, SO_2 and COS, whereas if higher sulphur levels were fed with the fuel in the gas engine, clean-up after the gas engine (following the combustion reactions) would predominantly concentrate on SO_2 removal (as most of the H_2S and COS would have been oxidized).

From an engine maintenance perspective, feeding a heavily contaminated gas into a reciprocating engine is not desirable. Also, because of the dilution effect (as air is added), the volumetric flow rate of the exhaust gas is approximately 3 x higher than the producer gas fed into the engine. So purely from a volumetric perspective, the size of gas clean-up equipment could increase and so would the associated operating costs.

5.2 THEORITICAL THERMODYNAMIC EQUILIBRIUM CALCULATIONS

5.2.1 Estimate Concentration of Sulphur Compounds

A situation, where 2,000 kg/h of RDF are fed into a gasifier and approximately 3,200 Nm^3/h of dry gas are produced, is considered. This corresponds to a plant that would produce enough gas to generate about 2 MW of electrical output (from a gas engine). If the sulphur content of the RDF was 0.17 wt.%, then this would correspond to 3.4 kg/h of sulphur in the feed, which could turn to approximately the same amount of sulphur in the gas produced. In reality, some of this sulphur will also be present in the char from the base of the gasifier (e.g. Cioni *et al.*, 2002). For biomass gasification, Paasen *et al.* (2006) suggested that 70 to 90 % of the sulphur is released as H_2S and COS, but when RDF is gasified:

- only 50 to 60 % of the sulphur is released in a gaseous form,
- 10 to 30 % is retained in the solid fractions, and
- the fate of the remaining 10 to 20 % of sulphur is unknown.

However, this aspect <u>is not</u> included in the example calculations that follow.

Example calculation:

Assuming that:

(a) The gasifier operates at an equivalence ratio of 0.25, and therefore that 25 % of the sulphur compounds react with the oxygen to produce SO_2. This would lead to 0.85 kg/h of sulphur producing 1.7 kg/h of SO_2.

(b) About 93 to 96 % of the sulphur (use 94.5 %) could be in the form of H_2S and the rest as COS (based on information in the literature described in Higman and Burgt (2008, p. 233)). This means that:

- 2.41 kg/h of the remaining sulphur could be in the form of H_2S, and
- 0.14 kg/h of sulphur could be in the form of COS.

The material balance for the key sulphur species is summarized in Table 5.1.

Table 5.1 Summary of simplified sulphur balance in the dirty gas (assuming 0.17 wt.% sulphur in the RDF feed).

Species	kg/h of sulphur	kg/h of species	Concentration of species in dry gas, if not cleaned, mg/Nm^3
SO_2	0.85	1.7	531
H_2S	2.41	2.560	800
COS	0.14	0.263	82
	Total 3.4		

5.2.2 Impact of Sulphur Compounds on WID Limit

Based on information presented earlier in Section 2.2.2 (Tables 2.8 and 2.9), the target WID limit that would relate to the sulphur species present in the discharge from such a plant for SO_2, is:

- Daily average: <50 mg/m^3
- Half hourly average <200 mg/m^3(100 %)
  <50 mg/m^3 (97 %)

Assuming that the gas is used as a fuel in a gas engine, then if all of the sulphur species in Table 5.1 were fed into the engine as fuel, then these would be converted to 6.8 kg/h of SO_2. Allowing for the fact that as air is added to the engine, the exhaust gas flow is approximately a factor of x 3 higher than the fuel flow to the engine (allowing for the air used to combust the fuel (Kolaczkowski, 2009b)), then the concentration of SO_2 in the exhaust would be:

$$\frac{6.8\ [kg/h]}{3\times 3200\ [Nm^3/h]} \approx 708\times 10^{-6}\, kg/Nm^3$$
$$= 708\, mg/Nm^3$$

This would clearly be in violation of the WID limit, and gas clean-up is essential.

This calculation can also be done for COS on its own. If the concentration of COS remained at 82 mg/Nm^3 in the gas (see Table 5.1), which was then used as fuel, then this would be converted to SO_2 in the gas engine, and contribute:

$$\frac{1}{3}\times\left(82\left[mg/Nm^3\right]\times\frac{64\,[g/mol]}{60\,[g/mol]}\right)\approx 29\ \ mg/Nm^3 \text{ in exhaust stream,}$$

where: 64 [g/mol] and 60 [g/mol] are molar masses of SO_2 and COS, respectively.

So even from a WID limit perspective, it is important to consider the contribution that any COS would make if it was not reduced to a low level in the gas clean-up process. Also, as a reminder, for these calculations a 0.17 wt.% of sulphur was assumed in the RDF feed, yet in the source of RDF for which this composition was obtained, this could peak at 0.3 wt.% of sulphur in the RDF.

5.2.3 Impact on Gas Clean-up after the Gas Engine

The fuel components fed into the gas engine consist predominantly of hydrogen, CO and some hydrocarbons. Because of incomplete combustion (and some fuel slippage past the pistons) then a significant level of CO is expected in the exhaust gas, and a lower level of hydrocarbons (e.g. see discussion in Knoef (2005, p. 294)). In addition, because of the presence of nitrogen species in the fuel (and in the air), the NOx level could also be significant. This means that CO, hydrocarbons and the NOx emissions would need to be reduced. If a catalytic process is use to control these emissions, then the effect that the sulphur species in the exhaust may have on the catalyst(s) will need to be considered most

carefully. Failure to remove sulphur species to an adequate level could easily lead to WID limits being exceeded, and also lead to a deterioration in the performance of catalyst system(s) which in turn would affect WID limits (if the catalyst(s) were not replaced).

5.2.4 Thermodynamic Equilibrium Calculation

Giving due consideration to the presence of other species in the producer gas, thermodynamic equilibrium conditions are calculated (as a function of temperature, 300 to 1200 ºC).

To illustrate the method, the following reversible chemical reaction is considered:

$$H_2S + CO \leftrightarrow H_2 + COS \tag{5.1}$$

The basic steps in the calculations that follow (Equations (5.2) to (5.9), are described in many text books (e.g. Hayes and Kolaczkowski (1997, pp. 126 - 28).

The thermodynamic equilibrium constant:

$$K_a = \frac{a_{H_2}\ a_{COS}}{a_{H_2S}\ a_{CO}} \tag{5.2}$$

where: a_i is the activity of species, and K_a can be determined using well established methods from:

$$\ln(K_a) = -\frac{\Delta G_R^o}{R_g\ T} \quad \text{or} \quad K_a = \exp\left(-\frac{\Delta G_R^o}{R_g T}\right) \tag{5.3}$$

For the value of K_a to be valid at the reaction temperature, T_2, then ΔG_R^o needs to be evaluated at that temperature. Alternatively, K_a may be calculated at T = 298 K (calculating ΔG_R^o at 298 K – using values in tables), and then the value of $K_{a,298K}$ is corrected for temperature using the van't Hoff equation:

$$\frac{d \ln K_a}{dT} = \frac{\Delta H_R^o}{R_g\ T^2} \tag{5.4}$$

In order to integrate this expression, ΔH_R^o should be represented as a function of temperature. However, if ΔH_R^o does not change much with temperature (which is often the case for gas phase reactions), then the value evaluated at 298K could be used. So after integrating the expression from 298 K to T_2, then:

$$\ln\left(\frac{K_{a,T_2}}{K_{a,298K}}\right) = -\frac{\Delta H^o_{R,298K}}{R_g}\left(\frac{1}{T_2} - \frac{1}{298}\right) \tag{5.5}$$

For a gas phase reaction, the activity is the ratio of the fugacity of the component in the mixture, to its fugacity in the standard state (1 atm).

$$a_i = \frac{\hat{f}_{iv}}{f^o_{iv}} \tag{5.6}$$

From the equation describing the gas phase fugacity coefficient,

$$\phi_i = \frac{\hat{f}_{iv}}{P_i} = \frac{\hat{f}_{iv}}{y_i\ P} \tag{5.7}$$

Substituting Equation (5.7) into (5.6), then:

$$a_i = \frac{y_i\ P\ \phi_i}{f^o_{iv}} \tag{5.8}$$

Note: For any gaseous species: $f^o_{iv} = 1\ atm \equiv 1.013$ bar.

Because activity is a ratio of fugacities, it is dimensionless. This means that K_a is also dimensionless. Assuming ideal gas behaviour, then $\phi_i = 1$, and after substituting Equation (5.8) into (5.2), then the equilibrium constant may be written in terms of mole fraction or partial pressures as follows:

$$K_A = \frac{y_{H_s}\ y_{COS}}{y_{H_2S}\ y_{CO}} = \frac{p_{H_2} \times p_{COS}}{p_{H_2S} \times p_{CO}} \tag{5.9}$$

Note: as the reaction in Equation (5.1) is equimolar, total system pressure does not affect the equilibrium.

5.2.4.1 Starting Composition of the Gas Phase

Next, a gas phase composition is assumed for the exit stream from the gasifier. This is summarized in Table 5.2.

Table 5.2 Assumed gas phase composition used as a starting point in the calculation of equilibrium values.

	Dry gas composition Vol.% see note(1)	**Adjusted wet gas composition(4) Vol.%**
Hydrogen	16.84	14.1
Carbon monoxide	18.6	15.5
Methane + HC	5.54	4.6
Carbon dioxide	15.53	13.0
Nitrogen	41.15	34.4
Oxygen	2.34	1.8379 see note(2)
Water vapour		16.5 see note(3)
SO_2		0.0155 ≡ 155 ppm
H_2S		0.0440 ≡ 440 ppm
COS		0.0026 ≡ 26 ppm
Total	100.00	100.0000

(1) Based on $1MW_e$ scale gasifier using Municipal Solid Waste (MSW) as fuel: values in Akay et. al. (2007).
(2) Oxygen content was adjusted to allow for inclusion of the sulphur species.
(3) Water vapour content was estimated from overall material balance.
(4) Wet gas composition was adjusted, and a wet gas flow of 3828 Nm^3/h from the gasifier was estimated. The presence of other contaminants was ignored in this analysis.

In Akay *et. al.* (2007), an oxygen content of 2.34 vol.% was reported. However, this looks on the high side and may reflect ingress of oxygen into the process down-stream of the gasifier. Nevertheless, this value has been used, and the presence of small amounts of oxygen is also reported in other measurements in the literature (e.g. Cioni *et al.* (2002) report 1.6 and 2.0 vol.% in wet raw gas).

5.2.4.2 Example Calculation (Simplified Situation)

For the gas phase composition described in Table 5.2, and considering only the simple equilibrium reaction described in Equation (5.1), then using as a basis 100 moles, the gas phase compositions can be represented as:

$$y_{H_2} = \frac{14.1+\varepsilon}{100};\ y_{H_2S} = \frac{0.044-\varepsilon}{100};\ y_{CO} = \frac{15.5-\varepsilon}{100};\ y_{COS} = \frac{0.0026+\varepsilon}{100} \qquad (5.10)$$

where ε is the change in moles to achieve equilibrium.

From Equations (5.9) and (5.10):

$$K_A = \frac{(14.1+\varepsilon)(0.0026+\varepsilon)}{(15.5-\varepsilon)(0.044-\varepsilon)} \qquad (5.11)$$

From Equations 5.5 and 5.11, the variable ε can now be calculated, and this was done with the aid of routines in Matlab (listed in Appendix 3). Knowing ε as a function of temperature, the composition of the species in the gas phase can be calculated, and these results for H_2S and COS are presented in Figures 5.1 and 5.2. In these calculations, the presence of CO and hydrogen at high concentrations in the producer gas was included and influenced the calculated outcome. However, equilibrium reactions between the other species (i.e. methane and HCs, CO_2, N_2 and O_2) listed in Table 5.1 did not feature in this simple calculation – they were treated as behaving in an inert manner, so they only participated in the calculation of partial pressures and mole fractions.

These results were then compared with calculations using a commercial package known as Aspen Plus® (version 7.1), using Gibbs free energy minimisation. A discussion of the Gibbs energy minimisation method features in a number of sources (e.g. Abbott and Van Ness (1972, p. 270); Baratieri *et al.* (2008)).

In Aspen Plus®, the option based on 'phase equilibrium and chemical equilibrium' was selected. In these calculations only the basic equation described in Equation (5.1) was considered. The results of these simulations are presented in Figures 5.1 and 5.2, where it is clear that a good match is obtained with the two techniques. As expected for the single reaction described in Equation (5.1), as this is a reversible exothermic reaction, then as temperature increases, the equilibrium would be shifted to the left, and less COS would be formed.

This check between the two methods provides confidence in the way Aspen Plus® is being used, and interactions between other key species are now considered.

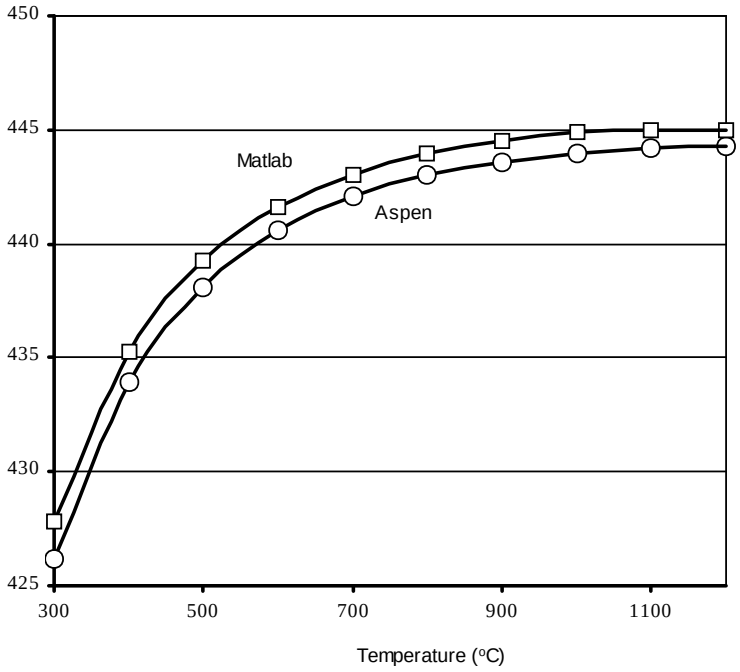

Figure 5.1 Variation in H_2S concentration – simulations using Matlab and Aspen.

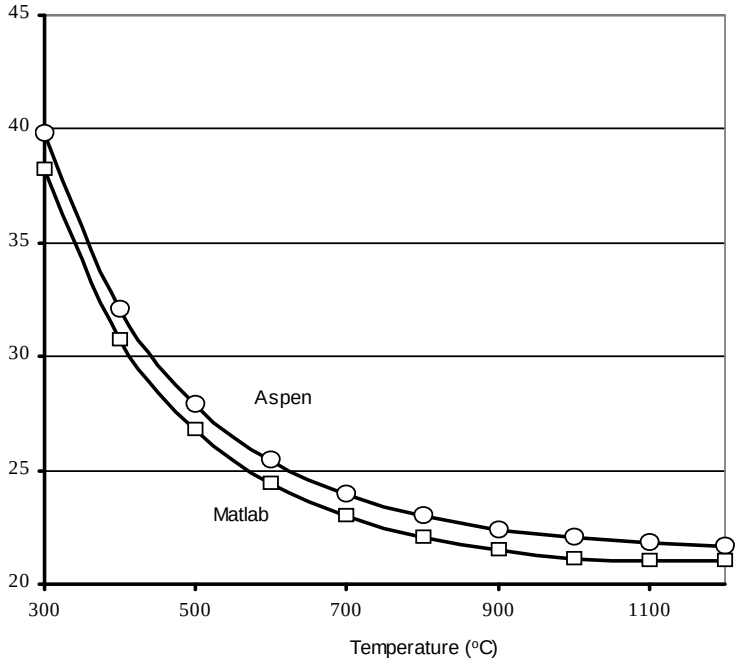

Figure 5.2 Variation in COS concentration – simulations using Matlab and Aspen.

5.2.4.3 More Complex Calculations

Making use of the software in Aspen Plus® (version 7.1), more complex calculations were performed where the interaction between many more species was considered, and this included: H_2, CO, CH_4. CO_2, N_2, O_2, H_2O, SO_2, SO_3, H_2S, COS, and CS_2.

(a) General discussion of species selected

To help explain the reason for the selection of some of these species, a brief discussion follows, in which the relevance of the species to a down-draft gasifier is discussed.

Based on information in the literature (e.g Yang *et al.*, 2008), COS is mainly formed by the following:

$$H_2S + CO \leftrightarrow H_2 + COS \quad \text{(key reaction)} \qquad (5.1)$$

In addition, COS may be formed from:

$$H_2S + CO_2 \leftrightarrow COS + H_2O \qquad (5.12)$$

From Equation (5.12), the presence of water has the effect of suppressing the formation of COS. Evidence for this may also be found in Yang *et al.* (2008), where experiments were performed on a ZnO/SiO_2 sorbent. In experiments on breakthrough in the bed (at 400ºC), the COS levels were:

- between 400 to 600 ppmv in the absence of water vapour, and
- 100 ppmv in the presence of 20 vol.% water vapour.

In a biomass gasification process, Reaction (5.12) is clearly important, as the water vapour content could be in the region of 15 vol.% (see Table 5.2). However, CO_2 also features in the gas, and from Reaction (5.12), an increase in CO_2 would push the equilibrium in the opposite direction and hence favour the formation of COS. In the particular example in Table 5.2, the CO_2 concentration is significant (i.e. 13 vol.%), but is less than the water

vapour content (15 vol.%). In further experiments in Yang *et al.* (2008), on the influence of CO_2 (on breakthrough in ZnO/SiO_2 sorbent), they concluded that CO_2 was not as active as CO in COS formation. Also of interest in their work is that they performed experiments in the absence of the sorbent (non-catalytic), and these indicated that the reactions observed in their sorbent bed were predominantly as a result of the catalytic effect. This is useful, as it provides an indication of how slow the homogeneous Reactions (5.1) and (5.12) would be at 400ºC.

They also stated that the COS formation mechanism is not well understood, and performed a number of experiments to try to understand the reaction pathway.

CS_2 has been included in the simulation, as it could be formed *via* the following reaction:

$$COS + H_2S \leftrightarrow CS_2 + H_2O \qquad (5.13)$$

However, in the biomass gasification reaction environment, in the presence of high water vapour content, the formation of CS_2 would be suppressed - so this reaction is probably of low importance. This is supported, as in a consideration of sulphur compounds that could be present in a coal gasifier (Wakker *et al.*, 1993), the presence of CS_2 is not even considered.

The range of sulphur species selected in this paper is also consistent with the range of sulphur species considered in Baratieri *et al.* (2008), where equilibrium calculations were performed on the syngas formed from the pyrolysis of pine saw dust.

(b) Simulations on a complex system using Aspen Plus®

The results of these simulations for H_2S and COS are presented in Figures 5.3 and 5.4. Comparing the results in Figures 5.3 and 5.4 with the simple reaction in Figures 5.1 and 5.2, it is clear that the change as a function of temperature is very different. This arises mainly because of the inclusion of additional species and the reversible reaction described in Equation (5.12). This has a very important effect on the way in which the equilibrium conditions will vary with temperature.

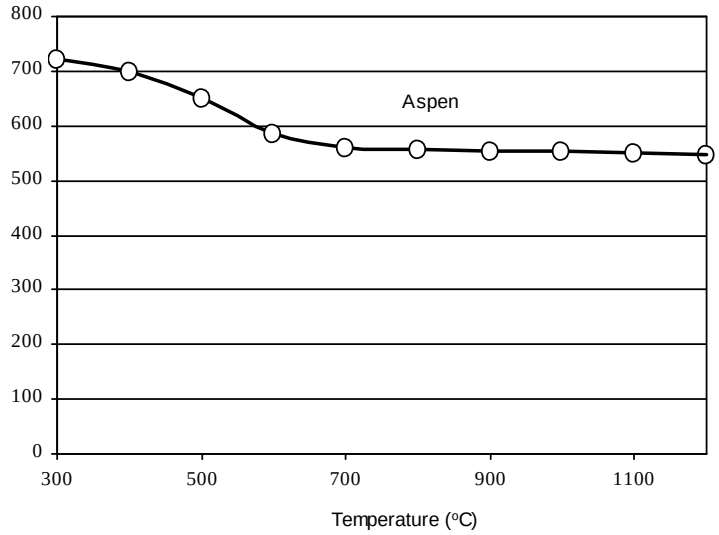

Figure 5.3 Variation in H_2S concentration – simulations on a complex system using Aspen Plus®.

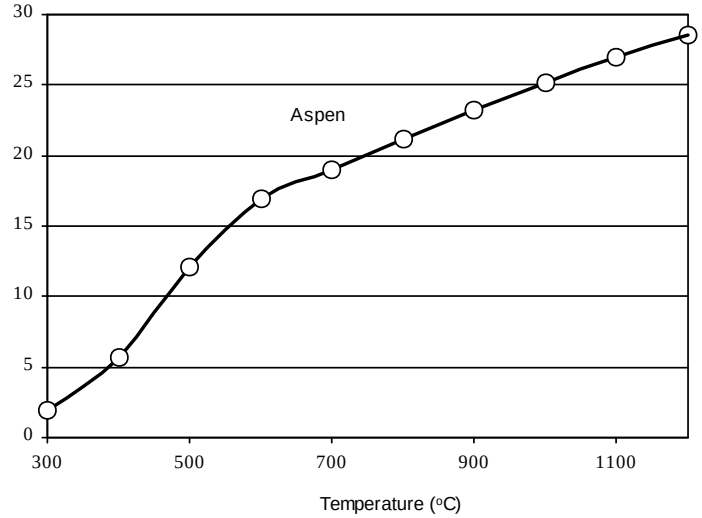

Figure 5.4 Variation in COS concentration – simulations on a complex system using Aspen Plus®.

The equilibrium conversion of all of the species considered is presented in Table 5.3.

Table 5.3 Variation of species – simulations on a complex system using Aspen Plus®.

Species	Temperature				
	300 °C	500 °C	700 °C	900 °C	1100 °C
H_2 (vol.%)	1.51	13.46	24.16	21.56	19.68
CO (vol.%)	0.05	4.33	16.62	19.68	21.56
CH_4 (vol.%)	12.50	7.39	0.15	0.00	0.00
CO_2 (vol.%)	26.00	23.67	14.16	11.15	9.27
N_2 (vol.%)	40.06	36.78	32.14	32.05	32.05
O_2 (vol.%)	0.00	0.00	0.00	0.00	0.00
H_2O (vol.%)	19.81	14.30	12.72	15.50	17.38
H_2S (ppmv)	721	652	561	555	551
COS (ppmv)	2	12	19	23	27
SO_2 (ppbv)	0	0	0	5	232
SO_3 (ppbv)	0	0	0	0	0
CS_2 (ppbv)	0	0	0	1	1

Looking more closely at Table 5.3, there are a number of interesting observations that can be made:

(i) The levels of CS_2 are very low. Based on earlier discussion, this is consistent with what was expected.

(ii) The SO_2 levels are very low, and SO_3 does not feature. So should the possible presence of SO_2 be neglected? This all depends on what is happening at the base of the down-draft gasifier:

- If the oxidation reactions are occurring in hot zones and the gases from those zones then mix with the gases produced from the pyrolysis/gasification oxygen-starved regions, SO_2 could be expected in the dirty syngas.
- However, if the gases from these two regions mix, and the residence time is adequate for further reactions to take place, then SO_2 concentrations would decrease and, depending on kinetics and residence time, would move in the direction of equilibrium.

If it can be assumed that:

- the reaction rate is high (at high temperature), and
- thermodynamic equilibrium could be reached quickly,

then the composition of the gas stream is established at high temperature (about 900°C) in the hot zone. Such results are also presented in the form of a simplified sulphur balance in Table 5.4. These can then be compared with the approximate calculations presented earlier in Table 5.1.

Table 5.4 Summary of simplified sulphur balance in the dirty gas (assuming 0.17 wt.% sulphur in the RDF feed; T = 900 ºC; thermodynamic equilibrium including the species: H_2, CO, CH_4. CO_2, N_2, O_2, H_2O, SO_2, SO_2, H_2S, COS, and SC_2).

Species	kg/h of sulphur	kg/h of species	Concentation of species, ppmv	Concentration of species in dry gas produced, mg/Nm^3	
			[From Table 5.4]		[Table 5.2]
SO_2	0.0	0.0	[0]	0	[531]
H_2S	3.264	3.468	[555]	1084	[800]
COS	0.136	0.255	[23]	80	[82]
	Total 3.4				

Table 5.4 shows that, at 900°C, the molar ratio of COS and H_2S is about 20:1.

By taking the values of the mass flow of sulphur in the Table 5.4, the percentage of sulphur in the feedstock converted into H_2S would be:

$$\frac{3.264[kg/h]}{3.4[kg/h]} \times 100\% = 96\%$$

and the rest was in the form of COS. This is still within the limits described earlier in Higman and Burgt (2008, p. 233).

5.2.4.4 Interim Concluding Remarks on Equilibrium Calculations

(a) The conversion of sulphur into SO_2 was considered at the very start, and then the distribution of sulphur between the COS and H_2S species was considered in more detail. With 0.17 wt.% sulphur in 2,000 kg/h RDF feed, and assuming 25% of the sulphur was oxidised, SO_2 concentrations could be significant in the dirty producer gas. However, when a more complex set of equilibrium calculations was performed, this indicated that SO_2 concentrations could be very low, and a greater quantity of H_2S and COS species would be formed from the sulphur in the feed.

(b) A closer study of the single $H_2S + CO \leftrightarrow H_2 + COS$ equilibrium reaction confirms the possibility of forming COS, and that its concentration decreases with an increase in temperature. This is consistent with the behaviour of an exothermic reaction. However, when a more complex scheme was considered (applying the Gibbs minimization technique), COS concentrations increased with temperature, and this was attributed to the inclusion of the $H_2S + CO_2 \leftrightarrow COS + H_2O$ reaction. However, what is interesting to observe is that COS concentrations varied from 12 ppmv at 500 ºC to 27 ppmv at 1100 ºC. This is a realistic range of temperatures in the reactions zones in a down-draft gasifier. Unfortunately, the situation is very complex in these zones, and it is difficult to assign a single temperature to represent the realistic conditions of reaction and attainment of equilibrium. The gas arises as a composite from various regions in the gasifier, and equilibrium conditions may not be attained.

(c) Using the more complex scheme of species, it would appear that SO_2 levels are predicted to be very low (< 1ppmv). However, the reality of this depends very much on the way in which the reactions take place in the gasifier. This is a complex matter, and it would be interesting to obtain some real plant data on this, when sulphur levels are high in the RDF. However, in practice it is probably less of a problem, as SO_2 is relatively easily scrubbed from the gas – although the production of more H_2S and COS species would need to be factored into the design.

(d) Considering the main basic reaction, $H_2S + CO \leftrightarrow H_2 + COS$, the presence of CO and H_2 species in the producer gas will affect the equilibrium calculations. However, as the concentration of CO and H_2 species was similar, they had opposing effects on the equilibrium reaction. On the other hand, the presence of both CO_2 and H_2O also influence the equilibrium in $H_2S + CO_2 \leftrightarrow COS + H_2O$, and as water vapour content is higher than the CO_2 content, then COS formation should be suppressed.

5.3 EXPERIMENTAL GASIFICATION IN QUARTZ-TUBE REACTOR

Using the experimental apparatus and techniques, described earlier in Chapter 3 (Section 3.2), experiments were performed with wood, straw, and RDF pellets, and the concentration of H_2S and COS species was quantified.

5.3.1 On-line Gas Analysis

Before the QMS could be used for on-line gas analysis, it is necessary to extend the methodology that had been developed earlier in Chapter 4 (Section 4.5).

The methodology was developed as follows:

(a) For COS the spectrum at m/z(60) was used.
(b) For H_2S the spectra at m/z(34) and m/z(35) were chosen. However, if O_2 is present in the gas stream, then it may contribute in the spectrum m/z(34); therefore, the partial pressure of H_2S was corrected by the contribution of O_2 at m/z(34).
(c) For O_2 the partial pressure of O_2 was derived from the m/z(32) peak, corrected for H_2S overlap.

Upgrading the QMS method developed in Chapter 4, the following equations were added:

For the partial pressure of COS:

$$P_{COS} = P_{m/z(60)} \tag{5.14}$$

For the partial pressure of H_2S at m/z(34), after correcting for O_2 overlap, then:

$$P_{H_2S} = P_{m/z(34)} - P_{O_2} \times C_{O_2(34)} \tag{5.15}$$

For the partial pressure of O_2 (after correcting for H_2S overlap), then:

$$P_{O_2} = P_{m/z(32)} - P_{H_2S} \times C_{H_2S(32)} \tag{5.16}$$

The spectrum at m/z(35) may also be affected by HCl. If HCl concentration can be considered to be very small, then this effect can be ignored. However, the chlorine content in some biomass fuel sources is quite high (e.g. Dias and Gulyurtlu, 2008; Kuramochi *et al.*, 2004; Drift *et al.*, 2001; Paasen *et al.*, 2006); thus, this may affect the accuracy of measuring H_2S in the producer gas stream.

According to Hiegl and Janssen (2009), commercial fuel pellets need to meet local requirements for their quality; e.g., the German standard, called DIN Plus, is applied for the United Kingdom. Therefore, if the wood and straw pellets used in this study met that standard, then their chlorine content would be less than 0.02 wt.%.

The chlorine content of RDF is expected to be higher than wood and straw pellets. An example of the chlorine content of the RDF can be found in Gendebien *et al.* (2003, p. 204), where it was reported to be typically in the range of 0.3 to 1.2 wt.% in dry basis, and mainly influenced by the level of plastics in the waste streams.

To correct for the partial pressure of H_2S at m/z(35) for the presence of HCl, a calibration mixture of HCl in N_2 is needed. In this study, H_2S was also measured using spectrum at m/z(35), but without correction of HCl overlap. The results from these measurements were then used to see if there was a presence of HCl in the gas streams produced from gasification of different biomass sources, and its influence on the accuracy of H_2S measurement at m/z(35).

Two methods were finally developed for the on-line analysis of the 8 gases, including: N_2, H_2, CO, CO_2, CH_4, O_2, H_2S and COS. In:

Method 1: the spectrum at m/z(34), with the correction of O_2 overlap, was used to measure H_2S.

Method 2: the spectrum at m/z(35), without the correction of HCl overlap, was used to measure H_2S.

The results from these two methods were then compared. To check on the accuracy of the methods, the following available gas mixtures were used:

- 2000 ppmv H_2S in N_2, and
- 200 ppmv COS in N_2.

These were tested in 'as supplied form', and they were also diluted by 50% with nitrogen (using rotameters). The results of such measurements are shown in Table 5.5.

From the results presented in Table 5.5, it is clear that both Method 1 and Method 2 could be used to measure the composition of H_2S and COS in the gas stream.

Table 5.5 Gas analysis with QMS – exploring the accuracy of the method developed.

Method 1 **m/z(34) for H_2S detection**			**Method 2** **m/z(35) for H_2S detection**			**m/z(60) for COS detection**		
Time (minute)	N_2 (vol.%)	H_2S (ppmv)	Time (minute)	N_2 (vol.%)	H_2S (ppmv)	Time (minute)	N_2 (vol.%)	COS (ppmv)
0:00:27	98.51	2060.55	0:00:27	99.16	0	0:00:27	97.9	192.83
0:01:00	99.35	2189.28	0:01:00	99.23	1109.25	0:01:00	98.3	195.45
0:01:33	98.71	2186.78	0:01:33	98.42	2103.22	0:01:33	98.38	193.52
0:02:09	99.29	2191.86	0:02:10	98.59	2012.04	0:02:06	98.61	197.69
0:02:54	99.07	2229.22	0:03:03	99.19	2083.66	0:02:54	98.49	197.31
0:03:42	99.04	2244.52	0:03:59	98.61	2107.85	0:03:48	98.99	193.12
0:04:31	98.76	2220.93	0:04:56	98.37	2097.54	0:04:43	98.36	195.41
0:05:19	98.61	2202.18	0:05:52	99.43	2112.45	0:05:37	98.17	201.12
0:06:08	98.84	2258.26	0:06:49	98.65	2126.37	**Extra dilution by 50% with N_2**		
0:06:57	99.11	2279.07	0:07:45	99.36	2159.46	0:06:32	98.89	98.68
0:07:45	98.87	2256.89	0:08:42	98.31	2124.6	0:07:29	98.66	96.15
Extra dilution by 50% with N_2			0:09:38	98.99	2155.53	0:08:26	98.84	96.38
0:08:33	99.26	1088.52	**Extra dilution by 50% with N_2**			0:09:23	97.88	95.98
0:09:22	99.06	1091.56	0:10:35	99.02	1073.83	0:10:20	97.78	95.92
0:10:11	98.98	1052.88	0:11:33	98.63	1035.25	0:11:17	98.42	95.92
0:10:59	98.84	1011.84	0:12:31	99.08	997.91	0:12:14	97.93	97
0:11:55	99.21	1009.11	0:13:30	99.4	992.46	0:13:11	97.85	118.84
0:12:49	98.98	1019.43	0:14:28	98.84	990.95	-	-	-
0:13:44	99.28	1021.13	0:15:26	99.16	996.18	-	-	-
0:14:37	99.51	1062.72	0:16:24	99.49	990.1	-	-	-

5.3.2 Composition of the Producer Gas from Gasification of Wood Pellets

Having established that the QMS method worked for a clean gas, a complex gas mixture was used, produced by the gasification of wood pellets. These experiments were performed with a small-scale 21 mm i.d. quartz-tube gasifier (see section 3.2.1 in Chapter 3) filled with wood pellets (5 mm diameter, and 13 mm long), to a depth of about 400 mm. The air flow was kept constant at 3 litre/min, and temperatures in the hot zone were in the region of 912 to 1046 °C.

If the wood pellets used in this study followed the German standard, DIN Plus, then the sulphur content would less than 0.04 wt.% (Hiegl and Janssen, 2009).

To stimulate the outlet temperature (approximately 600 ^{o}C) of the gas stream exiting the bottom of a down-draft gasifier, the lower half of the quartz tube contained an inert stainless steel support, which was then heated up to 600^{o}C by an electrical furnace during the experiment.

An example of measurements on dry gas (using Method 1, m/z(34) to measure H_2S) is shown in Figures 5.5(a) and 5.5(b).

In this example, the average trace gas concentrations were:

O_2 = 1,510 ppmv,

H_2S = 99 ppmv, and

COS = 10 ppmv.

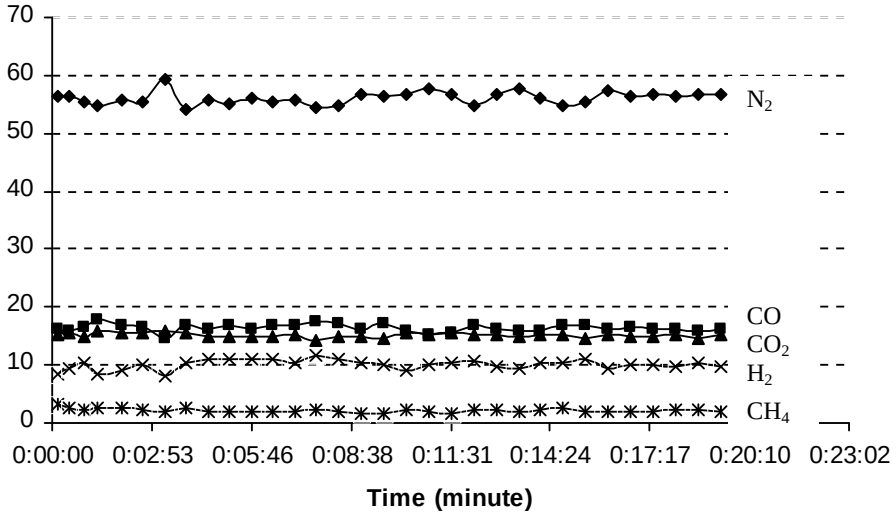

Figure 5.5(a) Composition (main gases) of dry gas from gasification of wood pellets.

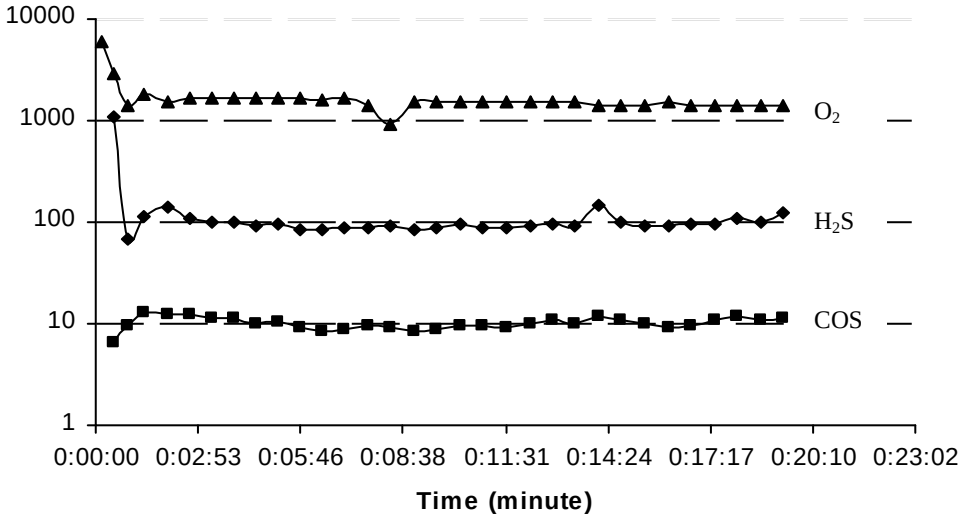

Figure 5.5(b) Composition (trace gases) of dry gas from gasification of wood pellets (Method 1, using spectrum at m/z(34)).

A sample of the producer gas from the gasification experiment was also taken using a plastic bag. The gas was then connected to the QMS sampling line. The method of measuring H_2S at spectrum m/z(34) (Method 1) was used to measure the H_2S concentration in this gas sample. The results are showed in Figures 5.6(a) and 5.6(b).

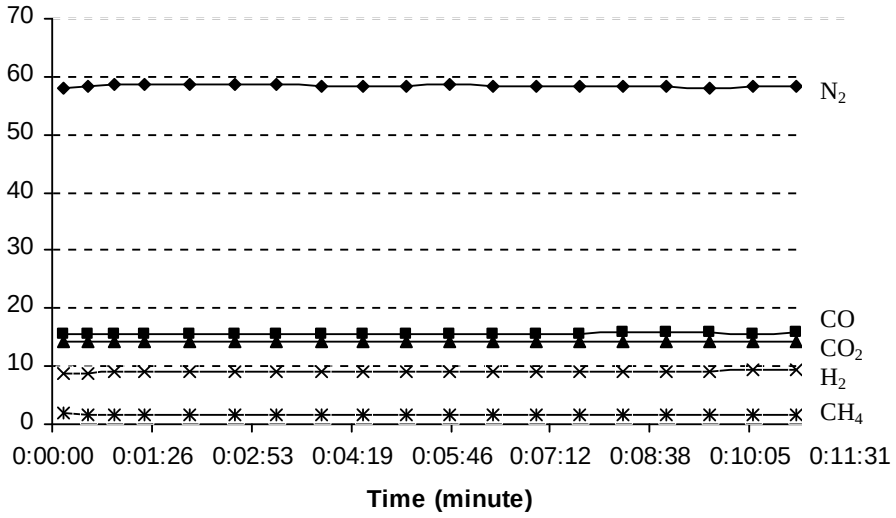

Figure 5.6(a) Composition (main gases) of dry off-line gas from gasification of wood pellets (Method 1, using spectrum at m/z(34)).

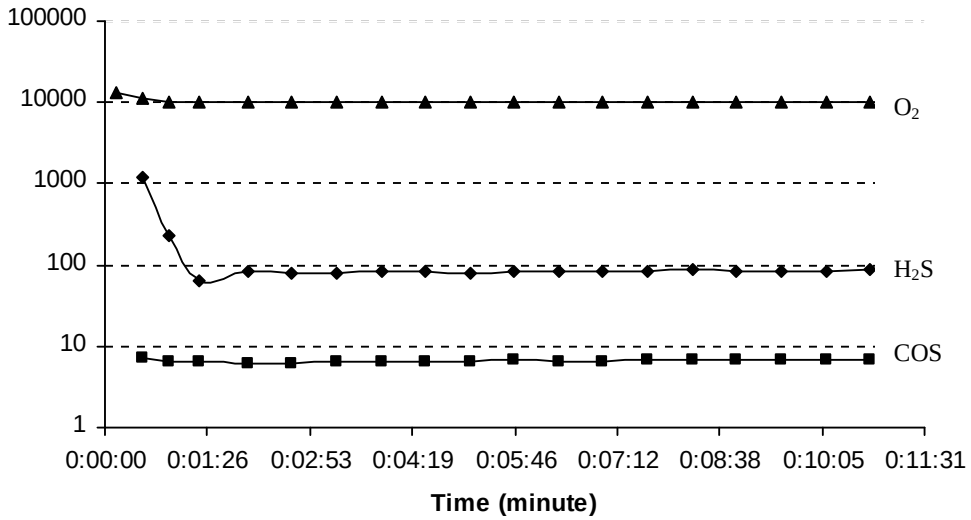

Figure 5.6(b) Composition (trace gases) of dry off-line gas from gasification of wood pellets (Method 1, using spectrum at m/z(34)).

The O_2 concentration of 10,000 ppmv is higher in Figures 5.6(b) compared with a value of 1,510 ppmv in Figure 5.5(b). This was because of a slight ingress of air into the plastic bag, as the gas sample was taken. However, one interesting thing is that the concentration of H_2S in the two different measurements is very similar (~ 90 ppmv) and has not be affected by the difference in the O_2 concentration. This means that the method of quantifying H_2S at m/z(34) with O_2 correction worked well.

Also, Method 2 was used to measure the H_2S (at spectrum m/z(35)) in this off-line gas sample collected in the bag. The results are shown in Figure 5.6(c).

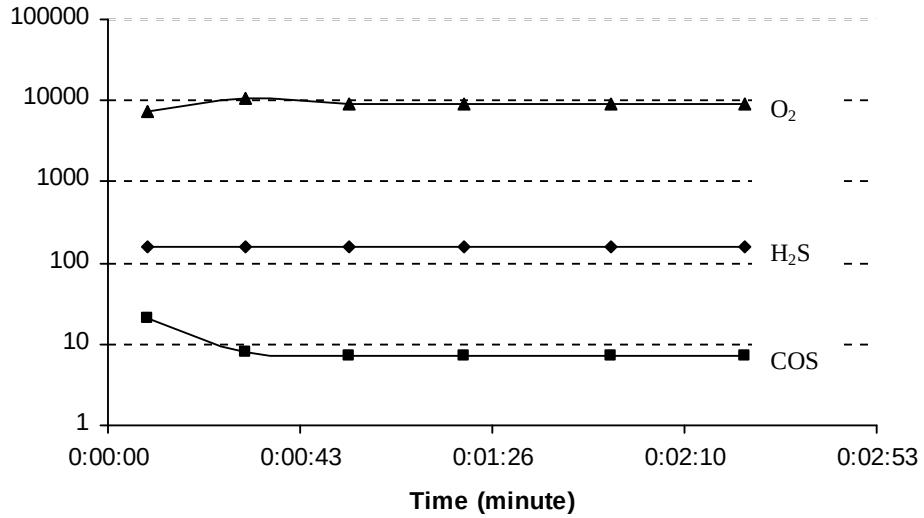

Figure 5.6(c) Composition (trace gases) of dry off-line gas from gasification of wood pellets (Method 2, using spectrum at m/z(35)).

As can be seen in Figure 5.6(c), the concentration of H_2S increased from 83 ppmv in Figure 5.6(b) to approximately 155 ppmv. This may be because of a possible contribution of HCl at the spectrum of m/z(35).

The results from Figures 5.6(a) and 5.6(b) were used to check the repeatability of measurements with the QMS. The repeatability was checked over a 10-minute period, during which it was found that the average concentrations of the species were: N_2 = 58.34 (± 0.28) vol.%; CO = 15.62 (± 0.16) vol.%; H_2 = 9.1 (± 0.16) vol.%; CO_2 = 14.31 (± 0.09) vol.%; CH_4 = 1.48 (± 0.01) vol.%; O_2 = 9987 (± 80) ppmv; H_2S = 83 (± 5) ppmv; COS = 6.55 (± 0.11) ppmv.

5.3.3 Composition of the Producer Gas from Gasification of Straw Pellets

Additional experiments were performed with straw pellets, and the results are compared with the wood pellets in Table 5.6. The straw pellets produce a slightly higher H_2S gas concentration, and the COS concentration is very similar.

According to Little (2010), the typical sulphur content in straw pellets was about 0.1 wt.%, which was higher than those of wood pellets made from heather (0.07 wt.%), gorse (0.08 wt.%), and rhododendron (0.02 wt.%).

Table 5.6 Comparison of gas compositions produced from different biomass sources.

Component	Previous results in Chapter 3 GC used for analysis		**QMS used for analysis**		
	Wood pellets	Straw pellets	Wood pellets	**Straw pellets**	-
CO, vol.%	15.8	14.7	16.44	**13.91**	-
H_2, vol.%	9.5	12.6	10.11	**12.83**	-
CH_4, vol.%	2.0	2.0	2.08	**2.11**	-
CO_2, vol.%	14.5	14.2	15.12	**17.17**	-
N_2, vol.%	58.2	56.5	56.06	**53.77**	-
O_2, ppmv	-	-	1510	**1736**	-
H_2S, ppmv	-	-	99	**123**	-
COS, ppmv	-	-	10	**11**	-

5.3.4 Composition of the Producer Gas from Gasification of RDF Pellets

An additional set of experiments was performed with RDF pellets. However, a number of difficulties arose:

(a) Because the length of RDF pellets was rather large (see Figure 5.7(a)) relative to the inside diameter of the quartz-tube (L_{pellet} = up to about 80 mm; i.d. tube = 21 mm), they had to be cut into smaller pieces (L_{pellet} = less than 10 mm). This was done.

(b) At the reaction temperatures in the quartz-tube, these pellets formed a sticky substance which restrained the movement of the pellets in the quartz-tube. This probably arose because of the presence of plastic material in the pellets, which as it melted stuck to the sides of the quartz-tube.

(c) Blockage occurred at the base of the quartz-tube, probably caused by the high ash content of the RDF pellets (see Table 5.7 for physical properties of RDF pellets). Thus, the experiment had to be stopped just after a few minutes.

Figure 5.7 Refuse derived fuel (RDF) pellets.

Table 5.7 RDF pellets analysis.

Properties	**RDF pellets**
Dimensions before the pellets were cut:	
Diameter, mm	14
Length, mm	30 – 80
Dimensions after the pellets were cut:	
Diameter, mm	14
Length, mm	less than 10
Moisture (wt.% in wet basic)	7.18
Volatiles (wt.% in dry basic)	42.82
Fix carbon (wt.% in dry basic)	31.49
Ash (wt.% in dry basic)	25.69

The results of brief measurements on the gasification of RDF pellets are presented in Figures 5.8(a) and 5.8(b) using Method 1 (H_2S at spectrum m/z(34)).

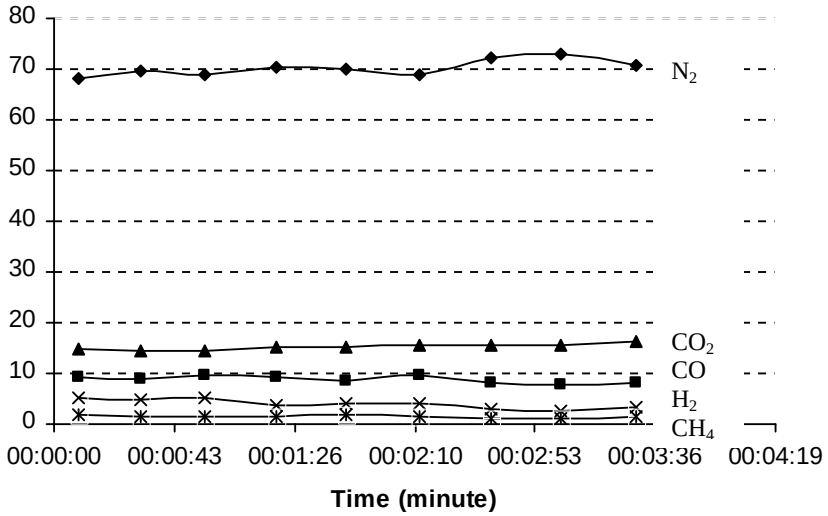

Figure 5.8(a) Composition (main gases) of dry gas from gasification of RDF pellets.

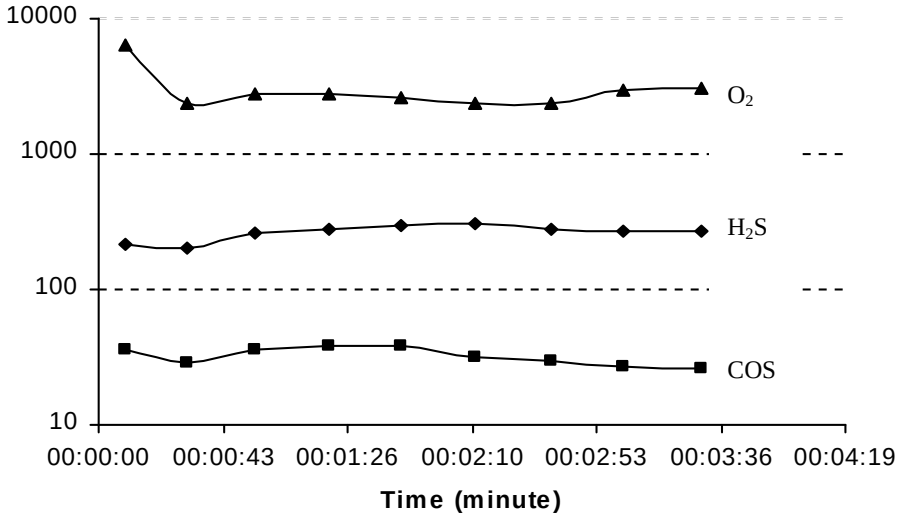

Figure 5.8(b) Composition (trace gases) of dry gas from gasification of RDF pellets (Method 1, using spectrum at m/z(34)).

A sample of the producer gas from the gasification experiment was also taken using a plastic bag. A measurement of this off-line gas sample was performed using Method 2 (H_2S at spectrum m/z(35)) for comparison. The results are shown in Figure 5.9.

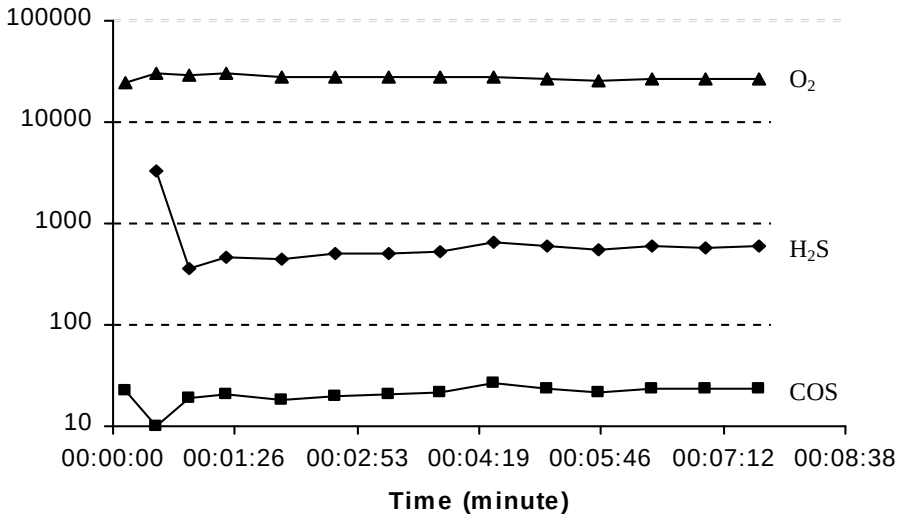

Figure 5.9 Composition (trace gases) of dry off-line gas from gasification of RDF pellets (Method 2, using spectrum at m/z(35)).

Comparing the results in Figures 5.9 and 5.8(b), the following observations can be made:

(a) Comparing the oxygen concentration, a small ingress of oxygen has occurred (as before) as the gas sample was collected in the bag. This also shows how difficult it is to take a truly representative gas sample with a bag for subsequent gas analysis.

(b) The H_2S concentration also increased dramatically from around 275 ppmv in Figure 5.8(b) to 550 ppmv in Figure 5.9. This difference may come from the contribution of HCl in the peak at m/z(35). Because the chlorine content in RDF is expected to be much higher than in wood and straw pellets, the impact on H_2S concentration using Method 2 would also be higher.

The fragment at m/z (34) of H_2S is the base peak. The concentration of O_2 in the producer gas is just around 1000 ppmv, so the contribution of O_2 at m/z(34) is very small (only around 0.45 % of the base peak at m/z(32)). Therefore, the concentration of H_2S derived from the spectrum at m/z(34), after being corrected for O_2 contribution, was not affected by the increased O_2 concentration in that gas mixture.

Nevertheless, the fragment at m/z(35) of H_2S is the daughter peak that is very small, around 2 % of the base peak at m/z 34. In addition, HCl, which may be present in the producer gas, also contributes significantly at m/z(35) (around 11 % of the base peak at m/z 37). Therefore, if the concentration of H_2S is derived from the spectrum m/z (35), it

must be corrected, otherwise the error of measurement will be very high. Unfortunately, HCl was not taken into the calibration step, so the method of detecting H_2S at m/z (35) gave considerable errors during that measurements.

An example of HCl formation can be found in Dias and Gulyurtlu (2008), where HCl concentration in the gas produced from a bubbling fluidized-bed gasifier fed with RDF was as high as 80 ppmv. More details about the concentration of sulphur and chloride compounds in the producer gas can be found in: Kuramochi *et al.* (2004), Drift *et al.* (2001), and Paasen *et al.* (2006).

Therefore, to avoid the negative effect of HCl on H_2S measurement, Method 1 was selected (H_2S at spectrum m/z(34)).

Additional experiments were then performed with the RDF pellets. However, this time a stainless steel tube was used (rather than the quartz-tube). The RDF pellets were also not cut to a smaller size, but instead, they were inserted in a vertical direction into the tube (see Figure 5.10). This was tried to see if it would help the RDF pellets to move more easily down the tube. The results are presented in Figures 5.11(a) and 5.11(b).

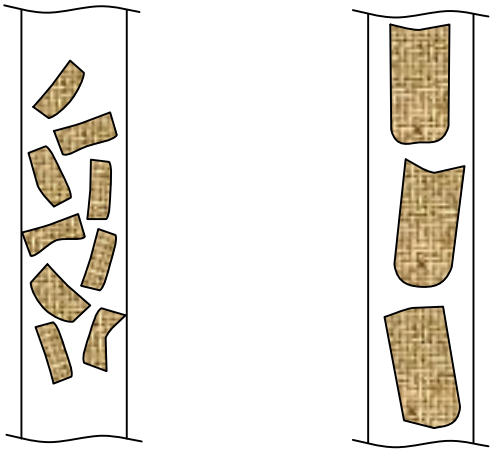

Figure 5.10 Schematic illustrating tube reactors filled with: (a) RDF pellets after they were cut; and (b) RDF pellets before they were cut.

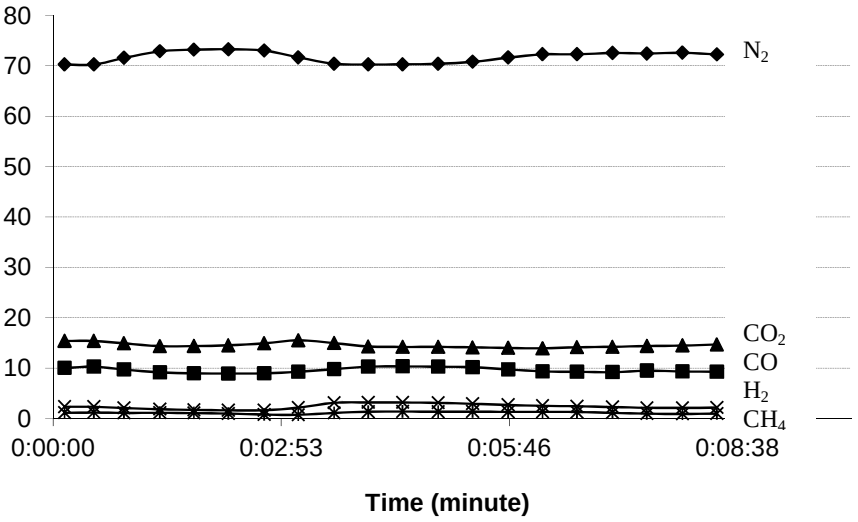

Figure 5.11(a) Composition (main gases) of dry gas from gasification of RDF pellets.

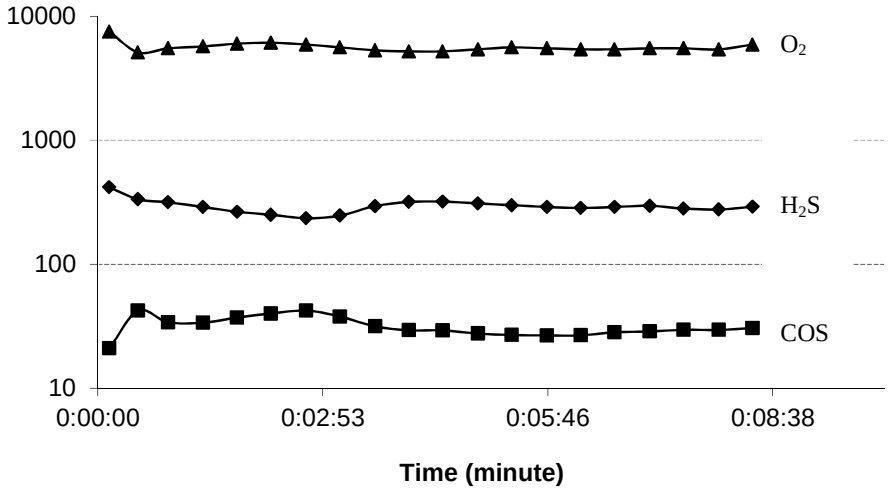

Figure 5.11(b) Composition (trace gases) of dry gas from gasification of RDF pellets (Method 1, H_2S spectrum at m/z(34)).

The results of this final set of measurements on the RDF pellets are also presented in Table 5.8, where it is compared with data for the wood and straw pellets.

Table 5.8 Comparison of gas compositions produced from different biomass sources.

Component	Previous results in Chapter 3, GC used for analysis		Current study, QMS used for analysis		
	Wood pellets	Straw pellets	Wood pellets	Straw pellets	**RDF pellets**
CO, vol.%	15.8	14.7	16.44	13.91	**10.39**
H_2, vol.%	9.5	12.6	10.11	12.83	**4.97**
CH_4, vol.%	2.0	2.0	2.08	2.11	**1.11**
CO_2, vol.%	14.5	14.2	15.12	17.17	**14.57**
N_2, vol.%	58.2	56.5	56.06	53.77	**67.90**
O_2, ppmv	-	-	1510	1736	**10063**
H_2S, ppmv	-	-	99	123	**286**
COS, ppmv	-	-	10	11	**28**

5.3.5 Thermodynamic Equilibrium Calculation for Producer Gas from Experiment

At this point, it was decided to calculate the thermodynamic equilibrium (using Aspen Plus) for the gas produced from experiments to see what would be predicted at different values of gas temperature, and to discover what temperature matched the data most closely. The gas produced from RDF gasification was chosen, and the moisture content in the gas stream was assumed to be the same (16.5 vol.%) as in Table 5.2. A range of reaction temperatures from 600 to 1200 ^{o}C was explored. The adjusted wet gas composition and the calculation results are shown in Tables 5.9 and 5.10, respectively.

Table 5.9 Adjusted gas composition used as a starting point in the calculation of equilibrium values.

	Dry gas composition **Vol.%, see Table 5.8**	**Adjusted wet gas composition[(1)]** **Vol.%**
Hydrogen	4.97	4.15
Carbon monoxide	10.39	8.68
Methane	1.11	0.93
Carbon dioxide	14.57	12.17
Nitrogen	67.90	56.71
Oxygen	1.01	0.84
Water vapour		16.5 see note[(1)]
H_2S	0.0286	0.0239 ≡ 239 ppmv
COS	0.0028	0.0023 ≡ 23 ppmv
Total	99.98	100.00

(1) Wet gas composition was adjusted for the moisture content in Table 5.2.

Table 5.10 Variation of species – simulations on a complex system using Aspen Plus®.

Species	**Temperature**					
	600 °C	700 °C	900 °C	1000 °C	**1100 °C**	1200 °C
H_2 (vol.%)	9.655	8.636	6.893	6.257	**5.739**	4.967
CO (vol.%)	4.809	6.062	7.814	8.450	**8.969**	9.757
CH_4 (vol.%)	0.065	0.002	0.000	0.000	**0.000**	0.000
CO_2 (vol.%)	16.710	15.493	13.742	13.105	**12.586**	11.797
N_2 (vol.%)	56.214	56.143	56.140	56.140	**56.140**	56.137
O_2 (vol.%)	0.000	0.000	0.000	0.000	**0.000**	0.000
H_2O (vol.%)	12.521	13.638	15.385	16.022	**16.540**	17.316
H_2S (ppmv)	253	251	247	244	**239**	224
COS (ppmv)	7	9	13	15	**17**	18
SO_2 (ppmv)	0	0	0	1	**4**	18
SO_3 (ppbv)	0	0	0	0	**0**	0
CS_2 (ppbv)	0	0	0	0	**0**	0

From Tables 5.9 and 5.10, it is likely that the gas composition estimated matches the experimental data at calculation temperatures higher than 900^{o}C. This may be reasonable because the reaction rate is high at high temperature, and thermodynamic equilibrium could be reached quickly. The temperature of 1100^{o}C seems to match the data most closely, and it is also nearly the highest temperature observed in the hot zone of gasification experiments (see Section 3.3.3).

It is interesting to see that the molar ratio of H_2S to COS at calculation temperature of 1100^{o}C is about 14:1, which is closer to the one (10:1) obtained from experiments. Also, the presence of SO_2 becomes significant (e.g. 4 ppmv at 1100^{o}C) at high temperature.

For thermodynamic equilibrium calculation, the concentrations of sulphur species also vary with the moisture content. It was found that, for set values of the moisture content between 8 to 20 vol.%, the temperature of 1100^{o}C always gave the best match. Therefore, it may be useful to see what moisture content matches the experimental data best at a temperature of 1100^{o}C. By adjusting the moisture content in the Aspen Plus model, it was found that the value of 10 to 13 vol.% of moisture gave the best match, where the molar ratio of H_2S to COS was approximately the same as the experimental value (10:1).

For example, the adjusted wet gas composition (for the moisture content of 13 vol.%), and the calculation results are presented in Tables 5.11 and 5.12, respectively.

Table 5.11 Adjusted gas composition used as a starting point in the calculation of equilibrium values.

	Dry gas composition **Vol.%, see Table 5.8**	**Adjusted wet gas composition[(1)]** **Vol.%**
Hydrogen	4.97	4.33
Carbon monoxide	10.39	9.04
Methane	1.11	0.97
Carbon dioxide	14.57	12.68
Nitrogen	67.95	59.07
Oxygen	1.01	0.88
Water vapour		13.00 see note[(1)]
H_2S	0.0286	0.0249 ≡ 249 ppmv
COS	0.0028	0.0024 ≡ 24 ppmv
Total	99.98	100.00

(1) Wet gas composition was adjusted for the moisture content found to match experiment data most closely at 13 vol.%.

Table 5.12 Variation of species – simulations on a complex system using Aspen Plus®.

Species	**Temperature**					
	600 °C	700 °C	900 °C	1000 °C	**1100 °C**	1200 °C
H_2 (vol.%)	9.170	8.181	6.462	5.843	**5.341**	4.932
CO (vol.%)	5.824	7.126	8.855	9.474	**9.977**	10.390
CH_4 (vol.%)	0.087	0.003	0.000	0.000	**0.000**	0.000
CO_2 (vol.%)	16.578	15.323	13.595	12.975	**12.472**	12.059
N_2 (vol.%)	58.571	58.472	58.469	58.469	**58.468**	58.468
O_2 (vol.%)	0.000	0.000	0.000	0.000	**0.000**	0.000
H_2O (vol.%)	9.742	10.869	12.592	13.212	**13.714**	14.125
H_2S (ppmv)	262	259	254	252	**247**	233
COS (ppmv)	9	11	16	18	**21**	22
SO_2 (ppmv)	0	0	0	1	**3**	16
SO_3 (ppbv)	0	0	0	0	**0**	0
CS_2 (ppbv)	0	0	0	0	**0**	1

5.4 CONCLUDING REMARKS

Looking at the data in Table 5.8, then:

(a) The concentration of H_2S and COS produced from RDF pellets is about three times higher than values from the wood and straw pellets. This is not surprising, as the RDF was expected to have higher sulphur content – however, even the absolute values measured will be very useful in the selection of future gas clean-up strategies.

(b) There is also consistency in the molar ratio of the concentration of H_2S to COS (around 10:1) for wood, straw and RDF. This information will also be very useful, when gas clean-up strategies need to be developed for commercial plants.

(c) This 10:1 ratio is also very different from the ratio determined in the thermodynamic equilibrium calculations earlier in Section 5.2.4.3. It is just because the thermodynamic equilibrium calculations predict a certain composition, it does not mean that the kinetics of the reaction have permitted that outcome to occur.

(d) The results also show that there is a certain amount of O_2 in the gas stream, and this can vary. This clearly depends on the design of the gasifier and operating parameters. For example, the concentration of O_2 in the gas from the RDF pellets was higher, because the pellets were too big for the i.d. of the tube (higher void fraction and wall channelling).

(e) The concentration of the main components in the gas is also compared with earlier experiments in Chapter 3, when the GC was used for gas analysis. Although there are slight differences, the comparison in general is very good. Slight differences probably arise from slight variations in operating conditions/composition of pellets used.

(f) The methodology for the QMS on-line method of gas analysis was successfully upgraded to measure up to 8 species, including the main gases (N_2, H_2, CO_2, CO, CH_4) and other trace gases (O_2, H_2S and COS). It was shown that an acceptable level of repeatability was attainable with the QMS. Also, provided that gas pre-cleaning was effective, the QMS was stable for months without needing to be re-calibrated.

From the earlier equilibrium calculations:

(g) Although not considered in any detail in this study, it is important to remember that sulphur compounds will also be present in the char from the base of the gasifier. If quantities are known, then this aspect can be factored into the calculations.

(h) In any interpretation of the results from theoretical equilibrium calculations, it is important to realise that because of kinetics and complexity of the reaction zones, the results may not match what is observed in an experiment. However, a useful indication is provided of what could occur.

(i) Finally, the importance of considering gas clean-up strategy, and how this may in turn affect the ability of the plant to meet the WID limits for SO_2 was explored, and how concentrations in the RDF translate into emissions. Also, the importance of considering the impact of contaminants on catalyst systems was emphasized, rather than just looking at WID limits on their own.

From the later equilibrium calculations:

(j) By adjusting the calculation temperature in the thermodynamic equilibrium model, it was found that 1100^{o}C was the best value that matches the experimental data most closely at every moisture content (from 8 to 20 vol.%) of the gas phase. This shows how interesting it is, because the temperature of about 1100^{o}C was also found to be the highest temperature observed in the hot zone of gasification experiments. It was likely that in the gas phase of the gasifier, thermodynamic equilibrium of reactions could be reached at this temperature, as the reaction rate would be high at high temperature.

(k) Also, by adjusting the moisture content in the thermodynamic equilibrium model, the range of 10 to 13 vol.% of moisture was found to give the best match, where the molar ratio of H_2S to COS was approximately the same as the experimental value (10:1).

REFERENCES

Abbott and Van Ness (1972). Schaum's outline of theory and problems of thermodynamics. 2nd edition, McGraw-Hill Inc.

Akay G., Dogru, M. and Calkan, O. (2007). Biomass to the rescue. The Chemical Engineer, Issue 786, pp. 55-57.

Baratieri, M., Baggio, P., Fiori, L. and Grigiante, M. (2008). Biomass as an energy source: Thermodynamic constraints on the performance of the conversion process. Bioresource Technology, Vol. 99, pp. 7063-7073.

Cioni, M., La Marca, C. and Riccardi, J. (2002). RDF gasification in a circulating fluidized bed gasifier: characterisation of syngas and ashes, Gasification: the Clean Choice for Carbon Management. Noordwijk, The Netherlands.

Dias, M. and Gulyurtlu, I. (2008). H_2S and HCl formation during RDF and Coal co-gasification: A comparison between predictions and experimental results. Proceedings of the biomass gasification technologies workshop MRC Gebze Campus-Turkiye.

Directive 7000/76/EC of the European Parliament and of the Council of 4 December 2000 on the incineration of waste, Official Journal of the European Communities.

Drift, A.V.D., Doorn, J.V. and Vermeulen, J.W. (2001). Ten residual biomass fuels for circulating fluidized-bed gasification. Biomass and Bioenergy, Vol. 20, pp. 45-56.

Gendebien, A., Leavens, A., Blackmore, K., Godley, A., Lewin, K., Whiting, K.J., Davis, R., Giegrich, J., Fehrenbach, H., Gromke, U., Bufalo, N.D. and Hogg, D. (2003). Refuse Derived Fuel, current practice and perspectives. Final Report, WRc plc.

Hayes, R.E. and Kolaczkowski, S.T. (1997). Introduction to catalytic combustion. CRC Press.

Hiegl, W. and Janssen, R. (2009). Development and promotion of a transparent European Pellets Market Creation of a European real-time Pellets Atlas. Final Report, WIP Renewable Engergy.

Higman, C. and Burgt, M.V.D. (2008). Gasification. Second edition, Elsevier.

Knoef, H.A.M., edited, (2005). Handbook Biomass Gasification. BTG biomass technology group.

Kolaczkowski, S., Le, C.D. and Awdry, S. (2011). Equilibrium reactions(s) involving H_2S and COS species – consideration of thermodynamics and implications on the biomass gasification process. In Proceedings of the bioten conference on biomass and biofuels 2010, Bridgwater, A.V. (Ed), CPL Press UK, pp. 733-744.

Kolaczkowski, S. (2009a). Private communication with Shanks Waste Management Ltd.

Kolaczkowski, S. (2009b). Private communication with Perkins Gas Engines.

Kuramochi, H., Wu, W. and Kawamoto, K. (2004). Prediction of the behaviors of H2S and HCl during gasification of selected residual biomass fuels by equilibrium calculation. Fuel, Vol. 84, pp. 377-387.

Little, J. (2010). Assessment of the use of landscape management arisings as a feedstock for commercial pellet production. Feasibility Report, Harvest Wood Fuels.

Paasen, S.V.B., Cieplik, M.K. and Phokawat, N.P. (2006). Gasification of non-woody biomass : Economic and Technical perspectives of chlorine and sulphur removal from product gas. Non-confidential version, Energy research Central of the Netherlands.

Yang, H., Sothen, R., Cahela, D.R. and Tatarchuk, B.J. (2008). Breakthrough characteristics of reformate desulphurisation using ZnO sorbents for logistic fuel cell powered systems. Ind. Eng. Chem. Res., Vol. 47, No. 24, pp. 10064 – 10070.

Wakker, J. P., Gerritsen, A.W. and Moulijn, J.A. (1993). High temperature H_2S and COS removal with MnO and FeO on γ-Al_2O_3 acceptors. Ind. Eng. Chem. Res., Vol. 32, pp. 139-149.

CHAPTER 6

Steam Gasification of Wood Charcoal and RDF-derived Char

In Chapter 2, it was concluded that there was great interest, within companies working on pilot-scale gasification technology (50 kW_e to 2 MW_e scale), in the conversion of the carbon in the char into a gaseous fuel. Otherwise the char had to be disposed off-site, which created a disposal cost and a loss in revenue from the potential of converting the carbon in the char into gaseous fuel. The presence of residual char was also very evident in the quartz-tube gasification experiments described in Chapter 3. These considerations led to the work described in this chapter, which consists of:

- Brief discussion of relevant literature.
- Experiments on the steam/air gasification of wood charcoal - this was selected to represent a relatively clean source of char from wood.
- Experiments on the steam/air gasification of char obtained from a commercial pilot-scale down-draft gasifier using RDF as a fuel - this enabled measurements to be performed on a realistic and difficult source of char.

6.1 INTRODUCTION

Based on information in the literature, it is well recognized that char is produced from the gasification of biomass (e.g. Wu *et al*., 2009; Knoef (2005, p.24); and Chaudhari *et al*. 2003). Besides converting the carbon in the char into gaseous fuel, the char could also be used as a carbon sequestration agent (Boateng, 2007; and Brewer *et al.*, 2009).

In the introduction to their paper on biochar, Brewer *et al*.(2009) commented that typically 15 to 20 % and 5 to 10 % of the feedstock mass are converted into char in fast pyrolysis and gasification of biomass, respectively. The best way of using this co-product varies and

depends on the local interests and the char properties. Char combustion to generate heat is common. However, the use of this char depends on its physical and chemical characteristics, although this usage is not yet well understood.

6.1.1 Char from Pyrolysis - Boateng (2007)

Based on work described in Boateng (2007), in a pyrolysis system it was proposed that charcoal could represent 15 to 20 % of the feed and this had an energy content in the 20,000 to 25,000 kJ/kg range. It was proposed that this could fulfil all of the energy requirements for the production of 60 to 70 wt.% bio-oil in a fast pyrolysis system. The charcoal derived from fluidized-bed fast pyrolysis oil production of switchgrass was characterized, and it was found that the charcoal had high ash content, ~27 wt.% on a dry basis. It was recognized that should such charcoal be buried or used for soil enrichment, then this could have led to large amounts of alkali metals in the ground. Boateng (2007) finally concluded that the surface areas for such char were low, and the crystallinity was high. This indicated that the char may not yet in a suitable form for use either as an activated charcoal, or for carbon sequestration (where higher surface areas were preferred). However, this charcoal could be a good combustion fuel, although the high ash content might present a slagging challenge (low-melting-point alkali metals might foul heat transfer equipment during combustion).

Taking these factors into account, then performing an additional gasification step on the carbon in the char might lead to a better disposal proposition, although the residual ash will still need to be disposed of in an approved manner.

6.1.2 Importance of Operating Parameters

In a downdraft gasification process, there will be thermal energy available which could be used to produce steam. Therefore, in this chapter, steam is selected as a gasifying reactant. Furthermore, air will also be used to provide the necessary energy to support the endothermic reactions, and to maintain the desired operating temperature in such a process.

Pressure, reactant and temperature are three main parameters in the operation of a gasifier. As summarized in Khor *et al.* (2006):

- Gasification at high pressure increases the overall reaction rates at the expense of added complexity and lower formation of carbon monoxide and hydrogen.
- The gasification process comprises of both endothermic and exothermic reactions. The changes in temperature were found to influence the producer gas composition. Operation at high temperature increases the reaction rate especially for chemical reaction rate controlled processes.
- The presence of methane, steam and carbon dioxide in the producer gas is favoured by low temperatures and high pressures, whereas the presence of hydrogen and carbon monoxide is favoured by high temperatures and low pressures.
- Equilibrium consideration points to a high temperature and a low operating pressure (unless methane is the desired product).

Operating at high temperatures also has a positive effect on tar elimination in biomass gasification process (Devi *et al.*, 2003). Obviously, high operating temperatures are preferred for producing clean gas with a high heating value, although the cost of such plant increases with temperature. Looking at the literature, when experiments on the steam gasification of charcoal are described, experiments in the temperature range of 700 to 1000 ^{o}C are often reported. For example, in:

Paviet *et al.* (2007) - char gasification experiments are performed with steam at 850, 900, 950 and 1000 ^{o}C.

Khor *et al.* (2006) - charcoal gasification experiments are performed with steam + air at 800 to 950 ^{o}C in the bed.

Chaudhari *et al.* (2003) - steam gasification of chars at 700, 750, and 800 ^{o}C.

6.1.3 Evolution of Char Structure

When char is gasified, the effect of evolution of the char structure, and the presence of alkali and alkaline earth metallic (AAEM) species, has raised great interest very recently (Wu *et al.*, 2009; and Yip *et al.*, 2010).

As reported in Yip *et al.* (2010), during char gasification, the reactivity of the raw biochars generally increased, while that of all acid-treated biochars (for removal of AAEM species) remained relatively unchanged with conversion. The results indicate that Na, K, and Ca retained in the biochars were the key catalytic species, with the catalytic effect appearing to be in the order K > Na > Ca during the steam gasification of the biochar.

A similar phenomena of increased reactivity of biochar with conversion was also observed and reported by Wu *et al.* (2009). The catalytic effect of the inherent AAEM species seems to in turn depend on the carbon structure that probably affects the catalyst dispersion. It was emphasized that the surface area of biochar increased with conversion, suggesting the formation of new pores and/or opening of closed pores as a result of steam activation during gasification.

Because of these factors, it will be of interest to compare the reactivity of wood charcoal and RDF-derived char – which is done in the following sections.

6.2 EXPERIMENTAL SETUP

The experimental work was performed in a fixed-bed reactor, operating at atmospheric pressure, as illustrated in Figures 6.1 and 6.2.

The reactor consisted of a vertical stainless steel tube (i.d. 9.5 mm), which was filled with wood charcoal pellets, or RDF-derived char (bed depth 330 mm), see Figures 6.3(a) and (b). This was positioned inside an electrically heated furnace, and the temperature inside the charcoal bed was measured using two thermocouples located 10 mm into the bottom of the bed, and also 10 mm into the top of the charcoal bed.

The reactants (steam and/or air) and nitrogen passed through a coiled stainless steel tube placed inside the furnace. This vaporized the water into steam, and preheated the gases before being fed into the bottom of the reactor. A small purge flow of nitrogen (or air) was fed into the bottom of the support bed to prevent any condensation of steam. The flow of reactants and nitrogen were adjusted with rotameters.

The gas from the top of the reactor flowed through a cooling coil, and condensate was trapped in a plastic vessel. The gas was passed through a glass wool filter, and then discharged into the vent from the fume cupboard, or drawn by a small sampling pump to a gas chromatography and/or a quadrupole mass spectrometer for gas analysis.

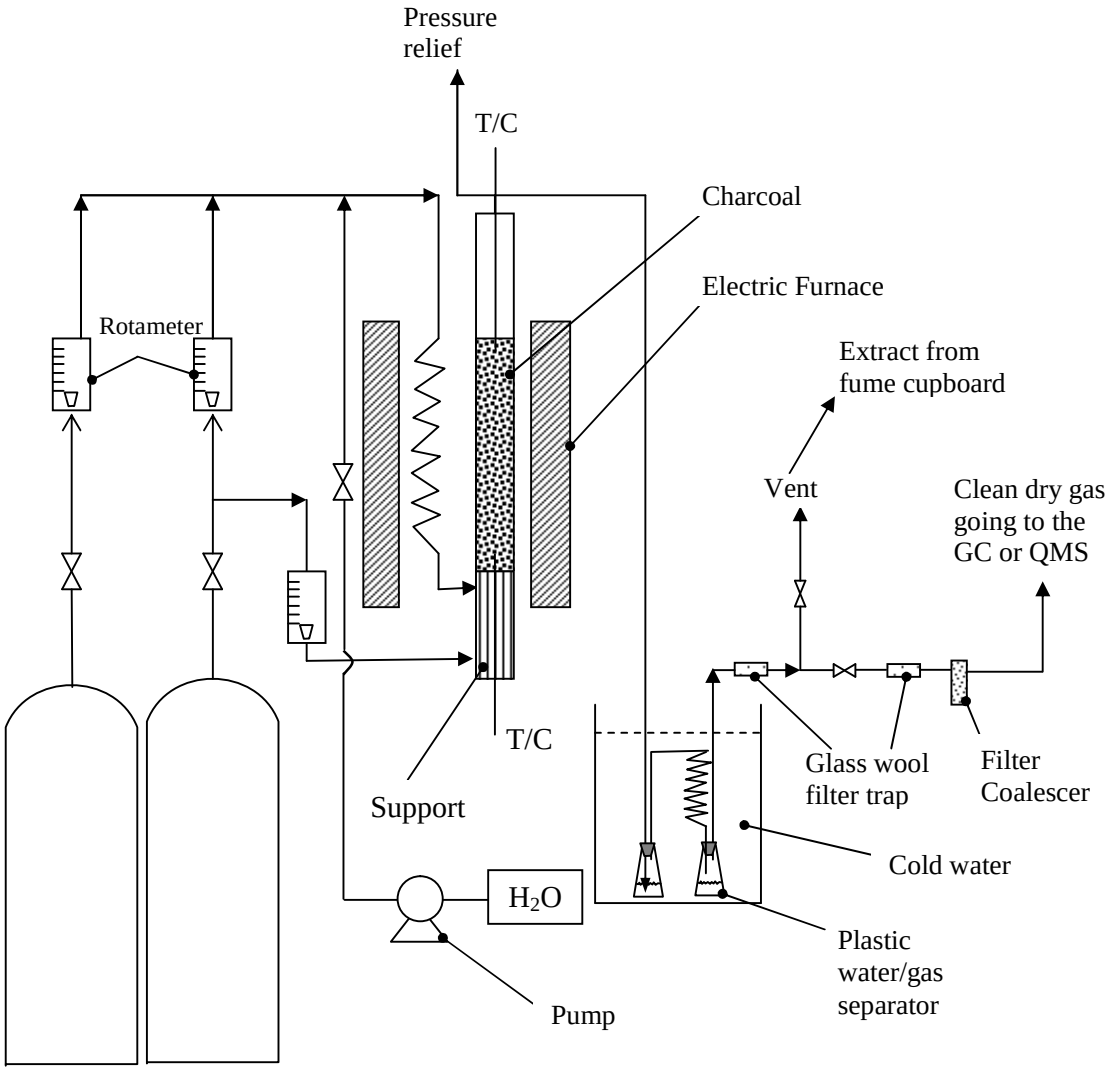

Figure 6.1 Schematic of the mini air/steam charcoal gasifier.

Figure 6.2 Experimental rig of small metal tube gasifier.

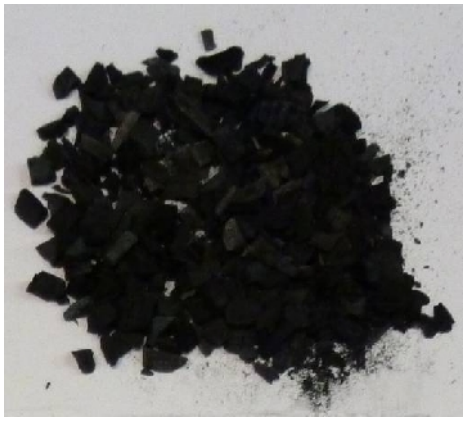

a) b)

Figure 6.3 Wood charcoal (a), and RDF-derived char (b).

6.3 STEAM GASIFICATION OF WOOD CHARCOAL

In the first set of experiments, wood charcoal was used (~4 mm in diameter). The charcoal bed was initially preheated to about 800 ^{o}C under the influence of nitrogen to prevent any oxidation reaction during this start-up phase (~3 hours), and this removed any volatiles. Steam and nitrogen with various ratios were used first as a gasifying agent.

6.3.1 Effect of Operating Temperature

Experiments were performed at different set points on the furnace, from 500 ^{o}C to 900 ^{o}C. Other experimental conditions:

- N_2 flow rate was kept at 0.1 litre/min (NTP).
- H_2O flow rate was kept at 0.148 g/min.
- The molar ratio of H_2O:N_2 = 2:1.
- For each new run at a set point temperature, the reactor was refilled with fresh charcoal.

Initially, the dry gas composition was analysed using a GC, and the results are presented in Figure 6.4. As the set point temperature was increased, the concentration of CO and H_2 also increased.

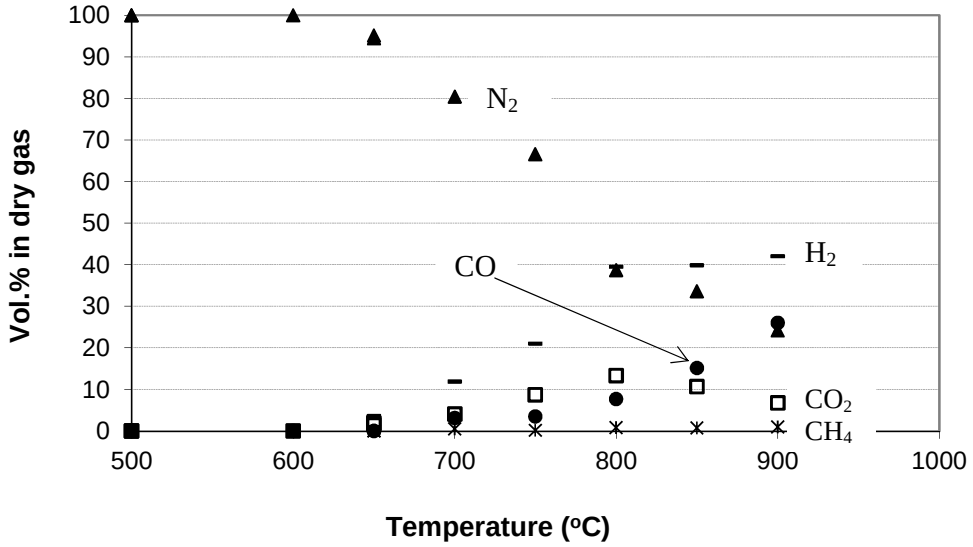

Figure 6.4 Steam gasification of wood charcoal (measurement with GC).

The QMS was then connected to the rig for on-line gas analysis, while the GC was also used to check the results obtained.

During one of the experimental runs, the temperature of the furnace was adjusted, increasing gradually from 600 ^{o}C to 900 ^{o}C. Gas composition was measured with the QMS (continuous), and on the GC (at 5 ½ minute intervals). The results of one run which lasted around 45 minutes are presented in Figure 6.5, and a good match is obtained between these two measurements. The QMS was then used on its own for the subsequent experiments.

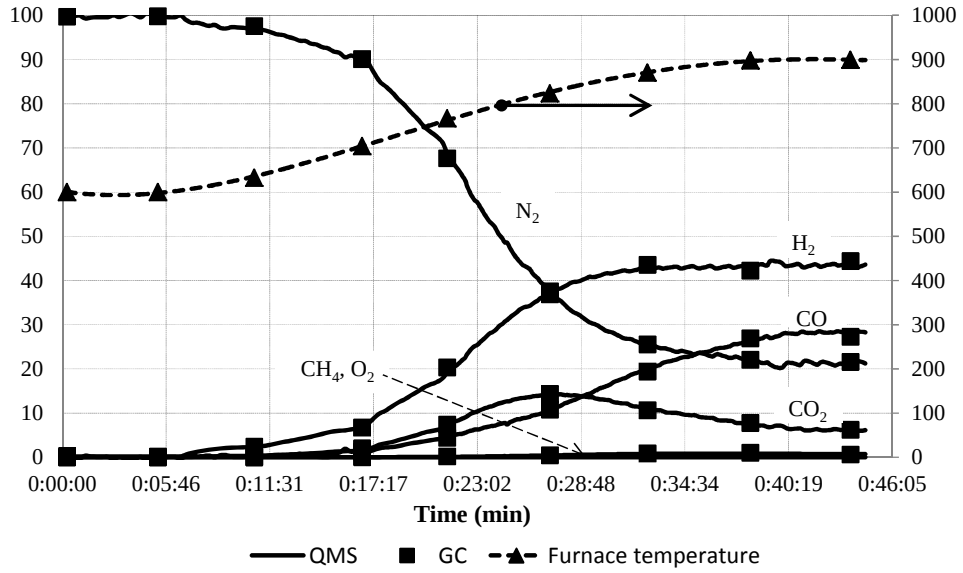

Figure 6.5 Steam gasification of wood charcoal (measurement with GC and QMS).

The results in Figure 6.5 also show the same trend as shown earlier in Figure 6.4, confirming the repeatability of the results. This provides a clear indication that at temperatures lower than 700 ^{o}C, reactions between steam and charcoal are slow and insignificant. However, at higher temperature (> 700 ^{o}C), charcoal starts to become reactive with steam. This observation is consistent with literature discussed earlier in Section 6.1.2.

In Figure 6.6 these results are presented in terms of the molar ratios of H_2:N_2 and CO:CO_2. If the ratio of H_2:N_2 is 2:1, then this indicates that 100 % of the steam was consumed. This condition is approached as the bed temperature approaches 900 ^{o}C.

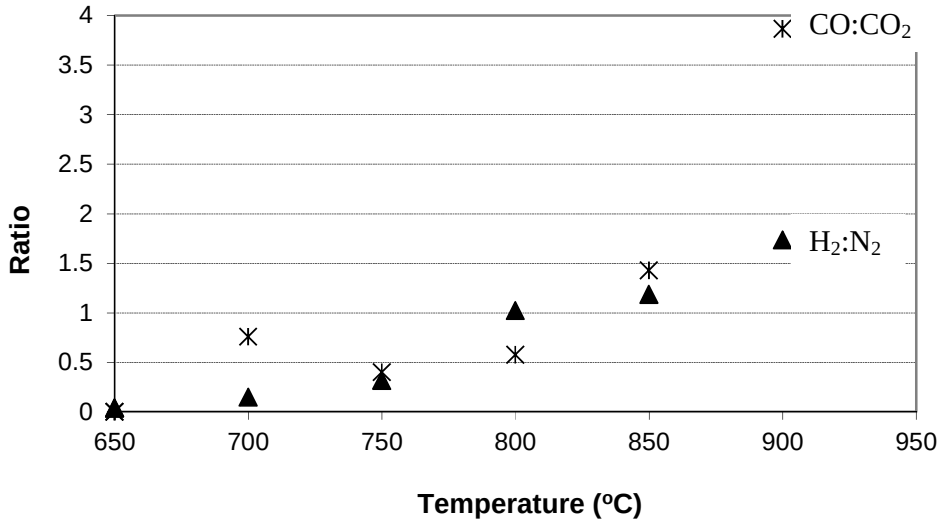

Figure 6.6 Molar ratios of H_2:N_2 and CO:CO_2 at different reaction temperatures.

The reactions that can take place are well described in the literature. For example, Chaudhari *et al.* (2003) proposed four important reactions to explain the steam gasification mechanism:

- the water gas reaction:

$$C + H_2O \leftrightarrow CO + H_2 \quad +131 \text{ MJ/kmol} \qquad (6.1)$$

- and the water gas shift reaction:

$$CO + H_2O \leftrightarrow CO_2 + H_2 \quad -40.9 \text{ MJ/kmol} \qquad (6.2)$$

- the Boudouard reaction:

$$C + CO_2 \leftrightarrow 2CO \quad +172 \text{ MJ/kmol} \qquad (6.3)$$

- the methane reaction:

$$C + 2H_2 \leftrightarrow CH_4 \quad -75 \text{ MJ/kmol} \qquad (6.4)$$

Yip *et al.* (2010) also compared the experimental ratios of CO_2:CO and H_2:CO, produced from the steam gasification of mallee biomass (from mallee trees growing in desert areas of Australia), and proposed that CO is likely to be the primary reaction product for the gasification of biochars used in their study. The reaction scheme: $C + H_2O \leftrightarrow CO + H_2$, and $CO + H_2O \leftrightarrow CO_2 + H_2$ contributed to the gaseous compositions observed, and the water gas shift reaction was primarily responsible for CO_2 formation. They also found that little CH_4 was formed during steam gasification of the biochars studied. Therefore, Reaction (6.4) was probably negligible.

From this discussion the increase in H_2 concentration (with temperature) is attributed to the increase in carbon conversion *via* Reaction (6.1). This also explains higher concentrations of CO and CO_2 at higher reaction temperatures. However, at higher temperatures the rate of the Boudouard reaction increases (Basu, 2010, pp. 123-124; Blasi, 2009), so CO_2 is converted into CO. Also, because the shift Reaction (6.2) is slightly exothermic, at higher temperatures the equilibrium is pushed to the left to create more CO, and all of these result in a higher $CO:CO_2$ ratio.

Chaudhari *et al.* (2003) in his paper concluded that: in the steam-carbon reaction, hydrogen atom and a hydroxyl radial, which adsorbs on adjacent carbon sites, are produced from dissociation of water at the carbon surface. This dissociation process normally forms hydroxyl species that are extremely active oxidizing agents. This mechanism is similar to that of the water gas shift reaction. Chaudhari *et al.* (2003) stated that carbon-oxide intermediate is involved in the reaction, while at typically high reaction temperature (>600 ^oC), hydrogen atoms quickly diffuse across carbon. Thus, the composition of the gas produced is determined by the relative rates of these reactions. Because of the complex interdependence of these gasification reactions, it is highly possible to produce syngas with desirable compositions by changing reactor design and operating conditions.

In conclusion, steam gasification of charcoal at high temperature produces a good quality gas stream with high concentration of H_2 and CO.

6.3.2 Charcoal Bed Temperature

During a set of experiments the temperature in the charcoal bed was recorded at:

- 10 mm into the top of the bed, and
- 10 mm into from the bottom of the bed.

The composition and flow of the exit dry gas were measured with the GC and a bubble flow meter, respectively.

Experimental conditions:

- N_2 flow rate was set at 0.1 litre/min (NTP).
- H_2O flow rate was set at 0.148 g/min.
- Molar ratio of H_2O:N_2 = 2:1.
- Temperature of the furnace was set at 500 ^oC, 600 ^oC, 700 ^oC and 750 ^oC.

For each run at each set point temperature of the furnace, the experiment lasted for 30 minutes. After that, the flow of water (steam) was stopped, and the temperatures were still observed continuously. From Figures 6.7(a) and (b) the following observations are made:

- At the lower set-point temperatures (500 and 600 ^oC) there were small variations in the bed temperature near the top of the bed.

- At higher operating temperatures (700 and 750 ^oC), temperatures remained relatively uniform.

This provides a good indication, with the combination of choice of tube i.d. for the reactor, and position inside the furnace, that relatively uniform temperatures were achieved throughout the course of an experiment in the charcoal bed.

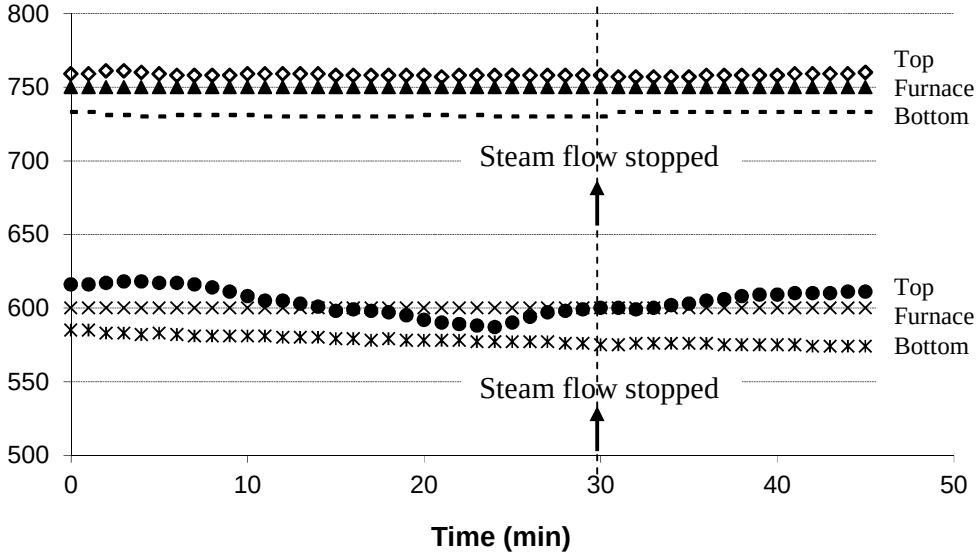

Figure 6.7(a) Temperatures in the bed - furnace temperature set at 600 ^{o}C and 750 ^{o}C.

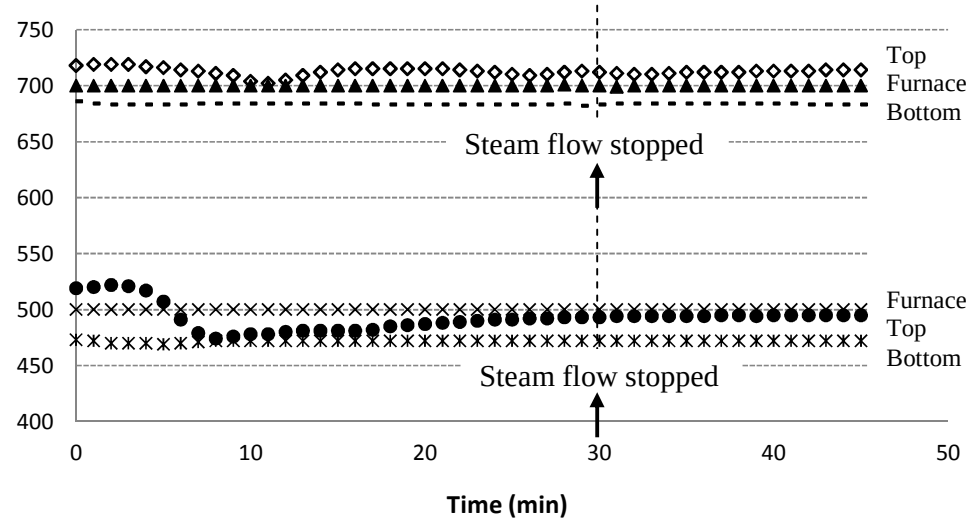

Figure 6.7(b) Temperatures in the bed - furnace temperature set at 500 ^{o}C and 700 ^{o}C.

From the results in Figure 6.7(c), because of the production of gas from the carbon in the char, the gas volume increases (molar expansion effect). This provides further evidence that steam gasification starts to become significant at T > 700 ^{o}C.

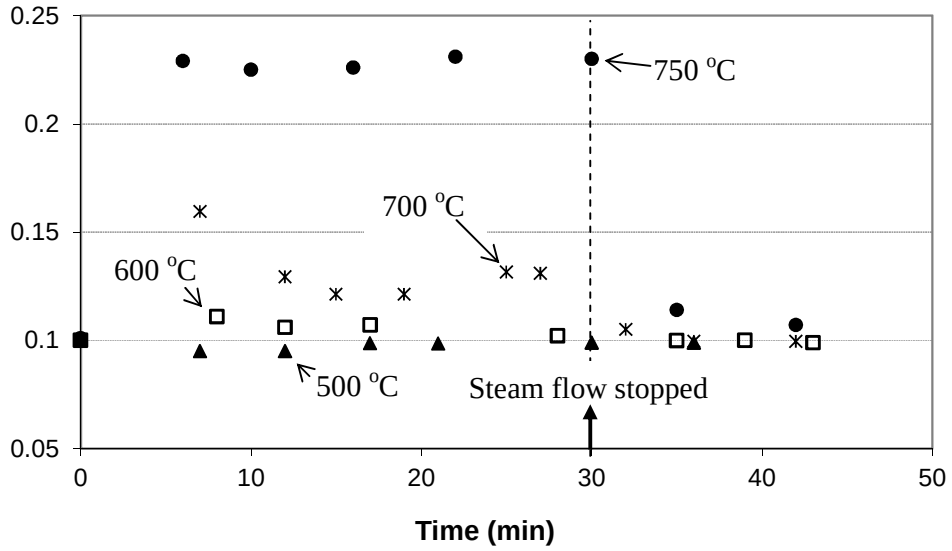

Figure 6.7(c) Dry gas flow from the reactor at different set-point temperatures.

Figures 6.7(d) and 6.7(e) represent the dry gas composition (GC measured) for two of the experimental runs at higher temperatures. The gas composition was stable after 10 minutes of operation.

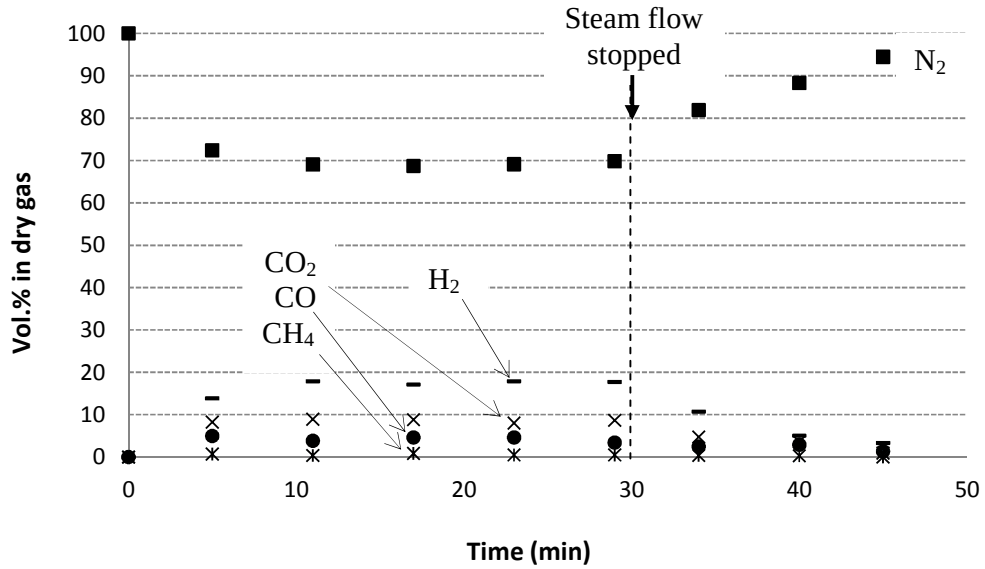

Figure 6.7(d) Dry gas composition at set-point temperature = 700 ^{o}C.

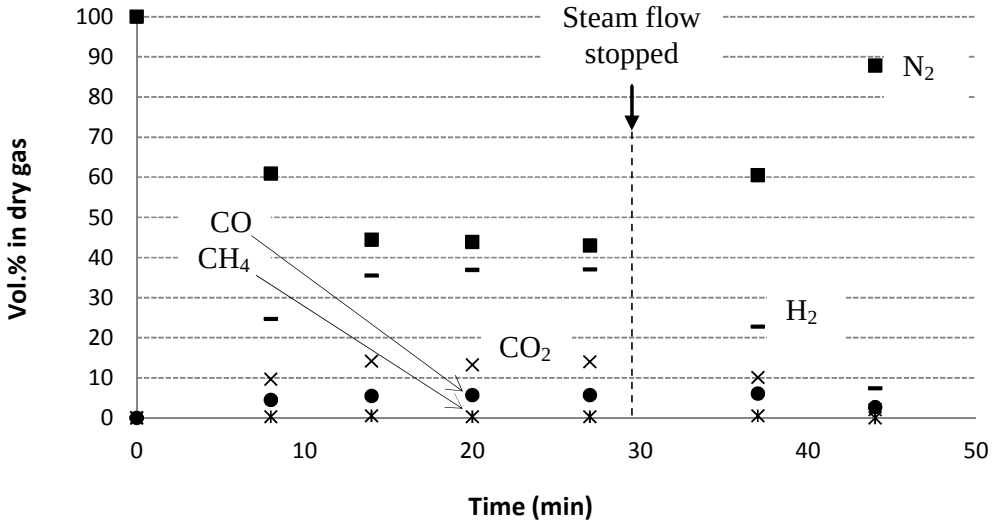

Figure 6.7(e) Dry gas composition at set-point temperature = 750 ^{o}C.

6.3.3 Effect of Molar Ratio of H_2O:N_2

To examine the effect of the molar ratio of H_2O:N_2, some experimental runs were performed at 700 and 750 ^{o}C, while the purge flow of N_2 was kept at 0.1 litre/min.

Experimental conditions:

- N_2 flow = 0.1 litre/min (NTP).
- H_2O flow was adjusted to vary the molar ratio of H_2O:N_2 from 1:3 to 10:1.
- Set-point furnace temperature at 700 ^{o}C and 750 ^{o}C.

A new run was started at each set point of molar ratio of $H_2O:N_2$. The dry gas composition was analysed using the GC. The results are showed in Figures 6.8 and 6.9.

Temperatures on the top and bottom of the char bed were observed during each run. It was shown that they were similar to data presented in Figures 6.7(a) and 6.7(b) (Section 6.3.2).

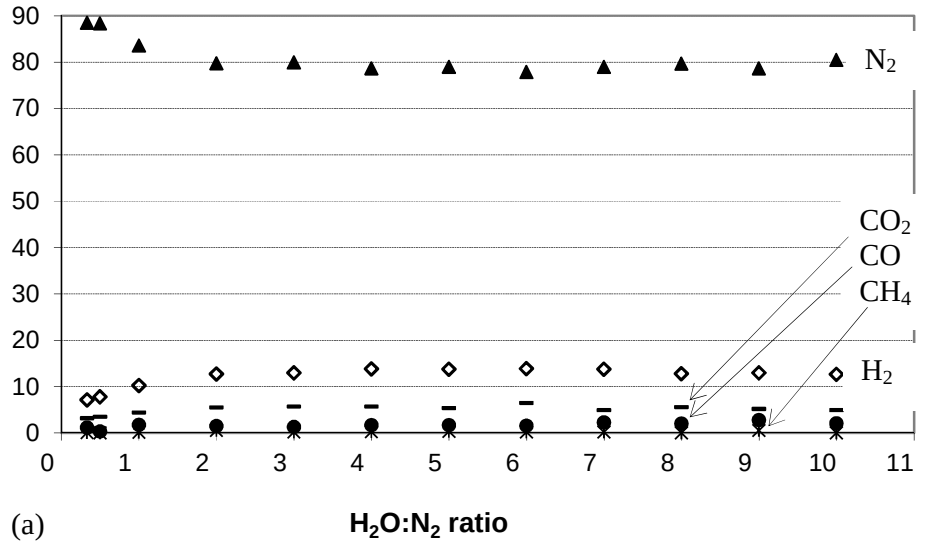

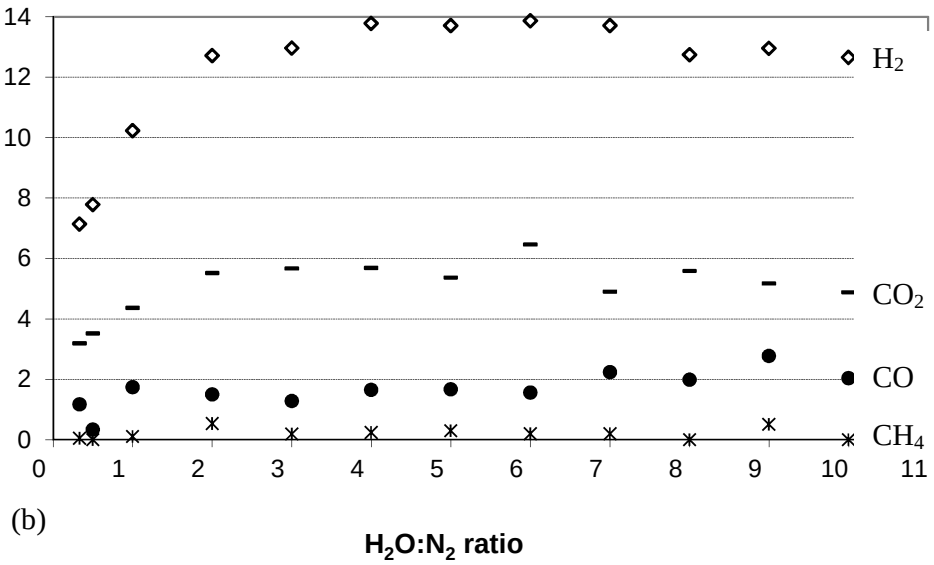

Figure 6.8 Furnace set at 700 ^oC: (a) dry gas composition, and (b) magnified view for H_2, CO_2, CO and CH_4.

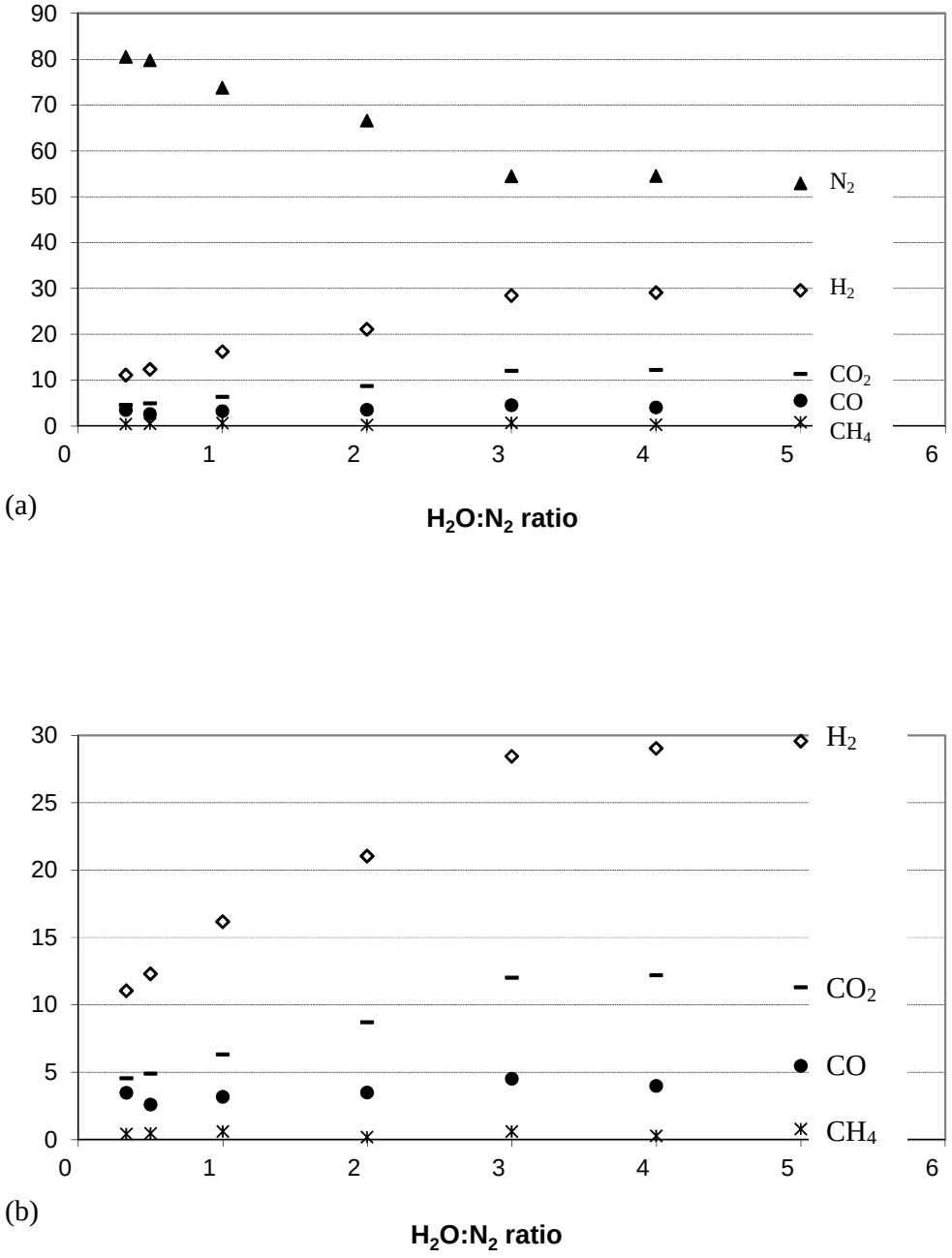

Figure 6.9 Furnace set at 750 ^{o}C: (a) dry gas composition, and (b) magnified view for H_2, CO_2, CO and CH_4.

As the ratio of H_2O:N_2 was increased from 0.5 to 3, then the concentration of H_2 increased. The concentration of CO remained relatively stable, while CO_2 increased. The increase in H_2 arises from the higher partial pressure of steam, that leads to an increase in carbon conversion *via* Reaction (6.1). It also enhances the water gas shift reaction (Reaction 6.2), resulting in an increase in the ratio of CO_2:CO in the gas stream. This matches observations made in Khor *et al.* (2006), and also in Chaudhari *et al.* (2003).

6.3.4 Effect of Gas Inlet Flow

Experimental conditions:

- N_2 gas flow was varied from 0.053 to 1 litre/min (NTP).
- H_2O flow was adjusted from 0.039 to 0.74 g/min, to keep the molar ratio of H_2O:N_2 = 1:1.
- Temperature of the furnace was set at 700 ^oC and 750 ^oC.

A new run was started at each set-point of gas flow, and dry gas composition was analysed using the GC. The results are showed in Figures 6.10, 6.11, 6.12 and 6.13.

Temperatures on the top and bottom of the char bed were also observed during each run. It was shown that they were similar to those presented in Figures 6.7(a) and 6.7(b) (Section 6.3.2).

Figures 6.10 and 6.12 indicate that in general, with an increase in gas velocity, the concentration of components H_2, CO and CO_2 tends to decrease. However, Figure 6.10 shows that above a N_2 flow of 0.7 litre/min, the change is relatively small.

Figures 6.11 and 6.13 present plots of H_2:N_2 ratio, which relates to the steam conversion, against the nitrogen flow rate, where team conversion decreases with gas velocity. Nevertheless, an insignificant trend was also observed at a high gas velocity, i.e. above a N_2 flow of 0.7 litre/min (Figure 6.11).

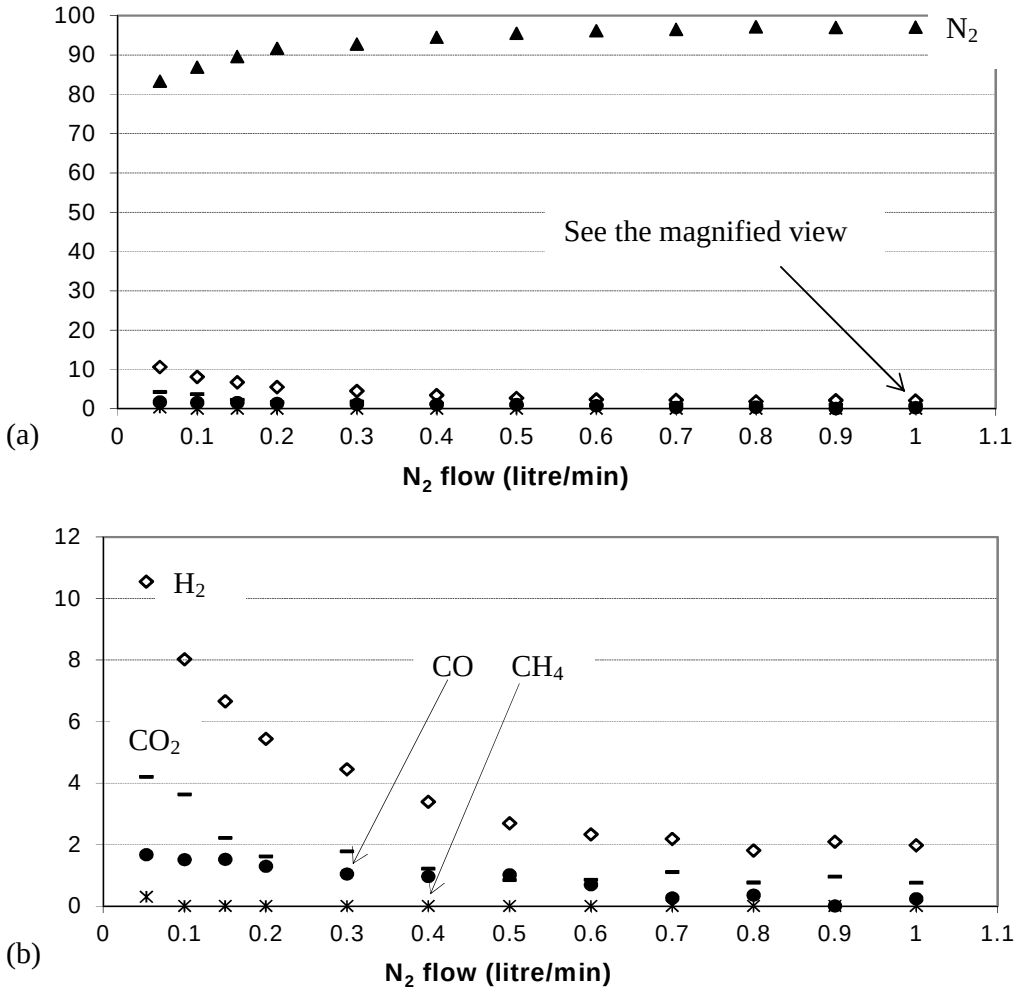

Figure 6.10 Furnace set at 700 ^{o}C: (a) gas composition, and (b) magnified view for H_2, CO_2, CO and CH_4.

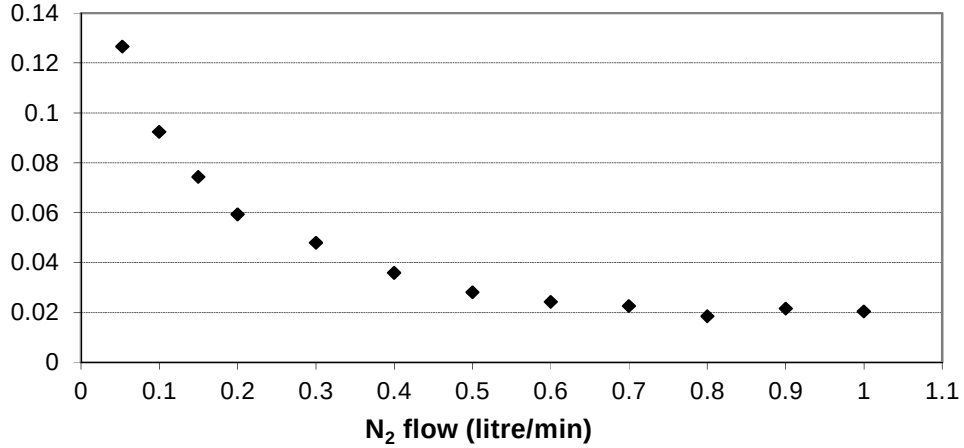

Figure 6.11 Experiments at 700 ^{o}C, the molar ratio of H_2:N_2 at different N_2 flows (with H_2:N_2 = 1 for 100 % conversion of steam).

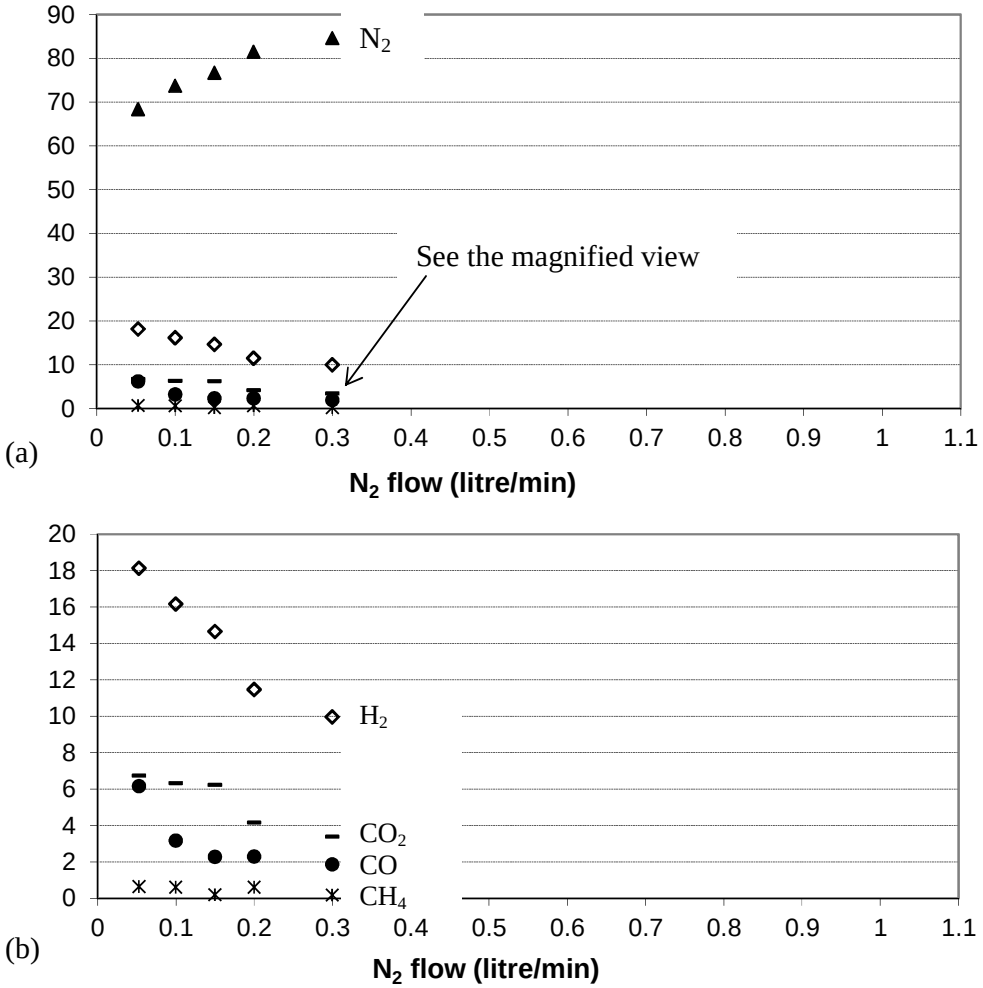

Figure 6.12 Furnace set at 750 ^{o}C: (a) gas composition, and (b) magnified view for H_2, CO_2, CO and CH_4.

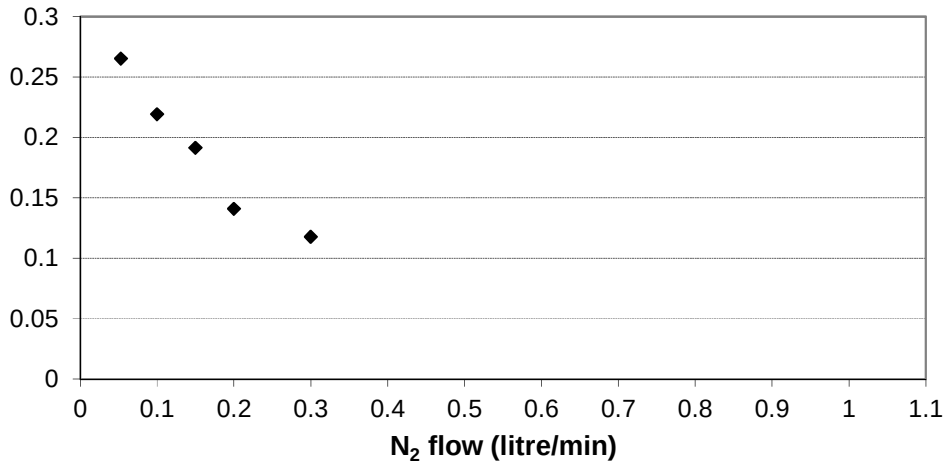

Figure 6.13 Experiments at 750 ^{o}C, the molar ratio of H_2:N_2 at different N_2 flows (with H_2:N_2 = 1 for 100 % conversion of steam).

In earlier experiments (Section 6.3.1) at 900 ^{o}C with 0.1 litre/min of N_2 flow and 0.148 g/min of H_2O, nearly 100 % of the steam was consumed. Therefore, it was decided to perform an extra experiment at these conditions, with the molar ratio of H_2O:N_2 at 2:1.

6.3.5 Extra Gas Flow Experiments for H_2O:N_2 at 2:1

Experimental conditions:

- N_2 flow was adjusted from 0.1 to 0.7 litre/min (NTP).
- H_2O flow was adjusted from 0.148 to 1.036 g/min, to keep molar ratio of H_2O:N_2 = 2:1
- Temperature of the furnace was set at 900 ^{o}C

This time both the QMS (continuous), and the GC (5½ min intervals) were used, and the results are shown in Figure 6.14.

Temperatures on the top and bottom of the char bed were observed to be the same as the furnace temperature (900 ^{o}C) during the experiment.

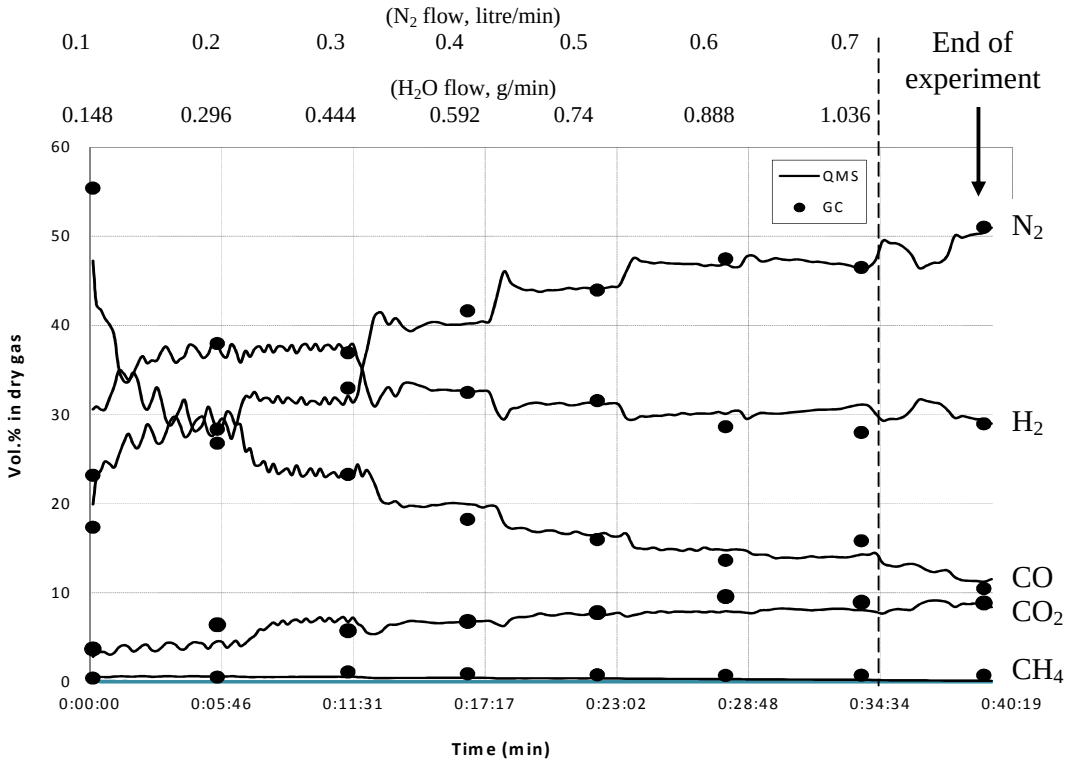

Figure 6.14 Furnace set at 900 ^{o}C and the nitrogen flow was varied (maintaining H2O:N2 = 2:1).

At this temperature of 900 ^{o}C, the change in H_2 concentration is relatively small, while the change in CO concentration is more significant.

It is expected (e.g. Paviet *et al.*, 2008) that at higher temperatures, diffusion effects will start to become more significant. Thus, at higher gas flows, the diffusion resistance (external mass transfer resistance) decreases, leading to an increase in char conversion rate. To explore this further, the production rates of CO, CO_2 and H_2 were calculated for this set of experiments.

For example, the production component *i* was calculated from:

$$F_i = \frac{y_i}{y_{N_2}} \times F_{N_2} \qquad (6.5)$$

where: F_i : molar flow rate of component i in the product stream, mol/h

y_i : mole fraction of component i in the product stream

Figures 6.15, 6.16, and 6.17 present the production rates of H_2, CO and CO_2, respectively.

From these results, across the range of conditions tested at 900 ^{o}C, the production rates of H_2, CO and CO_2 all increase with gas flow. The rates are higher than the experiments performed at the lower temperatures.

At this point it is worth mentioning that the reactivity of the charcoal may increase during the course of an experiment, and this could also lead to slightly higher rates of reaction as the gas flow was gradually increased. An increase in char activity with time has been observed in the literature (e.g. Wu *et al.*, 2009; and Yip *et al.*, 2010), and arises from the evolution of the char structure, and influence of alkali and alkaline earth metallic species. This includes changes in pore structure and size, and also catalytic activity.

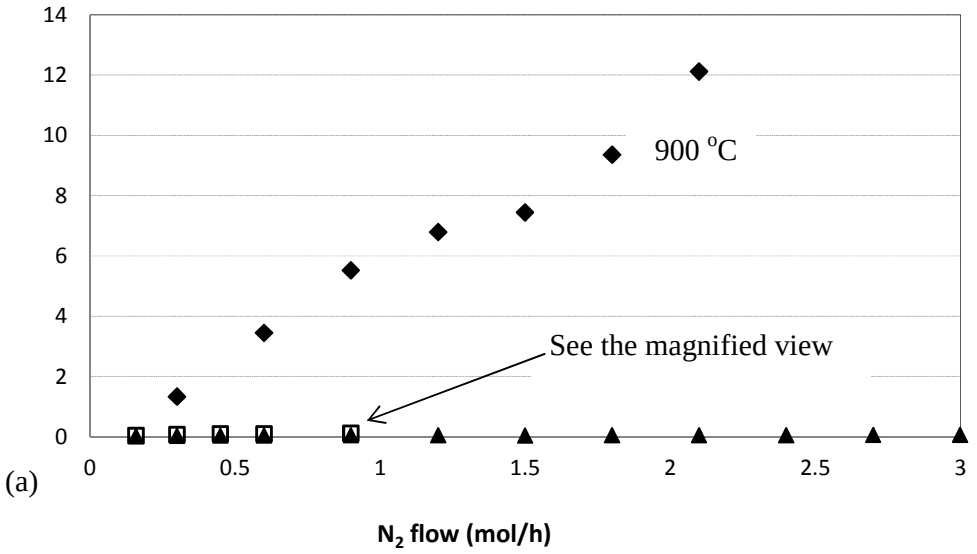

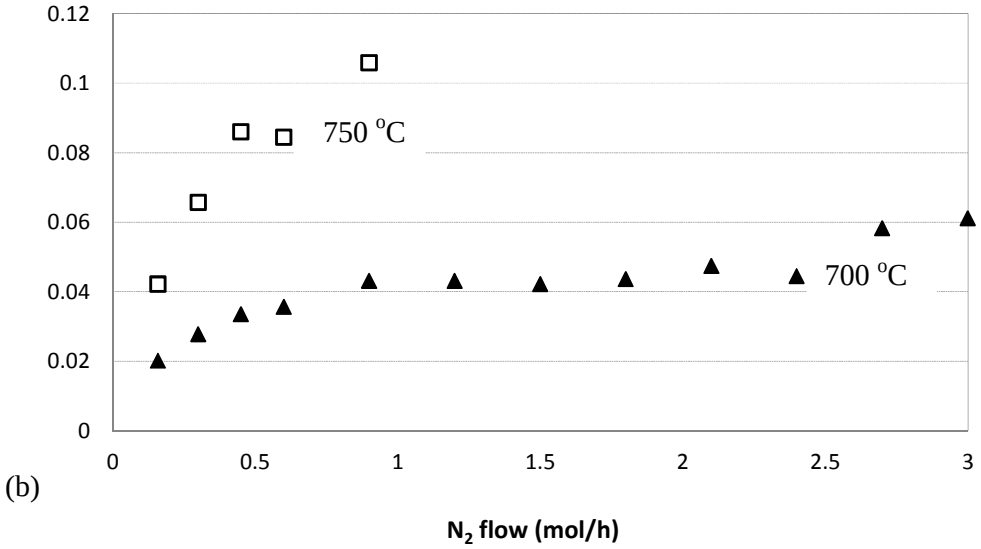

Figure 6.15 The production rate of H_2 (a) at 900 °C, and (b) magnified view at 700 °C and 750 °C.

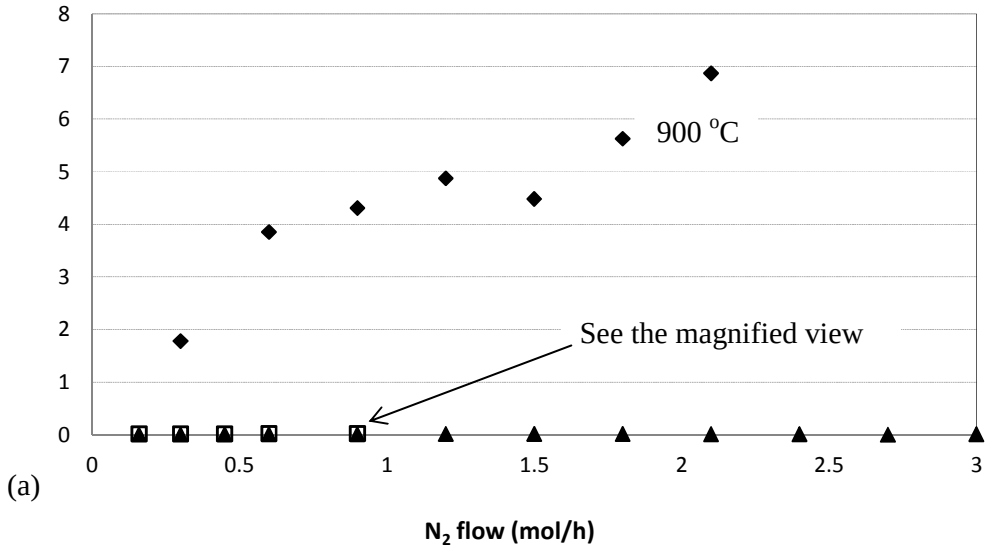

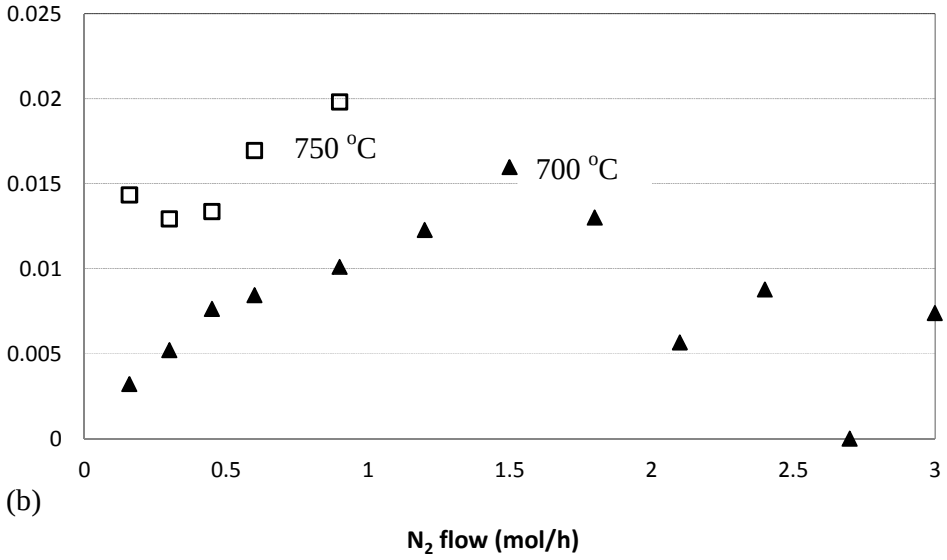

Figure 6.16 The production rate of CO (a) at 900 °C, and (b) magnified view at 700 °C and 750 °C.

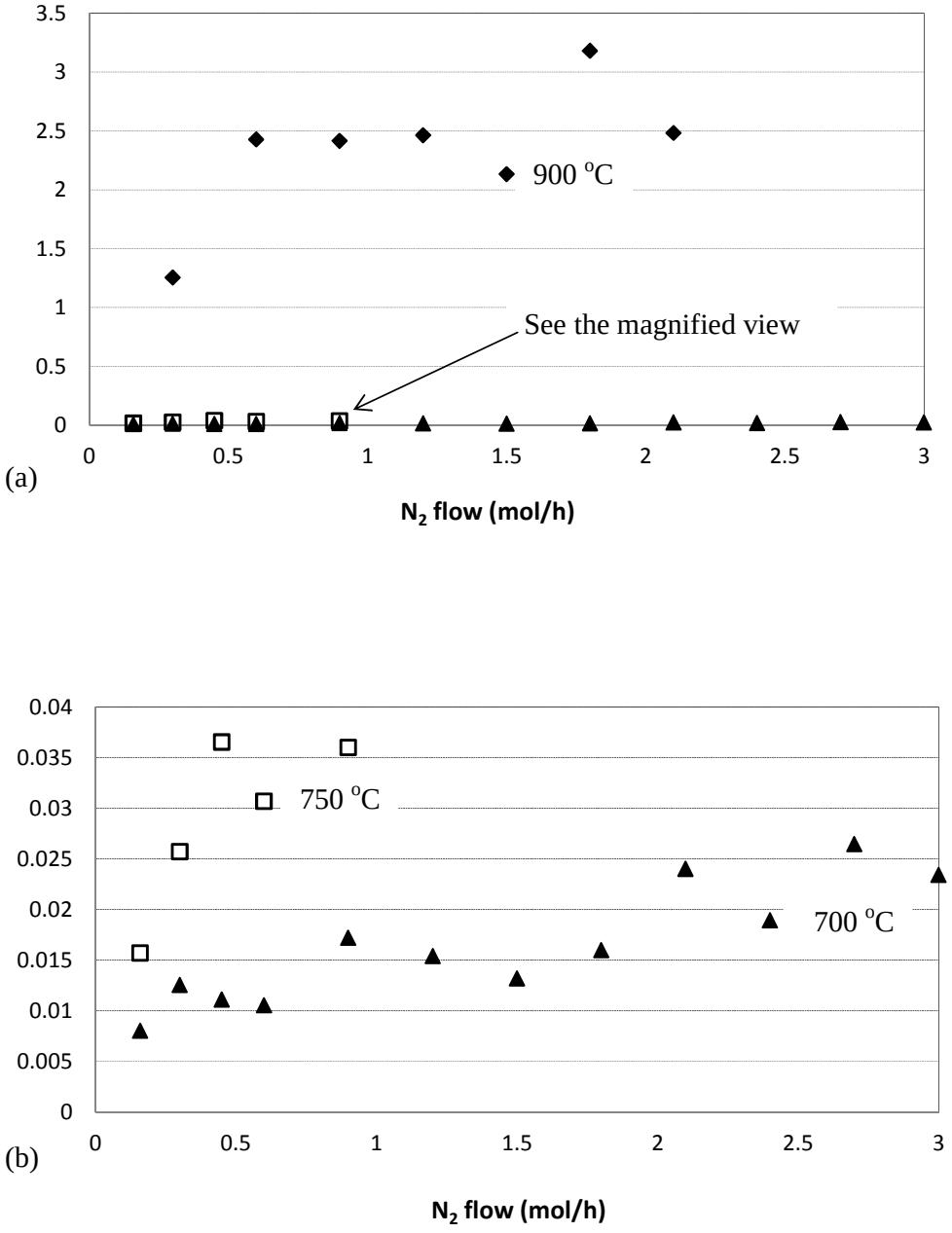

Figure 6.17 The production rate of CO_2 (a) at 900 ^oC, and (b) magnified view at 700 ^oC and 750 ^oC.

6.4 GASIFICATION OF WOOD CHARCOAL WITH AIR/STEAM

6.4.1 Using Charcoal Particles ~4 mm in Diameter

In the presence of a flow of air through the charcoal bed (~4 mm particles) it was found that the charcoal pellets started to become ignited at around 450 to 500 ^{o}C. This established a suitable temperature of operation. Then experiments were performed at different air to steam ratios, the QMS was used for analysis, and the results are presented in Figure 6.18. The flow of air and steam was increased gradually, resulting in a change in the wt.% of steam in the feed stream. The CO concentration reaches around 10 vol.%, while the H_2 concentration is low when the steam input is < 11.4 wt.%. However, at higher levels of steam input, the H_2 becomes more significant and reaches nearly 20 vol.% (when steam input was 27.8 wt.%), while the CO reaches 16 vol.%. At the end of the 25th minute as all of the charcoal in the bed had been consumed, then O_2 was detected in the gas.

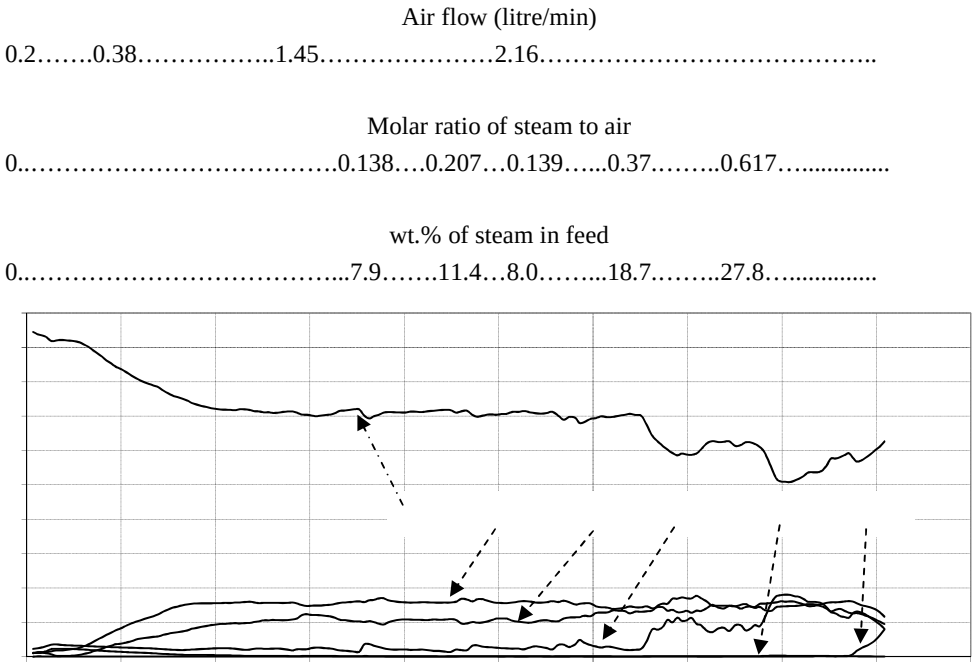

Figure 6.18 Steam/air gasification of 4 mm wood charcoal pellets (furnace temperature set at 500 ^{o}C).

6.4.2 Using Charcoal Powder

Samples of charcoal were then ground into a powder (particle size ~ 375 μm in mean diameter), and the experiment was repeated. The results are presented in Figure 6.19. In this case, there was a significant pressure drop across the charcoal, making it difficult to increase the gas flow, and to control the addition of water (steam) to the desired value.

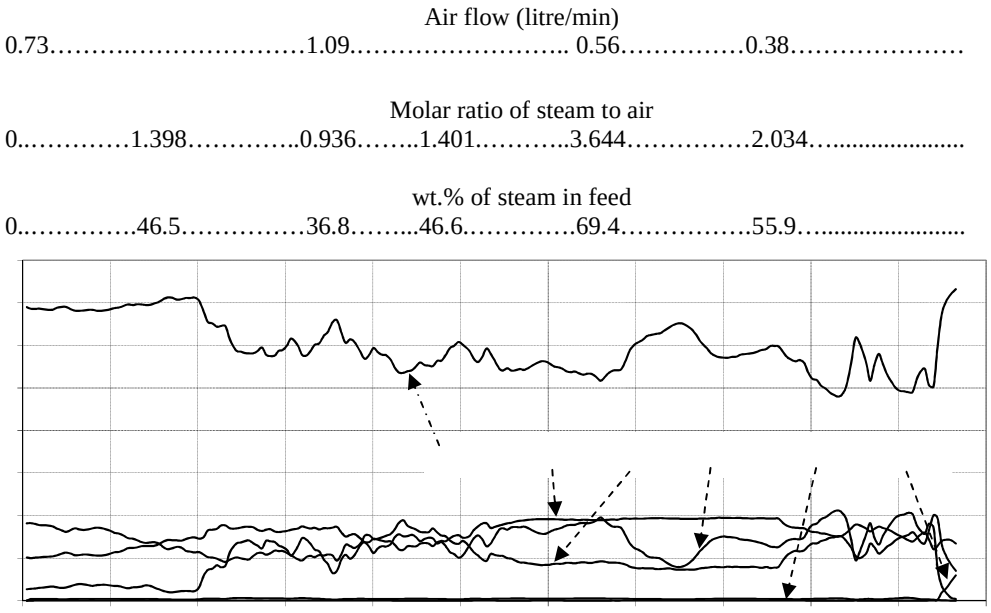

Figure 6.19 Steam/air gasification of wood charcoal powder (furnace temperature set at 500 ^{o}C).

From Figure 6.19, when steam input is 36.8 wt.%, the concentrations of CO and H_2 are quite high (more than 15 vol.% for each). Then when the steam flow is increased, a higher concentration of H_2 is produced, but a lower value of CO is obtained. This may be explained due to the equilibrium of two Reactions (6.1) and (6.2), meaning that more steam in the reactant stream would produce more H_2 and CO_2, but less CO. The higher rate of H_2 production with an increase in steam flow was also reported in a study carried out by Khor *et al.* (2006), where H_2 formation reached a peak of 21 vol.% with steam at 35 wt.% of the total reactant input.

When the steam feed rate is increased further to 69.4 wt.% (Figure 6.19), the H_2 concentration declines to about 10 vol.% The drop in H_2 evolution may be due to a drop in the temperature of the bed. This was also noted in Khor *et al.* (2006), where the H_2 formation decreased from 21 vol.% to about 18 vol.%, when the steam input rate was increased from 35 wt.% to 40 wt.%.

6.5 GASIFICATION OF RDF-DERIVED CHAR WITH AIR/STEAM

RDF-derived char (mainly in form of powder, ~ 305 μm in mean diameter) from a commercial pilot-scale gasifier (with about 50 wt.% ash) was used for new runs at different ratios of air/steam. The results of these experiments are presented in Figure 6.20.

From Figure 6.20, with a steam input < 25.5 wt.%, the H_2 concentration remains low (about 5 vol.%). When the steam input = 51 wt.%, then the H_2 concentration increases considerably to 20 vol.%, while CO is still stable at 10 vol.% in the dry producer gas.

From these results, a steam input of about 50 wt.% makes the gas composition look viable, although further work would be necessary to optimize the system for a particular design of reactor.

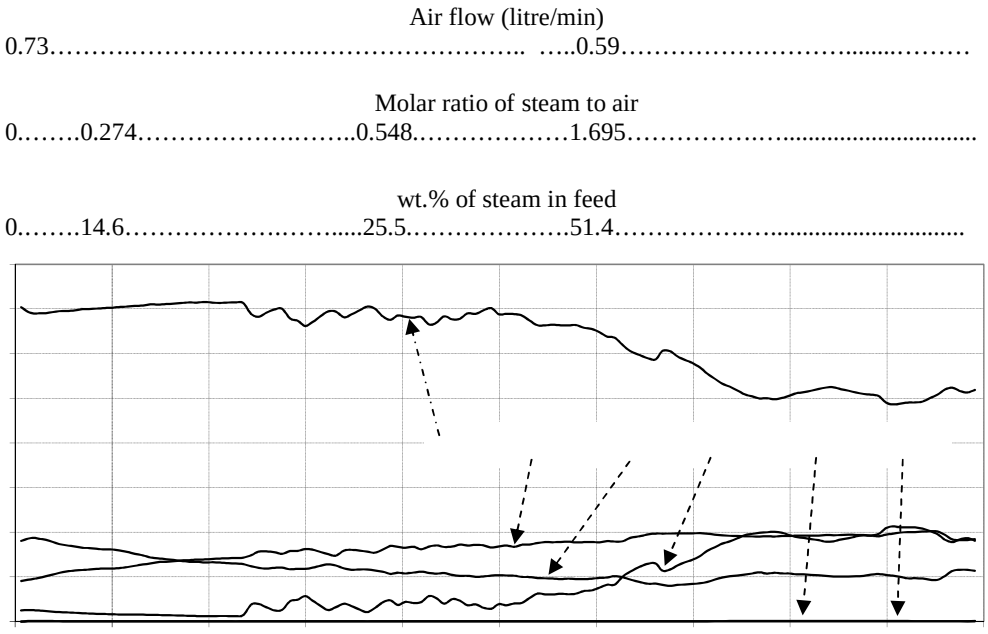

Figure 6.20 Steam/air gasification of RDF-derived char powder (furnace temperature set at 500 ^{o}C).

6.6 GASIFICATION OF RDF-DERIVED CHAR WITH AIR/STEAM IN A LARGER DIAMETER REACTOR

6.6.1 Experimental Setup

The small diameter metal tube (9.5 mm i.d.) in the furnace was now replaced by a 100 mm i.d. quartz tube, and this was filled with RDF-derived char (about 50 wt.% ash, particle size ~ 305 µm in mean diameter) from a real downdraft pilot-scale gasifier. The apparatus is illustrated in Figures 6.21, 6.22 and 6.23. Air and water streams were fed down a tube into the base of the quartz tube, where the water turned to steam, and the resulting gas mixture was preheated in the wire mesh zone in the furnace (see Figure 6.21). Although the top part of the quartz-tube was insulated, by removing this insulation, it was possible to see what was taking place inside this gasifier.

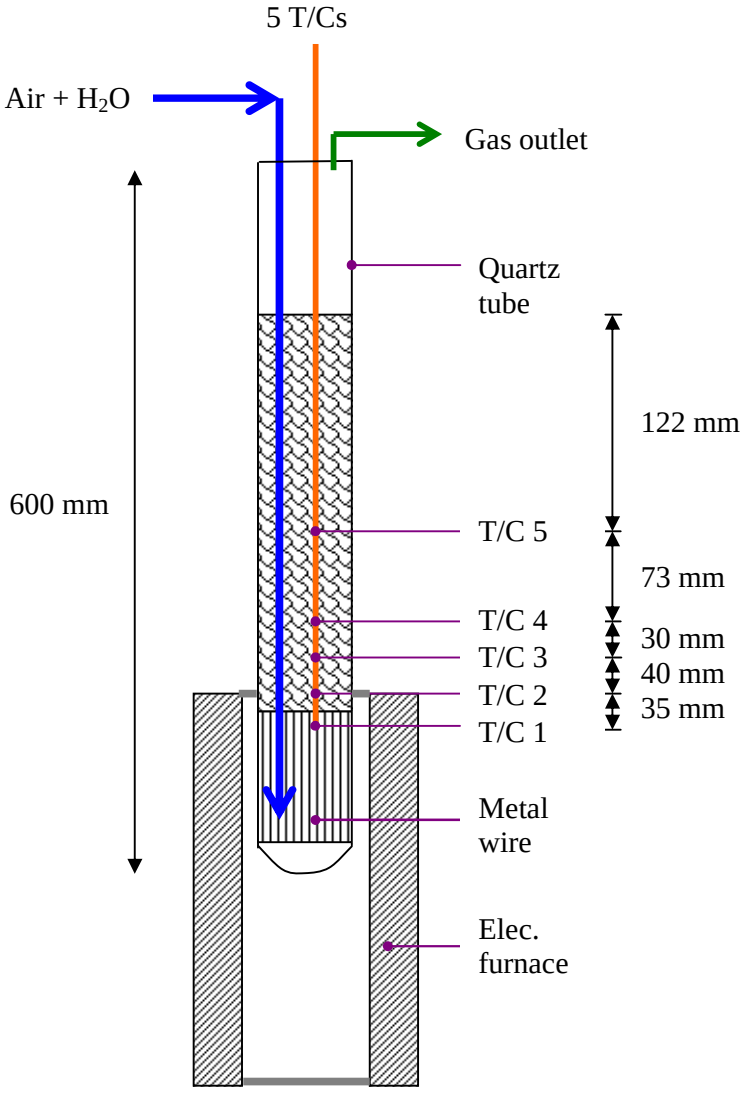

Figure 6.21 Schematic of the 100 mm i.d. quartz-tube char gasifier.

Figure 6.22 The 100 mm i.d. quartz-tube prepared for an experiment.

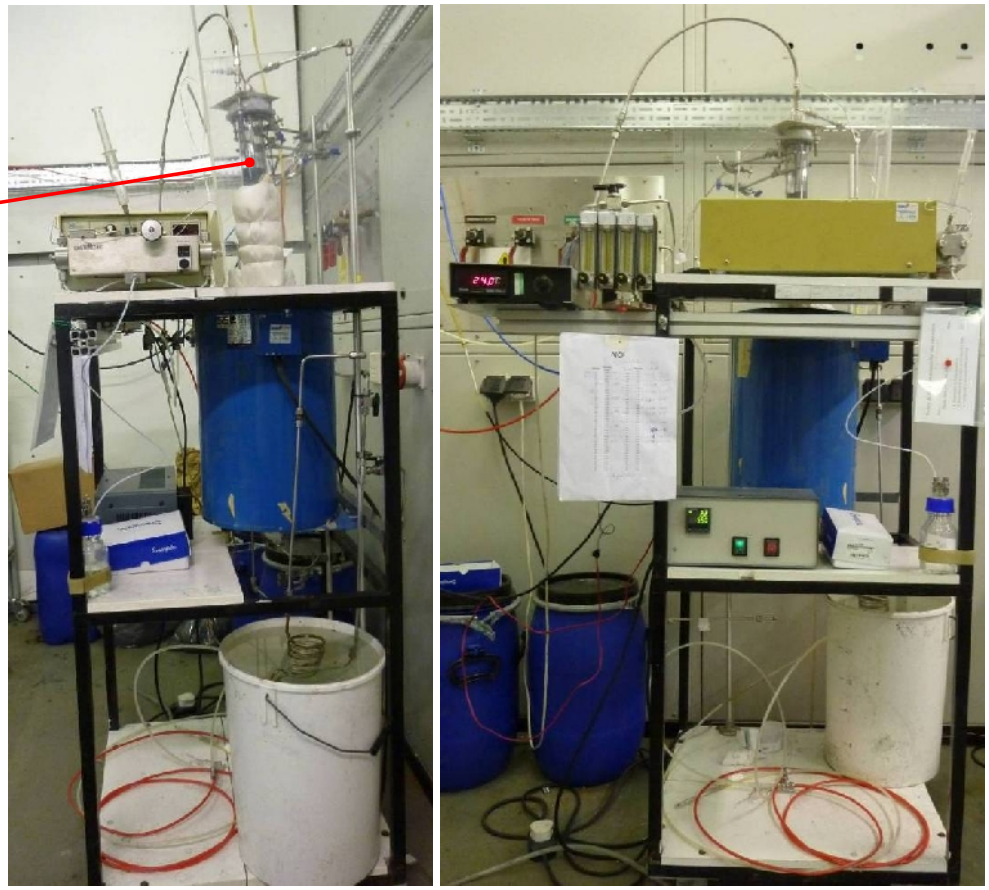

Figure 6.23 Photos of the apparatus – left picture shows the quartz-tube with insulation.

6.6.2 Experimental Results

This size of reactor is now starting to look like a small pilot-scale packed-bed gasifier, and because of the increase in the diameter of the tube, higher gas flows had to be used. Unfortunately, it was impossible to perform experiments above an air flow of about 3.5 litre/min, as above that the char bed started to expand (visual observation), and would then have become fluidized.

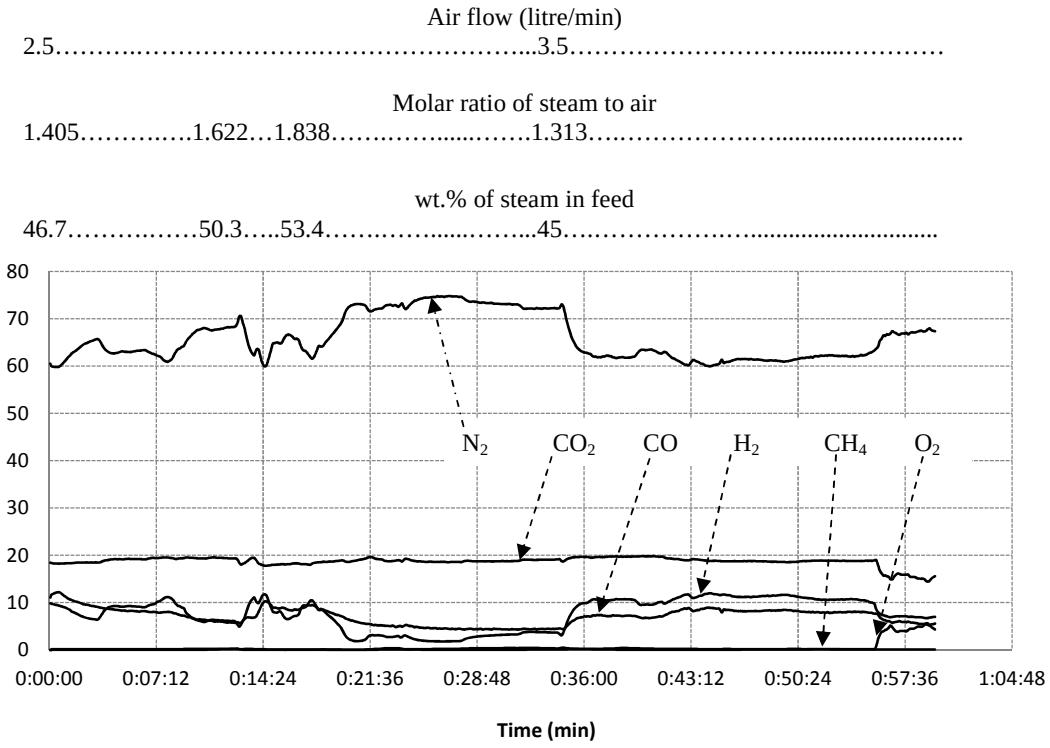

Figure 6.24 Experiments in 100 mm i.d. quartz-tube gasifier - steam/air gasification of RDF-derived char (furnace temperature set at 500 ^{o}C).

From Figure 6.24, between 45 to 50 wt.% of steam in the feed, the concentrations of CO and H_2 are significant (around 7 - 10 vol.%). At 53 wt.% of steam in feed, their concentrations decrease to around 5 vol.%. With the insulation lifted for a brief moment, photographs were taken during this experiment, and some are shown in Figure 6.25.

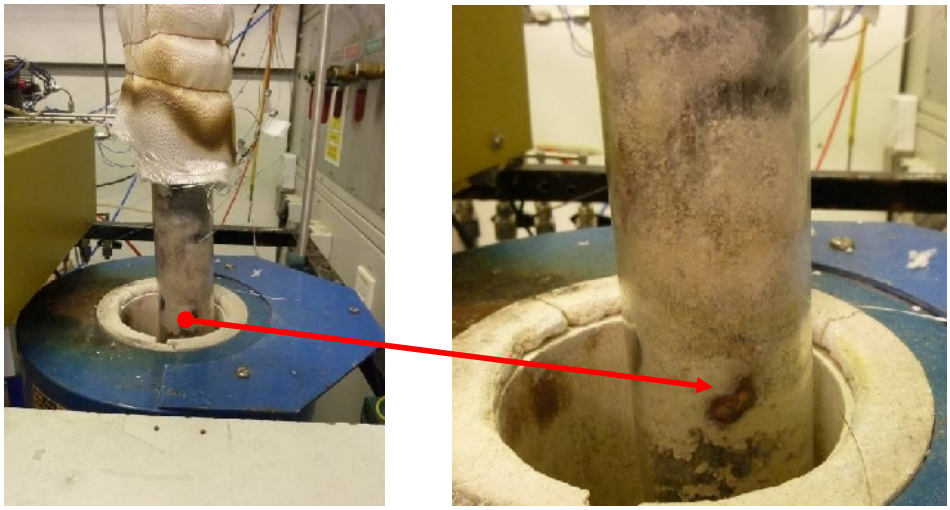

Figure 6.25 Photographs taken during an experiment.

This set of results is interesting for a number of different reasons:

a) They demonstrate that this approach is viable, although further work is clearly necessary.

b) They also highlight a number of practical difficulties in trying to scale-up experiments from a 9.5 mm i.d. tube, to a 100 mm i.d. tube.

- At higher gas flows the bed started to lift and become fluidized.
- Channelling was visible in the bed, and some of the regions became more active than others (evident from visual observations of hot zones, and also grey regions that had been turned into ash).
- Practical issues arose from the vaporisation of steam in this type of arrangement.
- It was not easy to heat the inside of the bed *via* an external method such as furnace – this aspect has to be factored into any conceptual design.

c) Measurement of temperatures was difficult, as when the reaction front moved from the bottom upwards in the bed, the temperature also changed depending on the position of the thermocouples in the bed. Temperatures were observed to peak at 1028 ^{o}C.

Finally, it is concluded that a reaction system in which the bed is fluidized, would probably be the best way to progress this further, though this is outside the scope of the work in this thesis. Nevertheless, some very useful basic data have now been acquired, which would assist such further work.

6.7 CONCLUDING REMARKS AND IMPLICATIONS FOR FURTHER WORK

From the steam gasification experiments of charcoal in the 9.5 mm i.d. stainless steel fixed bed gasifier:

(a) At temperatures above 700 ^{o}C, charcoal starts to be gasified by steam, becoming more significant as the temperature is increased up to 900 ^{o}C.

(b) The ratio of H_2:CO, and the ratio of CO:CO_2 in the gas stream can be adjusted slightly by changing the reaction temperature. This means that gas composition could be tuned to an end use application.

(c) In general, a rise in the partial pressure of steam increases desirable reactions, but there is a limit, which also depends on the design of the system.

(d) An increase in char reactivity with gas flow was also found, probably caused by enhanced external mass transfer, and possible changes in char structure with time. This aspect is also recommended for further work.

From the steam/air gasification experiments of wood charcoal:

(e) A steam input between 28 to 51 wt.% of the feed could be suitable, where H_2 and CO could reach 20 vol.% and 15 vol.%, respectively. However, these values also depend on the flow of air.

From the steam/air gasification experiments of RDF-derived char:

(f) When the steam input = 51 wt.%, then the H_2 concentration increased considerably to 20 vol.% while CO was still stable at 10 vol.% in the dry producer gas.

(g) Steam/air gasification of RDF-derived char is a viable process. However, as the particle size is small, a fluidized-bed gasifier rather than a packed-bed system should be considered for such an application.

In the next chapter, a kinetic study of the gasification of this RDF-derived char in steam is performed.

RERERENCES

Basu, P. (2010). Biomass Gasification and Pyrolysis. Elsevier Inc.

Blasi, C.D. (2009). Combustion and gasification rates of lignocellulosic chars. Process in Energy and Combustion Science, Vol. 35, pp. 121-140.

Boateng, A.A. (2007). Characterization and thermal conversion of charcoal derived from fluidized-bed fast pyrolysis oil production of switchgrass. Ind. Eng. Chem. Res., Vol. 46, No. 26, pp. 8857-8862.

Brewer, C. E., Schmidt-Rohr, K., Satrio, J.A. and Brown, R.C. (2009). Characterization of biochar from fast pyrolysis and gasification systems. Enviromental Progress & Systainable Energy, Vol. 28, No. 3, pp. 386-396.

Chaudhari, S. T., Dalai, A.K. and Bakhshi, N.N. (2003). Production of Hydrogen and/or Syngas (H_2 + CO) via steam gasification of biomass-derived chars. Energy and Fuel, Vol. 17, No. 4, pp. 1062-1067.

Devi, L., Ptasinski, K.J. and Ganssen, F.J.J.G. (2003). A review of the primary measures for tar elimination in biomass gasification processes. Biomass and Bioenergy, Vol. 24(2), pp. 125-140.

Khor, A., Ryu, C., Yang, Y., Sharifi, V.N. and Swithanbank, J. (2006). Clean Hydrogen Production via Novel Steam-Air Gasification of Biomass. WHEC 16/13-16, Lyon France.

Knoef, H.A.M.,edited, (2005). Handbook Biomass Gasification. BTG biomass technology group.

Paviet, F., Bals, O. and Antonini, G. (2008). The effects of diffusional resistance on wood char gasification. Process Safety and Environment Protection, Vol. 86, pp. 131-140.

Paviet, F., Bals, O. and Antonini, G. (2007). Kinetic study of various chars steam gasification. International Journal of Chemical Reactor Engineering, Vol. 5, Article A80.

Yip, K., Tian, F., Hayashi, J. and Wu, H. (2010). Effect of alkali and alkaline earth metallic species on biochar reactivitiy and syngas composition during steam gasification. Energy Fuels, Vol. 24, pp. 173-181.

Wu, H., Yip, K., Tian, F., Xie, Z. and Li, C.Z. (2009). Evolution of char structure during the steam gasification of biochars produced from the pyrolysis of various mallee biomass components. Ind. Eng. Chem. Res., Vol. 48, No. 23, pp. 10431-10438.

CHAPTER 7

Steam Gasification Kinetics of RDF-derived Char

In this chapter, the gasification kinetics of RDF-derived char with steam are explored further. During such experiments, the nature of the char particle changes with time (e.g. size, porosity, ash content and catalytic properties), which also results in a change in its reactivity. This creates additional challenges and makes this type of experiment to become very difficult. Nevertheless, this data is useful as it will help with the design of a unit (e.g. fluidized bed gasifier) in which the carbon content in these char particles could be converted into a gaseous fuel. Data on kinetics is useful as it helps to estimate the residence time required in a reactor to achieve the desired conversion.

This chapter consist of descriptions of:

- the RDF-derived char (properties and particle size variations),
- the experimental apparatus, and
- the kinetic experiments.

This work is novel as there is relatively little information in the literature on the gasification kinetics of RDF-derived char.

7.1 INTRODUCTION TO KINETICS OF CHAR GASIFICATION

There have been numerous studies on the kinetics of steam gasification of char (e.g. Paviet *et al.*, 2008; Ahmed and Gupta, 2010; and Wu *et al.*, 2006), and these studies have been performed on char from wood, food waste, or coal. It is well recognized that char reactivity depends not only on operating parameters (e.g. temperature, pressure, steam ratio), but also on the source of the char and how it was produced. For example, wood char reactivity is reported to increase with carbon conversion (Mermoud *et al.*, 2006a), whereas that of coal char decreases with carbon conversion (Liu *et al.*, 2006).

Temperature: Many of the studies in the literature on steam gasification kinetics of chars are performed at temperatures < 1000 ^{o}C, at which according to Blasi (2009), the rate of diffusion through the pores of reacting chars plays no role in determining the overall rate of reaction. These are usually referred to as the kinetically controlled conditions.

Gas velocity: The effect of gas velocity was also considered in some studies. For example, Paviet *et al.* (2008) reported that gas velocity had influence on the external mass transfer resistance, and at high gas velocity (from 10 to 20 cm/s) this influence could be considered to be negligible. Mermoud *et al.* (2006a) also suggested that gas velocity had a gentle influence on gasification, although there was no clear observation due to the repeatability of the experiments and the real effect of the gas velocity.

Particle size: Char particle size was reported to have no effect by some authors (e.g. Paviet *et al.*, 2008). Others have reported a retarding effect on the rate as the particle size is increased (e.g. Mermoud *et al.*, 2006a; and Mani *et al.*, 2011).

- Paviet *et al.* (2008), in an investigation of the effects of diffusional resistance on wood char gasification in a tubular kiln reactor, reported no significant influence on wood char gasification for mean char particle sizes of 0.1 mm and 0.47 mm. They suggested that the internal mass transfer at this condition could be considered to be negligible (experiments at T = 900 to 1000 ^{o}C, and steam partial pressure from 0.1 to 0.7 atm).

- Mali *et al.* (2011), in an investigation of reaction kinetics and mass transfer of wheat straw char with CO_2 using TGA, found that particle size (<60 - 925 μm) had

much influence on the char gasification reaction, and reactivity decreased as the particle size increased (experiments performed at T = 750 ^{o}C to 900 ^{o}C, with CO_2 partial pressure of 1 atm).

- Mermoud *et al.* (2006a) formed similar conclusions as Mali *et al.* (2011). However, they investigated the steam gasification of single wood charcoal particles (10 to 30 mm in size) at different temperatures (830 to 1030 ^{o}C), and different steam partial pressures (0.1 to 0.4 atm). They concluded that internal mass transfer was influencing the reaction under these operating conditions – although that is not surprising as the charcoal particles are large.

AAEM species: It is well-known that alkali and alkaline metallic (AAEM) species can be good catalysts for the combustion and gasification of solid carbonaceous fuels such as biomass or biochar (e.g. Wu *et al.*, 2009; and Yip *et al.*, 2010). Moreover, Wu *et al.* (2009) concluded that the catalytic effect seems also dependent on the biochar carbon structure that can probably affect the catalyst dispersion. Consideration of the effects of catalysts and evolution of carbon structure during gasification will not be considered in any detail in this chapter; however, they will be used to explain the evolution of reactivity of RDF-derived char during the gasification process.

Assumptions leading to experimental technique: There were a number of important assumptions made, which led to the choice of experimental technique:

(a) Everson *et al.* (2006) and Huang *et al.* (2010) concluded that char-CO_2 and char-steam reactions proceed on separate active sites at atmospheric pressure. Thus, in this present study, it was decided to study the steam gasification of char as a separate experiment.

(b) Although some authors (e.g. Everson *et al.*, 2006; Huang *et al.*, 2010) have presented evidence of the inhibition effects of CO in CO_2-char reactions, and H_2 in steam-char reactions, in this study it is assumed that there are no inhibition effects.

(c) The partial pressure of the gasifying agent (H_2O) is considered to remain unchanged along the reactor, even though it is inevitably consumed in reality. This

assumption was also applied in other studies in the literature (e.g. Ahmed and Gupta, 2010; Yip *et al.*, 2010; Wu *et al.*, 2006; and Cozzani, 2000).

(d) Many of the kinetic experiments on char gasification have been performed using a thermo gravimetric apparatus (TGA), and the carbon conversion was measured by the loss in the weight of the sample (e.g. Mani *et al.*, 2011; Huang *et al.*, 2010; Everson *et al.*, 2006; Mermoud *et al.*, 2006a; and Cozzani, 2000). However, there are also problems with this technique (use of low gas flows, and measurement of small changes, possible external mass transfer effects, Liu *et al.* (2006)). Hence, it was decided to perform such experiments in a small packed-bed reactor, which is often used in heterogeneous catalytic experiments.

7.2 EXPERIMENTAL APPARATUS

The experimental work was carried out using a batch type fixed-bed reactor at atmospheric pressure as illustrated in Figures 7.1 and 7.2. The reactor was a vertical stainless steel tube with an inner diameter of 15.6 mm, filled with RDF-derived char particles, in which the char bed depth could be varied from 1.6 to 23.7 mm. This was positioned inside an electrically heated furnace, and the temperature inside the char bed was measured using a thermocouple located at the top of the char bed. The char bed was supported by two quartz wool layers which retained the char and ash particles.

In experiments with steam, the water and nitrogen passed through a stainless steel tube put inside the furnace, which vaporized the water and preheated the gas. The nitrogen flow was adjusted with a rotameter, while that of the water was manipulated by using a metering pump.

The producer gas exiting from the top of the reactor flowed through a cooling coil, and condensate was trapped in two plastic vessels connected in series. The gas was passed through a glass wool filter, and then discharged into the vent from the fume cupboard. A gas stream was passed to a QMS for on-line gas analysis.

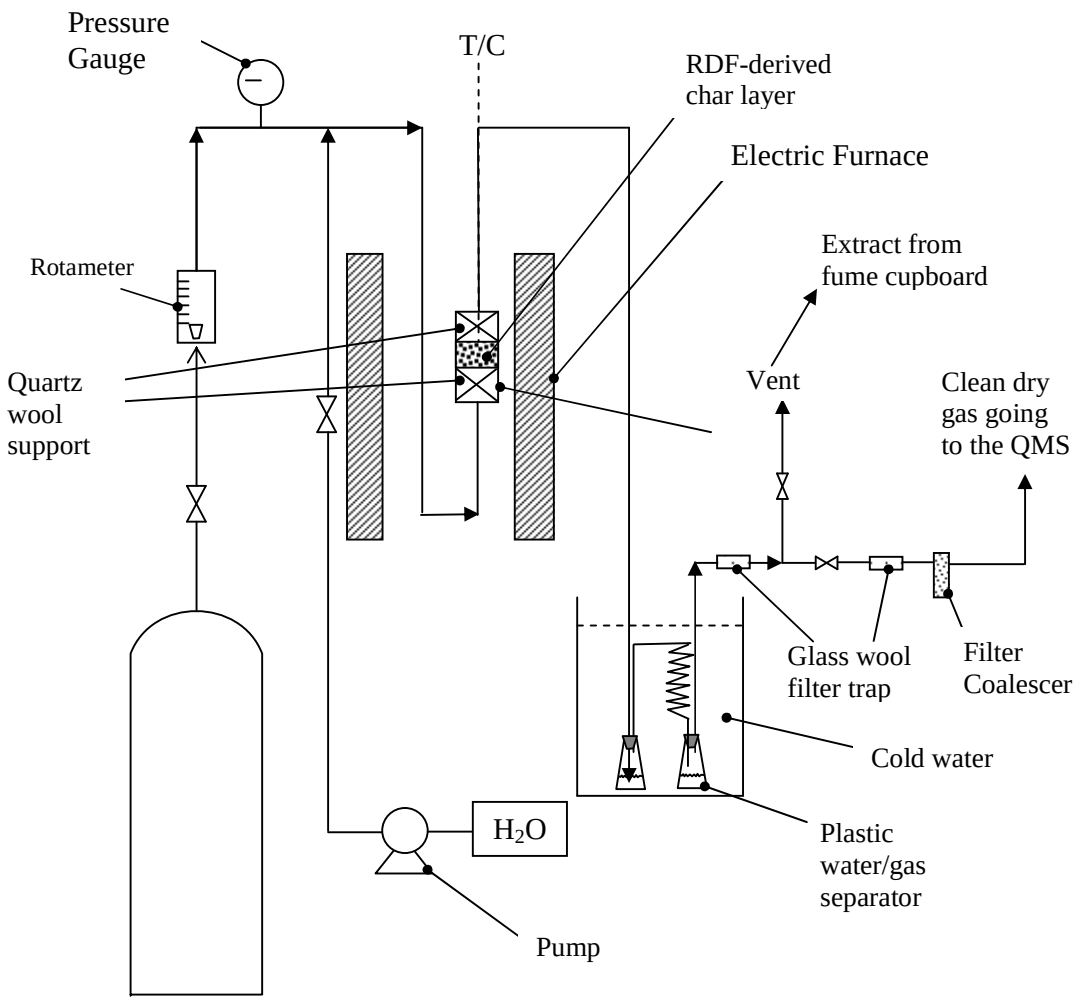

Figure 7.1 Schematic of the kinetic study apparatus.

a) b)

Figure 7.2 Small stainless steel tube reactor for kinetic studies.

7.3 RDF-DERIVED CHAR PARTICLE SIZE DISTRIBUTION

Sieves were used to classify by size the RDF-derived char that had been obtained from the commercial pilot-scale gasifier. The mass distribution of these char particles is shown in Table 7.1.

Table 7.1 RDF-derived char – particle size mass distribution.

Size range	Weight			
	1	2	3	Average
> 4000 μm	117.35	139.96	143.82	133.71
2000 – 4000 μm	165.18	189.94	168.89	174.67
1180 – 2000 μm	125.76	156.50	185.02	155.76
1000 – 1180 μm	47.22	56.96	60.90	55.03
500 – 1000 μm	154.04	186.13	200.25	180.14
250 – 500 μm	133.87	158.86	160.27	151
180 – 250 μm	91.10	109.14	113.92	104.72
120 – 180 μm	36.18	45.79	56.87	46.28
75 – 120 μm	113.60	134.77	135.81	128.06
0 – 75 μm	29.08	33.43	29.68	30.73
Total	1013.4	1211.48	1255.42	1160.1

From Table 7.1, the frequency mass fractions are calculated from:

$$q_i = \left(\frac{m}{\Delta d_q} \right)_i \quad \text{or} \quad \mathrm{Q_i} = \sum_{1}^{i} \left(q.\Delta d_q \right)_i \tag{7.1}$$

where: q_i is the differential frequency mass (or fixed carbon content) fraction of size interval i , 1/μm;

Q_i is the cumulative frequency mass (or fixed carbon content) fraction of particles smaller than size $(d_q)_i$;

$(\Delta d_q)_i$ is the size interval i, μm; and

m_i is the mass fraction of char particle in size interval i.

Then, the mean size of RDF-derived char particles is estimated from:

$$\bar{d}_q = \frac{1}{\sum^{all\ i}\left(m/d_q\right)_i} = 305.52\ \mu\text{m} \qquad (7.2)$$

Information on the fixed carbon content in the different char size ranges will be also be useful when designing a process, so this type of information is presented in Table 7.2 and Figures 7.3 and 7.4.

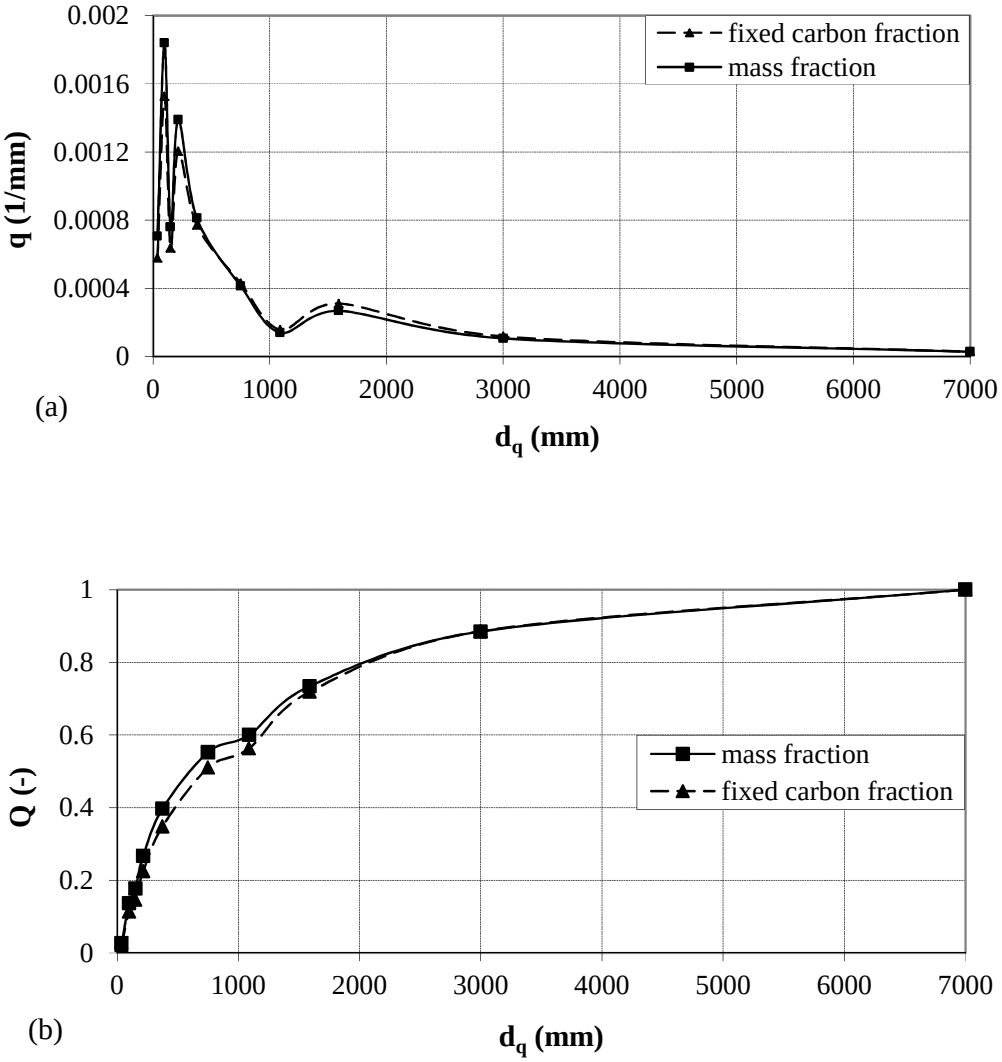

Figure 7.3 RDF-derived char particles: (a) Differential frequency mass and fixed carbon content distributions, (b) Cumulative frequency mass and fixed carbon content distributions.

Table 7.2 **(a)** RDF-derived char analysis

Properties	RDF-derived char
Moisture (wt.% in wet basis)	4.59
Volatiles (wt.% in dry basis)	10.71
Fixed carbon (wt.% in dry basis)	34.18
Ash (wt.% in dry basis)	55.10

(b) Properties based on size range

Size range	Weight (wt.% on dry basis)		
	Ash	Fixed carbon	Volatiles
0 – 75 μm	59.40	29.88	10.72
75 – 120 μm	59.99	30.23	9.78
180 – 250 μm	59.91	30.52	9.57
250 – 500 μm	57.88	31.56	10.56
500 – 1000 μm	55.15	34.54	10.31
1000 – 1180 μm	50.12	37.83	12.05
120 – 180 μm	48.67	41.15	10.18
1180 – 2000 μm	44.16	42.23	13.61
2000 – 4000 μm	46.30	40.31	13.39
> 4000 μm	49.70	36.15	14.15

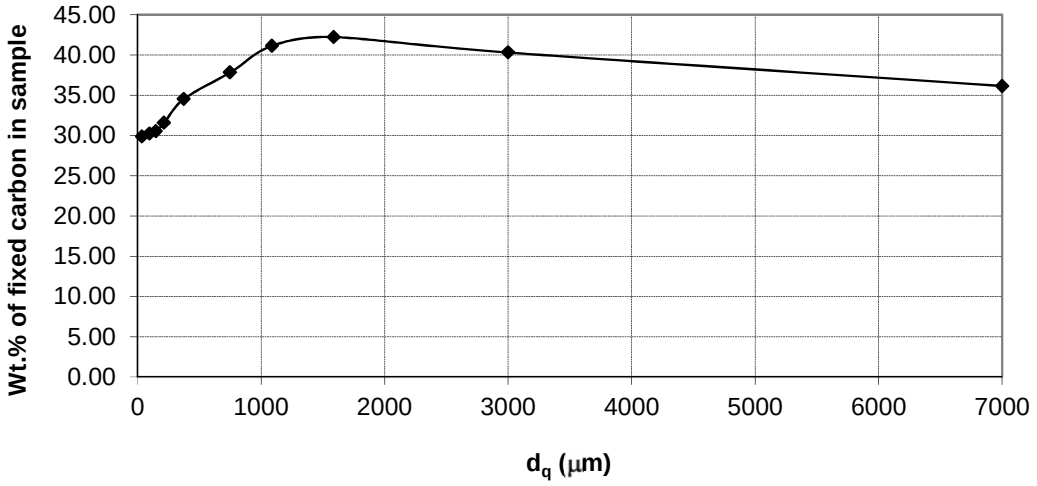

Figure 7.4 RDF-derived char: fixed carbon content based on char particle size range.

From the data on the fixed carbon content, it is interesting to note that this changes slightly with particle size, and this is most probably related to the part of the process from which that carbon particle arose (e.g. carried in the gas stream and trapped in a cyclone, or retained in the char stream from the base of the gasifier).

Decision taken: From these measurements, it was decided to use char in the size range of 250-500 μm for the kinetic experiments.

7.4 EXPERIMENTAL METHODOLOGY

Char conditioning: Samples of char were first conditioned by heating for 3 hours in a flow of N_2 at 800 ^oC, and this removed any volatiles (checked with the QMS).

Experimental procedure: N_2 was first fed into the reactor during the heating-up period to the desired operating temperature. This was then followed by steam injection, and the experiment was started. The system pressure was atmospheric (open end of reactor). After each run, air was passed through the reactor to burn out any residual carbon. Finally, the reactor was cooled, and the remaining ash was collected and weighed.

Carbon reactivity of the char: This can be inferred from the molar flow rate of CO and CO_2 for the reactor. This approach has been used in many studies, making use of the flow of an inert sweeping gas (e.g. N_2 or Argon) to perform such calculations (e.g. Parviet *et al.*, 2008; Parviet *et al.*, 2007; Ahmed and Gupta, 2010; Wu *et al.*, 2006; and Liu *et al.*, 2006). If the formation of CH_4 was significant then it would have to be included, but this was checked and found not to be the case in the experiments described.

The experimental conversion of carbon in the char, *X*, may be defined (e.g. Paviet *et al.*, 2008) as:

$$X = \frac{w_0 - w}{w_0 - w_{ash}} \tag{7.3}$$

where: w_0 is the initial sample weight, w is the sample weight at any time t and w_{ash} is the ash content measured after reaction.

The evolution of sample weight, *w(t)*, as a function of time is unknown, but it can be deduced from the gas composition. The experimental kinetic rate, at any time *t*, can thus be calculated (e.g. Cozzani, 2000) from:

$$\frac{dX}{dt} = \lim_{\Delta t \to 0}\left(\frac{X_{t_2} - X_{t_1}}{\Delta t}\right) \qquad (7.4a)$$

where: X_{t_1} and X_{t_2} are carbon conversion at time t_1 and t_2, respectively,

$\Delta t = t_2 - t_1 \approx 20s$ is the measurement step of the gas analysis method.

or (e.g. Paviet *et al.*, 2008) from:

$$\frac{dX}{dt} = \frac{12\left(F_{CO} + F_{CO_2}\right)}{w_0 - w_{ash}} \qquad (7.4b)$$

where: F_{CO} and F_{CO_2} are molar flow rates (mol/min) of CO and CO_2, respectively, in the producer gas stream.

Both Equations (7.4a) and (7.4b) were used to calculate the carbon conversion rate, and they produced the same results. Hence, equation (7.4b) was selected to use in this study.

A wide range of different preliminary experiments was performed, and these are summarized in this section.

7.4.1 Practical Experimental Problems (and Experimental Errors)

There were many challenges and the key ones are listed:

- Quartz wool (rather than glass wool) had to be used to contain the char/ash in the bed (to withstand high operating temperatures).

- At high operating temperature, the threads on the fittings were damaged, even though they were protected by a special lubricant (oil-based thread lubricant, named Silver Goop®, for use on stainless steel and high-temperature alloys). This was because the working temperature for this lubricant is only up to 815^{o}C.

- Small particles (mainly metal oxides from the walls of the reactor) in the gas stream were not all captured by the filter coalescer, resulting in the fact that some of the particles reached the sampling point connected to the QMS. This caused blockage inside the filter just before the capillary line to the QMS. This in turn changed the base pressure of the QMS during an experiment.

- Blockage by small metal oxide particles could also occur in the small gas exit lines (3.8 mm i.d.). This in turn could lead to a build-up of pressure inside the reactor, which was easily detected.

- If experiments were performed with a high flow of H_2O, the flow of N_2 was not stable because of the vaporization of H_2O in the inlet line, causing pressure fluctuations.

- In general, the concentration measurements with the QMS were very reliable. However, measurement of CO at low concentrations (< 1 vol.%) were within ± 7 %). In future work, it would be better to use argon as a carrier gas (but this would also mean that the QMS method of analysis would need to be refined).

- At low liquid flows (< 0.074 g/min), the water feed pump did not work well, resulting in fluctuations in the flow of steam into the char bed. These low flows were avoided. Reported liquid flows at 0.074 g/min were within ± 4 %.

- The balance used to weigh the initial sample and the ash remaining after each run was not suitable for small quantities (< 0.1 g). Reported weights at 0.1 g are within ± 10 %.

- Errors in the readings on the QMS can arise either because of a change in the Base Pressure during experiment, or from measurements at low concentrations of CO (< 1 vol.%). The accuracy of the QMS was enhanced by using the by-pass valve to adjust the Base Pressure.

- Errors could also arise from the N_2 rotameter reading, so a bubble flow-meter was used to check the gas flow during an experiment (reported gas flows at 0.2 litre/min were within ± 2 %).

- At very high temperature (e.g. 900 ºC), some reactions took place between the steam and the metal tube wall, leading to a small amount of hydrogen being produced. This also damaged the inside of the tube, and created fine particles of metal oxide, which were transported in the gas effluent from the reactor.

- Temperatures were measured with Type-K thermocouples, and these are accurate to within ± 4 ºC for temperature < 1000 ºC.

7.4.2 Example of an Experimental Run

The following test conditions were applied:

- Furnace temperature was set at 900 ºC.
- RDF-derived char sample weight was 0.5 gram (particle size from 250 to 500 μm).
- N_2 flow set point = 0.2 litre/min (NTP), but actual measured value = 0.194 litre/min.
- H_2O flow = 0.148 g/min.
- Expected molar ratio of H_2O:N_2 = 1:1.

Figure 7.5 shows the composition of dry gas stream exiting the reactor *versus* the reaction time. The ash remaining at the end of the experiment (w_{ash}) was 0.3 g.

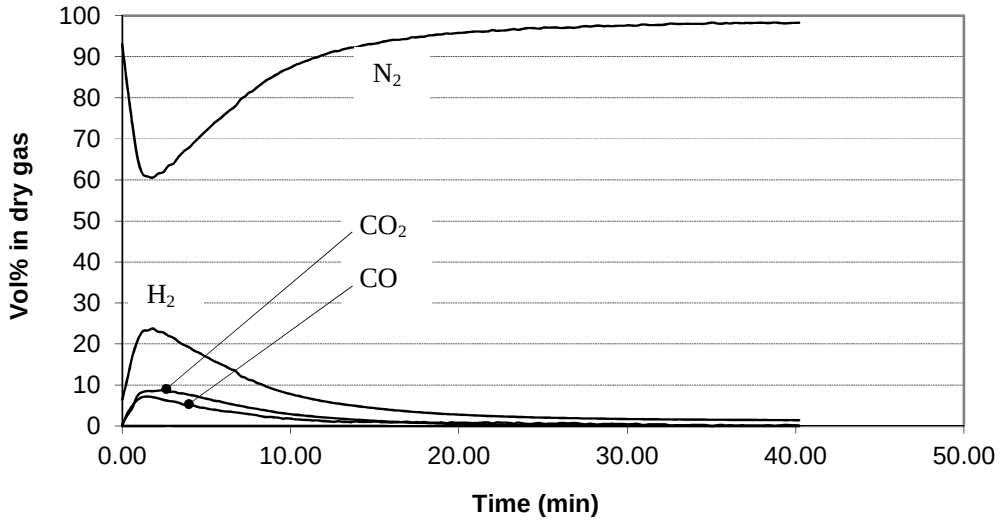

Figure 7.5 Dry gas composition for steam gasification of RDF-derived char.

From the measured composition of the dry gas, the molar flow rate of species i (mol/min), is given by:

$$F_i = y_i \times \frac{F_{N_2}}{y_{N_2}} \tag{7.5}$$

where: y_i is the mole fraction of species i.

The mass flow rate of species i (g/min), is then estimated from:

$$f_i = F_i \times M_i \tag{7.6}$$

where: M_i is the molar mass of species i, g/mol

The carbon mass fraction conversion rate can then be calculated:

$$\frac{dX}{dt} = \frac{12\left(F_{CO} + F_{CO_2}\right)}{w_0 - w_{ash}} \tag{7.7}$$

The experimental fractional conversion of carbon, *X*, at any time, *t*, can be obtained by integrating Equation (7.7) as a function of time. The results of this experiment are presented in Figures 7.6 to 7.9.

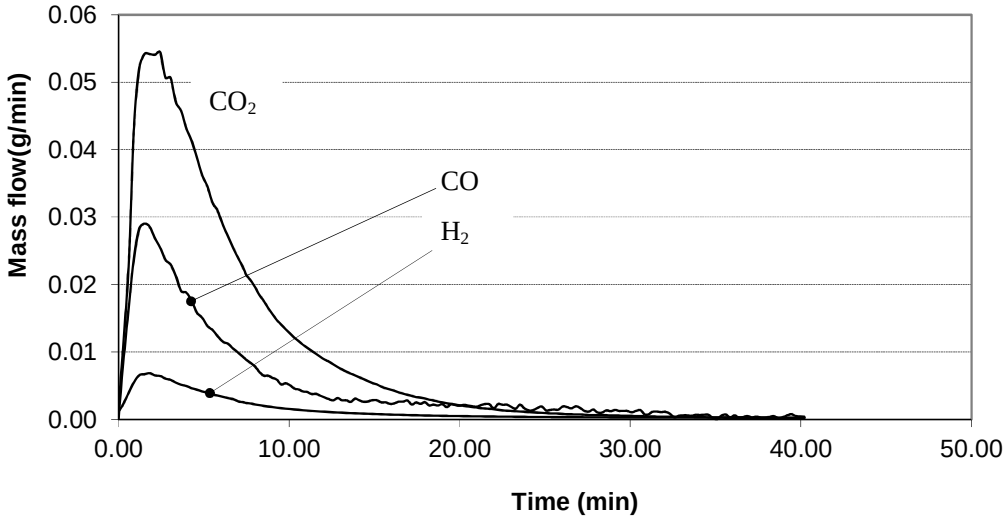

Figure 7.6 Mass flow of gaseous products (steam gasification of RDF-derived char).

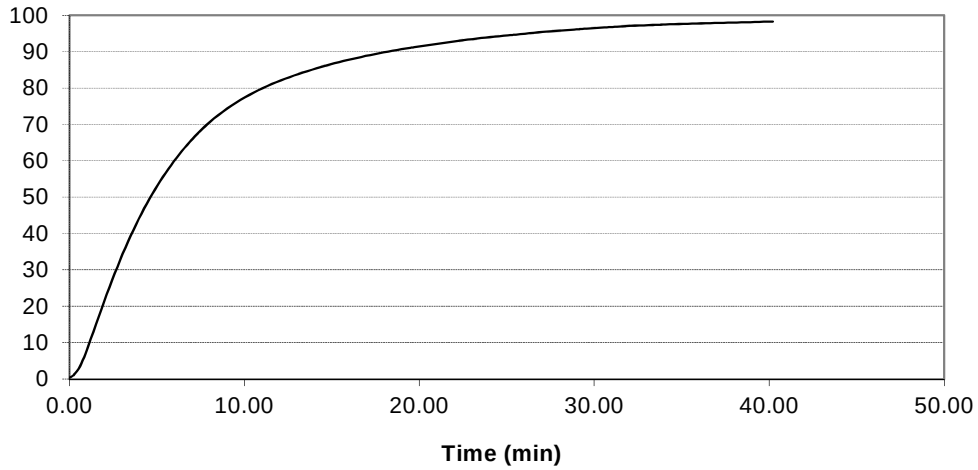

Figure 7.7 Carbon conversion expressed as a % (steam gasification of RDF-derived char).

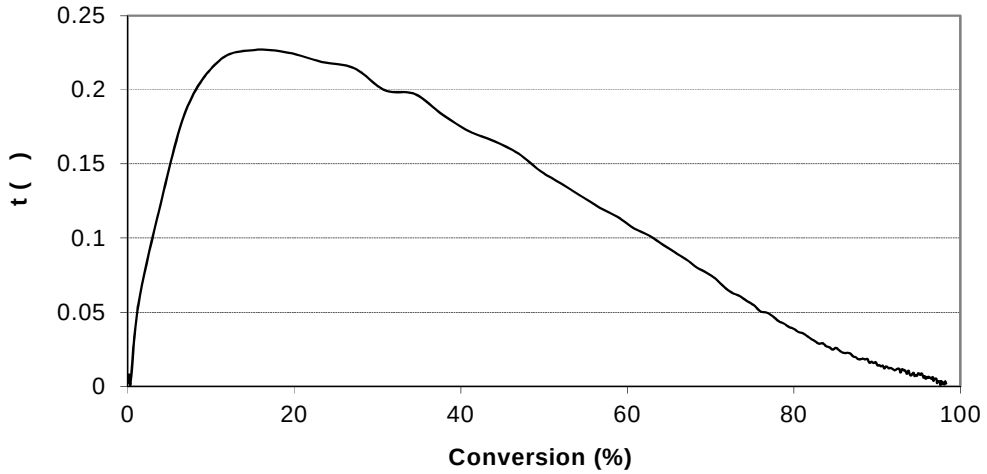

Figure 7.8 Rate of carbon conversion *versus* % conversion (steam gasification of RDF-derived char).

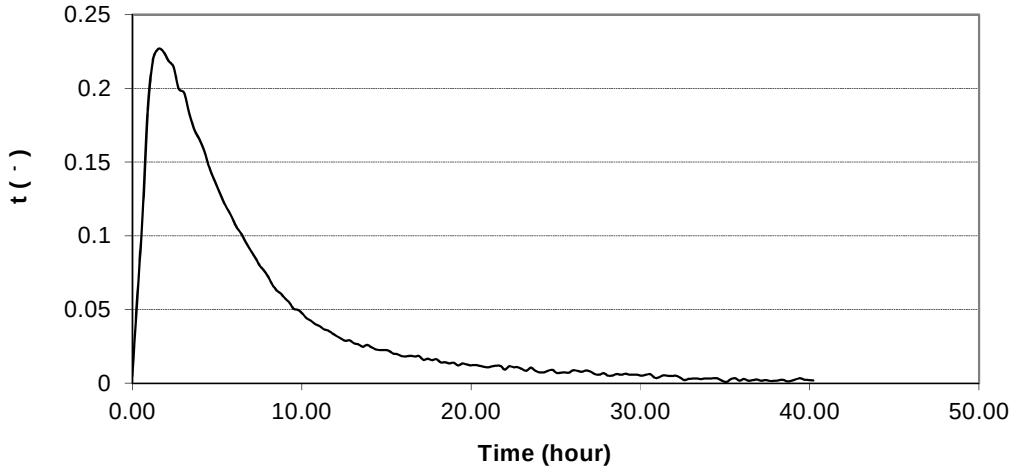

Figure 7.9 Rate of carbon conversion *versus* time (steam gasification of RDF-derived char).

Check on carbon consumption: To check the validity of this method, the experiment was kept running until only a very small and unchanged concentration of CO_2 (~0.06 vol.%) was detected in the gas outlet stream (because CO measurement was not reliable at low concentration). This should then correspond to almost 100 % carbon conversion. Using the method described (Equations (7.5) to (7.7)), 98 % of the carbon had been converted after 40 minutes, and this features in Figure 7.7. This was a very pleasing outcome.

From Figure 7.7, it is clear that 70 % of the carbon had been consumed after 8 minutes of reaction. After a conversion of 18 %, the rate of carbon conversion decreases (see Figure 7.8).

Repeatability experiments: To check the repeatability of the method, two additional runs were performed at the same set of experimental conditions, and the repeatability is evident in Figures 7.10, 7.11 and 7.12.

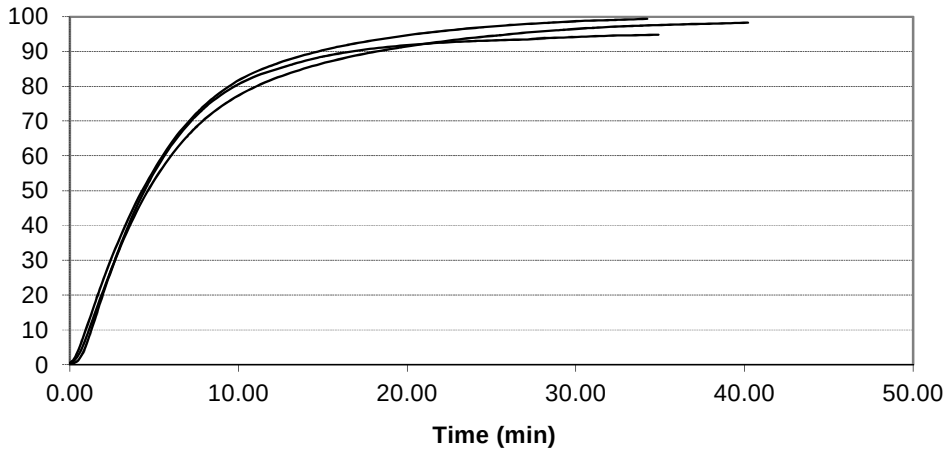

Figure 7.10 Repeatability check on carbon conversion *versus* reaction time.

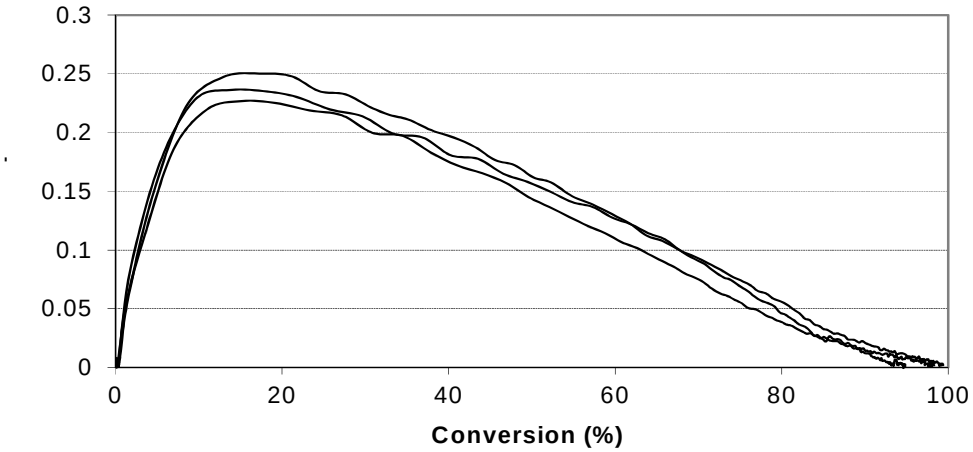

Figure 7.11 Repeatability check on rate of carbon conversion *versus* carbon conversion.

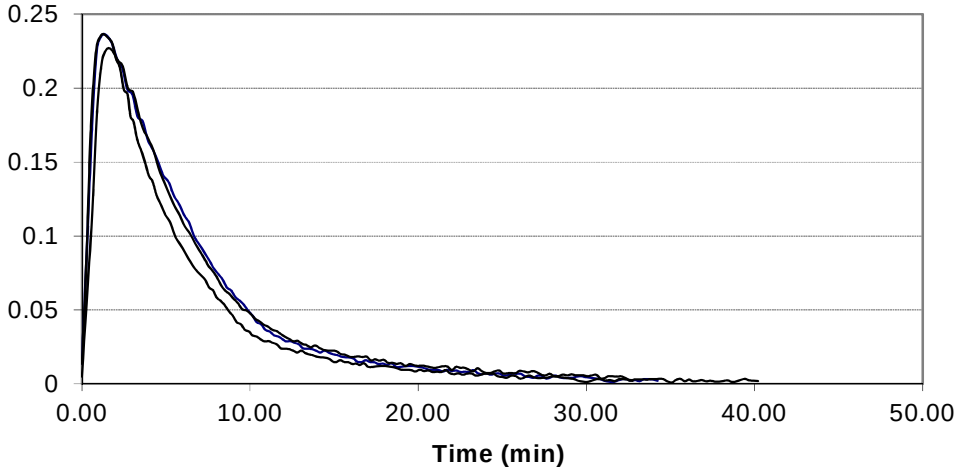

Figure 7.12 Repeatability check on rate of carbon conversion *versus* reaction time.

Concluding remark: This set of preliminary experiments provides a good indication of experimental errors, as well as confidence in the planned technique.

7.4.3 Effect of Char Bed Length

Experiments were performed with different char bed lengths, corresponding to different initial mass of char (the bulk density of the char = 500 kg/m^3):

Char bed length (mm)	1.6	5.7	8.2	16.8	23.7
Mass of char (g)	0.1	0.35	0.5	1.03	1.45

Experiments were performed at:

- Furnace temperature set at 900 ^oC; Char particles from 250 to 500 μm.
- N_2 flow set at 0.2 litre/min; H_2O flow = 0.148 g/min.
- Expected molar ratio of H_2O:N_2 = 1:1

The results obtained are shown in Figure 7.13.

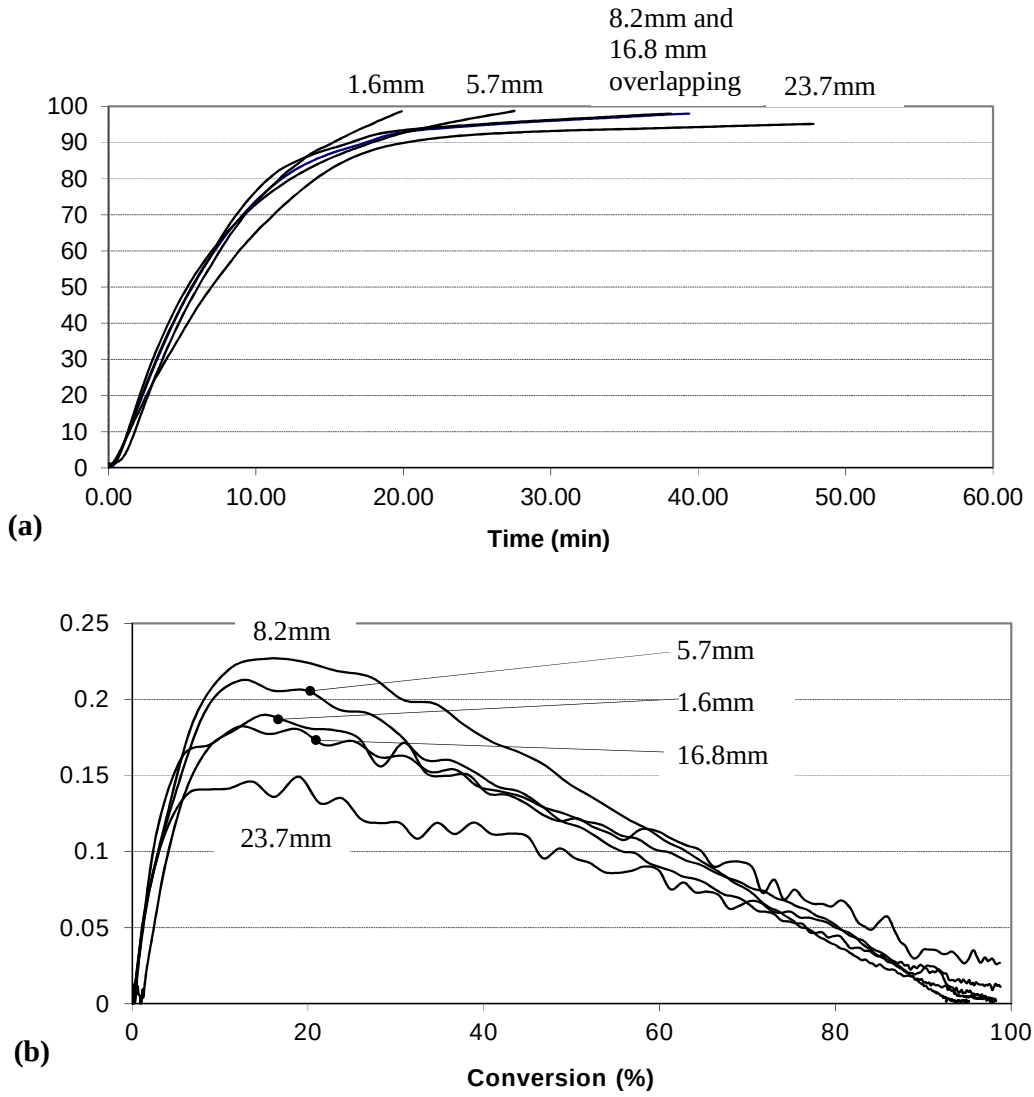

Figure 7.13 Influence of RDF-derived char bed length: (a) carbon conversion, (b) rate of carbon conversion.

As can be seen in Figure 7.13(a), performance of bed lengths from 1.6 to 16.8 mm is very similar and about 70 % of carbon in the char was consumed after eight minutes. For the planned kinetics study, it was decided to select a small initial bed length to reduce any secondary reactions, and to minimize the change in the partial pressure of steam along the char bed.

Decision taken: If a bed length < 5.7 mm was used, then CO concentration would be low, leading to measurement errors. Therefore, an initial char bed length of 8.2 mm was selected for all subsequent experiments.

7.4.4 Effect of Gas Flow

Experiments were performed at different gas inlet flows, which corresponded to different superficial velocities in the packed bed:

N_2 flow (litre/min)	0.2	0.4	0.6	0.7
H_2O flow (g/min)	0.148	0.296	0.444	0.518
Superficial velocity (m/sec)	0.218	0.437	0.655	0.764

Otherwise, the experiments were performed at the following conditions:

- Furnace temperature set at 900 ^oC; Char bed length = 8.2 mm.
- Char particles from 250 to 500 μm.
- Expected molar ratio of H_2O:N_2 = 1:1.

The results obtained are shown in Figure 7.14.

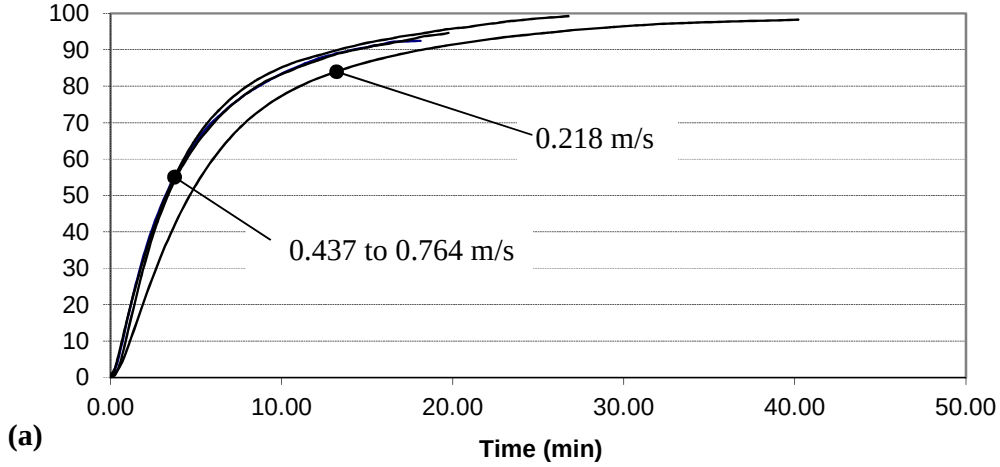

(a)

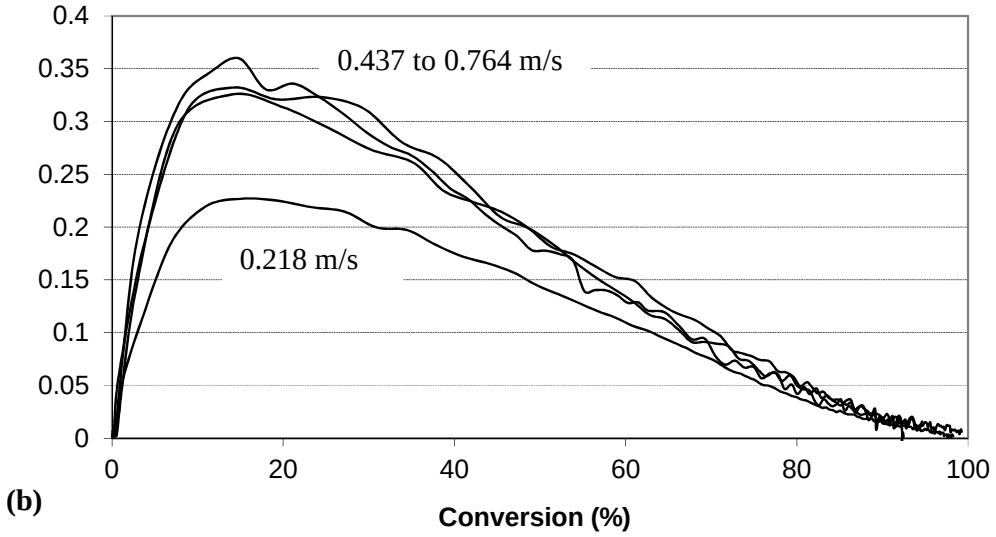

(b)

Figure 7.14 Influence of gas velocity: (a) carbon conversion, (b) rate of carbon conversion.

From Figure 7.14, at the high gas superficial velocities (0.437 to 0.764 m/s), this parameter has little influence on char gasification, indicating that external mass transfer resistance is low. In Paviet *et al.* (2008), superficial gas velocities at 10 to 20 cm/s (0.1 to 0.2 m/s) had little influence on external mass transfer.

Decision taken: Although high gas velocities are preferred, this leads to higher errors in CO measurements in the outlet gas stream; hence, a gas velocity of 0.218 m/s was selected for subsequent experiments.

7.4.5 Effect of Char Particle Size

Experiments were performed with char particles that had the following size range: 180 to 250 μm; 250 to 500 μm; 1000 to 1180 μm; and 2000 to 4000 μm.

The experiments were performed at:

- Furnace temperature set at 900 ^{o}C; Char bed length = 8.2 mm
- N_2 flow set at 0.2 litre/min; H_2O flow set at 0.148 g/min.
- Expected molar ratio of H_2O:N_2 = 1:1

The results obtained are shown in Figure 7.15.

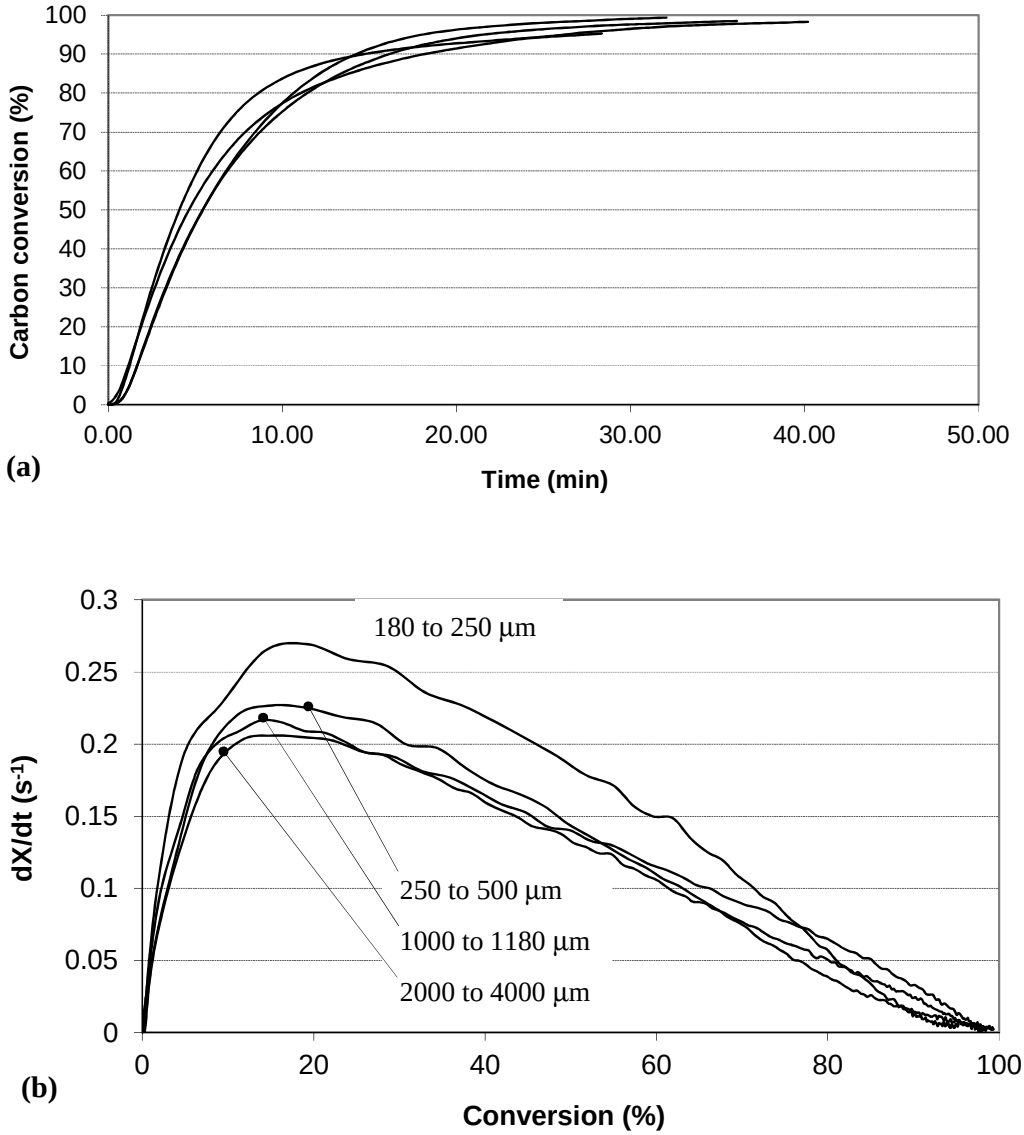

Figure 7.15 Influence of char particle size: (a) carbon conversion, (b) rate of carbon conversion.

As can be seen in Figure 7.15, the rate of carbon conversion increases as the particle size is reduced.

Decision taken: Because the measured mean particle size of RDF-derived char was ~ 305 µm, particles in the range of 250 to 500 µm were chosen for the subsequent kinetic experiments.

7.4.6 Effect of Reaction Temperature

To explore the effect of reaction temperature, experiments were performed at: 800, 850, and 900 ^{o}C. This set of experiments (at different reaction temperature) was repeated at various H_2O flows, while N_2 flow was kept constant at 0.2 litre/min. This helps to determine kinetic parameters that will be described later.

One example of the conditions in the reactor for one set of experiments was:

- N_2 flow rate = 0.2 litre/min
- Char bed length = 8.2 mm
- H_2O flow = 0.222 g/min.
- Expected molar ratio of H_2O:N_2 = 3:2

As expected, reaction rates increased with temperature, see Figure 7.16.

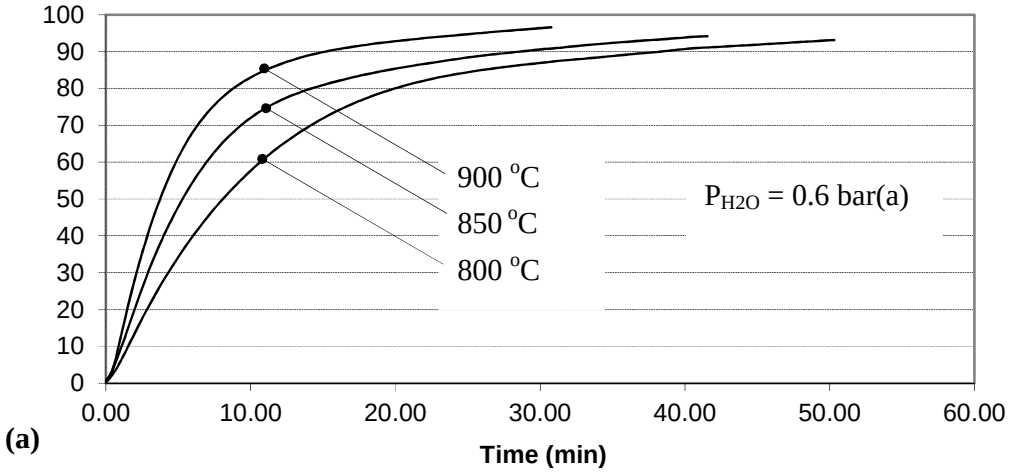

(a)

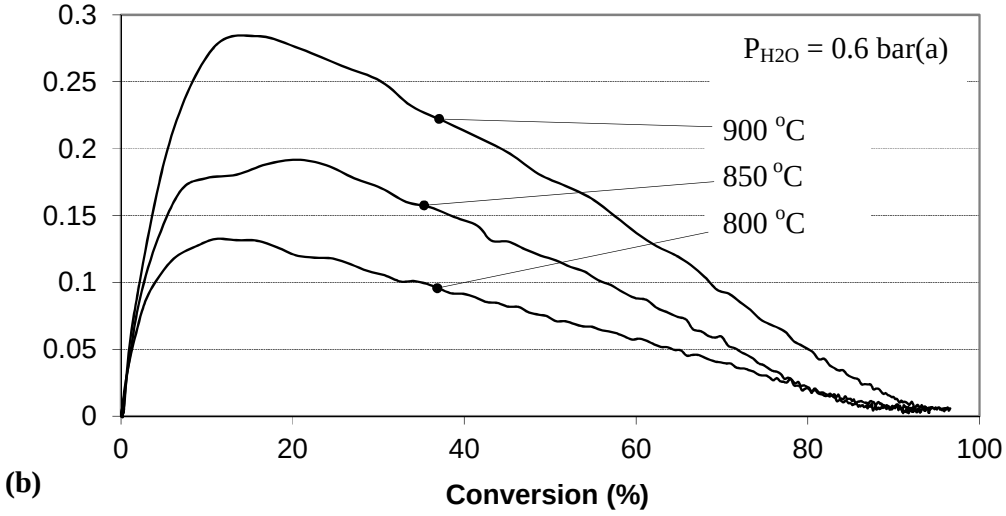

(b)

Figure 7.16 Influence of reaction temperature: (a) carbon conversion, (b) rate of carbon conversion.

7.4.7 Effect of Partial Pressure of Steam

As a reminder, for each reaction temperature (800 ^{o}C, 850 ^{o}C, or 900 ^{o}C), experiments were performed at different partial pressures of H_2O, which corresponded to different H_2O flows, while N_2 flow was kept constant at 0.2 litre/min.

H_2O flow (g/min)	0.074	0.148	0.222	0.296
Molar ratio of H_2O : N_2	1:2	1:1	3:2	2:1
Partial pressure (bar(a))	0.333	0.5	0.6	0.667

One example of the conditions in the reactor was:

- Furnace temperature set = 850 ^{o}C
- N_2 flow = 0.2 litre/min
- Char bed length = 8.2 mm

The results are presented in Figure 7.17, for experiments performed at 850^{o}C. From these experiments, char reactivity increases with steam partial pressure.

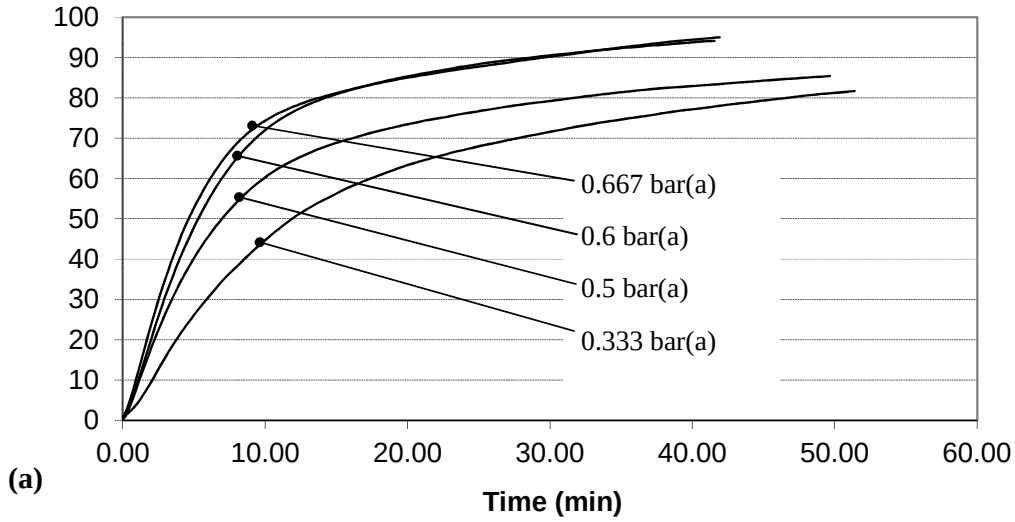

(a)

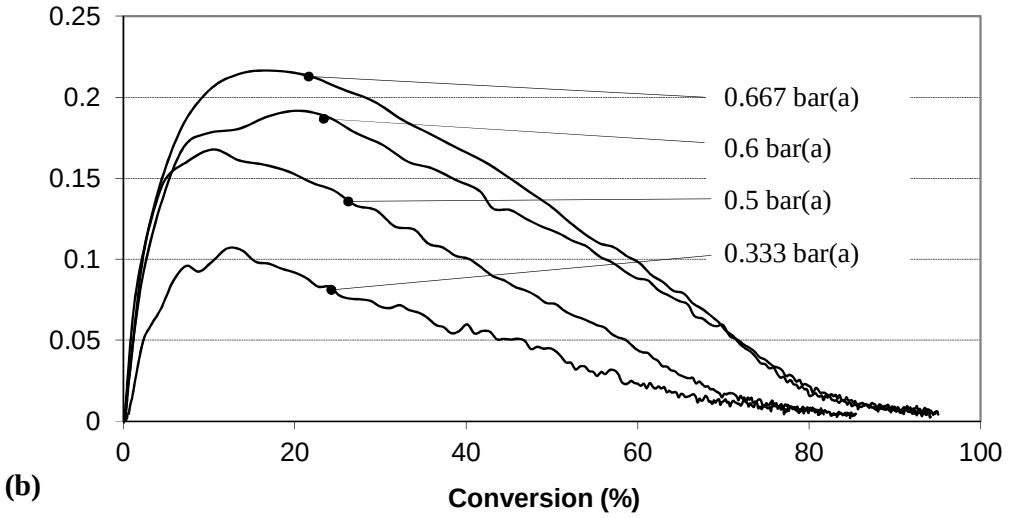

(b)

Figure 7.17 Influence of steam partial pressure at 850 ^{o}C: (a) carbon conversion, (b) rate of carbon conversion.

7.5 KINETICS OF STEAM GASIFICATION REACTION

There are a number of various well established techniques that can be used to describe the reacting char. Because the ash content in the RDF-derived char is high, then according to Levenspiel (1999, pp. 568-579) and Kunii and Levenspiel (1991, pp. 450-456), the Uniform-Reaction and Shrinking-Core models for porous solids of unchanging size, where the overall size of the particle remains constant during gasification process, are normally applied. In general:

- small particles follow the **Uniform-Reaction Model**, while
- large particles follow the **Shrinking-Core Model** (with ash diffusion controlling at high temperatures, but reaction controlling at low temperatures, Kunii and Levenspiel (1991, p. 455)).

In this thesis, both of these models are considered.

7.5.1 Estimate of Kinetic Parameters for the Shrinking-Core Model

The theoretical development of this model is based on Levenspiel (1999, pp. 570-576) and Kunni and Levenspiel (1991, pp. 451-453).

For a Shrinking-Core model, the reaction front advances from the outer surface into the particle, leaving behind a layer of ash. Thus, at any time there exists an unreacted core of carbon which shrinks in size during the reaction.

One char particle is considered for the purpose of constructing the equations. The reaction rate, r_C, is proportional to the available surface, S_C, of the unreacted core. Therefore, the mole balance on carbon in one particle at any instant in time, t, yields the following equation:

$$-r_C \times S_C = \frac{dN_C}{dt} \tag{7.8}$$

where: N_C represents the number of moles of carbon in the particle at time t, and can be expressed as a function of carbon conversion, X:

$$N_C = N_0(1-X), \tag{7.9}$$

with N_0 is the initial number of moles of carbon in the particle,

The available surface of unreacted core with diameter d_C is calculated from:

$$S_C = \pi.d_C^2 \tag{7.10}$$

where: π is the constant *pi*.

Now, replacing S_C and N_C in Equation (7.8) by Equations (7.9) and (7.10), and rearranging give:

$$r_C \times (\pi d_C^2) = N_0 \times \frac{dX}{dt} \tag{7.11}$$

where: $$N_0 = \frac{1}{6}\pi\rho D^3 \tag{7.12}$$

$$1-X = \frac{volume\ \text{of unreacted core}}{total\ \text{volume of particle}} = \frac{\frac{1}{6}\pi d_C^3}{\frac{1}{6}\pi D^3} = \left(\frac{d_C}{D}\right)^3 \tag{7-13}$$

with D is the diameter of the particle, and ρ is the molar density of carbon in the particle,

then, combining Equations (7.11), (7.12), (7.13), and rearranging give:

$$r_C = \left(\frac{1}{6}\rho D\right)\frac{1}{(1-X)^{2/3}}\frac{dX}{dt} \tag{7-14}$$

For the steam gasification of char, an nth-order reaction model is commonly used (e.g. Basu (2010, p. 212), Ahmed and Gupta (2010)):

$$r_C = k_C.P_{H_2O}^n \tag{7-15}$$

where: P_{H_2O} is the partial pressure of steam, that is considered as the partial pressure of steam in the inlet gas stream.

Combining Equations (7-14) and (7-15) gives:

$$r_C = \left(\frac{1}{6}\rho D\right)\frac{1}{(1-X)^{2/3}}\frac{dX}{dt} = k_C.P_{H_2O}^n \tag{7-16}$$

By calling:

$$r = \frac{1}{(1-X)^{2/3}}\frac{dX}{dt} \qquad \text{and } k = \frac{6k_C}{\rho D}, \qquad \text{then Equation (7-16) becomes:}$$

$$r = \frac{1}{(1-X)^{2/3}}\frac{dX}{dt} = k.P_{H_2O}^{n} \tag{7-17}$$

where: $r = \frac{1}{(1-X)^{2/3}}\frac{dX}{dt}$ is called specific (or apparent) reactivity of char in gasification reaction (Yip *et al.*, 2010).

A similar equation to Equation (7-17) can also be seen in the literature (e.g. Liliedahl and Sjostrom, 1997; and Basu, 2010, p. 140).

Now, Equation (7.17) can be rewritten as,

$$\frac{1}{r} = \frac{1}{k}.\frac{1}{P_{H_2O}^{n}} \tag{7.18}$$

where: $r = \frac{1}{(1-X)^{2/3}}\frac{dX}{dt}$ for the **Shrinking-Core Model**,

Taking a logarithm of Equation (7.18),

$$\ln\left(\frac{1}{r}\right) = \ln\left(\frac{1}{k}\right) + n\ln\left(\frac{1}{P_{H_2O}}\right) \tag{7.19}$$

Data on the apparent reactivity of the char (r, s^{-1}) at different partial pressures of steam was gathered from the experiments. Using such data, graphs were plotted of $\ln\left(\frac{1}{r}\right)$ *versus* $\ln\left(\frac{1}{P_{H_2O}}\right)$. The *y*-intercept will give the value of ln(1/k), and the slope will give the value of *n*. Figure 7.18 shows an example of the plots to determine the values of *k* and *n* at 850 ^{o}C at different degrees of conversion (*X*). These results are very encouraging as the data points are positioned close to the 'best-fit' straight lines. Values of *k* and *n* at various reaction temperatures are shown in Table 7.3.

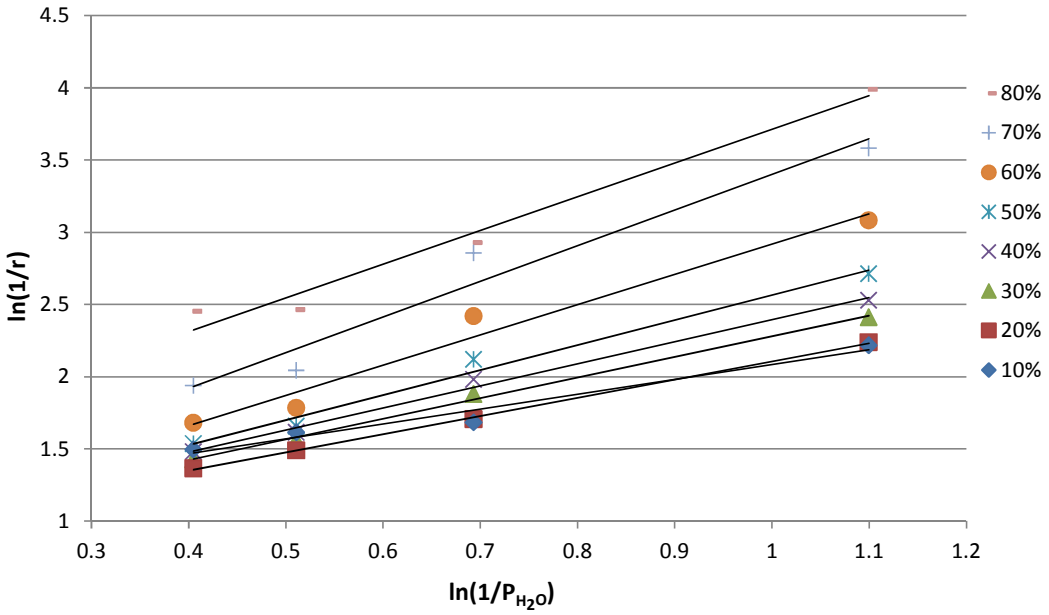

Figure 7.18 Example of plot to determine the values of *k* and *n* at 850 °C (Shrinking-Core Model).

Table 7.3 Values of *k* and *n* at various reaction temperatures (Shrinking-Core Model).

Carbon conversion (%)	900 °C		850 °C		800 °C	
	k	***n***	***k***	***n***	***k***	***n***
10	0.585	1.453	0.347	1.025	0.232	0.889
20	0.660	1.413	0.429	1.261	0.261	1.075
30	0.607	1.370	0.427	1.429	0.239	1.179
40	0.594	1.409	0.421	1.529	0.226	1.216
50	0.639	1.579	0.435	1.732	0.235	1.382
60	0.693	1.878	0.439	2.092	0.254	1.810
70	0.684	2.286	0.393	2.466	0.248	2.351
80	0.537	2.676	0.252	2.333	0.126	2.937

Next, from the Arrhenius equation, *k* can be expressed as:

$$k = A.\exp\left(-\frac{E}{R_g T}\right) \tag{7.20}$$

where *A* is the pre-exponential factor, and *E* is the activation energy. Equation (7.20) can be rewritten as,

$$\ln(k) = \ln(A) - \frac{E}{R_g}\frac{1}{T} \tag{7.21}$$

This equation shows that if a graph of ln(k) *versus* 1/T is plotted, the y-intercept will give the value of ln(A), and the slope will give the value of ($-E/R_g$). Figure 7.19 presents such a plot, and values of A and E are shown in Table 7.4.

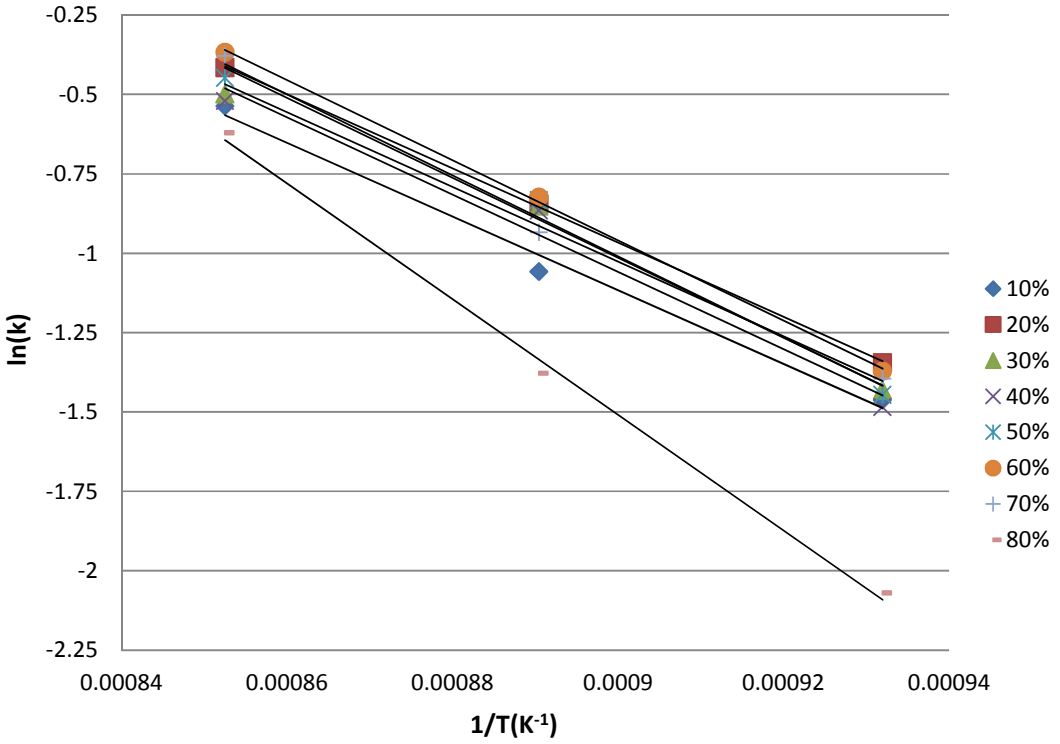

Figure 7.19 Arrhenius plot for the kinetics of char conversion (Shrinking-Core Model).

Table 7.4 Activation energies and pre-exponential factors (Shrinking-Core Model).

Carbon conversion (%)	**Arrhenius equation** $\ln(k)=\ln(A)-\frac{E}{R_g}\frac{1}{T}$	**Activation energy, *E* (kJ/mol)**	**Pre-exponential factor, *A* ($bar^{-n}.s^{-1}$)**
10	y=9.342 – 11620x	96.6	11407
20	y=9.5596 – 11696x	97.2	14180
30	y= 9.5651 – 11768x	97.8	14258
40	y= 9.9045 – 12182x	101.3	20020
50	y=10.323 – 12597x	104.7	30424
60	y=10.42 – 12644x	105.1	33523
70	y=10.471 – 12756x	106.1	35277
80	y=13.31 – 18220x	151.5	2925570

Once again, these results are encouraging as good straight line fits were obtained with the experimental data. The activation energy varies from 96 to 106 kJ/mol across the 10 to 70 % conversion range, and then it increased dramatically to 152 kJ/mol at 80 % carbon conversion.

Blasi (2009) reviewed data on the steam gasification of a number of different biochars, and reported that *E* varied from 143 to 237 kJ/mol (with a large part of the values around 180 to 200 kJ/mol), depending on reaction conditions and biochar source. This indicates that the RDF-derived char used in this thesis may be very active.

From data in Table 7.4, the value of the pre-exponential factor increases slightly with conversion across the 10 to 70 % range, but more rapidly after that. This change may be due to the evolution of the char structure with carbon conversion. Ahmed and Gupta (2010) suggested that ash might have increased the adsorption rate of steam to the char surface, leading to an increase of the pre-exponential factor. However, (a) increased porosity, and (b) access to the ash (which may have catalytic properties), may also have a role to play (e.g. Wu *et al.* (2006), and Wu *et al.*(2009)). The effects of carbon structure on char reactivity are also discussed in Aarna and Suuberg (1998), where they concluded that the micropores (< 2 nm) probably did not participate in the gasification reaction of chars, and that the surface developed by the macropores and the mesopores (2 nm < diameter < 50 nm) was a better indicator of the reactive surface, than the total pore surface area. This conclusion is consistent with others (e.g. Paviet et al, 2008; Mermoud *et al*., 2006b)

In other studies on the steam gasification of biochars (e.g. Wu *et al.*, 2009; Yip *et al.*, 20010; Golfier *et al.*, 2009; Mermoud *et al.*, 2006a; and Ahmed and Gupta, 2010) pore surface area and reactivity of chars increased with conversion, while an opposite trend was observed for the steam gasification of coal chars (e.g. Wu *et al.*, 2006; Liliedahl and Sjostrom, 1997; and Xu *et al.*, 2011).

The 70 to 80 % carbon conversion region: This region was examined in more detail, and more data points were added. Figure 7.20 shows the Arrhenius plot for conversions from 71 to 80 %.

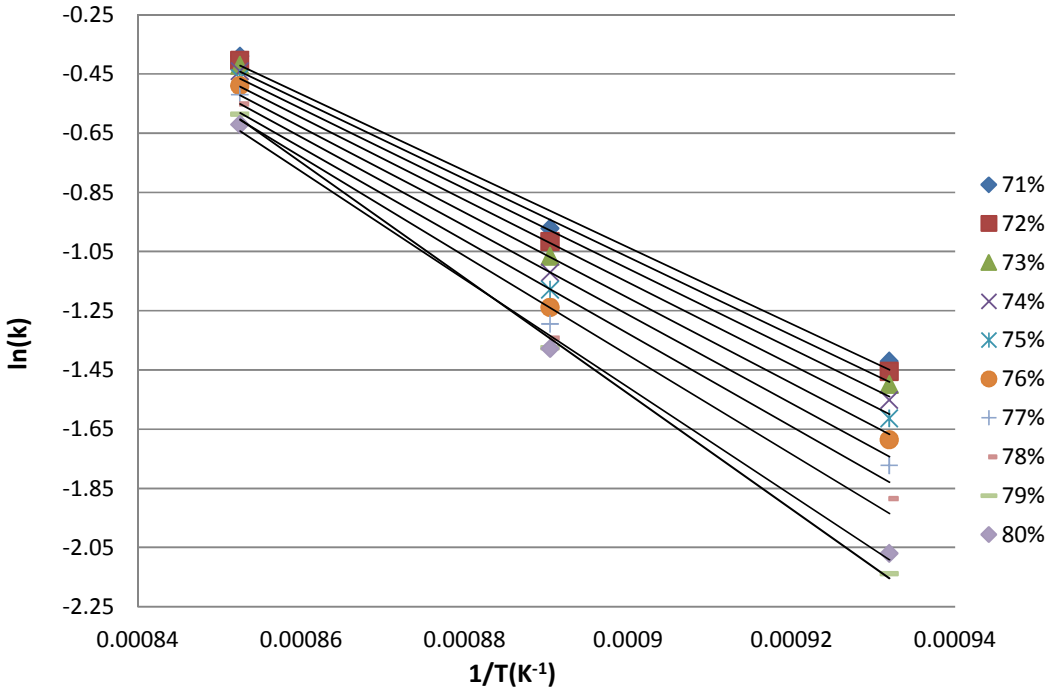

Figure 7.20 Arrhenius plot for conversions from 71 to 80% (Shrinking-Core Model).

A 'compensation effect' is observed here, where there is a simultaneous increase in activation energy and pre-exponential factor with conversion, see Table 7.5. This 'compensation effect' or 'isokinetic effect' has been observed and reported in literature for char-gas reactions (e.g. Wu *et al.*, 2006; Ahmed and Gupta, 2010), and explains the observed change that took place.

Table 7.5 Activation energies and pre-exponential factors (Shrinking-Core Model).

Carbon conversion (%)	Arrhenius equation $\ln(k)=\ln(A)-\frac{E}{R_g}\frac{1}{T}$	Activation energy, E (kJ/mol)	Pre-exponential factor, A ($bar^{-n}.s^{-1}$)
71	y=10.612 – 12942x	107.6	40619
72	y=10.806 – 13195x	109.7	49316
73	y= 11.061 – 13522x	112.4	63640
74	y= 11.379 – 13926x	115.8	87466
75	y= 11.765 – 14412x	119.8	128669
76	y=12.225 – 14987x	124.6	203822
77	y=12.798 – 15695x	130.5	361494
78	y= 13.651 – 16724x	139.0	848309
79	y= 16.035 – 19516x	162.3	9202631
80	y= 14.889 – 18220x	151.5	2925570

7.5.2 Estimate of Kinetic Parameters for the Uniform-Reaction Model

The theoretical development of this model is based on Kunii and Levenspiel (1991, pp. 450-451).

In a Uniform-Reaction Model, gaseous reactant(s) enter and react throughout the particle. Thus, the solid carbon is converted continuously and progressively at any location within the char particle. The gasification rate is proportional to the mass of unreacted carbon in the particle.

$$-r_C \times N_C = \frac{dN_C}{dt} \tag{7.22}$$

Replacing N_C in Equation (7.22) by Equation (7.9), combining with Equation (7.15), and rearranging give:

$$r_C = \frac{1}{1-X}\frac{dX}{dt} = k_C.P_{H_2O}^n \tag{7.23}$$

Equation (7.23) can be rewritten as:

$$r = \frac{1}{1-X}\frac{dX}{dt} = k.P_{H_2O}^n \tag{7.24}$$

where: $r = r_C = \frac{1}{1-X}\frac{dX}{dt}$ is the specific (or apparent) reactivity of char,

and $k = k_C$

A similar equation to Equation (7.24) can also be seen in the literature (e.g. Liliedahl and Sjostrom, 1997; Kunii and Levenspiel, 1991, p. 450; and Basu, 2010, p. 140).

Now, Equation (7.22) can be rewritten as:

$$\frac{1}{r} = \frac{1}{k}.\frac{1}{P_{H_2O}^n} \tag{7.25}$$

where $r = \frac{1}{1-X}\frac{dX}{dt}$ for the **Uniform-Reaction Model**.

For this model, the values of the activation energies (*E*) and pre-exponential factors (*A*) at different degrees of conversion (*X*) are calculated and presented in Table 7.6.

Table 7.6 Activation energies and pre-exponential factors (Uniform-Reaction Model).

Carbon conversion (%)	**Arrhenius equation** $\ln(k)=\ln(A)-\frac{E}{R_g}\frac{1}{T}$	**Activation energy, *E* (kJ/mol)**	**Pre-exponential factor, *A* ($bar^{-n}.s^{-1}$)**
10	y=9.3771 – 11620x	96.6	11815
20	y=9.6351 – 11697x	97.2	15292
30	y= 9.684 – 11768x	97.8	16059
40	y= 10.075 – 12182x	101.3	23742
50	y=10.555 – 12598x	104.7	38369
60	y=10.725 – 12644x	105.1	45479
70	y=10.873 – 12756x	106.1	52733
71	y=11.023 – 12941x	107.6	61267
72	y=11.231 – 13195x	109.7	75433
73	y= 11.498 – 13522x	112.4	98519
74	y= 11.828 – 13926x	115.8	137036
75	y= 12.227 – 14412x	119.8	204230
76	y=12.7 – 14987x	124.6	327748
77	y=13.228 – 15695x	130.5	590072
78	y= 14.155 – 16723x	139.0	1404230
79	y= 16.525 – 19482x	162.0	15021604
80	y=15.426 – 18220x	151.5	5005260

For comparison, one can see that values of the activation energy (*E*) presented in Table 7.6 are almost similar to those in Tables 7.4 and 7.5. However, values of the pre-exponential factor (*A*) in the Uniform-Reaction Model are different from those in the Shrinking-Core Model. Mathematically, this comes from the fact that the pre-exponential factor in Shrinking-Core Model includes the factor of $\frac{6k_C}{\rho D}$, whereas that in the Uniform-Reaction Model does not; see Equations (7.16) and (7.24).

7.6 SIMULATIONS USING THE KINETIC PARAMETERS

Using the kinetic parameters evaluated, simulations were performed (see Figure 7.23), using the Shrinking-Core Model and the Uniform-Reaction Model. The functions of the reaction order, pre-exponential factor, activation energy *versus* carbon conversion for two models are $f_{1s}(X,T)$ and $f_{1u}(X,T)$; $e^{f_{2s}(X)}$ and $e^{f_{2u}(X)}$; $f_{3s}(X)$ and $f_{3u}(X)$, respectively, see Appendix 4. Across the range of conditions tested, the two models produced very similar results, and just as an example, a comparison is shown with the experimental data in Figures 7.21 and 7.22.

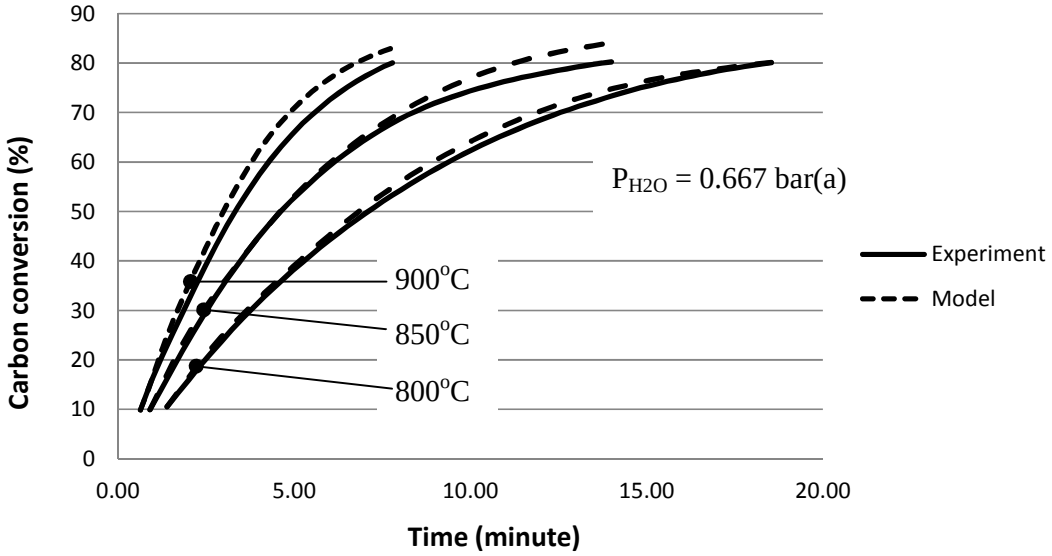

Figure 7.21 Experimental and simulated values at P_{H2O} = 0.667 bar(a).

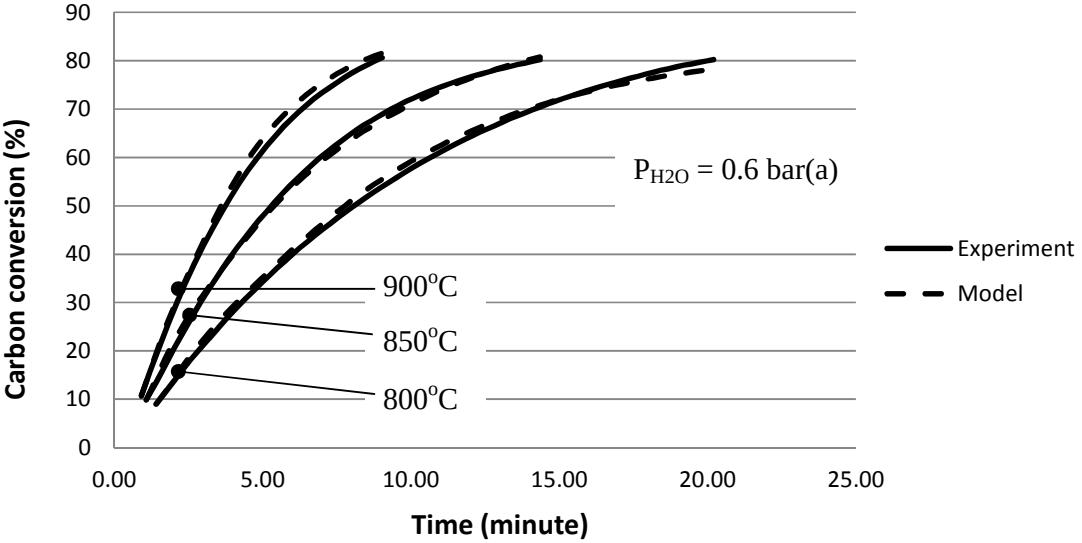

Figure 7.22 Experimental and simulated values at P_{H2O} = 0.6 bar(a).

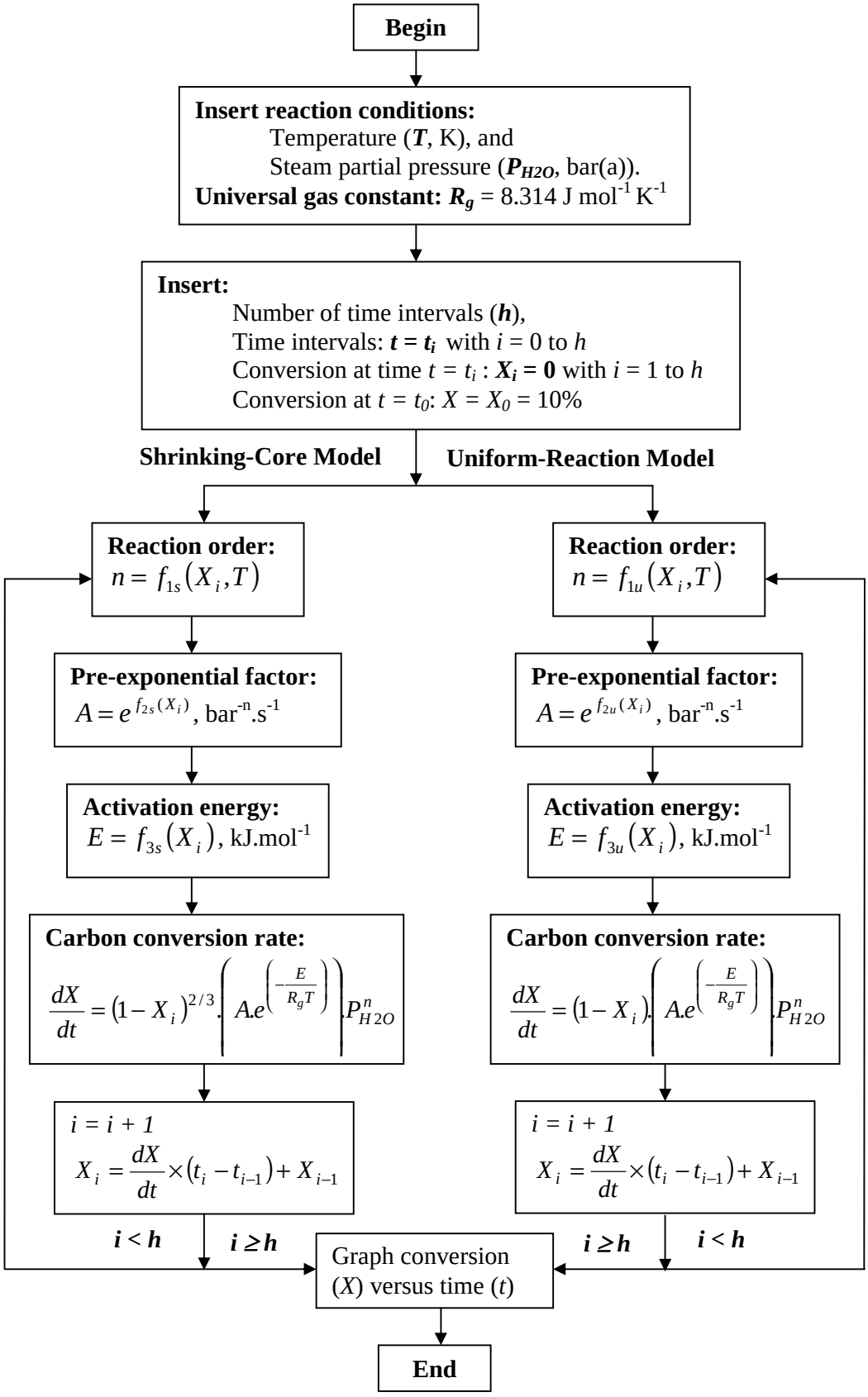

Figure 7.23 Flowchart of the simulation program for two models.

7.7 COMPARISON BETWEEN RDF-DERIVED CHAR AND WOOD CHARCOAL

Experiments were performed with a wood charcoal, obtained from a small commercial gasification reactor (the same as the wood charcoal used in Chapter 6). Two different ranges of wood charcoal particles were used (250 to 500 μm and 2000 to 4000 μm) and tested. All of these experiments were performed at:

- Furnace temperature set at 900 ^{o}C; Char bed length = 8.2 mm.
- N_2 flow set at 0.2 litre/min; H_2O flow set at 0.148 g/min.
- Expected molar ratio of H_2O:N_2 = 1:1.

The results are shown in Figure 7.24.

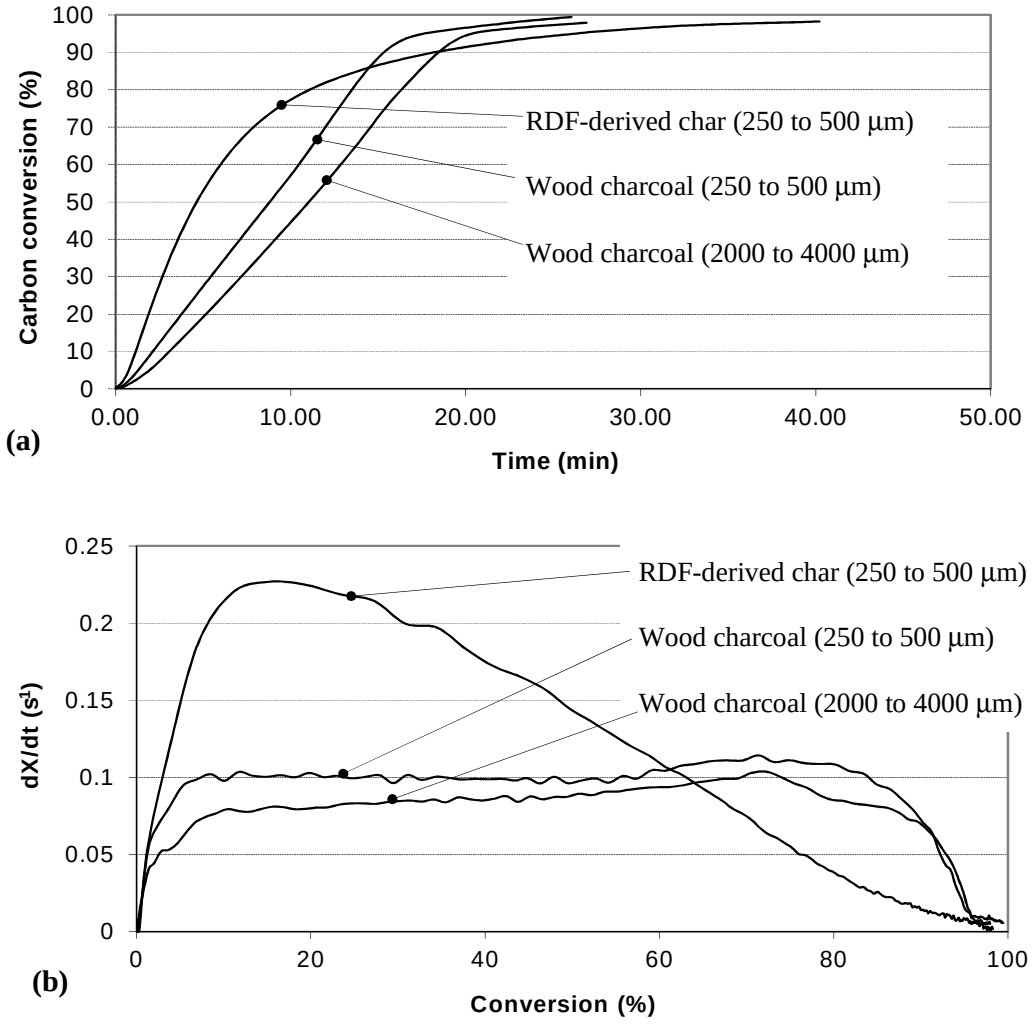

Figure 7.24 Comparisons between RDF-derived char and wood charcoal at 900 ^{o}C: (a) carbon conversion, (b) rate of carbon conversion.

From this data, it is clear that at low carbon conversion (< 60 %), the RDF-derived char is much more reactive than wood charcoal. However, at higher carbon conversions the opposite is true.

In some studies (e.g. Yip *et al.*, 2010; Xu *et al.*, 2011), the reactivity of gasification of char are presented as the specific (or apparent) reactivity, r. If the Shrinking-Core Model is selected, then $r = \frac{1}{(1-X)^{2/3}} \frac{dX}{dt}$. Figure 7.25 shows the evolution of apparent reactivity of char with carbon conversion.

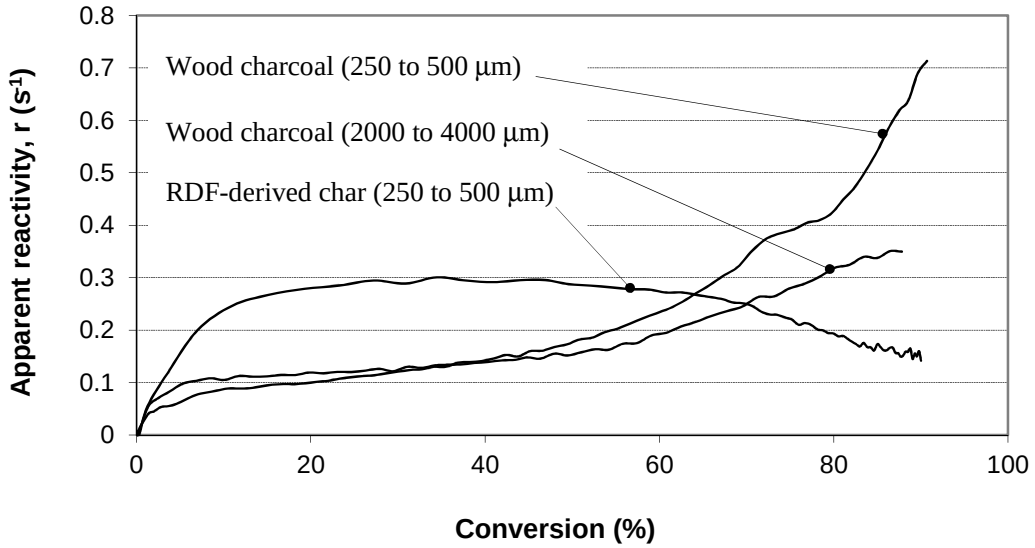

Figure 7.25 Apparent reactivity of RDF-derived char and wood charcoal.

From Figure 7.25, above a carbon conversion of 50 %, the apparent RDF-derived char reactivity decreases sharply with carbon conversion. This behaviour of RDF-derived char is opposite to that of other biochars such as mallee-bimass-derived char (Yip *et al.*, 2010) or food-waste-derived char (Ahmed and Gupta, 2010); however, it is similar to that of coal char (e.g. Wu *et al.*, 2006; Liliedahl and Sjostrom, 1997; Xu *et al.*, 2011; and Liu *et al.*, 2006).

Mermoud *et al.* (2006a), in a study of steam gasification of single wood charcoal particles (with a diameter of 10 to 30 mm), observed that reactivity of wood charcoal increased continuously with conversion due to a continuous increase in the surface area. However, Liu *et al.* (2006) reported a decrease in coal char reactivity with conversion because of a decrease in the surface area.

7.8 CO_2 GASIFICATION OF RDF-DERIVED CHAR AND WOOD CHARCOAL

It is well known that CO_2 will also gasify char, so some preliminary experiments were performed to compare its behaviour with RDF-derived char and wood charcoal (250 to 500 μm, and 2000 to 4000 μm), and to see how these compare with the earlier steam gasification experiments. All experiments were performed at:

- Furnace temperature set at 900 ^oC; Char bed length = 8.2 mm.
- N_2 flow set at 0.177 litre/min.
- CO_2 flow set at 0.083 litre/min.

Comparison of carbon conversion rates are shown in Figures 7.26.

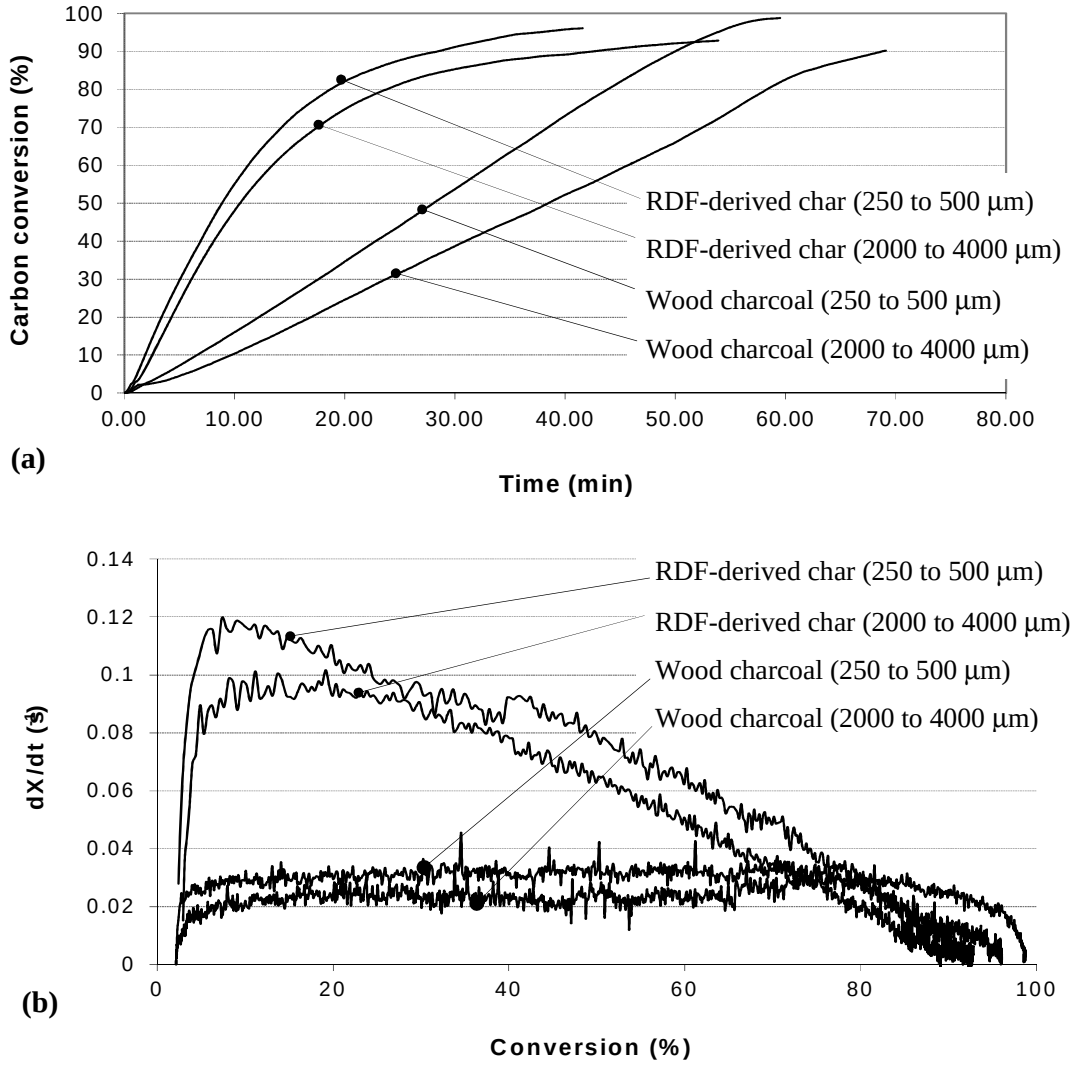

Figure 7.26 Gasification with CO_2 of RDF-derived char and wood charcoal at 900 ^oC: (a) carbon conversion, (b) rate of carbon conversion.

From these experiments, at low carbon conversion (< 70 %), the RDF-derived char is much more reactive than wood charcoal. However, at higher carbon conversions, the reactivity decreases. This is similar to what was observed earlier with the steam gasification experiments.

Kinetic experiments: Some preliminary kinetic experiments were also performed on this CO_2 gasification reaction; however difficulties were encountered with the form of rate expressions tried, and because of limitations in time, this was left as a recommendation for further work.

7.9 CONCLUDING REMARKS

The work in this chapter has provided valuable additional information on the steam gasification of RDF-derived char, and also how this compares with the char derived from wood.

(a) From samples obtained of RDF-derived char from a pilot-scale commercial gasifier: the char contained ~55 wt.% of ash (dry basis), fixed carbon (~35 wt.%) and volatiles (~10 wt.%). The mean particle size was ~ 305 μm.

(b) On char reactivity, the influence of char bed length, char particle size range, gas flow, steam partial pressure, and temperature, were all explored.

(c) Kinetic parameters were then evaluated for the steam gasification of the char, and the results were tabulated as a function of char conversion. This led to the development of the rate expressions as presented in Appendix 4.

(d) For steam gasification, the activation energy *E* varied from 96 to 162 kJ/mol. The reactivity of the RDF-derived char (at carbon conversions from 10 to 70 %) appears be higher than other biochars reported in the literature. However, at high conversions (> 50 %), the apparent reactivity of the RDF-derived char deceases with carbon conversion, behaving in a similar manner to coal structures.

(e) Across a char conversion range of 10 to 60 %, it was most interesting to find that the RDF-derived char was found to be much more reactive than the wood charcoal (both for steam and carbon dioxide gasification).

(f) For the gasification of RDF-derived char with steam, comparisons between the use of the Shrinking-Core Model and the Uniform-Reaction Model produced almost identical results.

(g) The data obtained will be most useful to the exploration of design concepts for the steam gasification of RDF-derived chars (probably in a fluidized-bed reactor).

REFERENCES

Aarna, I. and Suuberg, E.M. (1998). Change in reactive surface area and porosity during char oxidation. Twenty-Seventh Symposium (International) on Combustion/The Combustion Institute, pp. 2933-2939.

Ahmed, I.I. and A.K. Gupta (2010). Pyrolysis and gasification of food waste: Syngas characteristics and char gasification kinetics. Applied Energy, Vol. 87, pp. 101-108.

Basu, P. (2010). Biomass Gasification and Pyrolysis. Elsevier Inc.

Blasi, C.D. (2009). Combustion and gasification rates of lignocellulosic chars. Process in Energy and Combustion Science, Vol. 35, pp. 121-140.

Cozzani, V. (2000). Reactivity in oxygen and carbon dioxide of char formed in the pyrolysis of refuse-derived fuel. Ind. Eng. Chem. Res., Vol. 39, pp. 864-872.

Everson, R.C., Neomagus, H.W.J.P., Kasaini, H. and Njapha, D. (2006). Reaction kinetics of pulverized coal-chars derived from inertinite-rich coal discards: Gasification with carbon dioxide and steam. Fuel, Vol. 85, pp. 1076-1082.

Golfier, F., Van de steene, L., Salvador, S., Mermoud, F., Oltean, C. and Bues, M.A. (2009). Impact of peripheral fragmentation on the steam gasification of an isolated wood charcoal particle in a diffusion-controlled regime. Fuel, Vol. 88, pp. 1498–1503.

Huang, Z., Zang, J., Zhao, Y., Zhang, H., Yue, G., Suda, T. and Narukawa, M. (2010). Kinetic studies of char gasification by steam and CO_2 in the presence of H_2 and CO. Fuel Processing Technology, Vol. 91, pp. 843-847.

Kunii, D. and O. Levenspiel (1991). Fluidization Engineering. 2nd edition. Butterworth-Heinemann.

Levenspiel, O. (1999). Chemical Reaction Engineering. 3rd edition, John Wiley & Sons.

Liliedahl, T. and K. Sjostrom (1997). Modeling of char-gas reaction kinetics. Fuel, Vol. 76, No. 1, pp. 29–37.

Liu, H., Luo, C., Kato, S., Uemiya, S., Kaneko, M. and Kojima, T. (2006). Kinetics of CO_2 gasification at elevated temperatures. Part I: Experimental results. Feul Processing Technology, Vol. 87, pp. 775-781.

Mani, T., Mahinpey, N. and Murugan, P. (2011). Reaction kinetics and mass transfer studies of biomass char gasification with CO_2. Chemical Engineering Science, Vol. 66, pp. 36-41.

Mermoud, F., Golfier, F., Salvador, S., Van de Steene, L. and Dirion, J.L. (2006a). Experimental and numerical study of steam gasification of a single charcoal particle. Combustion and Flame, Vol. 145, pp. 59-79.

Mermoud, F., Salvador, S., Van de Steene, L. and Golfier, F. (2006b). Influence of the pyrolysis heating rate on the steam gasification rate of large wood char particles. Fuel, Vol. 85, pp. 1473-1482.

Paviet, F., Bals, O. and Antonini, G. (2008). The effects of diffusional resistance on wood char gasification. Process Safety and Environment Protection, Vol. 86, pp. 131-140.

Paviet, F. Bals, O., and Antonini, G. (2007). Kinetic study of various chars steam gasification. International Journal of Chemical Reactor Engineering, Vol. 5, Article A80.

Xu, Q., Pang, S. and Levi, T. (2011). Reaction kinetics and producer gas compositions of steam gasification of coal and biomass blend chars, part 1: Experimental investigation. Chemical Engineering Science, Vol. 66, pp. 2141-2148.

Yip, K., Tian, F., Hayashi, J. and Wu, H. (2010). Effect of alkali and alkaline earth metallic species on biochar reactivitiy and syngas composition during steam gasification. Energy Fuels, Vol. 24, pp. 173-181.

Wu, H., Yip, K., Tian, F., Xie, Z. and Li, C.Z. (2009). Evolution of char structure during the steam gasification of biochars produced from the pyrolysis of various mallee biomass components. Ind. Eng. Chem. Res., Vol. 48, No. 23, pp. 10431-10438.

Wu, S., Wu, J., Li, L., Wu, Y. and Gao, J. (2006). The reactivity and kinetics of yanzhou coal chars from elevated pyrolysis temperatures during gasification in steam at 900-1200^{o}C. Trans IchemE, Part B, Process Safety and Environmental Protection, Vol. 84(B6), pp. 420-428.

CHAPTER 8

Gas Analysis on a Commercial Pilot-scale Plant

In this chapter, the results of gas analysis measurements, which were taken on a commercial pilot-scale plant operated by Refgas Ltd, are described. A 'waste-wood' was used as a fuel. The term 'waste-wood' is used to describe a material that has been mainly produced from used wood, but may also contain a small amount of other contaminants (e.g. plastic, paper).

In its present configuration, this pilot-plant had a nominal capacity of 150 to 250 kg/h, depending on the material fed into the gasifier and the choice of operating conditions. The potential electrical output from the gas produced from this plant could vary from 150 to 250 kW_e. The data obtained from such a study is extremely useful, as:

- Data on the operation of commercial pilot-scale units of this size is scarce, and when it is published, it often lacks the scientific rigour to connect the values reported with actual operating conditions on the plant.

- The techniques developed with the QMS in the laboratory (Chapter 4) are now applied on the pilot-plant, and on-line gas analysis measurements are obtained (N_2, CO, CO_2, H_2, CH_4 and O_2). These can also be compared with gas measurements obtained from the laboratory-scale quartz-tube reactor (Chapter 3).

- Measurements are also made of the sulphur compounds (H_2S and COS), which had been discussed extensively in Chapter 5 (Section 5.3). Data of this type is also scarce in the literature, yet it is so important in terms of the development of suitable gas clean-up strategies.

- Finally, data was gathered on the variation in O_2 concentration of the gas produced during start-up of the gasifier. This helps to identify the length of time over which potential flammable conditions could exists within the ductwork and parts of the plant as the process is started-up. Although this safety concern is discussed in the literature, there is a lack of actual plant data.

8.1 THE REFGAS PILOT-PLANT

The pilot-plant was operational at a test site in Sandycroft (near Chester, UK). It is important to emphasize that this was a pilot-scale plant, whose design continued to evolve. The configuration described reflects the unit operations on the plant at the time these measurements were made. However, it does not reflect the configuration of units, which would be selected for a commercial application. The configuration would also depend on the nature of the feed material, and the customer's requirements between the relative amounts of thermal *versus* electrical energy from such a process. In many of the planned commercial configurations, additional process units would need to be added to the gas-clean-up stages, and additional heat recovery would also be installed.

A simplified schematic of the process flow diagram is shown in Figure 8.1, and this consists of the following main unit operations:

- The waste-wood chips were fed from a hopper into the gasifier.
- The down-draft gasifier operates under a negative pressure, and the gases are drawn from the gasifier by the centrifugal gas blower.
- Because of the negative pressure in the gasifier, air is drawn into the gasifier, and this supports the combustion and partial oxidation reactions that take place inside this unit.
- Some of this air is preheated in the outer jacket around the two cyclones. Another quantity of air is fed at ambient temperature directly into the gasifier along the central shaft.
- The gas leaves the reactor at the bottom of the unit, at a temperature of about $550^{o}C$.
- Char is discharged from the base of the gasifier, and char fines/ash are also trapped in the two cyclones.
- The dirty gas from the cyclones is quenched with water, and then passes through a HESS unit (which is a high efficiency water scrubber).
- The gas then passes through a heat exchanger (chiller), where additional residual water/tars are condensed.
- The blower draws the gas from the gasifier, and then blows it (under positive pressure) through the filters, into the storage tank, and then to the gas engine, and/or to the gas flare.
- The gas engine has the capacity to produce electrical energy.

During the course of measurements on the plant, the gas was discharged to flare.

Photographs of the pilot-plant are shown in Figure 8.2.

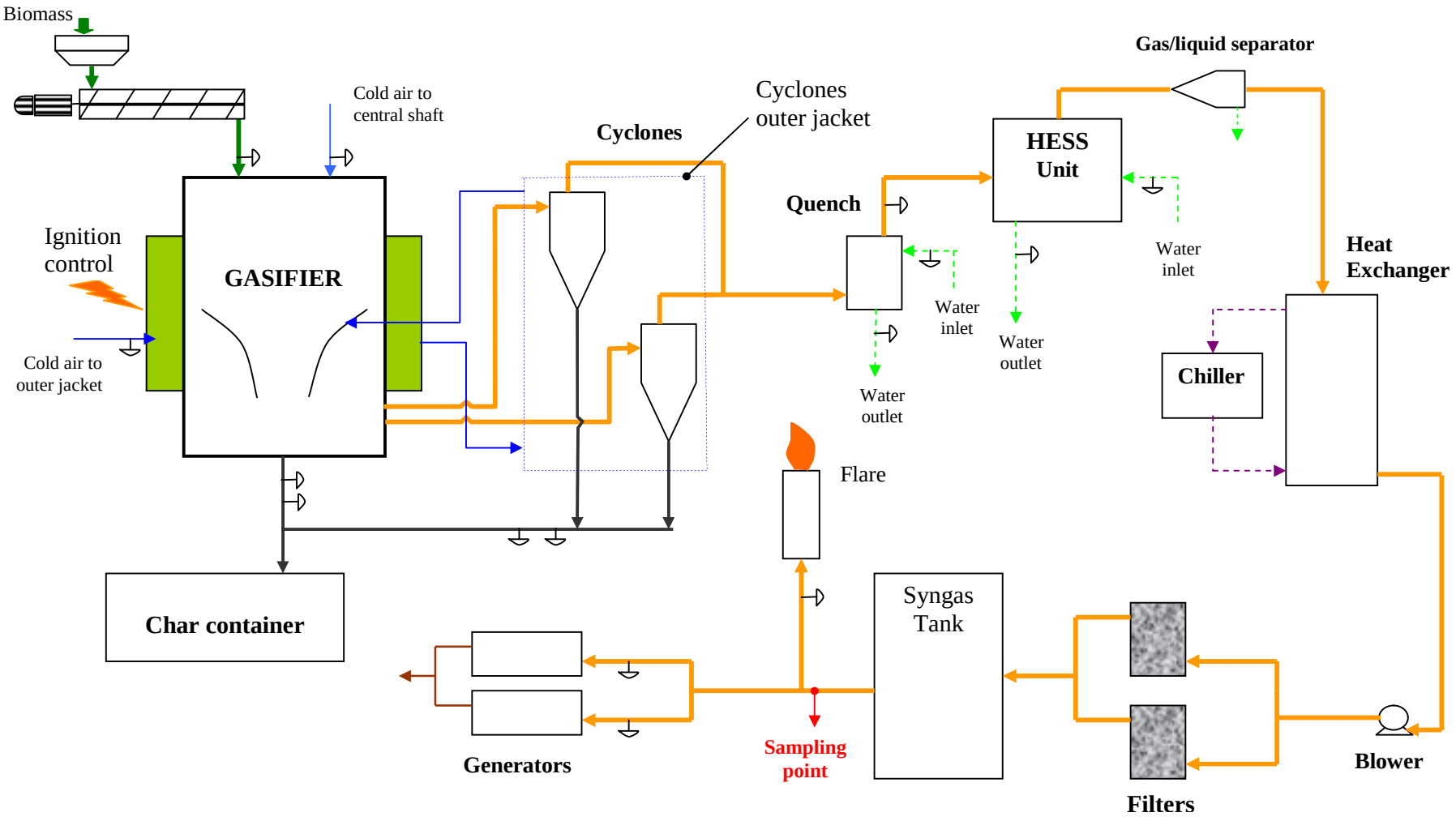

Figurer 8.1 Simplified process flow diagram of the commercial pilot-scale plant.

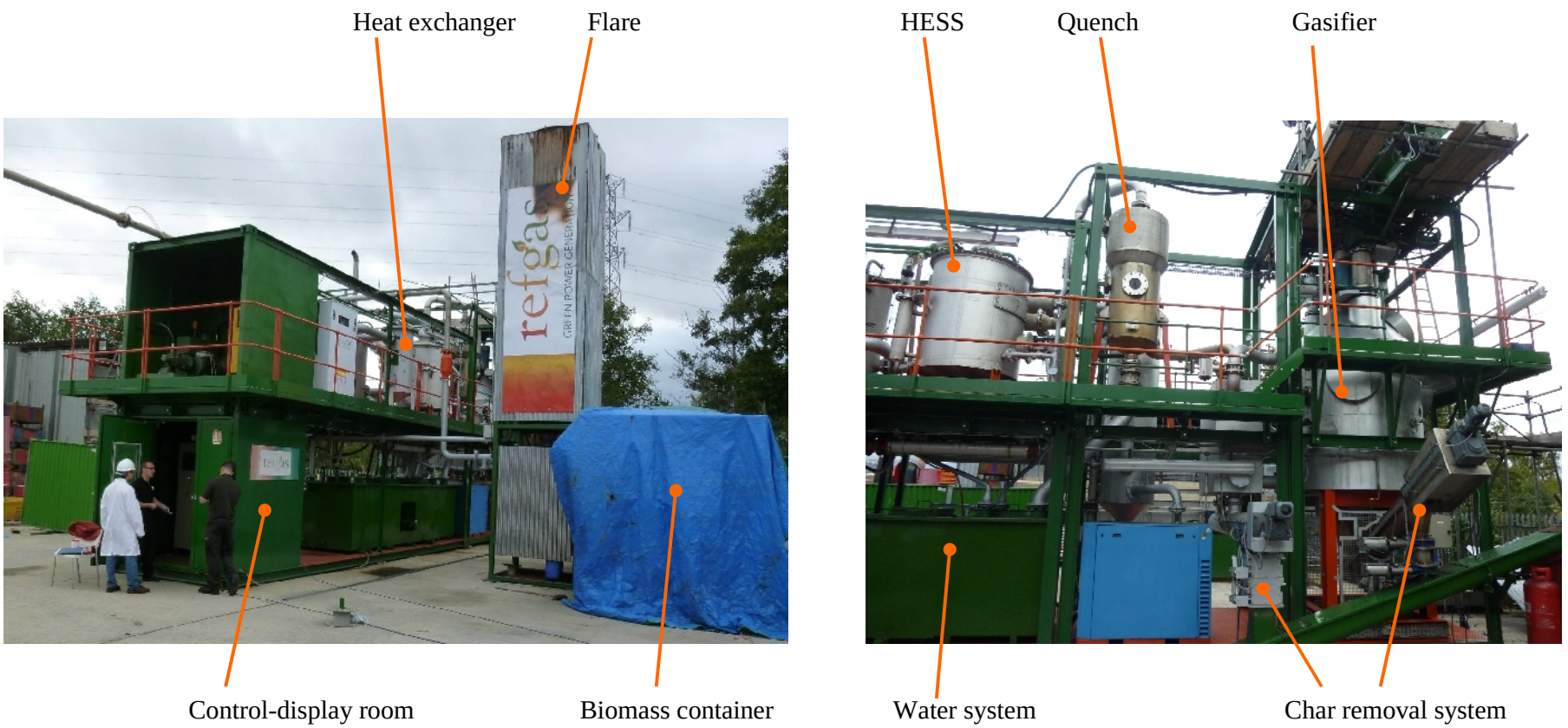

Figure 8.2 Photographs of the pilot-scale plant (author on left in white laboratory coat).

8.2 GAS ANALYSIS

The gas sample to the QMS was drawn from the line, at the point where the gas was sent to flare (see Figure 8.1). At this point, the gas was at positive pressure. The flow of gas was controlled by a needle valve (see Figure 8.3(a)). The gas sample then flowed through a glass wool filter (Figure 8.3(b)) and a filter coalescer before going to the QMS for analysis. These filters helped to remove the majority of any residual tars and particulates from the gas stream, so as not to damage the QMS.

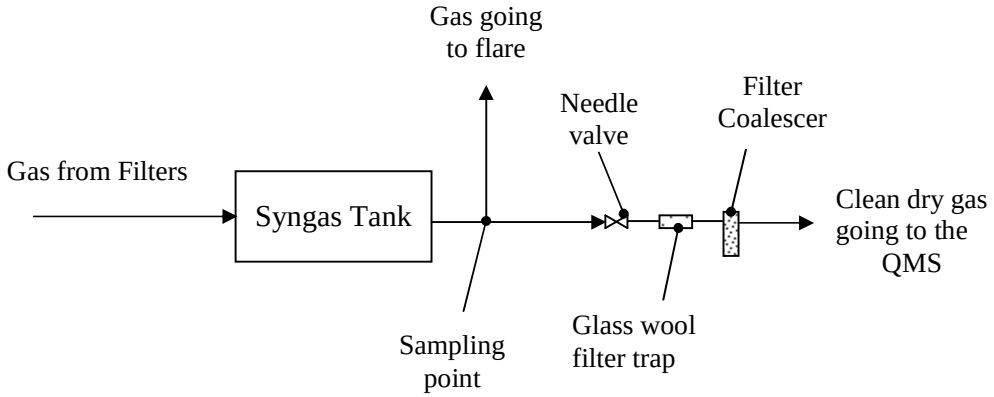

(a)

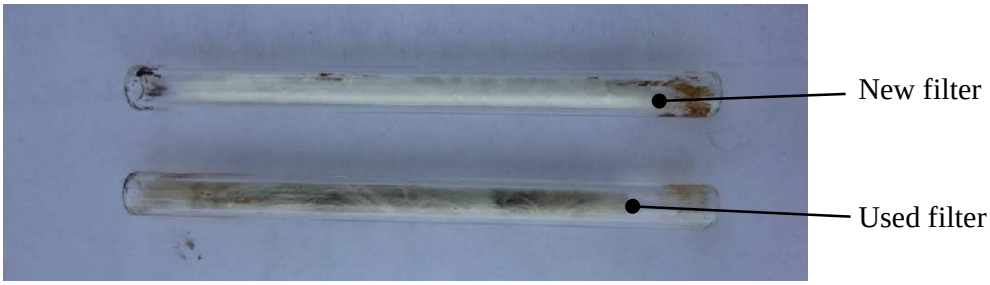

(b)

Figure 8.3 Gas clean-up prior to the QMS (a) schematic, (b) glass wool filters before and after used.

Gas analysis techniques, for:

- N_2, CO, CO_2, H_2, CH_4 and O_2: same as described in Section 4.5.
- H_2S and COS: same as described in Section 5.3.

8.3 COMPOSITION OF WASTE-WOOD

8.3.1 The Actual Waste-wood Processed

Samples were taken of the waste-wood that was processed, and this is illustrated in Figure 8.4. It clearly shows that the sample consists of wood from a variety of different sources (e.g. bark, used wood, painted wood), and that it also contains small quantities of cardboard, brown paper, and even plastics.

Figure 8.4 Photograph of a sample of waste-wood used.

A sample was also taken of the char from the base of the gasifier, and this is illustrated in Figure 8.5.

Figure 8.5 Photograph of a sample of char from the base of the gasifier.

Samples of the waste-wood and waste-wood-derived char (see Figure 8.5), were analyzed, and their key properties are summarised in Table 8.1. Samples of this waste-wood were also reduced to char and then ash in the laboratory quartz-tube gasifier, and Figure 8.6 shows photographs taken.

Table 8.1 Proximate analysis of the waste-wood and the char derived (wt.% wet basis).

Property	Moisture	Volatiles	Fixed carbon	Ash
Waste-wood	9.97	70.57	19.13	0.33
Waste-wood-derived char	5.56	17.97	75.16	1.31

a) b) c)

Figure 8.6 Photos of (a) waste-wood, (b) wood reduced to char, and (c) char reduced to ash.

8.3.2 General Discussion on Composition of Waste-wood

Atkins and Donovan (1996) studied the nature of waste-wood, and classified this material into the following three main categories:

- Wood products manufactured with glues, binders, or resins, such as structural and non-structural panels (e.g., polywood, particleboard, masonite, waferboard, and wood laminates).
- Wood products treated with paints, stains, or coatings.
- Wood products impregnated with preservatives such as creosote, pentachlorophenol, or chromium copper arsenate (e.g., railroad ties, utility poles, and exterior grade lumber).

An analysis of different types of waste-wood is presented in Table 8.2.

Table 8.2 Analysis of waste-wood, data from Atkins and Donovan (1996).

Sample type	Fixed carbon	Volatiles	Ash	C	H	O	N	S	HHV, Btu/lb
Polywood scraps	18.87	79.63	1.5	54.74	6.13	37.28	0.31	0.04	9178
Pressure treated 1	16.22	79.97	3.81	55.17	6.03	34.71	0.25	0.03	9363
Pressure treated 2	18.04	80.96	1	50.97	6.27	41.51	0.23	0.02	8349
Fire treated	30.04	68.73	1.23	50.19	6.24	40.44	1.89	0.01	8280
Particle board (hardwoods)	19.36	80.4	0.24	51.83	5.81	39.13	2.96	0.03	8315
Particle board (pine fine)	19.91	79.54	0.55	52.99	6.09	37.39	2.95	0.03	8842
Particle board (pine medium)	20.77	78.84	0.39	55.01	5.65	35.76	3.16	0.03	8975
Particle board (pine coarse)	19.32	79.73	0.95	53.51	5.92	36.04	3.5	0.08	8947
Telephone poles	19.02	78.57	2.41	55.65	6.02	34.92	0.44	0.56	9415
Railroad ties	15.67	82.96	1.37	56.11	6.06	35.87	0.47	0.12	9434
Birch furniture polywood	14.3	85.32	0.38	51.25	5.94	38.94	3.48	0.01	8309
Furniture waste	17.86	81.06	1.08	50.88	6.13	40.29	1.6	0.02	8429
Laminated wood	20.44	78.05	1.51	49.71	6.08	39.29	3.36	0.05	8348

From Table 8.2, it is interesting to note that the sulphur content can vary considerably, and this depends on the source of wood. Atkins and Donovan (1996) concluded that high levels of sulphur in a waste-wood stream indicate that either the waste-wood contains: creosote-treated materials, or non-wood contaminants (such as tarpaper, shingles, and asphalt).

Looking at other sources in the literature (see Table 8.3), the sulphur content was found to vary from 0.0 wt.% (e.g. fresh wood like redwood, maple) to 1.0 wt.% (e.g. kiln dried wood).

Table 8.3 Sulphur content of waste-wood.

Biomass Fuels	Sulphur, wt.% (dry basis)	Reference source
Redwood (waste)	0.1	Boley and Landers (1969) as presented in Basu (2010, p. 51)
Redwood	0.0	Tillman (1987) as presented in Basu (2010, p. 51)
Maple	0.0	
Douglas fir	0.0	
Wood, chipped	0.08	Anonymous (1979) as presented in Kaupp and Goss (1984, p. 144)
Wood, general	0.02	
Wood, pine bark	0.1	Bailie (1977) as presented in Reed and Das (1988, p. 15)
Wood, green fir	0.06	
Wood, kiln dried	1.0	
Wood, air dried	0.08	
Red Alder	0.07	Gaur and Reed (1998, p. 235)
Tan Oak	0.03	
Western Hemlock	0.1	
Spruce Bark	0.1	
Paper	0.2	Bowerman (1969) as presented in Reed and Das (1988, p. 13)
Brown paper	0.1	Kreith and Goswami (2007, pp. A4-1 – A4-2)
Cardboard	0.1	
Garbage	0.5	
Garden plant wastes	0.3	

To represent a sample of waste-wood, samples were taken by Atkins and Donovan (1996) directly from a range of waste-woods and the average values are shown in Table 8.4.

Table 8.4 Ultimate and proximate analysis of waste-wood, Atkins and Donovan (1996).

	Fixed carbon	Volatiles	Ash	C	H	O	N	S	HHV, Btu/lb
Average (wt.% dry basis)	15.25	79.59	5.16	50.28	5.92	38.07	0.46	0.12	8238

8.4 CALCULATION OF AIR FLOW AND WASTE-WOOD FEED RATE

8.4.1 Flow of Air

As data on the flow of air and waste-wood was more difficult to measure on the pilot-plant, this was back-calculated from other measured parameters.

Starting with an overall material balance for the process:

$$\begin{bmatrix}\text{Waste}-\text{wood In}\\(\text{kg/h})\end{bmatrix}+\begin{bmatrix}\text{Air In}\\(\text{kg/h})\end{bmatrix}=\begin{bmatrix}\text{Gas Out}\\(\text{kg/h})\end{bmatrix}+\begin{bmatrix}\text{Char removal}\\(\text{kg/h})\end{bmatrix}+\begin{bmatrix}\text{Condensates}\\(\text{kg/h})\end{bmatrix} \quad (8.1)$$

Char was removed from the bottom of the gasifier and the cyclones (duration 2 minutes in a 10 minute cycle). The char removal rate was thus calculated to be 19.44 kg/h.

The flow of gas to the flare was measured and recorded. Therefore, if the composition of the gas is measured (on QMS) then the flow rate of each species can be calculated from:

$$f_i = (y_i \times F_{gas}) \times M_i \qquad \text{(kg/h)} \qquad (8.2)$$

where: y_i is mole fraction of species i

M_i is the molar mass of species i, kg/kmol

F_{gas} is the total molar flow of producer gas, and can be calculated from:

$$F_{gas} = \frac{Q_{std}}{V_o} \qquad \text{(kmol/h)} \qquad (8.3)$$

where: Q_{std} is standard volume flow of producer gas, m^3/h

V_o is the standard volume of one mole gas at normal conditions (25 ^oC, 101.325 kPa), 24.47 m^3/kmol.

On the plant, the volumetric flow of producer gas (Q) was measured at atmospheric pressure and temperature, T (^oC), of the gas from the Syngas Tank (see Figure 8.1). Therefore, Q_{std} can be calculated:

$$Q_{std} = Q \times \frac{298}{T + 273} \qquad (m^3/h) \qquad (8.4)$$

The recorded values of the volumetric flow of gas on the plant had to be re-calculated, following the use of a turbine meter for gas flow measurement, see Figure 8.7.

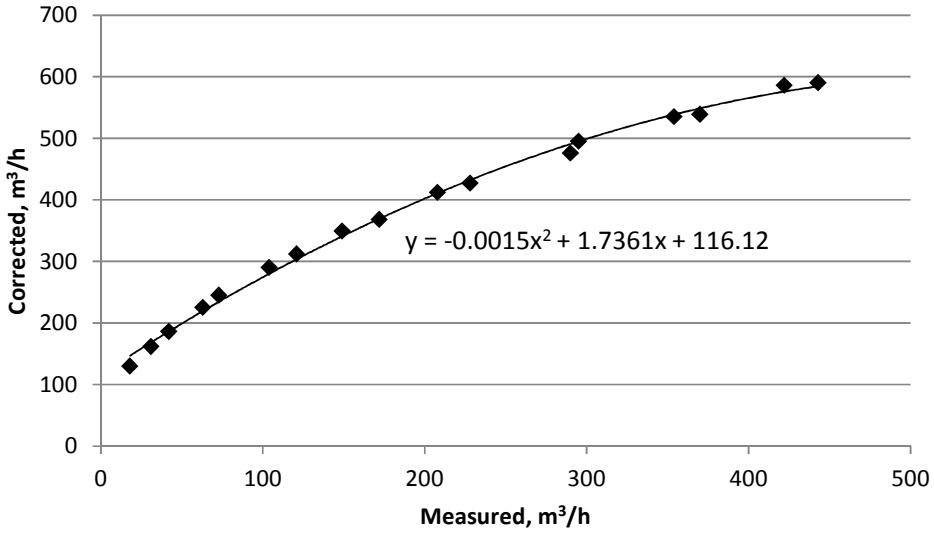

Figure 8.7 Calibration curve to correct volumetric flow of gas.

Because nitrogen is considered as an inert gas during the gasification process, the flow of air into the process can be back-calculated from the flow of nitrogen in the producer gas:

$$f_{air} = f_{N_2} + f_{O_2} = f_{N_2} + F_{N_2} \times \frac{21}{79} \times M_{O_2} \qquad \text{(kg/h)} \qquad (8.5)$$

8.4.2 Waste-wood Feed Rate

A mass balance on carbon is then performed, to calculate the mass flow of waste-wood.

$$\begin{bmatrix}\text{Total carbon in}\\ \text{waste - wood}\\ \text{(kg/h)}\end{bmatrix} = \begin{bmatrix}\text{Total carbon}\\ \text{in gas (kg/h)}\end{bmatrix} + \begin{bmatrix}\text{Total carbon in}\\ \text{char removed}\\ \text{(kg/h)}\end{bmatrix} + \begin{bmatrix}\text{Total carbon in}\\ \text{condensates}\\ \text{(kg/h)}\end{bmatrix} \qquad (8.6)$$

To simplify Equation (8.6), it was assumed that:

- The waste-wood had the composition as described in Table 8.4.
- The moisture content of the waste-wood was 9.97 wt.% (as measured, see Table 8.1).
- The waste-wood-derived char contained 1.31 wt.% ash, 5.56 wt.% moisture and the rest was carbon (93.13 wt.%), as measured in Table 8.1.
- Carbon in the form of condensates (e.g. tars) was small and neglected.

From Equation (8.6), the feed of waste-wood is estimated:

$$\left[\begin{matrix}\text{Waste - wood feed}\\(\text{kg/h})\end{matrix}\right] = \left[\left(\begin{matrix}\text{Total carbon}\\\text{feeding (kg/h)}\end{matrix}\right) \times \frac{100}{\left(\begin{matrix}\text{Carbon content}\\(\text{wt.\%})\end{matrix}\right)}\right] \times \left[\frac{100}{100 - \left(\begin{matrix}\text{Moisture content}\\(\text{wt.\%})\end{matrix}\right)}\right] \tag{8.7}$$

8.4.3 Air Equivalence Ratio

The equivalence ratio (ER) is defined as:

$$ER = \frac{Actual\ \text{air}}{Stoichiometric\ \text{air}} \tag{8.8}$$

where the stoichiometric air (f_{air}^{0}, kg/h) is the theoretical air requirement for complete combustion of a unit mass of a fuel, and the actual air (f_{air}) is calculated from Equation (8.5).

The stoichiometric air requirement can be calculated either from the composition of the waste-wood, or from the compositions of the gas and char produced.

From a mass balance on oxygen:

$$f_{air}^{0} = \begin{bmatrix} \text{Actual air} \\ \text{consumed (kg/h)} \end{bmatrix} + \begin{bmatrix} \text{Air required for} \\ \text{complete combustion} \\ \text{of producer gas (kg/h)} \end{bmatrix} + \begin{bmatrix} \text{Air required for} \\ \text{complete combustion} \\ \text{of char (kg/h)} \end{bmatrix} + \begin{bmatrix} \text{Air required for} \\ \text{complete combustion} \\ \text{of condensates (kg/h)} \end{bmatrix} \text{, kg/h} \tag{8.9}$$

The air for the combustion of condensates was considered to be very small and neglected.

8.4.4 An Example Calculation

For one 'snap-shot' in Table 8.5(c):

From the corrected value of producer gas flow into the flare (Q = 477 m^3/h), the total molar flow of gas produced is estimated from Equations (8.3) and (8.4):

$$F_{gas} = Q \times \left(\frac{298}{T + 273} \right) \times \frac{1}{V_0} = 477 \times \left(\frac{298}{18 + 273} \right) \times \frac{1}{24.47} = 19{,}962 \quad \text{mol/h}$$

$$= 19.962 \quad \text{kmol/h}$$

The mass flow rate of each species is then calculated from Equation (8.2). For example, for N_2:

$$f_{N_2} = \left(y_{N_2} \times F_{gas} \right) \times M_{N_2} = \frac{(53.31 \times 19.962)}{100} \times 28 = 297.97 \ \text{kg/h}$$

The flow of air fed into the gasifier is then calculated from Equation (8.5):

$$f_{air} = f_{N_2} + F_{N_2} \times \frac{21}{79} \times M_{O_2} = 297.97 + \frac{(53.31 \times 19.962)}{100} \times \frac{21}{79} \times 32 \approx 388 \ \text{kg/h}$$

The total carbon in the waste-wood is now calculated from Equation (8.6):

$$\begin{bmatrix}\text{Total carbon in}\\ \text{waste - wood}\\ \text{(kg/h)}\end{bmatrix} = \begin{bmatrix}\text{Total carbon}\\ \text{in gas (kg/h)}\end{bmatrix} + \begin{bmatrix}\text{Total carbon in}\\ \text{char removed}\\ \text{(kg/h)}\end{bmatrix}$$

$$= \left[12 \times \left(y_{CO} + y_{CO_2} + y_{CH_4}\right) \times F_{gas}\right] + \left[(Char \text{ removal}) \times \frac{93.13}{100}\right]$$

$$= \left[12 \times \left(\frac{16.13 + 15.89 + 1.4}{100}\right) \times 19.962\right] + \left[19.44 \times \frac{93.13}{100}\right]$$

$$\approx 98.16 \text{ kg/h}$$

The waste-wood feed is then calculated from Equation (8.7):

$$[\text{Waste - wood feed}] = 98.16 \times \frac{100}{50.28} \times \frac{100}{100 - 9.97} \approx 217 \text{ kg/h}$$

The stoichiometric air is estimated either from the composition of waste-wood (Table 8.4), and it is: $f_{air}^{0} = 1543$ kg/h, or from the compositions of the gas and char produced:

$$f_{air}^{0} = \begin{bmatrix}\text{Actual air}\\ \text{consumed (kg/h)}\end{bmatrix} + \begin{bmatrix}\text{Air required for}\\ \text{complete combustion}\\ \text{of producer gas (kg/h)}\end{bmatrix} + \begin{bmatrix}\text{Air required for}\\ \text{complete combustion}\\ \text{of char (kg/h)}\end{bmatrix}$$

$$\approx 388 + 516 + 201 = 1105 \text{ kg/h}$$

Therefore, from Equation (8.8) the equivalence ratio (ER) is:

$$ER = \frac{f_{air}}{f_{air}^{0}} = \begin{cases} \dfrac{388}{1543} \approx 0.25 & \text{from the waste - wood composition.} \\ \text{or } \dfrac{388}{1105} \approx 0.35 & \text{from the compositions of the gas and char produced.} \end{cases}$$

8.5 EXPERIMENTAL RESULTS

Over a period of two days, a total of three runs were performed.

Initiation of reactions in the gasifier: At the start of each run, reactions in the gasifier are initiated, by:

- starting the blower, which draws air into the gasifier, and draws gas from the gasifier, and
- then inserting an ignited lance (through which propane flows) into the throat of the gasifier, which sustains a flame to initiate reactions in the gasifier.

When temperatures start to rise in the throat of the gasifier, and gas temperatures from the gasifier also rise, the supply of propane is turned-off, and the lance is withdrawn.

8.5.1 Test Run 1 – Cold Stage Start-up

By selecting the following key parameters:

- temperatures at the top and bottom of the throat (in the gasifier, but measured near the wall of the throat), and producer gas flow,
- producer gas composition (N_2, CO, CO_2, H_2, CH_4 and O_2),
- the sulphur species, H_2S and COS, in the gas,

the results of this first Test Run are summarized in Figure 8.8. In general, during this run, temperatures fluctuated at the top and the bottom of the throat, and gas flow varied depending on the choice of operating conditions. When the gasifier was started-up from cold, such fluctuations can occur in the initial phase.

This first Test Run was used as a preliminary trial, and measurements that correspond to various moments in time, known as ‘snap-shots’, are captured in Appendix 5. However, at this point, they are not discussed further as this was just a preliminary run.

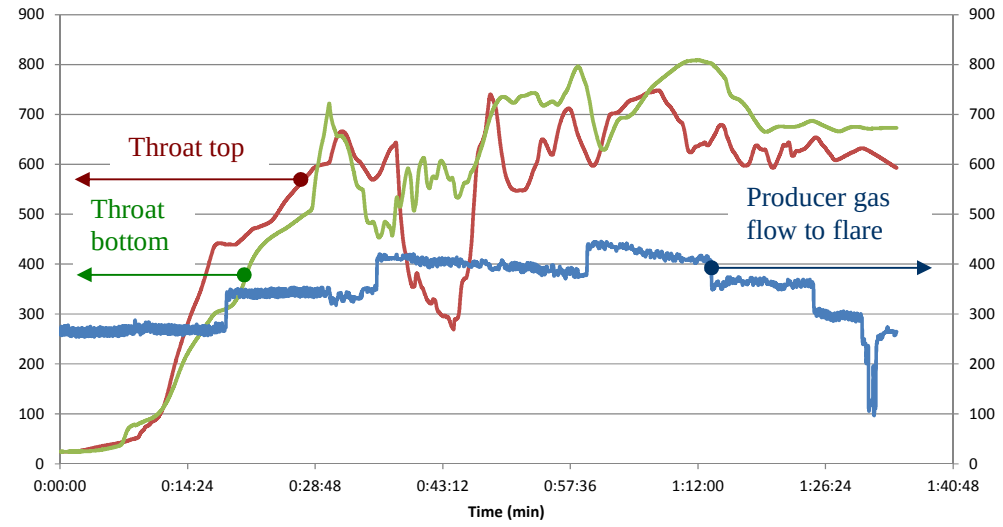

(a) Temperature and gas flow.

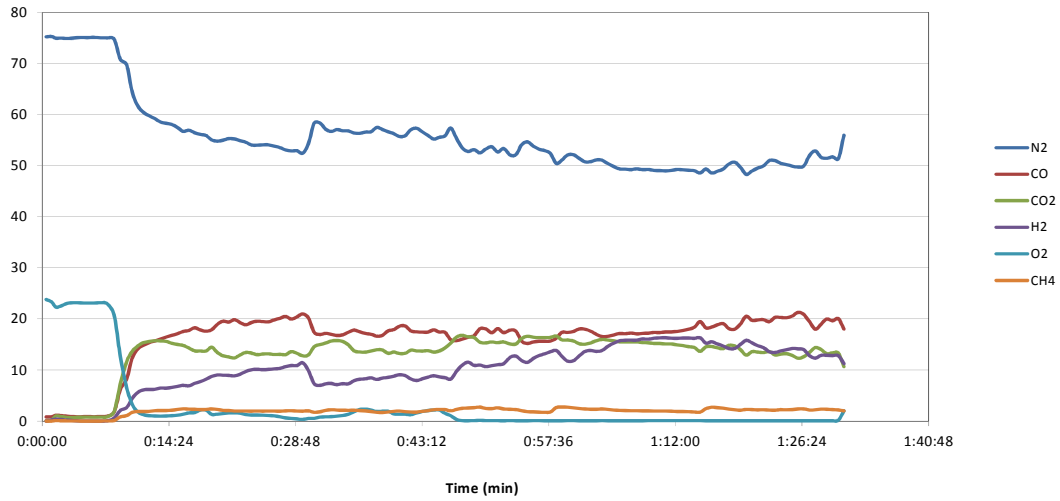

(b) Dry gas composition.

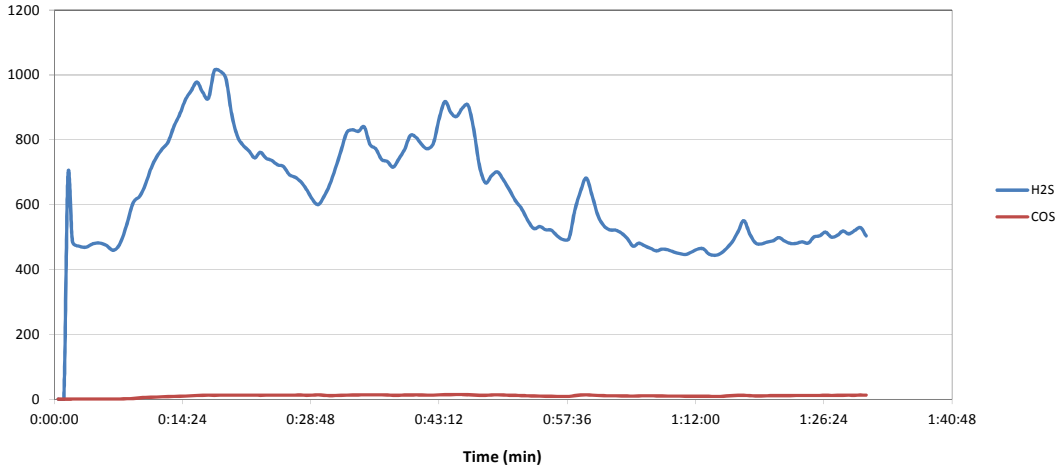

(c) Concentrations of H_2S and COS in dry gas.

Figure 8.8 Test Run 1.

8.5.2 Test Run 2 – Warm Stage Start-up

The results of this second Test Run are summarized in Figure 8.9. Because the gasifier was started-up from a warm condition, recorded temperatures at the top and bottom of the throat (Figure 8.9(a)) were more stable (than in Test Run 1, Figure 8.8(a)).

In this run, the blower speed was set at an initial low value (30 %), and then it was increased by a 10 % interval, up to a value of 40 %, and then down to 30 %. This was to explore the effect of air flow on producer gas composition. After one hour of operation, a small blockage occurred inside the gas/liquid separator after the HESS, and this led to an increase in pressure drop, and the gasifier thus was shut-down.

In Tables 8.5(a) to (e), snap-shots at moments in time are shown, corresponding to operating points at different speeds of the blower, and some of the parameters, that were calculated from the material balances described earlier in Section 8.4, are presented in Table 8.6. This data is now discussed in more detail. Looking at the data, the following general observations can be made:

- As the blower speed was increased, the flow of air into the gasifier increased, and temperatures in the gasifier increased. The flow of gas from the gasifier also increased, as more gas was drawn by the centrifugal blower.
- As the unit was started-up, the composition of the gas changed (see Figure 8.9 (b)), providing a very clear indication of the point at which H_2 and CO started to be produced, and O_2 was consumed.
- In general, as temperatures in the gasifier increase (above and below the throat), the concentration of CO decreases (from 23 to 16 vol.%), whereas that of H_2 increases (from 10 to 15 vol.%).
- At various fixed operating speeds of the blower, the gas composition fluctuates (for example, see Figure 8.9 (b), and this most probably arises from the nature of the gasification process (and composition of waste-wood) that is taking place in the throat of the gasifier. Although some gas back-mixing will occur in the pipework and process units before the gas sampling point, the fact that these fluctuations still

remain indicates the presence of far bigger variations in gas composition at the base of the actual gasifier. However, considering the nature of the waste-wood feedstock, and the variations in size of the feedstock (Figure 8.4), this is not surprising. For example, for a fixed operating speed of the blower at 40 %, it is interesting to see that these variations are approximately: CO = 16.0 (± 1.8) vol.%, H_2 = 11.9 (± 2.9) vol.%, CO_2 = 15.8 (± 1.4) vol.%, N_2 = 54.1 (± 3.3) vol.%, CH_4 = 1.9 (± 0.7) vol.%, O_2 = 0.3 (± 0.2) vol.%.

- From the calculated parameters, there are two sets of equivalence ratio (e.g. they vary in ranges of 0.32 to 0.35, and 0.23 to 0.25). The later range of the equivalence ratio estimated from assumed composition of the waste-wood feed looks more reasonable because they are approximately 0.25, which is considered (Knoef (2005, p. 17)) as a typical value for such a down-draft gasification process.

- In Figure 8.9(c), the changes in H_2S and COS levels are shown. The concentration of H_2S varies from about 200 to 700 ppmv, which is slightly lower than in Test Run 1, while the COS concentration is still quite low (~10 ppmv). The variations in H_2S levels are not surprising as this will vary depending on the composition of the waste-wood that is being gasified at a particular moment in time. This will be discussed further in Section 8.6.

- Looking more closely at Table 8.5(a), the gas outlet temperature from the gasifier has two different values (176 and 157 ºC), corresponding to two different positions from which the gas was withdrawn. As the speed of the blower is increased to 40 %, these two gas temperature increase up to 486 and 559 ºC (see Table 8.5 (d)).

- In the data in the snap-shots, the gas flow to the flare has two values. For example, in Table 8.5(a), 162 m^3/h is the recorded value, and 358 m^3/h is the corrected reading (after calibration of the instrument). The reported gas flows in Figure 8.9(a) are the corrected gas flows.

- The initial start-up period, provides some interesting data on the oxygen content in the gas, and this will be discussed further in Section 8.7.

- These gas measurements can be compared with earlier experiments in Chapter 3. From these, for example, the concentration of CO is 15.8 vol.%, and for H_2 is 9.5 vol.% in the gas stream produced from gasification of wood pellets.

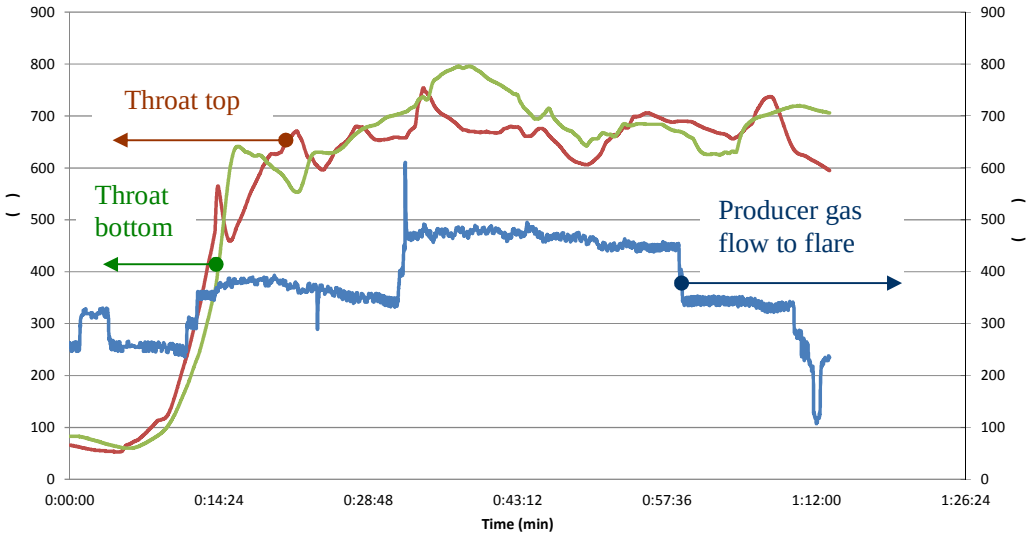

(a) Temperature and gas flow.

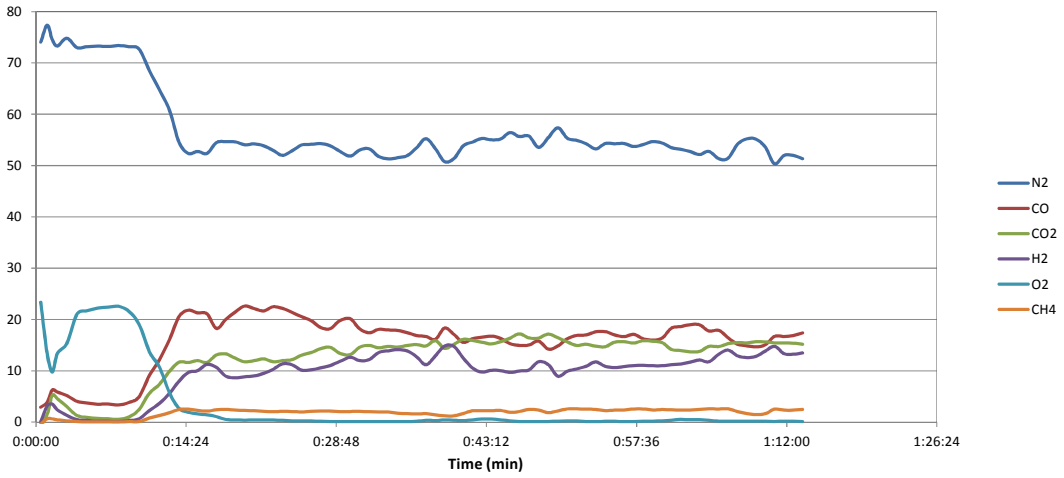

(b) Dry gas composition.

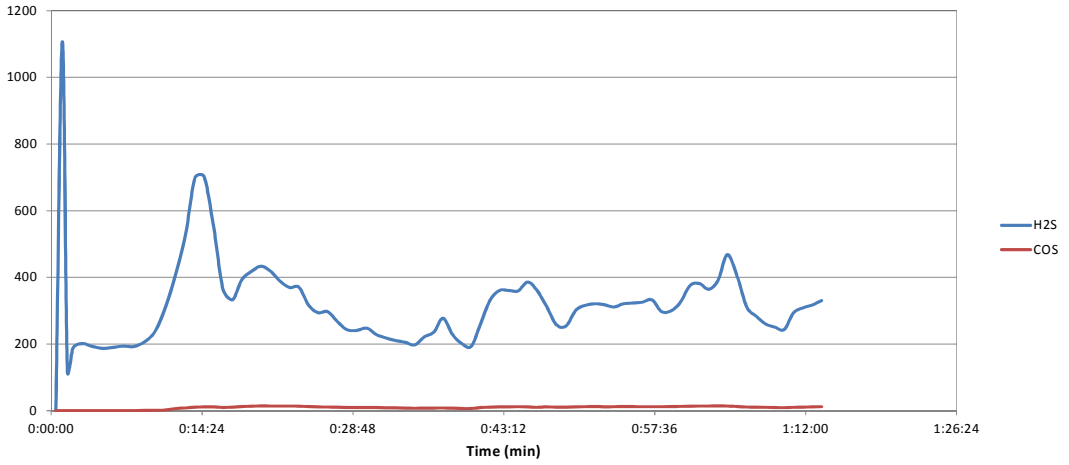

(c) Concentration of H_2S and COS in dry gas.

Figure 8.9 Test Run 2.

Table 8.5(a) Test Run 2: Snap Shot 1 at 00:13:43.

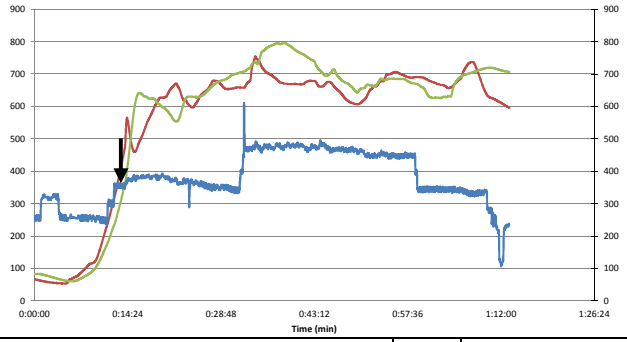

Producer gas			
		Temperature (°C)	Pressure (mbar)
Gasifier	Out	176 and 157	-
Cyclones	In	see note *(1)*	-
	Out	80	-
Quench	In		-
	Out	40	- 70
HESS	In		
	Out	13	-
Heat Exchanger	In		-
	Out	11	- 100
Blower	In		
	Out	-	-
Filters	In		
	Out	16	103
Syngas Tank			
Flare		571	
Flow into Flare (m^3/h): *162* (recorded value) **358** (corrected value)			

Gasifier	
Top	-9 (mbar) 117 (°C)
Throat Top	448
Throat Bottom	341
Bottom	-

Air	
Into cyclones	24 (°C) *(2)*
Out cyclones	30 (°C) *(2)*
Into gasifier	66 (m^3/h) *(3)*

Water	
Into quench	15 (°C) *(2)*
Out quench	36 (°C) *(4)*
Into HESS	18 (°C)
Out HESS	20 (°C) *(2)*
Tank	21 (°C)

Gas Composition (vol.%)	
N_2	54.53
CO	20.56
CO_2	11.68
H_2	8.0
O_2	2.68
CH_4	2.45
H_2S	698 (ppmv)
COS	10.3 (ppmv)

Chiller	
Fluid Out	11 (°C) *(4)*
Fluid In	10 (°C) *(2)*

Blower	
Speed	30 (%)

1. The producer gas leaves the base of the gasifier via two separate pipes (at 180º from each other), so two gas temperatures are reported (one for each pipe).
2. These values was read from in-line gauges
3. Air passing through the outer jacket of the cyclones and then into the gasifier, is measured at NTP. Air entering via the central shaft in the gasifier was not measured.
4. Values were measured using a hand held temperature probe.

Table 8.5(b) Test Run 2: Snap Shot 2 at 00:28:12.

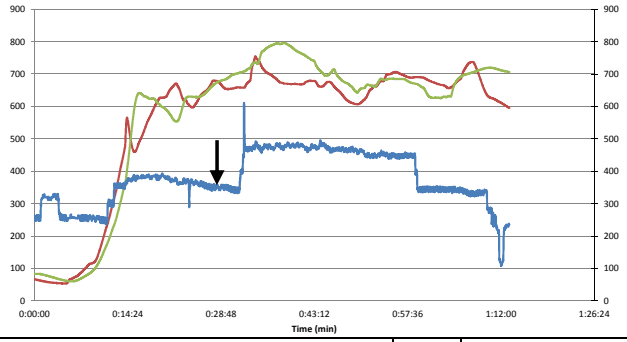

Producer gas			
		Temperature (°C)	Pressure (mbar)
Gasifier	Out	418 and 400	-
Cyclones	In	see note *(1)*	-
	Out	262	-
Quench	In		-
	Out	61	- 50
HESS	In		
	Out	23	-
Heat Exchanger	In		-
	Out	13	- 91
Blower	In		
	Out	-	-
Filters	In		
	Out	17	104
Syngas Tank			
Flare		619	
Flow into Flare (m^3/h): 160 (recorded value) **356** (corrected value)			

Gas Composition (vol.%)	
N_2	53.86
CO	18.2
CO_2	14.59
H_2	11.02
O_2	0.12
CH_4	2.15
H_2S	243 (ppmv)
COS	9.7 (ppmv)

Gasifier	
Top	-12 (mbar) 116 (°C)
Throat Top	678
Throat Bottom	674
Bottom	-

Air	
Into cyclones	26 (°C) *(2)*
Out cyclones	70 (°C) *(2)*
Into gasifier	82 (m^3/h) *(3)*

Water	
Into quench	16 (°C) *(2)*
Out quench	42 (°C) *(4)*
Into HESS	8 (°C)
Out HESS	23 (°C) *(2)*
Tank	21 (°C)

Chiller	
Fluid Out	12 (°C) *(4)*
Fluid In	12 (°C) *(2)*

Blower	
Speed	30 (%)

1. The producer gas leaves the base of the gasifier via two separate pipes (at 180º from each other), so two gas temperatures are reported (one for each pipe).
2. These values was read from in-line gauges
3. Air passing through the outer jacket of the cyclones and then into the gasifier, is measured at NTP. Air entering via the central shaft in the gasifier was not measured.
4. Values were measured using a hand held temperature probe.

Table 8.5(c) Test Run 2: Snap Shot 3 at 00:38:18.

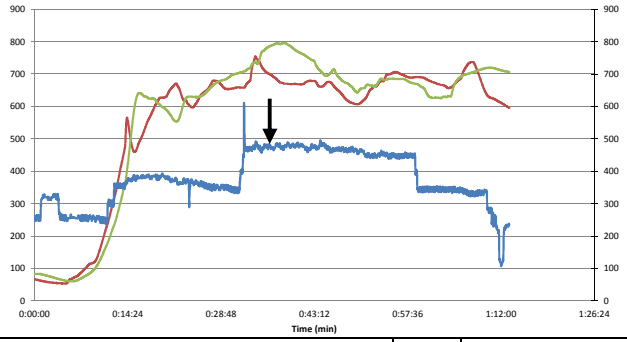

Producer gas			
		Temperature (°C)	Pressure (mbar)
Gasifier	Out	473 and 549 see note *(1)*	-
Cyclones	In		-
	Out	397	-
Quench	In		-
	Out	70	- 44
HESS	In		
	Out	31	-
Heat Exchanger	In		-
	Out	14	- 127
Blower	In		
	Out	-	-
Filters	In		
	Out	18	57
Syngas Tank			
Flare		521	
Flow into Flare (m^3/h): 272 (recorded value) **477** (corrected value)			

Gasifier	
Top	-17 (mbar) 183 (°C)
Throat Top	672
Throat Bottom	759
Bottom	-

Air	
Into cyclones	28 (°C) *(2)*
Out cyclones	100 (°C) *(2)*
Into gasifier	101 (m^3/h) *(3)*

Water	
Into quench	16 (°C) *(2)*
Out quench	41 (°C) *(4)*
Into HESS	2 (°C)
Out HESS	35 (°C) *(2)*
Tank	21 (°C)

Gas Composition (vol.%)	
N_2	53.31
CO	16.13
CO_2	15.89
H_2	12.91
O_2	0.31
CH_4	1.4
H_2S	228 (ppmv)
COS	7.37 (ppmv)

Chiller	
Fluid Out	14 (°C) *(4)*
Fluid In	15 (°C) *(2)*

Blower	
Speed	40 (%)

1. The producer gas leaves the base of the gasifier via two separate pipes (at 180º from each other), so two gas temperatures are reported (one for each pipe).
2. These values was read from in-line gauges
3. Air passing through the outer jacket of the cyclones and then into the gasifier, is measured at NTP. Air entering via the central shaft in the gasifier was not measured.
4. Values were measured using a hand held temperature probe.

Table 8.5(d) Test Run 2: Snap Shot 4 at 00:57:20.

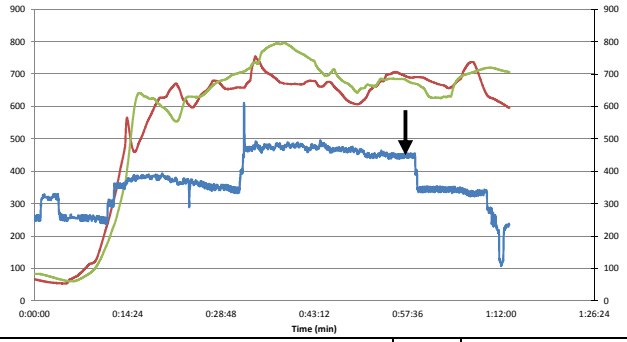

Producer gas			
		Temperature (^oC)	Pressure (mbar)
Gasifier	Out	486 and 559 see note *(1)*	-
Cyclones	In		-
	Out	443	-
Quench	In		-
	Out	82	- 33
HESS	In		
	Out	46	-
Heat Exchanger	In		-
	Out	26	- 110
Blower	In		
	Out	-	-
Filters	In		
	Out	23	54
Syngas Tank			
Flare		601	
Flow into Flare (m^3/h): 237 (recorded value) **443** (corrected value)			

Gas Composition (vol.%)	
N_2	53.7
CO	17.09
CO_2	15.43
H_2	11.02
O_2	0.13
CH_4	2.57
H_2S	332 (ppmv)
COS	12 (ppmv)

Gasifier	
Top	-17 (mbar) 180 (^oC)
Throat Top	692
Throat Bottom	681
Bottom	-

Air	
Into cyclones	30 (^oC) *(2)*
Out cyclones	160 (^oC) *(2)*
Into gasifier	103 (m^3/h) *(3)*

Water	
Into quench	20 (^oC) *(2)*
Out quench	44 (^oC) *(4)*
Into HESS	-7 (^oC)
Out HESS	45 (^oC) *(2)*
Tank	21 (^oC)

Chiller	
Fluid Out	24 (^oC) *(4)*
Fluid In	25 (^oC) *(2)*

Blower	
Speed	40 (%)

1. The producer gas leaves the base of the gasifier via two separate pipes (at 180º from each other), so two gas temperatures are reported (one for each pipe).
2. These values was read from in-line gauges
3. Air passing through the outer jacket of the cyclones and then into the gasifier, is measured at NTP. Air entering via the central shaft in the gasifier was not measured.
4. Values were measured using a hand held temperature probe.

Table 8.5(e) Test Run 2: Snap Shot 5 at 01:07:17.

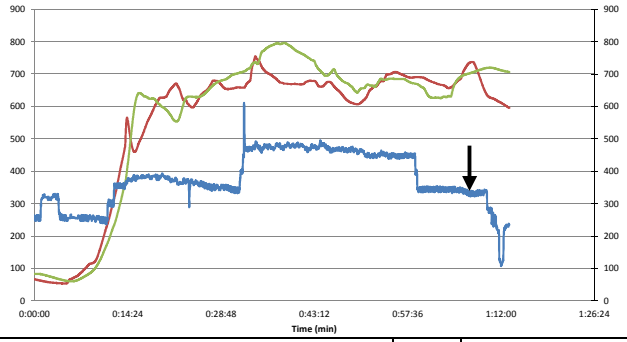

Producer gas			
		Temperature (°C)	Pressure (mbar)
Gasifier	Out	462 and 521	-
Cyclones	In	see note *(1)*	-
	Out	380	-
Quench	In		-
	Out	75	- 29
HESS	In		
	Out	41	-
Heat Exchanger	In		-
	Out	29	- 62
Blower	In		
	Out	-	-
Filters	In		
	Out	27	38
Syngas Tank			
Flare		611	
Flow into Flare (m^3/h): 139 (recorded value) **329** (corrected value)			

Gas Composition (vol.%)	
N_2	54.15
CO	15.17
CO_2	15.5
H_2	12.9
O_2	0.16
CH_4	2.06
H_2S	283 (ppmv)
COS	10.7 (ppmv)

Gasifier	
Top	-10 (mbar) 270 (°C)
Throat Top	736
Throat Bottom	703
Bottom	-

Air	
Into cyclones	32 (°C) *(2)*
Out cyclones	170 (°C) *(2)*
Into gasifier	71 (m^3/h) *(3)*

Water	
Into quench	20 (°C) *(2)*
Out quench	46 (°C) *(4)*
Into HESS	2 (°C)
Out HESS	39 (°C) *(2)*
Tank	21 (°C)

Chiller	
Fluid Out	25 (°C) *(4)*
Fluid In	26 (°C) *(2)*

Blower	
Speed	30 (%)

1. The producer gas leaves the base of the gasifier via two separate pipes (at 180º from each other), so two gas temperatures are reported (one for each pipe).
2. These values was read from in-line gauges
3. Air passing through the outer jacket of the cyclones and then into the gasifier, is measured at NTP. Air entering via the central shaft in the gasifier was not measured.
4. Values were measured using a hand held temperature probe.

Table 8.6 **Test Run 2**: Calculated parameters corresponding to snap-shots in time.

Test Run 2 - on Wednesday 12 October 2011						
Time	00:13:43	00:28:12	00:38:18	00:57:20	01:07:17	-
Blower Speed (%)	30	30	40	40	30	-
Air inlet flow (kg/h)	300	294	388	357	264	-
Char removal rate (kg/h)	19.44	19.44	19.44	19.44	19.44	-
Producer gas flow (kg/h)	416	407	539	497	359	-
Waste-wood feed rate (kg/h)	179	178	217	210	156	-
HHV (MJ/Nm^3)	4.60	4.57	4.25	4.59	4.39	-
LHV (MJ/Nm^3)	4.35	4.26	3.94	4.28	4.05	-
Heat flow (kW)	473	464	576	569	398	-
Equivalence ratio *1)*	0.32	0.32	0.35	0.32	0.32	-
Equivalence ratio *2)*	0.24	0.23	0.25	0.24	0.24	
Throat Top, ^oC	448	678	672	692	736	-
Throat Bottom, ^oC	341	674	759	681	703	-

1) Equivalence ratio was estimated by calculating total air required for complete combustion of producer gas and char received.

2) Equivalence ratio was estimated by assuming the composition of the waste-wood fed into the gasifier.

8.5.3 Test Run 3 – Warm Stage Start-up

The results of this third Test Run are summarized in Figure 8.10.

In this Test Run, the blower speed was started from an initial low value (20 %), and then it was increased to 30, 40, 45, and finally 50 %. At that point a blockage occurred in the gas/liquid separator after the HESS, and the plant was shut-down (1 hour of operation achieved). Snap-shots which correspond to data at various time intervals in this Test Run 3 are presented in Appendix 6.

Looking at the data in Figure 8.10, the following general observations can be made:

- As the blower speed was increased, the flow of air into the gasifier increased, and temperatures in the gasifier increased. The flow of gas from the gasifier also increased, as more gas was drawn by the centrifugal blower. This follows a similar pattern to earlier experiments.

- Because the gasifier was started-up from a warm condition, recorded temperatures at the top and bottom of the throat remained more stable than in Test Run 1. However, their stability is of a similar order of magnitude to Test Run 2.

- Concentration of H_2S varied from about 200 to 700 ppmv, which is closer to the values in Test Run 2, while COS levels remained low ~10 ppmv.

- In general, as the temperatures increase (as gas flow increases), the CO levels remain high, and H_2 levels gradually increase; however, when the blower speed is increased to 50 %, the concentrations drop, but this also coincides with a small blockage in the gas/liquid separator after the HESS, and a drop in recorded temperatures in the gasifier (see Figure 8.10(a)). The levels of H_2S also peak at this point (see Figure 8.10(c)).

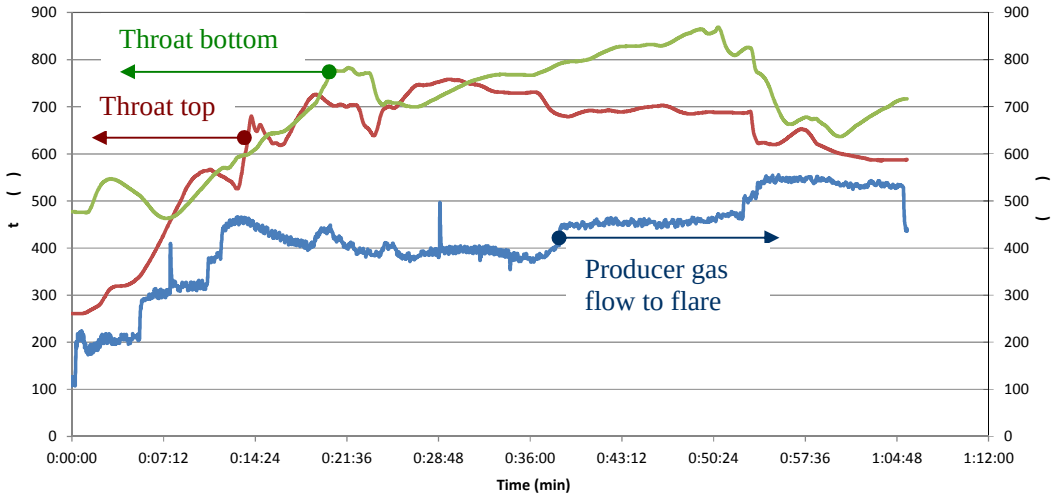

(a) Temperature and gas flow.

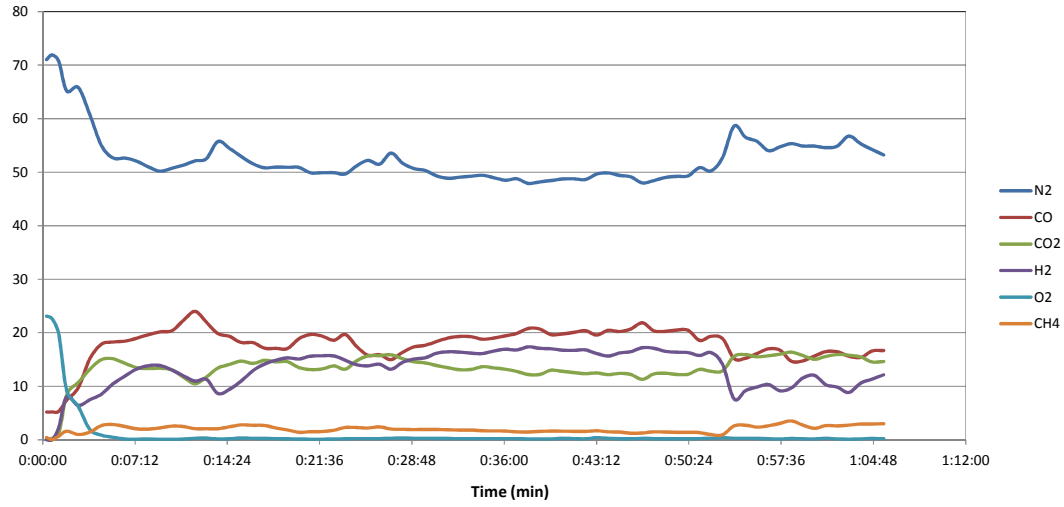

(b) Dry gas composition.

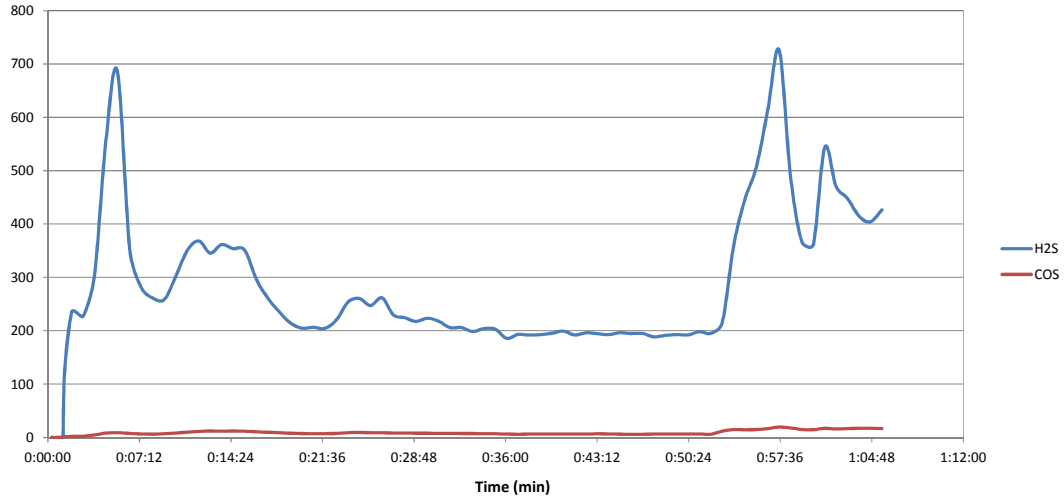

(c) Concentration of H_2S and COS in dry gas.

Figure 8.10 Test Run 3.

8.6 H_2S AND COS LEVELS IN THE PRODUCER GAS

8.6.1 H_2S Levels: Measurement and Calculation

In Test Runs 1, 2 and 3, the concentration of H_2S varies during the runs, and this is not surprising, as this will depend on the nature of the sulphur content in the waste-wood stream being gasified at that moment in time in the gasifier.

To explore how these values may compare with the thermodynamic simulations performed in Chapter 5, at a number of snap-shots in time, the thermodynamic equilibrium calculations were performed, using the measure values of gas composition at these points, and assuming a moisture content of 16.5 vol.% in the wet producer gas from the gasifier. Then, temperatures were adjusted to identify a suitable temperature which would correspond to the composition of the gas stream obtained. This is a similar technique, to that used in Chapter 5, Section 5.3.5.

The results of measured and calculated values are shown in Tables 8.7(a), 8.7(b), and 8.8(a) and 8.8(b) for snap-shots presented in Table 8.5(c) and 8.5(d), respectively.

Looking at the results in Tables 8.7(a), 8.7(b), and 8.8(a), 8.8(b), the following conclusions can be formed:

- There is a good match in the gas composition at a calculation temperature between 800 to 900 ^{o}C.
- The assumed moisture content of 16.5 vol.% is within values (8 to 20 vol.%) which could exist in the gas phase inside the gasifier.
- The measured concentration of COS in the producer gas stream is just slightly lower (e.g. 2 ppmv lower) than the theoretically calculated values (e.g. 12 ppmv).

Table 8.7(a) Adjusted gas composition (from Table 8.5(c)), used as a starting point in the calculation of equilibrium values.

	Dry gas composition Vol.%, see Table 8.5(c)	**Adjusted wet gas composition[(1)] Vol.%**
Hydrogen	12.91	10.783
Carbon monoxide	16.13	13.472
Methane	1.4	1.169
Carbon dioxide	15.89	13.272
Nitrogen	53.31	44.526
Oxygen	0.31	0.259
Water vapour		16.50 see note[(1)]
H_2S	0.0228	0.019 ≡ 190 ppmv
COS	0.000737	0.0006 ≡ 6 ppmv
Total	99.97	99.98

(1) Wet gas composition was adjusted for the moisture content in Table 5.2 (Chapter 5).

Table 8.7(b) Variation of species – simulations on a complex system using Aspen Plus®.

Species	**Temperature**					
	600 °C	700 °C	800 °C	900 °C	1000 °C	1100 °C
H_2 (vol.%)	16.346	15.957	14.619	13.493	12.576	11.825
CO (vol.%)	9.247	11.778	13.210	14.342	15.260	16.010
CH_4 (vol.%)	0.651	0.029	0.002	0.000	0.000	0.000
CO_2 (vol.%)	17.803	15.553	14.133	13.002	12.084	11.333
N_2 (vol.%)	44.187	43.644	43.620	43.619	43.619	43.618
O_2 (vol.%)	0.000	0.000	0.000	0.000	0.000	0.000
H_2O (vol.%)	11.747	13.019	14.396	15.525	16.443	17.193
H_2S (ppmv)	189	186	185	184	183	181
COS (ppmv)	6	7	8	9	10	11
SO_2 (ppmv)	0	0	0	0	0	0
SO_3 (ppbv)	0	0	0	0	0	0
CS_2 (ppbv)	0	0	0	0	0	0

Table 8.8(a) Adjusted gas composition (from Table 8.5(d)), used as a starting point in the calculation of equilibrium values.

	Dry gas composition Vol.%, see Table 8.5(d)	**Adjusted wet gas composition[(1)] Vol.%**
Hydrogen	11.02	9.204
Carbon monoxide	17.09	14.274
Methane	2.57	2.146
Carbon dioxide	15.43	12.887
Nitrogen	53.7	44.851
Oxygen	0.13	0.109
Water vapour		16.50 see note[(1)]
H_2S	0.0332	0.0277 ≡ 277 ppmv
COS	0.0012	0.001 ≡ 10 ppmv
Total	99.97	99.97

(1) Wet gas composition was adjusted for the moisture content in Table 5.2 (Chapter 5).

Table 8.8(b) Variation of species – simulations on a complex system using Aspen Plus®.

Species	**Temperature**					
	600 °C	700 °C	800 °C	900 °C	1000 °C	1100 °C
H_2 (vol.%)	16.987	17.066	15.750	14.619	13.698	12.944
CO (vol.%)	10.446	13.348	14.809	15.948	16.870	17.624
CH_4 (vol.%)	0.925	0.045	0.003	0.000	0.000	0.000
CO_2 (vol.%)	17.280	14.762	13.320	12.182	11.260	10.506
N_2 (vol.%)	43.846	43.088	43.052	43.050	43.050	43.050
O_2 (vol.%)	0.000	0.000	0.000	0.000	0.000	0.000
H_2O (vol.%)	10.488	11.662	13.039	14.173	15.095	15.849
H_2S (ppmv)	272	266	264	263	261	260
COS (ppmv)	9	10	12	13	15	16
SO_2 (ppmv)	0	0	0	0	0	0
SO_3 (ppbv)	0	0	0	0	0	0
CS_2 (ppbv)	0	0	0	0	0	0

8.6.2 COS Hydrolysis Reaction

Because of the low COS levels measured on the pilot-plant (e.g. 10 ppmv), information in the literature was considered in more detail, and this would help to understand why these values were so low relative to H_2S levels.

In a recent patent, McDaniel (2001) reported a method and apparatus for removing COS from a producer gas stream *via* wet scrubbing in the presence of ash particles. The ash particles contained alumina oxide, which could exhibit catalytic properties for the reaction.

$$H_2O + COS \underset{catalyst}{\leftrightarrow} CO_2 + H_2S \qquad (8.10)$$

Williams *et al.* (1999) also reported that such a reaction can take place at temperatures in the range of 30 to 250^{o}C, with higher rates occurring at higher temperatures. McDaniel (2001) found that if the producer gas stream from the gasifier went directly into a wet scrubber (without passing through any other particulate removal devices), then up to a 30 % drop in the COS occurred across the scrubber. This depended on the design of the scrubber and its operating conditions, and flooding conditions were preferred.

8.6.3 COS Hydrolysis Reaction and Pilot-plant

Looking back at the data in some of the snap-shots (e.g. Table 8.5(d)), the producer gas enters the quench at 443 ºC and leaves at 82 ºC. It then enters the HESS and leaves at 46 ºC. All of these temperatures are adequate to support hydrolysis reactions. It is proposed that as the gas is scrubbed, char fines and ash accumulate and are circulated in the scrubbing liquor, providing potential catalytic sites to support the hydrolysis reactions.

It would have been interesting to measure the composition of the dirty gas after the cyclones and before the quench. Unfortunately, this was not possible because of accidental contamination of the feed supply line to the QMS. The experiments were stopped, and there was insufficient time to repeat that set of planned experiments.

8.7 OXYGEN LEVELS IN THE GAS STREAM DURING START-UP

8.7.1 Flammability Limits

It is well recognized that during start-up of the gasifier, there is a risk of an explosive gas mixture existing in the lines/units from the gasifier, and that is why the provision of explosion relief is recommended on gasifiers (e.g. Reed and Das, 1988, p. 122). Such situations can exist with fuel-air mixtures between the lower flammability limit (LFL) and upper limit (UFL). The flammability limit of a gas mixture depends on the gas composition, temperature and pressure. For example, for gas compositions with higher contribution of inert species, such as N_2, a reduction of the flammability range can be observed, whereas an increase in temperature will see an opposite trend (e.g. Knoef, 2005, p. 306; and Timmerer and Lettner, 2005). Table 8.9 shows the flammability limits for CO, H_2 and CH_4 at 20 ^oC and atmospheric pressure.

Table 8.9 Flammability limits and autoignition temperatures for some combustible species in the producer gas, adapted from Carson and Mumford (2002, pp. 183-191).

Species	LFL vol.% in air	UFL vol.% in air	Autoignition temperature (^oC)
CO	12.5	74	609
H_2	4	75	585
CH_4	5	15	537

The flammable range is often expressed in terms of an explosion triangle, and such a diagram is illustrated in Figure 8.11.

From Figure 8.11, if a gas mixture (at 25 ^oC and 1 bar) of H_2, CO and CH_4 (in N_2 and CO_2), has an air content > 20 vol.% (this means > 4 vol.% oxygen), then a flammable mixture could exists. This could be used to assess explosions risks during start-up of the gasification plant.

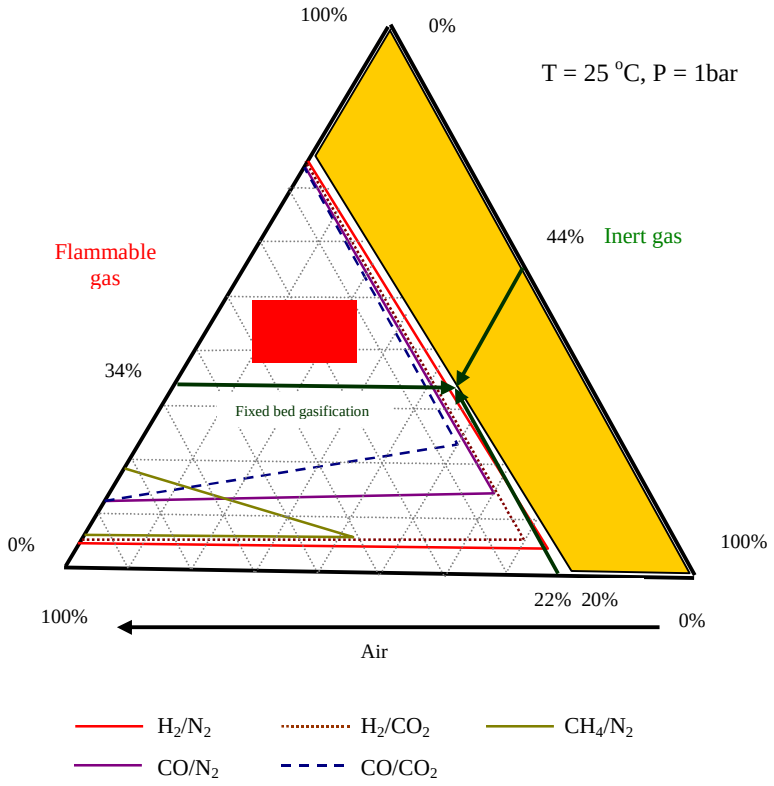

Figure 8.11 Explosion triangles for CH_4, CO and H_2 in air, and nitrogen and carbon dioxide as inert agents at 25 °C and 1 bar, adapted from Knoef (2005, p. 310).

8.7.2 Explosion Risk Assessment during Start-up

From data measured during Test Runs 1, 2 and 3, there are short periods (e.g 3 to 5 mins), where such conditions could exist. Larger scale plots of the early parts of Figures 8.8 (b), 8.9(b), and 8.10(b) are shown in Figures 8.12. Oxygen levels start at about 20 vol.% (which is what is expected for air in the gasifier), and then reduce, as the air in the lines and vessels is displaced initially with a mixture of products of the combustion reactions from the pilot- burner (propane) and the products of the gasification reaction. As oxygen levels decrease, then the concentration of flammables increases.

From Figures 8.12, it is useful to see how the variation of the gas mixture during start-up period is expressed in the explosion triangle in Figure 8.11. Some snap-shots were taken from Figure 8.12 (b) in Test Run 2, and they were presented in the explosion triangle. Table 8.10 and Figure 8.13 show the composition of the gas mixtures and their expression in the explosion triangle, respectively.

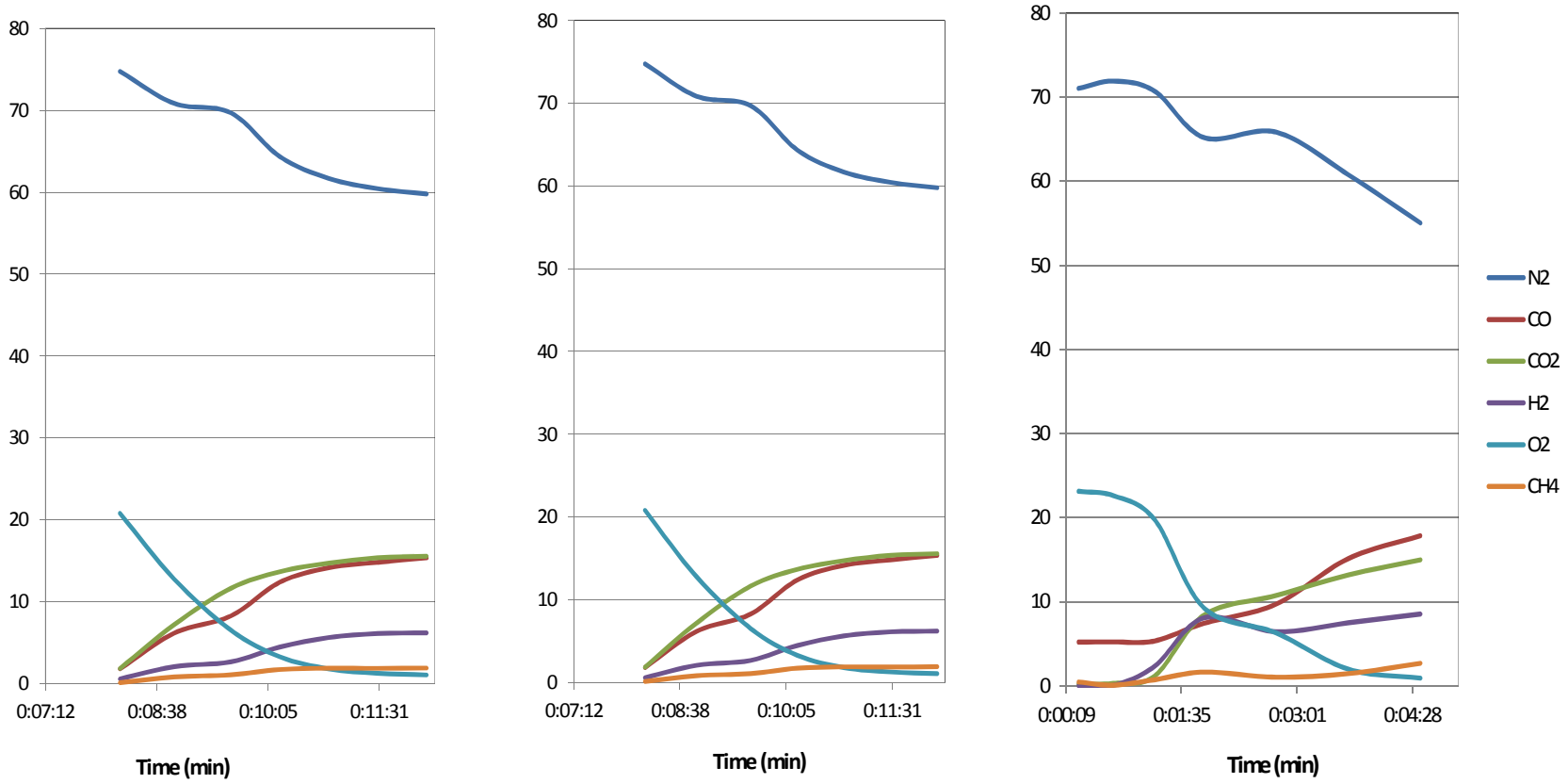

(a) **(b)** **(c)**

Figure 8.12 Oxygen levels in the producer gas during start-ups of the gasifier, magnified view of: (a) Figure 8.8(b) Test Run 1, (b) Figure 8.9(b) Test Run 2, and (c) Figure 8.10(b) Test Run 3.

Table 8.10 Variation of gas composition during start-up period in Test Run 2.

Species	Time				
	00:09:53 (point 1)	**00:10:52 (point 2)**	**00:11:50 (point 3)**	**00:12:49 (point 4)**	**00:13:43 (point 5)**
H_2	0.66	2.23	3.65	5.64	8.0
CO	4.94	9.04	12.19	16.18	20.56
CH_4	0.12	0.97	1.28	1.85	2.45
Total flammable gas:	5.72	12.24	17.12	23.67	31.01
CO_2	2.46	5.58	7.38	9.93	11.68
N_2	72.71	68.53	64.74	60.68	54.53
O_2	19.06	13.77	10.7	5.63	2.45

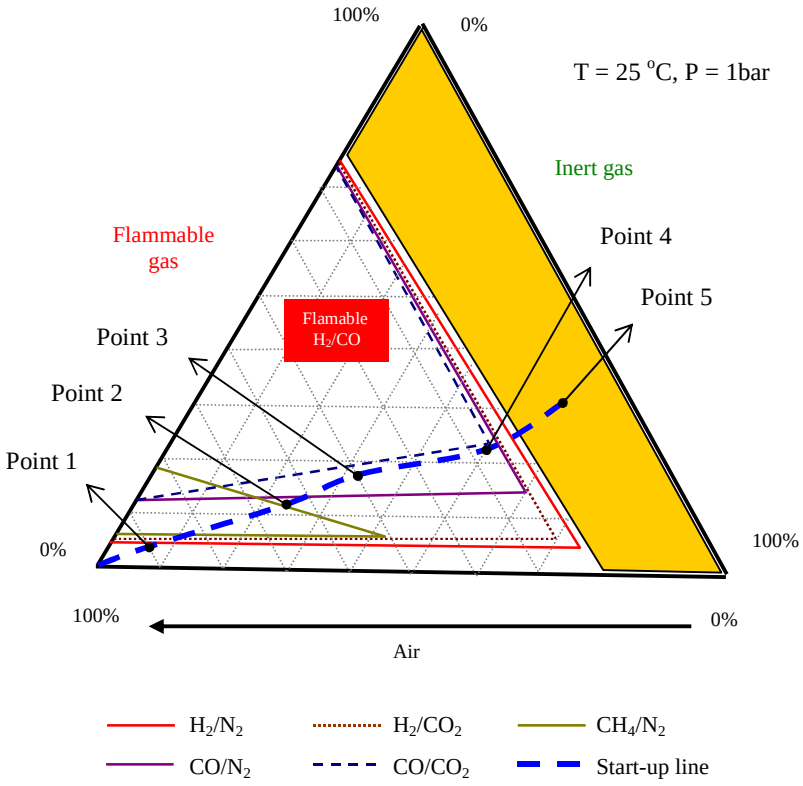

Figure 8.13 Explosion triangles for CH_4, CO and H_2 in air, and nitrogen and carbon dioxide as inert agents at 25 °C and 1 bar.

From Figure 8.13, it is clear that a flammable gas mixture could exist during the start-up period of Test Run 2.

8.8 CONCLUDING REMARKS

Using a QMS, valuable data was gathered on the real-time composition of producer gas from a commercial pilot-scale down-draft gasifier in which waste-wood was used as a fuel.

(a) O_2 levels were recorded during start-up, and these helped to identify the time period over which there was potential for a flammable mixture of gas to exist in the pipes and process plant. This lasted for about 3 to 5 mins after start-up.

(b) During normal operating conditions, the equivalence ratio was calculated and found to vary from 0.21 to 0.25. This is close to the theoretical value of 0.25, for this type of plant.

(c) The temperatures recorded at the top and bottom of the throat in the gasifier only provide an indication of temperatures at these locations (and how they change). They do not reflect actual maximum temperatures inside the hot zone in the throat.

(d) Gas outlet temperatures from the base of the gasifier provide a good indication of gas temperatures at this point. During stable operating periods, these varied from 400 to 580 ºC.

(e) During more stable operating periods of the gasifier, the dry gas concentrations reached maximum values of: CO = 20.5 vol.%; H_2 = 16.5 vol.% and CH_4 =2.5 vol.%. Consequently, the highest HHV of the gas produced was 5.35 MJ/Nm^3.

(f) Concentrations of two key sulphur compounds (H_2S and COS) in the producer gas were measured. Concentrations of H_2S varied from 200 to 1000 ppmv, and this is probably connected to the variation in the composition of the waste-wood fed into the gasifier. In addition, the thermodynamic calculated H_2S levels broadly match the experimental measurements for all calculation ranges (e.g. temperature is from 600 to 1200 ^oC, and moisture content is from 8 to 20 vol.%).

(g) The COS concentrations were in the region of 6 to 17 ppmv. These are ~30 times smaller than the concentrations of H_2S. This is different from the findings in Chapter 5, where the molar ratio of H_2S : COS was around 10:1 for all three types of biomass (wood pellets, straw pellets and RDF). This difference might arise from the possibility of COS hydrolysis reactions taking place in the water quench and HESS units - if it occurred, this would lead to the conversion of COS into H_2S.

REFERENCES

Atkins, R.S. and Donovan, C.T. (1996). Wood Products in the Waste Stream – Characterization and Combustion Emissions. United States Environmental Protection Agency. Volume 1, Technical Report.

Basu, P. (2010). Biomass Gasification and Pyrolysis. Elsevier Inc.

Carson, P.A. and Mumford, C.J. (2002). Hazards Chemicals Handbook. 2nd Edition, Elsevier.

Gaur, S., and Reed, T.B. (1998). Thermal data for natural and synthetic fuels. Marcel Dekker, Inc.

Kaupp, A. and Goss, J.R. (1984). Small scale gas producer-engine systems. Friedr. Vieweg & Sohn Braunschweig/Wiesbaden.

Knoef, H.A.M., edited, (2005). Handbook Biomass Gasification. BTG biomass technology group.

Kreith, F., and Goswami, D.Y., edited, (2007). Handbook of energy efficiency and renewable energy. CRC Press, Taylor & Francis Group.

McDaniel, J.E. (2001). Method and apparatus for removing carbonyl sulfide from a gas stream via wet scrubbing. US Patent, No. US 6322763 B1.

Reed, T.B. and Das, A. (1988). Handbook of biomass downdraft gasfier engine systems. U.S. Department of Energy, SERI/SP-271-3022.

Timmerer, H. and Lettner, F. (2005). Explosion parameters and explosion protection in biomass gasification plants. ThermalNet, Health, Safety and Environment of Biomass Gasification, pp. 114-127.

Williams, B.P., Young, N.C., West, J., Rhodes, C. and Hutchings, G.J. (1999). Carbonyl sulphide hydrolysis using alumina catalysts. Catalysis Today, Vol. 49, pp. 99-104.

CHAPTER 9

Conclusions and Recommendations

9.1 CONCLUSIONS

Related to gasification reactions:

(a) The experiments performed in the small glass quartz-tube gasifier (21 mm i.d.) proved to be most informative, as they provided a good indication of the likely gas composition from such a process (e.g. CO = 15.8 vol.%, H_2 = 9.5 vol.%, CO_2 = 14.5 vol.%, N_2 = 58.2 vol.%, and CH_4 = 2.0 vol.%). These values also compared well with data that was then gathered on the commercial pilot-scale plant (e.g. CO = 24.01 vol.%, H_2 = 11.83 vol.%, CO_2 = 11.74 vol.%, N_2 = 47.90 vol.%, CH_4 = 3.05 vol.%, and other hydrocarbons = 1.47 vol.%). Because of the nature of the quartz-tube gasifier, and as it was possible to view the contents within, important observations were made about the depth and movement of the hot zone, and how it moved downwards or upwards depending on the flow of gas. This in turn helped to develop a picture of the three dimensional shape that such hot zones may have in the throat of a gasifier.

(b) In the quartz-tube experiments, when the gases were passed through a fixed bed of hot charcoal (at a temperature of 600 to 900 °C), the improvement in the concentrations of CO and H_2 were not significant. This raised some unanswered questions about the effectiveness of this zone in a full scale gasifier, and whether it functions as often portrayed in simplified one dimensional schematics. It was postulated that the 1D form of representation is far too simplistic.

(c) However, when experiments were performed on the gasification of wood charcoal with steam, it was clear that above a gas temperature of 700 °C the reactions are initiated and a temperature of 750 °C is required before they become significant.

(d) Theoretical thermodynamic equilibrium calculations were performed looking closely at the key components in the gas. These showed that a good match was obtained with data from the quartz-tube, when an equilibrium temperature of 1100 ^{o}C was assumed, and in the commercial pilot-plant, when an equilibrium temperature of 800 to 900 ^{o}C was assumed. This is helpful as it shows the application of such calculations in a real situation. It is however emphasized that the kinetics of the individual and complex reactions may not match the equilibrium calculations.

Related to on-line gas analysis with QMS:

(e) A method was developed which enabled a QMS to be used to provide on-line, and in real-time quantitative gas analysis – this was not a trivial task. Special care had to be taken, with clashes in the mass spectra of N_2, CO and CO_2. The method was used to detect the main species in the producer gas (i.e. CO, H_2, CO_2, N_2, CH_4 and O_2), and the technique was later enhanced to measure the presence of COS and H_2S species.

Related to the presence of H_2S and COS in the producer gas:

(f) To help with the development of suitable gas clean-up strategies, the presence of two key sulphur species, H_2S and COS, was considered in more detail. It was shown that information on COS levels was particularly important, as this substance is difficult to remove from the gas, and can cause downstream problems (when the producer gas is utilised e.g. in an engine).

(g) From experiments on the small quartz-tube gasifier, the molar ratio of H_2S to COS was around 10:1. The concentration of H_2S (286 ppmv) and COS (28 ppmv) generated from the RDF pellets was about three times higher than values from the wood (H_2S = 99 ppmv; COS = 10 ppmv) and straw pellets (H_2S = 123 ppmv; COS = 11 ppmv). This is not surprising, as the RDF was expected to have a higher sulphur content.

(h) Thermodynamic equilibrium calculations were also completed to predict the concentration of sulphur species in the producer gas stream. A particularly interesting set of results relate to experimental measurements on the commercial pilot-scale plant, and how these compared with thermodynamic simulations. These showed, for example, that:

- the experimentally measured values on the pilot plant were: H_2S (277 ppmv) and COS (10 ppmv), (adjusted for a wet producer gas), whereas
- the simulations indicated a value of H_2S (264 ppmv) and COS (12 ppmv), corresponding to a temperature of 800^oC, and an assumed moisture content of 16.5 vol.%.

Related to the steam gasification of wood and RDF-derived chars:

(i) It is possible to generate a valuable producer gas from chars, and there is scope to tune the gas composition to match the end application (e.g. by adjusting the ratio of steam to air in the feed). For example, for a steam input between 28 to 51 wt.% of the feed, the H_2 and CO generated from wood charcoal could reach 20 vol.% and 15 vol.%, respectively. However, when the steam input = 51 wt.%, then the H_2 concentration produced from RDF-derived char increased considerably to 20 vol.%, while CO concentration remained stable at 10 vol.% in the dry producer gas.

(j) Because the particle size of RDF-derived char is small (e.g. 305 μm in mean diameter), then it is likely that a fluidized-bed reactor would be used to gasify the char.

(k) A kinetic study of the steam gasification of RDF-derived char was completed, and the kinetic parameters were evaluated and tabulated as functions of carbon conversion. Both Shrinking-Core and Uniform-Reaction models were used to interpret the results, and both produced very similar results.

(l) For the steam gasification of RDF-derived char, at a carbon conversion from 10 to 70 % they appear to be more reactive than other biochars reported in the literature. However, at high conversion (> 50 %), its apparent reactivity decreases with carbon conversion, behaving in a similar manner to coal chars.

Related to commercial pilot-scale gasifier:

(m) Measurements of the gas produced using waste-wood as a fuel showed that the following levels can be achieved: CO = 20.5 vol.%; H_2 = 16.5 vol.% and CH_4 = 2.5 vol.% (in dry producer gas). Consequently, the highest HHV of the fuel gas produced was 5.35 MJ/Nm^3.

(n) In general, as temperatures in the gasifier increase (above and below the throat), the concentration of CO decreases (from 23 to 16 vol.%), whereas that of H_2 increases (from 10 to 15 vol.%).

(o) The molar ratio of H_2S:COS in the measurement on the plant was about 30:1, compared with 10:1 in the quartz-tube experiments. This may arise from the hydrolysis of the COS on the pilot plant as the gas is scrubbed with water and comes into contact with ash (catalytic effect). This is a very useful piece of information, as the COS levels were low (e.g. 10 ppmv).

(p) The O_2 levels in the producer gas were monitored during start-up of the gasifier, and this provides a useful indication of when a flammable atmosphere could exist in the lines and associated vessels. Over a time period of about 4 minutes, the O_2 levels drop from 19 down to 2 vol.%, as the concentration of the flammable gases increases: CO (from 5 to 21 vol.%) and H_2 (from 1 to 8 vol.%).

9.2 RECOMMENDATIONS

(a) **Upgrading the QMS method:** There is scope to improve the method further, by including more of the trace contaminant species into the methodology (e.g. NH_3, SO_2, HCl). For some of the lab-scale kinetic experiments, especially when low CO levels need to be measured, it would be better to use argon rather than nitrogen as the carrier gas.

(b) **Hydrolysis of COS on the commercial pilot-plant:** Measurements should be performed before and after the gas quench and scrubbing systems, to quantify if there is a reduction in COS levels across these units and a corresponding increase in H_2S levels.

(c) **Start-up and shut-down:** Further information should be gathered on oxygen and flammable gas levels during plant start-up and shut-down, and in the development of strategies to mitigate such problems.

(d) **Kinetics of CO_2 char gasification:** Although some preliminary experiments were performed, further work is recommended to gather such data on RDF-derived char.

(e) **RDF-derived char structure:** It would be interesting to study in more detail, both the content of AAEM species in the char and the char structure (during gasification), and their impact on the catalytic properties.

(f) **Design of a fluidized-bed gasifier for the char:** Information obtained for this thesis could be used to help with the design of a fluidized-bed char gasifier.

(g) **Tar conversion to gas & waste water treatment:** These were not considered in this thesis, but were encountered as problem areas, and should be explored in further work.

APPENDIX 1

Further Information on H_2S Removal

Further information on reactions in the 3rd scrubber discussed in Section 2.3.4.1 for the removal of H_2S (based mainly on information in Wang *et al.* (2004, pp.265-271)).

With **sodium hypochlorite**, the following reactions are likely to occur:

$$H_2S + 2NaOH \rightarrow Na_2S + 2H_2O \quad \text{(A1.1)}$$

$$NaOCl + H_2O \rightarrow HOCl + NaOH \quad \text{(A1.2)}$$

$$3HOCl + Na_2S \rightarrow Na_2SO_3 + 3HCl \quad \text{(A1.3)}$$

$$HOCl + Na_2SO_3 \rightarrow Na_2SO_4 + HCl \quad \text{(A1.4)}$$

$$HCl + NaOH \rightarrow NaCl + H_2O \quad \text{(A1.5)}$$

The overall reaction may be written as:

$$2NaOH + 4NaOCl + H_2S \rightarrow Na_2SO_4 + 4NaCl + 2H_2O \quad \text{(A1.6)}$$

If **hydrogen peroxide** is used, then:

$$4H_2O_2 + 2NaOH + H_2S \rightarrow Na_2SO_4 + 6H_2O \quad \text{(A1.7)}$$

In either case it is necessary to have an excess of the oxidizing agent.

Fagan (2009) states that the use of H_2O_2 is more advantages (than NaOCl) as H_2O_2 rapidly oxidizes H_2S and is a more cost effective alternative for facilities considering elimination of chlorine gas.

In simplified terms, if the oxidizing agent is a solution of caustic and sodium hypochlorite, then from equation (A1.6), at least 8.76 mg of NaOCl is required to oxidize 1 mg H_2S, whereas from equation (A1.7), the 4 mg of H_2O_2 is required to oxidize 1mg H_2S. As a result, less H_2O_2 is required compared to NaOCl. There are also differences in the volume requirements of each chemical. The volume of NaOCl solution needed on a daily basis is much larger than that of H_2O_2 to treat the same amount of H_2S. Obviously, larger capital outlays will be required for NaOCl storage vessels, pumping systems, piping and scrubbing systems.

H_2O_2 also has other advantages:

(a) It is considered to be more of an environmentally friendly oxidizer that produces no chlorinated by-products.

(b) As NaOCl will also react rapidly with organics, it may form undesirable chlorinated by-products, which may be toxic or refractory to biological treatment.

(c) When NaOCl reacts with low molecular weight organics, then VOCs (Volatile Organic Compounds) can be produced, posing air quality concerns, while H_2O_2 has fewer tendencies to react with organics.

(d) H_2O_2 has the benefit of adding dissolved oxygen to the waste stream, which helps to maintain aerobic conditions and inhibit H_2S regeneration.

(e) Although both H_2O_2 and NaOCl experience some decomposition during storage, H_2O_2 (50 wt.%) loses less than 1 % per year, as compared to NaOCl (12.5 wt.%) can lose 1 to 2 % per month. The chlorine gas resulting from NaOCl decomposition is scrubbed (extra cost) or vented to the atmosphere, contributing to air emissions from the process.

(f) Also, about 1 % NaOCl reacts with H_2S to form S deposits, ($H_2S + NaOCl \rightarrow S + NaCl + H_2O$), resulting in fouling problems and consuming additional chemicals.

APPENDIX 2
Events Sequence for the QMS Method

A2.1 Events Sequence for Calibrating the QMS

HIDEN ANALYTICAL

User : STK20, University of Bath
Event editor - HAL 7 RC RGA 201 #133280 : Hiden Analytical\calibration_syngas_H2S_COS.exp View:1

Events	
Trips	
f(x)1	f(x): Run EventSequence1 for each step in scan Scan 9 : CO RS 1.00 and get y value fro
f(x)2	f(x): Run gas3_factor for each step in scan Scan 10 : CO2 RS 1.00 and get y value from
f(x)3	f(x): Run gas4_factor for each step in scan Scan 11 : H2 RS 1.00 and get y value from g
f(x)4	f(x): Run gas5_factor for each step in scan Scan 12 : O2 RS 1.00 and get y value from g
f(x)5	f(x): Run gas6_factor for each step in scan Scan 13 : CH4 RS 1.00 and get y value from
f(x)6	f(x): Run gas7_factor for each step in scan Scan 14 : H2S RS 1.00 and get y value from
f(x)7	f(x): Run gas8_factor for each step in scan Scan 15 : COS RS 1.00 and get y value from
EventSequence1	Event Sequence : EventSequence1
gas1_get	Get data from Scan 1 : N2 + CO + CH4 at 14.00
gas2_get	Get data from Scan 2 : CO + N2 + CO2 at 28.00
gas3_get	Get data from Scan 3 : CO2 at 44.00
gas4_get	Get data from Scan 4 : H2 at 2.00
gas5_get	Get data from Scan 5 : O2 + H2S at 32.00
gas6_get	Get data from Scan 6 : CH4 at 15.00
gas7_get	Get data from Scan 7 : H2S + O2 at 34.00
gas8_get	Get data from Scan 8 : COS at 60.00
%gas1	**USER ENTRY** N2 concentration
%gas2	**USER ENTRY** CO concentration
%gas3	**USER ENTRY** CO2 concentration
%gas4	**USER ENTRY** H2 concentration
%gas5	**USER ENTRY** O2 concentration
%gas6	**USER ENTRY** CH4 concentration
%gas7	**USER ENTRY** H2S concentration
%gas8	** USER ENTRY** COS concentration
factor1	Evaluate : gas1_get * 100 / 5.2 : N2 at 28
factor2	Evaluate : gas3_get * 9.8 / 100 : CO2 at 28
gas2_correct	Evaluate : gas2_get - factor1 - factor2 : CO correction
factor3	Evaluate : gas2_correct * 0.52 / 100
factor4	Evaluate : gas6_get * 14.9 / 100 : CH4 at 14
gas1_correct	Evaluate : gas1_get - factor3 - factor4 : N2 correction
factor1+	Evaluate : gas1_correct * 100 / 5.2 : N2 at 28
gas2_correct+	Evaluate : gas2_get - factor1+ - factor2 : CO correction
factor3+	Evaluate : gas2_correct+ * 0.52 / 100 : CO at 14
gas1_correct+	Evaluate : gas1_get - factor3+ - factor4 : N2 correction
factor5	Evaluate : gas5_get * 0.45 / 100 : O2 at 34
gas7_correct	Evaluate : gas7_get - factor5 : H2S correction
factor6	Evaluate : gas7_correct * 39.7 / 100 : H2S at 32
gas5_correct	Evaluate : gas5_get - factor6 : O2 correction
factor5+	Evaluate : gas5_correct * 0.45 / 100 : O2 at 34
gas7_correct+	Evaluate : gas7_get - factor5+ : H2S correction
factor6+	Evaluate : gas7_correct+ * 39.7 / 100 : H2S at 32
gas5_correct+	Evaluate : gas5_get - factor6+ : O2 correction
Sum1	Evaluate : gas1_correct+ + gas2_correct+ + gas3_get + gas4_get + gas5_correct+
SumTotal	Evaluate : Sum1 + gas6_get + gas7_correct+ + gas8_get
gas1%	Evaluate : gas1_correct+ / SumTotal
gas2%	Evaluate : gas2_correct+ / SumTotal
gas3%	Evaluate : gas3_get / SumTotal
gas4%	Evaluate : gas4_get / SumTotal
gas5%	Evaluate : gas5_correct+ / SumTotal
gas6%	Evaluate : gas6_get / SumTotal
gas7%	Evaluate : gas7_correct+ / SumTotal
gas8%	Evaluate : gas8_get / SumTotal
gas1_factor	Evaluate : gas1% / %gas1 : Relative factor for calculation of other factors
gas2_factor	Evaluate : gas2% / gas1_factor / %gas2
gas3_factor	Evaluate : gas3% / gas1_factor / %gas3

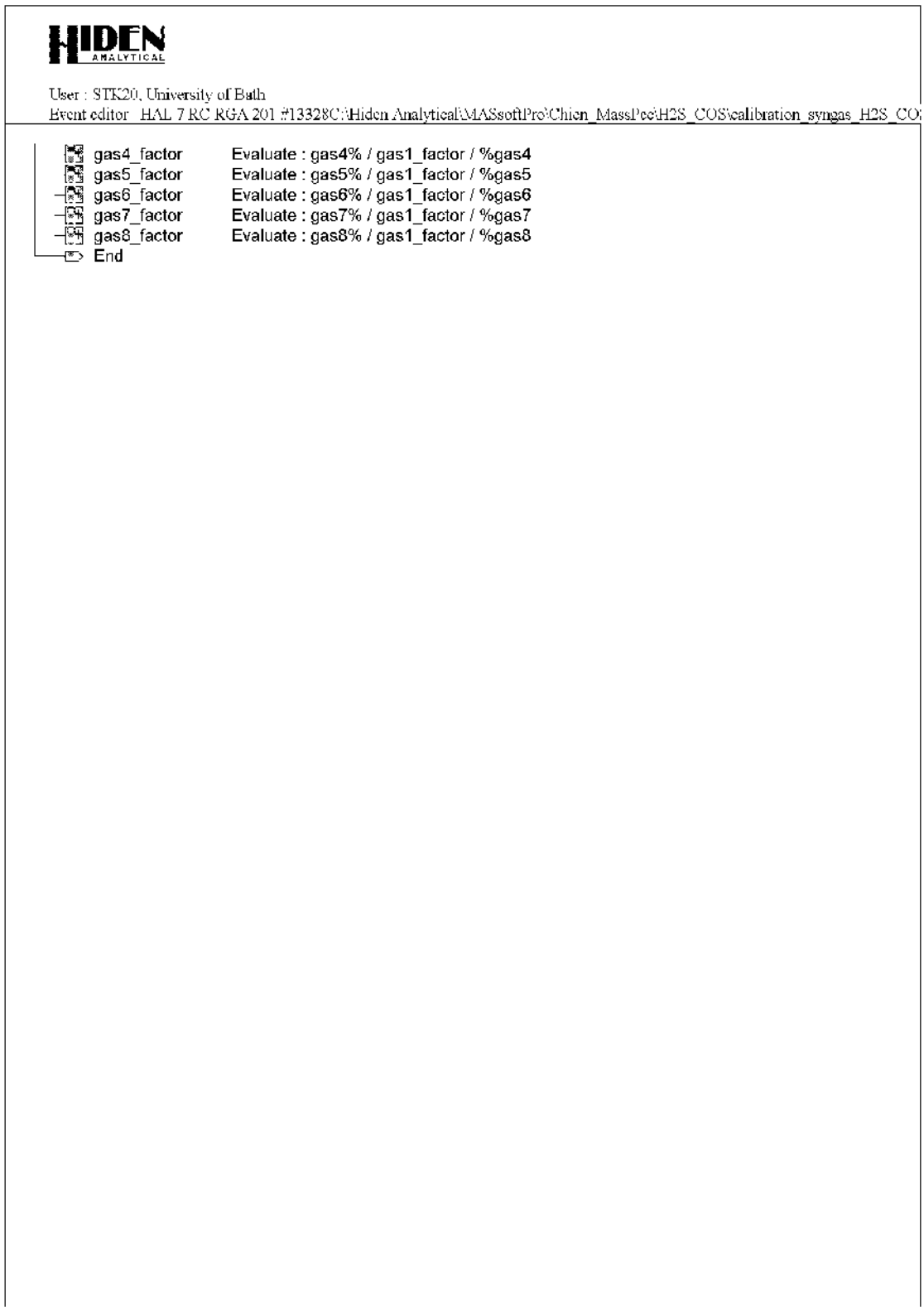
HIDEN
ANALYTICAL
User : STK20, University of Bath
Event editor HAL 7 RC RGA 201 #13328C:\Hiden Analytical\MASsoft\Pro\Chien_MassPec\H2S_COS\calibration_syngas_H2S_CO
gas4_factor Evaluate : gas4% / gas1_factor / %gas4
gas5_factor Evaluate : gas5% / gas1_factor / %gas5
gas6_factor Evaluate : gas6% / gas1_factor / %gas6
gas7_factor Evaluate : gas7% / gas1_factor / %gas7
gas8_factor Evaluate : gas8% / gas1_factor / %gas8
End

A2.2 Events Sequence for Quantifying the Composition of the Producer Gas

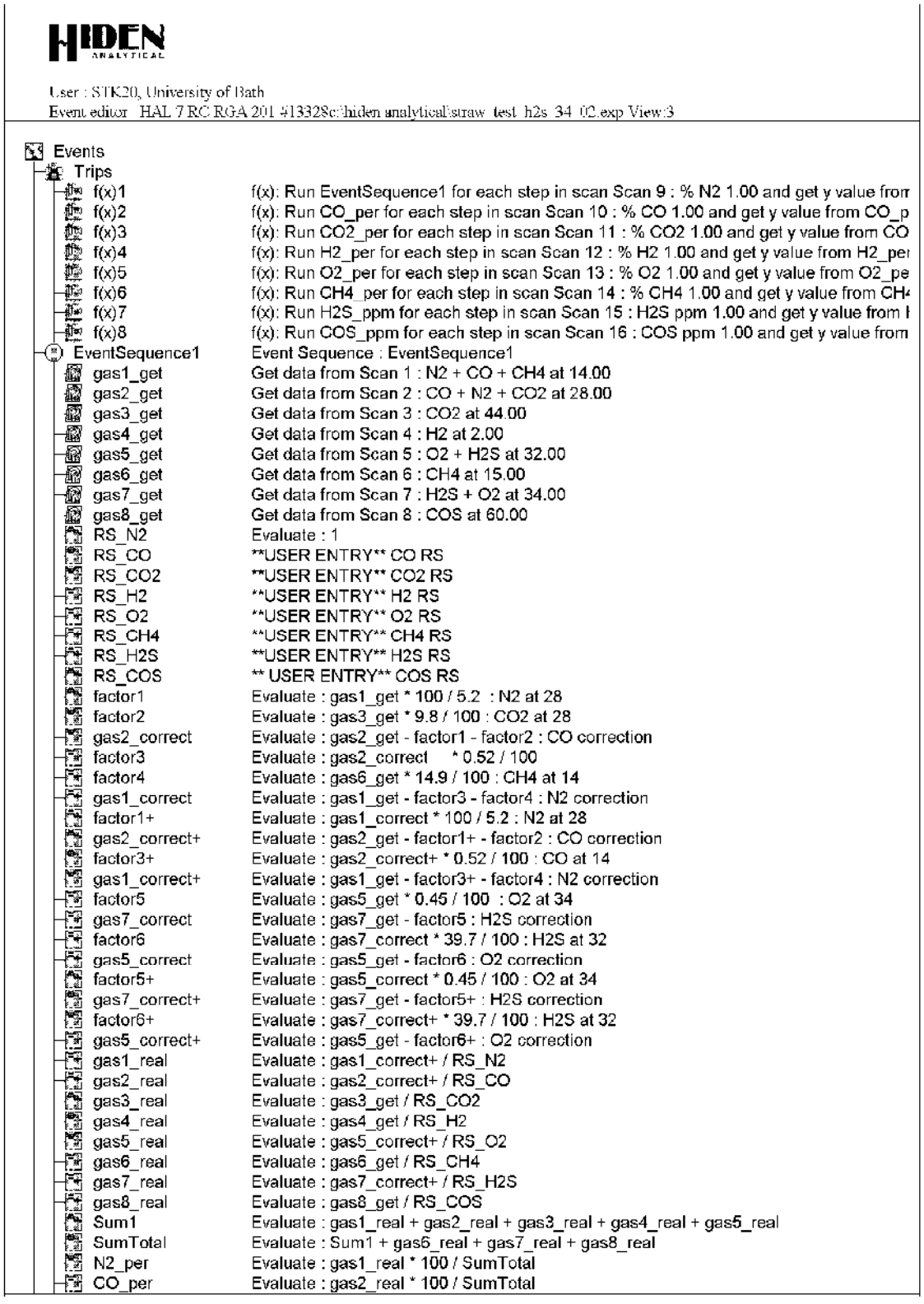

User : STK20, University of Bath
Event editor HAL 7 RC RGA 201 413328c:\hiden analytical\straw_test_h2s_34_02.exp View:3

Events	
Trips	
f(x)1	f(x): Run EventSequence1 for each step in scan Scan 9 : % N2 1.00 and get y value from
f(x)2	f(x): Run CO_per for each step in scan Scan 10 : % CO 1.00 and get y value from CO_p
f(x)3	f(x): Run CO2_per for each step in scan Scan 11 : % CO2 1.00 and get y value from CO
f(x)4	f(x): Run H2_per for each step in scan Scan 12 : % H2 1.00 and get y value from H2_per
f(x)5	f(x): Run O2_per for each step in scan Scan 13 : % O2 1.00 and get y value from O2_pe
f(x)6	f(x): Run CH4_per for each step in scan Scan 14 : % CH4 1.00 and get y value from CH4
f(x)7	f(x): Run H2S_ppm for each step in scan Scan 15 : H2S ppm 1.00 and get y value from H
f(x)8	f(x): Run COS_ppm for each step in scan Scan 16 : COS ppm 1.00 and get y value from
EventSequence1	Event Sequence : EventSequence1
gas1_get	Get data from Scan 1 : N2 + CO + CH4 at 14.00
gas2_get	Get data from Scan 2 : CO + N2 + CO2 at 28.00
gas3_get	Get data from Scan 3 : CO2 at 44.00
gas4_get	Get data from Scan 4 : H2 at 2.00
gas5_get	Get data from Scan 5 : O2 + H2S at 32.00
gas6_get	Get data from Scan 6 : CH4 at 15.00
gas7_get	Get data from Scan 7 : H2S + O2 at 34.00
gas8_get	Get data from Scan 8 : COS at 60.00
RS_N2	Evaluate : 1
RS_CO	**USER ENTRY** CO RS
RS_CO2	**USER ENTRY** CO2 RS
RS_H2	**USER ENTRY** H2 RS
RS_O2	**USER ENTRY** O2 RS
RS_CH4	**USER ENTRY** CH4 RS
RS_H2S	**USER ENTRY** H2S RS
RS_COS	** USER ENTRY** COS RS
factor1	Evaluate : gas1_get * 100 / 5.2 : N2 at 28
factor2	Evaluate : gas3_get * 9.8 / 100 : CO2 at 28
gas2_correct	Evaluate : gas2_get - factor1 - factor2 : CO correction
factor3	Evaluate : gas2_correct * 0.52 / 100
factor4	Evaluate : gas6_get * 14.9 / 100 : CH4 at 14
gas1_correct	Evaluate : gas1_get - factor3 - factor4 : N2 correction
factor1+	Evaluate : gas1_correct * 100 / 5.2 : N2 at 28
gas2_correct+	Evaluate : gas2_get - factor1+ - factor2 : CO correction
factor3+	Evaluate : gas2_correct+ * 0.52 / 100 : CO at 14
gas1_correct+	Evaluate : gas1_get - factor3+ - factor4 : N2 correction
factor5	Evaluate : gas5_get * 0.45 / 100 : O2 at 34
gas7_correct	Evaluate : gas7_get - factor5 : H2S correction
factor6	Evaluate : gas7_correct * 39.7 / 100 : H2S at 32
gas5_correct	Evaluate : gas5_get - factor6 : O2 correction
factor5+	Evaluate : gas5_correct * 0.45 / 100 : O2 at 34
gas7_correct+	Evaluate : gas7_get - factor5+ : H2S correction
factor6+	Evaluate : gas7_correct+ * 39.7 / 100 : H2S at 32
gas5_correct+	Evaluate : gas5_get - factor6+ : O2 correction
gas1_real	Evaluate : gas1_correct+ / RS_N2
gas2_real	Evaluate : gas2_correct+ / RS_CO
gas3_real	Evaluate : gas3_get / RS_CO2
gas4_real	Evaluate : gas4_get / RS_H2
gas5_real	Evaluate : gas5_correct+ / RS_O2
gas6_real	Evaluate : gas6_get / RS_CH4
gas7_real	Evaluate : gas7_correct+ / RS_H2S
gas8_real	Evaluate : gas8_get / RS_COS
Sum1	Evaluate : gas1_real + gas2_real + gas3_real + gas4_real + gas5_real
SumTotal	Evaluate : Sum1 + gas6_real + gas7_real + gas8_real
N2_per	Evaluate : gas1_real * 100 / SumTotal
CO_per	Evaluate : gas2_real * 100 / SumTotal

HIDEN ANALYTICAL

User : STK20, University of Bath
Event editor : ITAL 7 RC RGA 201 #13328c3\hiden analytical\straw_test_h2s_34_02.exp View:1

CO2_per	Evaluate : gas3_real * 100 / SumTotal
H2_per	Evaluate : gas4_real * 100 / SumTotal
O2_per	Evaluate : gas5_real * 100 / SumTotal
CH4_per	Evaluate : gas6_real * 100 / SumTotal
H2S_ppm	Evaluate : gas7_real * 1000000 / SumTotal
COS_ppm	Evaluate : gas8_real * 1000000 / SumTotal
End	

APPENDIX 3
Matlab Single Reaction Equilibrium Model

```
% Calculation of equilibrium at diff. temperatures
% Caculation for only one reaction: H2+COS-->CO+H2S
% initial number of mole NT0 = 100
% Rely on Robert and et al. book
function H2S_COS_equi
clear all
clc
global NT0 K1 delA1 delB1 delC1 delD1

% define constants
NT0=100; % the initial mole of H2O
R=8.314;
%delta A, B, C, D at Cp equations
delA1=1.4554; delB1=-12.0914e-3; delC1=1.6489e-5; delD1=-0.6814e-8;

%standard heat and Gibbs-engery change of reactions at 298.15 K
delHo=10770; %heat of reactions at 298.15 K, J/mol
delGo=-1529; %the changes of Gibbs engeries of reactions at 298.15 K,
J/mol

% calculation of the changes of Gibbs energies of each reaction
%set initial temperatures point
TvectorC=300; % temperature, oC
TvectorK=TvectorC+273.15;  % changing unit from oC to K
delG1=delHo-(TvectorK/298.15)*(delHo-
delGo)+R*(quad(@Cp1,298.15,TvectorK))-
R*TvectorK*(quad(@Cpp1,298.15,TvectorK));

% calculation of equilibrium constants
K1=exp(-delG1/(R*TvectorK));
%loop to calculate K at diff. temp.
K1_vector=K1; %creat Ki_vector to store K values
T_vector=TvectorC; %store temperature vector
h=25; % step size
step=1; %count the number of steps
while TvectorC < 1200
    TvectorC=TvectorC+h; % increase temperature by step h
    TvectorK=TvectorC+273.15;  % changing unit from oC to K
    delG1=delHo-(TvectorK/298.15)*(delHo-
delGo)+R*(quad(@Cp1,298.15,TvectorK))-
R*TvectorK*(quad(@Cpp1,298.15,TvectorK));
    %calculation of equilibrium constants
    K1=exp(-delG1/(R*TvectorK));
    %store Ki into Ki_vector
    K1_vector=[K1_vector,K1];
    T_vector=[T_vector,TvectorC];
    step=step+1; %increase the number of steps
end %end the while loop

% Finding ei values
% Initial guess and set tolerance
```

```
%set initial conditions
% the loop to calculate compositions of species at equilibrium
K1=K1_vector(1); %take Ki values at 300 oC
%call fsolve
e = fsolve(@myfun,0.001);
ff = feval(@myfun, e);
errr=abs(ff);
err=sqrt(sum(errr));
y_H2S=((0.044+e)/NT0)*1000000; %mole fraction
y_COS=((0.0026-e)/NT0)*1000000;
%e_vector=e;  %store e values
%err_vector=err;  %store error values
y_H2S_vector=y_H2S;%store mole fraction values
y_COS_vector=y_COS;
%Show results of e values
disp('temperature')
disp(T_vector(1))
disp('error')
disp(err)
disp(e);
for i=2:step
K1=K1_vector(i); %take Ki values at each temperature point
%call fsolve
e = fsolve(@myfun,0.001);
ff = feval(@myfun, e);
errr=abs(ff);
err=sqrt(sum(errr));
y_H2S=((0.044+e)/NT0)*1000000; %mole fraction
y_COS=((0.0026-e)/NT0)*1000000;
%e_vector=e;  %store e values
%err_vector=err;  %store error values
y_H2S_vector=[y_H2S_vector,y_H2S];%store mole fraction values
y_COS_vector=[y_COS_vector,y_COS];
%Show results of e values
disp('temperature')
disp(T_vector(i))
disp('error')
disp(err)
disp(e);
end %end the for loop
% Show the results
for i=1:step
disp('Equilibirum constant at temperature')
disp(T_vector(i))
disp(K1_vector(i))
disp('Concentration of H2S and COS, respectively')
disp(y_H2S_vector(i))
disp(y_COS_vector(i))
end %end the for loop for showing results

%Graph of equilibrium concentration of H2S versus temperature
figure1 = figure('Name',...
    'Equilibrium concentration of H2S as a function of temperature');

% Create axes
axes1 = axes('Parent',figure1);
box(axes1,'on');
hold(axes1,'all');

% Create plot
```

```
plot(T_vector,y_H2S_vector,'Parent',axes1,'Color',[0 0.5
0],'DisplayName','H2S');

% Create xlabel
xlabel('Temperature, oC');

% Create ylabel
ylabel('mole fraction, ppm');

% Create title
title('Equilibrium concentration of H2S as a function of temperature');


% Graph of equilibrium concentration of COS versus temperature
figure2 = figure('Name',...
    'Equilibrium concentration of COS as a function of temperature');

% Create axes
axes2 = axes('Parent',figure2);
box(axes2,'on');
hold(axes2,'all');

% Create plot
plot(T_vector,y_COS_vector,'Parent',axes2,'Color',[0 0
1],'DisplayName','COS');

% Create xlabel
xlabel('Temperature, oC');

% Create ylabel
ylabel('mole fraction, ppm');

% Create title
title('Equilibrium concentration of COS as a function of temperature');


% Calculation of changes of heat capacity of reactions (deltaCp/R)
function f=Cp1(T)
global delA1 delB1 delC1 delD1
f=(delA1+delB1*T+delC1*T.^2+delD1*T.^3); %J/mol

% function deltaCp/R.T
function f=Cpp1(T)
global delA1 delB1 delC1 delD1
f=(delA1+delB1*T+delC1*T.^2+delD1*T.^3)./T; %J/mol


% equilibrium conversion equations
function f = myfun(x)
global NT0 K1
% x are the concentrations of the seven species. x(1) is the
concentration of species a,
% x(2) is the concentration of b etc.
f(1)= (15.5+x)*(0.044+x)-K1*(14.1-x)*(0.0026-x);
```

APPENDIX 4
Rate Expressions for Steam Gasification of RDF-derived Char

A4.1 Shrinking-Core Model

Rate expression:

$$r = \frac{1}{(1-X)^{2/3}} \cdot \left(A.e^{\left(-\frac{E}{R_g T}\right)} \right) . P_{H2O}^{n} \qquad \text{(A4-1)}$$

where:

The reaction order is a function of carbon conversion (X) at different reaction temperature:

$$n = -1.753\times10^{-7} X^4 + 3.17\times10^{-5} X^3 - 1.448\times10^{-3} X^2 + 1.893\times10^{-2} X + 1.387 \quad \text{at } 900\ ^{o}\text{C} \qquad \text{(A4-2)}$$

$$n = 3.153\times10^{-10} X^6 - 9.069\times10^{-8} X^5 + 9.568\times10^{-6} X^4 - 4.59\times10^{-4} X^3 + 1.004\times10^{-2} X^2 - 6.835\times10^{-2} X + 1.064 \quad \text{at } 850\ ^{o}\text{C} \qquad \text{(A4-3)}$$

$$n = 4.369\times10^{-10} X^6 - 1.139\times10^{-7} X^5 + 1.11\times10^{-5} X^4 - 4.907\times10^{-4} X^3 + 9.563\times10^{-3} X^2 - 5.302\times10^{-2} X + 0.856 \quad \text{at } 800\ ^{o}\text{C} \qquad \text{(A4-4)}$$

Pre-exponential factor: $A = e^{f_{2s}(X)}$, where:

$$f_{2s}(X) = -4.007\times10^{-10} X^6 + 2.556\times10^{-7} X^5 - 4.084\times10^{-5} X^4 + 2.743\times10^{-3} X^3 - 8.535\times10^{-2} X^2 + 1.169X + 4.18 \qquad \text{(A4-5)}$$

Finally, activation energy is calculated from:

$$E = 2.056\times10^{-9} X^6 + 8.019\times10^{-7} X^5 - 2.074\times10^{-4} X^4 + 1.595\times10^{-2} X^3 - 0.518X^2 + 7.07X + 66.314 \qquad \text{(A4-6)}$$

A4.2 Uniform-Reaction Model

Rate expression:

$$r = \frac{1}{(1-X)} \cdot \left(A.e^{\left(-\frac{E}{R_g T}\right)} \right) . P_{H2O}^{n} \qquad \text{(A4-7)}$$

where:

The reaction order is a function of carbon conversion at different temperature:

$$n = -1.753\times10^{-7} X^4 + 3.17\times10^{-5} X^3 - 1.448\times10^{-3} X^2 + 1.893\times10^{-2} X + 1.387 \quad \text{at } 900\ ^{o}\text{C} \qquad \text{(A4-8)}$$

$$n = 3.153\times10^{-10} X^6 - 9.069\times10^{-8} X^5 + 9.568\times10^{-6} X^4 - 4.59\times10^{-4} X^3 + 1.004\times10^{-2} X^2 - 6.835\times10^{-2} X + 1.064 \quad \text{at } 850\ ^{o}\text{C} \qquad \text{(A4-9)}$$

$$n = 4.369\times10^{-10} X^6 - 1.139\times10^{-7} X^5 + 1.11\times10^{-5} X^4 - 4.907\times10^{-4} X^3 + 9.563\times10^{-3} X^2 - 5.302\times10^{-2} X + 0.856 \quad \text{at } 800\ ^{o}\text{C} \qquad \text{(A4-10)}$$

Pre-exponential factor: $A = e^{f_{2s}(X)}$, where:

$$f_{2s}(X) = -4.035\times10^{-10} X^6 + 2.563\times10^{-7} X^5 - 4.09\times10^{-5} X^4 + 2.745\times10^{-3} X^3 - 8.537\times10^{-2} X^2 + 1.173X + 4.18 \qquad \text{(A4-11)}$$

Finally, activation energy is calculated from:

$$E = 2.001\times10^{-9} X^6 + 8.134\times10^{-7} X^5 - 2.083\times10^{-4} X^4 + 1.598\times10^{-2} X^3 - 0.518X^2 + 7.074X + 66.309 \qquad \text{(A4-12)}$$

APPENDIX 5

Test Run 1 – on the Refgas Pilot-plant

Snap-shots in time are presented in Tables A5-1 to A5-6, which correspond to the conditions described in Section 8.5.1, and in Figure 8.8.

Calculated parameters are also presented in Table A5-7.

Table A5-1 Test Run 1: Snap Shot 1 at 00:08:52.

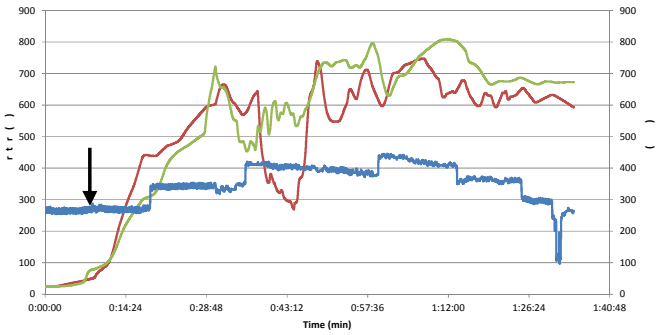

Producer gas			
		Temperature (°C)	Pressure (mbar)
Gasifier	Out	168 and 151 see note *(1)*	-
Cyclones	In		-
	Out	58	-
Quench	In		-
	Out	20	- 16
HESS	In		
	Out	15	-
Heat Exchanger	In		-
	Out	15	- 27
Blower	In		
	Out	-	-
Filters	In		
	Out	20	35
Syngas Tank			
Flare		18	
Flow into Flare (m^3/h) : 101 (recorded value) 276 (corrected value)			

Gas Composition (vol.%)	
N_2	70.85
CO	6.17
CO_2	7.2
H_2	2.08
O_2	12.78
CH_4	0.82
H_2S	606 (ppmv)
COS	1.82 (ppmv)

Gasifier	
Top	-12 (mbar) 67 (°C)
Throat Top	54
Throat Bottom	80
Bottom	-

Air	
Into cyclones	22 (°C) *(2)*
Out cyclones	20 (°C) *(2)*
Into gasifier	90 (m^3/h) *(3)*

Water	
Into quench	14 (°C) *(2)*
Out quench	18 (°C) *(4)*
Into HESS	24 (°C)
Out HESS	12 (°C) *(2)*
Tank	15 (°C)

Chiller	
Fluid Out	9 (°C) *(4)*
Fluid In	12 (°C) *(2)*

Blower	
Speed	20 (%)

1. The producer gas leaves the base of the gasifier via two separate pipes (at 180º from each other), so two gas temperatures are reported (one for each pipe).
2. These values was read from in-line gauges
3. Air passing through the outer jacket of the cyclones and then into the gasifier, is measured at NTP. Air entering via the central shaft in the gasifier was not measured.
4. Values were measured using a hand held temperature probe.

Table A5-2 Test Run 1: Snap Shot 2 at 00:17:58.

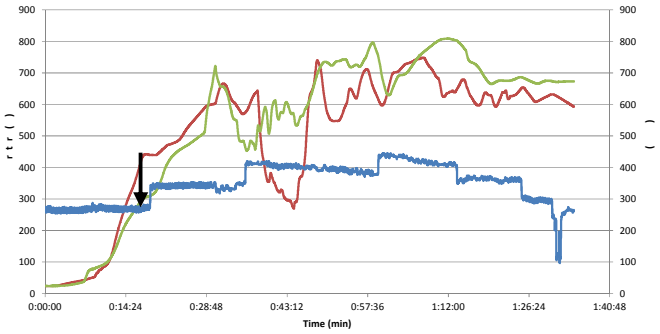

Producer gas			
		Temperature (°C)	Pressure (mbar)
Gasifier	Out	277 and 271 see note *(1)*	-
Cyclones	In		-
	Out	176	-
Quench	In		-
	Out	59	- 14
HESS	In		
	Out	19	-
Heat Exchanger	In		-
	Out	14	- 29
Blower	In		
	Out	-	-
Filters	In		
	Out	20	35
Syngas Tank			
Flare		515	
Flow into Flare (m^3/h): 98 (recorded value) 272 (corrected value)			

Gas Composition (vol.%)	
N_2	56.13
CO	17.86
CO_2	13.73
H_2	7.74
O_2	2.15
CH_4	2.25
H_2S	1013 (ppmv)
COS	11.9 (ppmv)

Gasifier	
Top	-8 (mbar) 71 (°C)
Throat Top	442
Throat Bottom	306
Bottom	-

Air	
Into cyclones	24 (°C) *(2)*
Out cyclones	35 (°C) *(2)*
Into gasifier	79 (m^3/h) *(3)*

Water	
Into quench	14 (°C) *(2)*
Out quench	38 (°C) *(4)*
Into HESS	18 (°C)
Out HESS	21 (°C) *(2)*
Tank	16 (°C)

Chiller	
Fluid Out	9 (°C) *(4)*
Fluid In	12 (°C) *(2)*

Blower	
Speed	20 (%)

1. The producer gas leaves the base of the gasifier via two separate pipes (at 180º from each other), so two gas temperatures are reported (one for each pipe).
2. These values was read from in-line gauges
3. Air passing through the outer jacket of the cyclones and then into the gasifier, is measured at NTP. Air entering via the central shaft in the gasifier was not measured.
4. Values were measured using a hand held temperature probe.

Table A5-3 Test Run 1: Snap Shot 3 at 00:27:02.

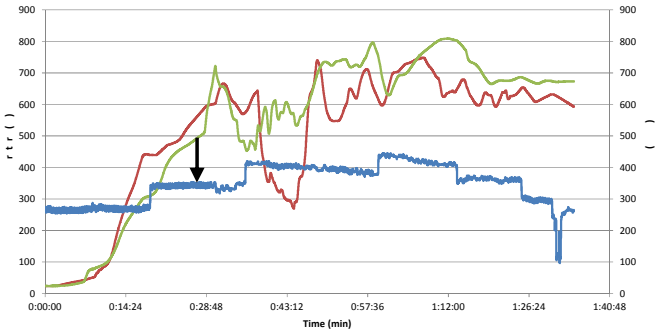

Producer gas			
		Temperature (°C)	Pressure (mbar)
Gasifier	Out	429 and 332	-
Cyclones	In	see note *(1)*	-
	Out	262	-
Quench	In		-
	Out	63	- 14
HESS	In		
	Out	24	-
Heat Exchanger	In		-
	Out	14	- 46
Blower	In		
	Out	-	-
Filters	In		
	Out	19	50
Syngas Tank			
Flare		629	
Flow into Flare (m^3/h): 151 (recorded value) 344 (corrected value)			

Gas Composition (vol.%)	
N_2	53.54
CO	20.14
CO_2	13.08
H_2	10.33
O_2	0.85
CH_4	1.96
H_2S	685 (ppmv)
COS	12.4 (ppmv)

Gasifier	
Top	-8 (mbar) 77 (°C)
Throat Top	560
Throat Bottom	492
Bottom	-

Air	
Into cyclones	26 (°C) *(2)*
Out cyclones	70 (°C) *(2)*
Into gasifier	73 (m^3/h) *(3)*

Water	
Into quench	14 (°C) *(2)*
Out quench	44 (°C) *(4)*
Into HESS	12 (°C)
Out HESS	27 (°C) *(2)*
Tank	15 (°C)

Chiller	
Fluid Out	10 (°C) *(4)*
Fluid In	12 (°C) *(2)*

Blower	
Speed	25 (%)

1. The producer gas leaves the base of the gasifier via two separate pipes (at 180º from each other), so two gas temperatures are reported (one for each pipe).
2. These values was read from in-line gauges
3. Air passing through the outer jacket of the cyclones and then into the gasifier, is measured at NTP. Air entering via the central shaft in the gasifier was not measured.
4. Values were measured using a hand held temperature probe.

Table A5-4 Test Run 1: Snap Shot 4 at 00:51:48.

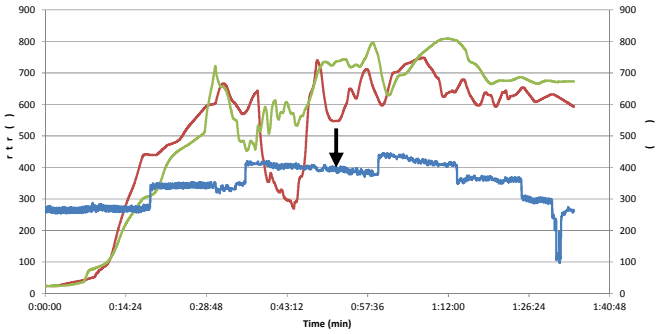

Producer gas			
		Temperature (°C)	Pressure (mbar)
Gasifier	Out	497 and 515	-
Cyclones	In	see note *(1)*	-
	Out	329	-
Quench	In		-
	Out	75	- 33
HESS	In		
	Out	38	-
Heat Exchanger	In		-
	Out	20	- 79
Blower	In		
	Out	-	-
Filters	In		
	Out	20	64
Syngas Tank			
Flare		643	
Flow into Flare (m^3/h): 193 (recorded value) 395 (corrected value)			

Gas Composition (vol.%)	
N_2	52.68
CO	18.12
CO_2	15.36
H_2	11.06
O_2	0.09
CH_4	2.61
H_2S	612 (ppmv)
COS	11.6 (ppmv)

Gasifier	
Top	-11 (mbar) 208 (°C)
Throat Top	548
Throat Bottom	733
Bottom	-

Air	
Into cyclones	30 (°C) *(2)*
Out cyclones	120 (°C) *(2)*
Into gasifier	81 (m^3/h) *(3)*

Water	
Into quench	16 (°C) *(2)*
Out quench	48 (°C) *(4)*
Into HESS	1 (°C)
Out HESS	37 (°C) *(2)*
Tank	16 (°C)

Chiller	
Fluid Out	16 (°C) *(4)*
Fluid In	18 (°C) *(2)*

Blower	
Speed	30 (%)

1. The producer gas leaves the base of the gasifier via two separate pipes (at 180º from each other), so two gas temperatures are reported (one for each pipe).
2. These values was read from in-line gauges
3. Air passing through the outer jacket of the cyclones and then into the gasifier, is measured at NTP. Air entering via the central shaft in the gasifier was not measured.
4. Values were measured using a hand held temperature probe.

Table A5-5 Test Run 1: Snap Shot 5 at 01:10:53.

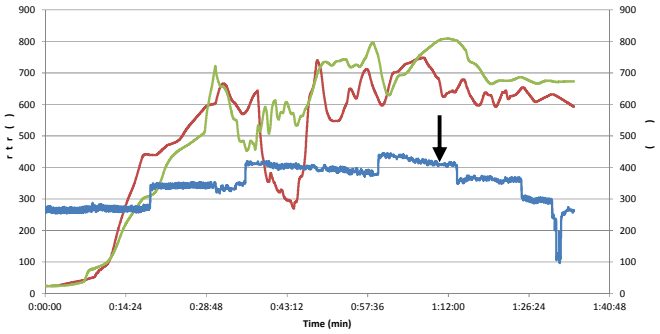

Producer gas			
		Temperature (°C)	Pressure (mbar)
Gasifier	Out	534 and 468	-
Cyclones	In	see note *(1)*	-
	Out	373	-
Quench	In		-
	Out	74	- 75
HESS	In		
	Out	37	-
Heat Exchanger	In		-
	Out	23	- 114
Blower	In		
	Out	-	-
Filters	In		
	Out	24	72
Syngas Tank			
Flare		625	
Flow into Flare (m^3/h): 205 (recorded value) 409 (corrected value)			

Gasifier	
Top	-13 (mbar) 163 (°C)
Throat Top	628
Throat Bottom	807
Bottom	-

Air	
Into cyclones	34 (°C) *(2)*
Out cyclones	155 (°C) *(2)*
Into gasifier	96 (m^3/h) *(3)*

Water	
Into quench	18 (°C) *(2)*
Out quench	47 (°C) *(4)*
Into HESS	7 (°C)
Out HESS	35 (°C) *(2)*
Tank	16 (°C)

Gas Composition (vol.%)	
N_2	48.98
CO	17.45
CO_2	15.1
H_2	16.33
O_2	0.09
CH_4	1.97
H_2S	446 (ppmv)
COS	9 (ppmv)

Chiller	
Fluid Out	20 (°C) *(4)*
Fluid In	20 (°C) *(2)*

Blower	
Speed	35 (%)

1. The producer gas leaves the base of the gasifier via two separate pipes (at 180º from each other), so two gas temperatures are reported (one for each pipe).
2. These values was read from in-line gauges
3. Air passing through the outer jacket of the cyclones and then into the gasifier, is measured at NTP. Air entering via the central shaft in the gasifier was not measured.
4. Values were measured using a hand held temperature probe.

Table A5-6 Test Run 1: Snap Shot 6 at 01:23:59.

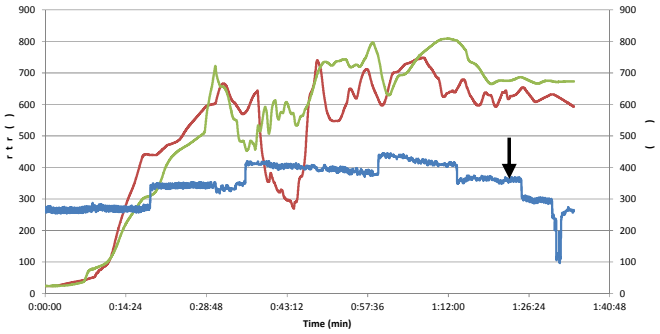

Producer gas			
		Temperature (°C)	Pressure (mbar)
Gasifier	Out	519 and 473	-
Cyclones	In	see note *(1)*	-
	Out	372	-
Quench	In		-
	Out	75	- 45
HESS	In		
	Out	37	-
Heat Exchanger	In		-
	Out	23	- 89
Blower	In		
	Out	-	-
Filters	In		
	Out	26	62
Syngas Tank			
Flare		625	
Flow into Flare (m^3/h): 166 (recorded value) 363 (corrected value)			

Gasifier	
Top	-11 (mbar) 140 (°C)
Throat Top	621
Throat Bottom	733
Bottom	-

Air	
Into cyclones	38 (°C) *(2)*
Out cyclones	170 (°C) *(2)*
Into gasifier	84 (m^3/h) *(3)*

Water	
Into quench	19 (°C) *(2)*
Out quench	46 (°C) *(4)*
Into HESS	9 (°C)
Out HESS	35 (°C) *(2)*
Tank	16 (°C)

Gas Composition (vol.%)	
N_2	50.45
CO	20.29
CO_2	13.13
H_2	13.73
O_2	0.07
CH_4	2.25
H_2S	485 (ppmv)
COS	11.2 (ppmv)

Chiller	
Fluid Out	20 (°C) *(4)*
Fluid In	20 (°C) *(2)*

Blower	
Speed	30 (%)

1. The producer gas leaves the base of the gasifier via two separate pipes (at 180º from each other), so two gas temperatures are reported (one for each pipe).
2. These values was read from in-line gauges
3. Air passing through the outer jacket of the cyclones and then into the gasifier, is measured at NTP. Air entering via the central shaft in the gasifier was not measured.
4. Values were measured using a hand held temperature probe.

Table A5-7 **Test Run 1**: Calculated parameters corresponding to snap-shots in time.

Test Run 1 - on Tuesday 11 October 2011						
Time	00:08:52	00:17:58	00:27:02	00:51:48	01:10:53	01:23:59
Blower Speed (%)	20	20	25	30	35	30
Air inlet flow (kg/h)	297	232	280	316	300	272
Char removal rate (kg/h)	19.44	19.44	19.44	19.44	19.44	19.44
Producer gas flow (kg/h)	333	317	390	448	435	388
Waste-wood feed rate (kg/h)	83	141	174	197	193	180
HHV (MJ/Nm^3)	1.39	4.16	4.66	4.75	5.08	5.22
LHV (MJ/Nm^3)	1.31	3.92	4.38	4.43	4.68	4.86
Heat flow (kW)	108	320	454	530	579	525
Equivalence ratio *1)*	0.49	0.31	0.31	0.31	0.29	0.28
Equivalence ratio *2)*	0.50	0.23	0.23	0.23	0.22	0.21
Throat Top, ^oC	54	442	560	548	628	621
Throat Bottom, ^oC	80	306	492	733	807	733

1) Equivalence ratio was estimated by calculating total air required for complete combustion of producer gas and char received.
2) Equivalence ratio was estimated by assuming the composition of the waste-wood fed into the gasifier.

APPENDIX 6

Test Run 3 – on the Refgas Pilot-plant

Snap-shots in time are presented in Tables A6-1 to A6-5, which correspond to the conditions described in Section 8.5.3, and in Figure 8.10.

Calculated parameters are also presented in Table A6-6.

Table A6-1 Test Run 3: Snap Shot 1 at 00:02:46.

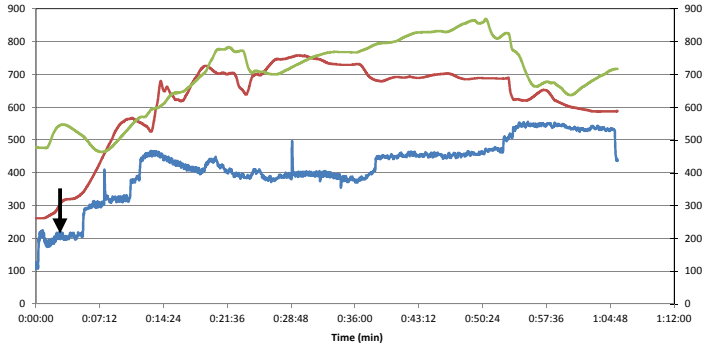

Producer gas			
		Temperature (°C)	Pressure (mbar)
Gasifier	Out	216 and 296	-
Cyclones	In	see note *(1)*	-
	Out	81	-
Quench	In		-
	Out	33	- 15
HESS	In		
	Out	14	-
Heat Exchanger	In		-
	Out	12	- 23
Blower	In		
	Out	-	-
Filters	In		
	Out	19	70
Syngas Tank			
Flare		118	
Flow into Flare (m^3/h): 55 (recorded value) 207 (corrected value)			

Gas Composition (vol.%)	
N_2	65.84
CO	9.71
CO_2	10.72
H_2	6.42
O_2	6.27
CH_4	1.0
H_2S	227 (ppmv)
COS	2.2 (ppmv)

Gasifier	
Top	-5 (mbar) 130 (°C)
Throat Top	305
Throat Bottom	545
Bottom	-

Air	
Into cyclones	22 (°C) *(2)*
Out cyclones	50 (°C) *(2)*
Into gasifier	40 (m^3/h) *(3)*

Water	
Into quench	24 (°C) *(2)*
Out quench	32 (°C) *(4)*
Into HESS	25 (°C)
Out HESS	30 (°C) *(2)*
Tank	32 (°C)

Chiller	
Fluid Out	8 (°C) *(4)*
Fluid In	10 (°C) *(2)*

Blower	
Speed	20 (%)

1. The producer gas leaves the base of the gasifier via two separate pipes (at 180º from each other), so two gas temperatures are reported (one for each pipe).
2. These values was read from in-line gauges
3. Air passing through the outer jacket of the cyclones and then into the gasifier, is measured at NTP. Air entering via the central shaft in the gasifier was not measured.
4. Values were measured using a hand held temperature probe.

Table A6-2 Test Run 3: Snap Shot 2 at 00:10:05.

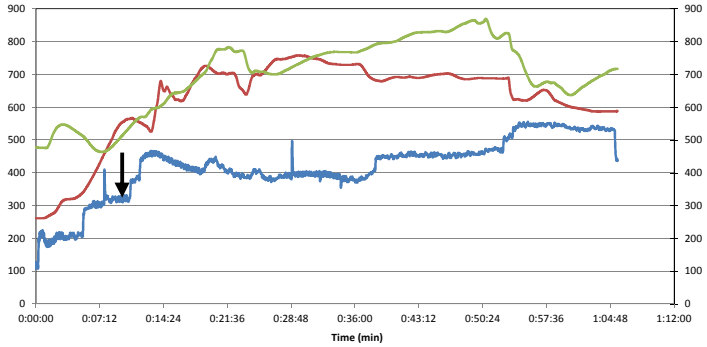

Producer gas			
		Temperature (°C)	Pressure (mbar)
Gasifier	Out	336 and 427 see note *(1)*	-
Cyclones	In		-
	Out	166	-
Quench	In		-
	Out	54	- 42
HESS	In		
	Out	15	-
Heat Exchanger	In		-
	Out	12	- 66
Blower	In		
	Out	-	-
Filters	In		
	Out	19	81
Syngas Tank			
Flare		613	
Flow into Flare (m^3/h): 128 (recorded value) 314 (corrected value)			

Gas Composition (vol.%)	
N_2	50.73
CO	20.41
CO_2	13.07
H_2	13.04
O_2	0.11
CH_4	2.58
H_2S	304(ppmv)
COS	8.2 (ppmv)

Gasifier	
Top	-9 (mbar) 167 (°C)
Throat Top	561
Throat Bottom	524
Bottom	-

Air	
Into cyclones	48 (°C) *(2)*
Out cyclones	50 (°C) *(2)*
Into gasifier	67 (m^3/h) *(3)*

Water	
Into quench	25 (°C) *(2)*
Out quench	39 (°C) *(4)*
Into HESS	20 (°C)
Out HESS	15 (°C) *(2)*
Tank	32 (°C)

Chiller	
Fluid Out	9 (°C) *(4)*
Fluid In	10 (°C) *(2)*

Blower	
Speed	30 (%)

1. The producer gas leaves the base of the gasifier via two separate pipes (at 180º from each other), so two gas temperatures are reported (one for each pipe).
2. These values was read from in-line gauges
3. Air passing through the outer jacket of the cyclones and then into the gasifier, is measured at NTP. Air entering via the central shaft in the gasifier was not measured.
4. Values were measured using a hand held temperature probe.

Table A6-3 Test Run 3: Snap Shot 3 at 00:33:25.

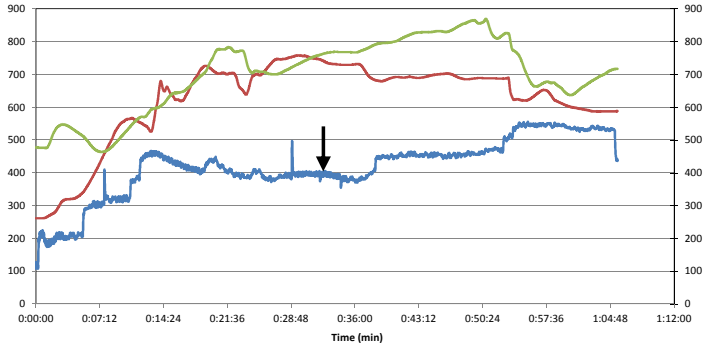

Producer gas			
		Temperature (°C)	Pressure (mbar)
Gasifier	Out	484 and 534 see note *(1)*	-
Cyclones	In		-
	Out	369	-
Quench	In		-
	Out	62	- 119
HESS	In		
	Out	27	-
Heat Exchanger	In		-
	Out	16	- 159
Blower	In		
	Out	-	-
Filters	In		
	Out	22	82
Syngas Tank			
Flare		612	
Flow into Flare (m^3/h): 190 (recorded value) 392 (corrected value)			

Gasifier	
Top	-8 (mbar) 154 (°C)
Throat Top	732
Throat Bottom	768
Bottom	-

Air	
Into cyclones	48 (°C) *(2)*
Out cyclones	125 (°C) *(2)*
Into gasifier	77 (m^3/h) *(3)*

Water	
Into quench	26 (°C) *(2)*
Out quench	39 (°C) *(4)*
Into HESS	10 (°C)
Out HESS	25 (°C) *(2)*
Tank	31 (°C)

Gas Composition (vol.%)	
N_2	49.25
CO	19.27
CO_2	13.16
H_2	16.2
O_2	0.24
CH_4	1.83
H_2S	199(ppmv)
COS	7.3 (ppmv)

Chiller	
Fluid Out	12 (°C) *(4)*
Fluid In	14 (°C) *(2)*

Blower	
Speed	40 (%)

1. The producer gas leaves the base of the gasifier via two separate pipes (at 180º from each other), so two gas temperatures are reported (one for each pipe).
2. These values was read from in-line gauges
3. Air passing through the outer jacket of the cyclones and then into the gasifier, is measured at NTP. Air entering via the central shaft in the gasifier was not measured.
4. Values were measured using a hand held temperature probe.

Table A6-4 Test Run 3: Snap Shot 4 at 00:47:40.

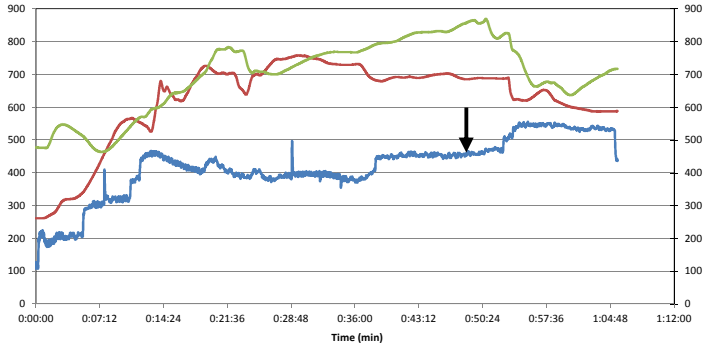

Producer gas			
		Temperature (°C)	Pressure (mbar)
Gasifier	Out	538 and 583	-
Cyclones	In	see note *(1)*	-
	Out	425	-
Quench	In		-
	Out	66	- 90
HESS	In		
	Out	29	-
Heat Exchanger	In		-
	Out	18	- 141
Blower	In		
	Out	-	-
Filters	In		
	Out	24	136
Syngas Tank			
Flare		616	
Flow into Flare (m^3/h): 250 (recorded value) 456 (corrected value)			

Gasifier	
Top	-10 (mbar) 155 (°C)
Throat Top	690
Throat Bottom	847
Bottom	-

Air	
Into cyclones	46 (°C) *(2)*
Out cyclones	155 (°C) *(2)*
Into gasifier	80 (m^3/h) *(3)*

Water	
Into quench	26 (°C) *(2)*
Out quench	39 (°C) *(4)*
Into HESS	9 (°C)
Out HESS	26 (°C) *(2)*
Tank	31 (°C)

Gas Composition (vol.%)	
N_2	48.43
CO	20.38
CO_2	12.31
H_2	17.11
O_2	0.22
CH_4	1.49
H_2S	189(ppmv)
COS	6.2 (ppmv)

Chiller	
Fluid Out	14 (°C) *(4)*
Fluid In	15 (°C) *(2)*

Blower	
Speed	45 (%)

1. The producer gas leaves the base of the gasifier via two separate pipes (at 180º from each other), so two gas temperatures are reported (one for each pipe).
2. These values was read from in-line gauges
3. Air passing through the outer jacket of the cyclones and then into the gasifier, is measured at NTP. Air entering via the central shaft in the gasifier was not measured.
4. Values were measured using a hand held temperature probe.

Table A6-5 Test Run 3: Snap Shot 5 at 00:57:31.

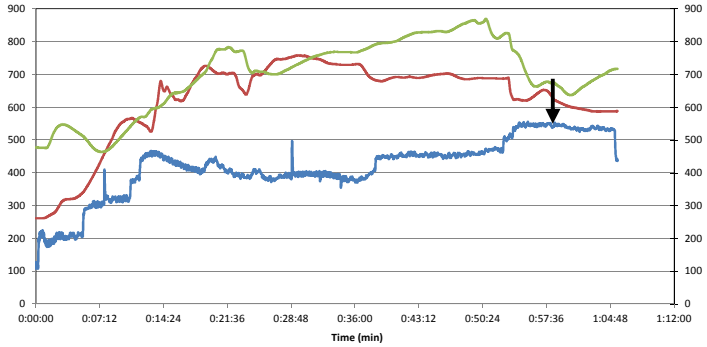

Producer gas			
		Temperature (°C)	Pressure (mbar)
Gasifier	Out	534 and 544 see note *(1)*	-
Cyclones	In		-
	Out	483	-
Quench	In		-
	Out	76	- 34
HESS	In		
	Out	46	-
Heat Exchanger	In		-
	Out	21	- 155
Blower	In		
	Out	-	-
Filters	In		
	Out	26	159
Syngas Tank			
Flare		641	
Flow into Flare (m^3/h): 360 (recorded value) 547 (corrected value)			

Gas Composition (vol.%)	
N_2	54.74
CO	16.74
CO_2	16.0
H_2	9.16
O_2	0.17
CH_4	3.08
H_2S	725(ppmv)
COS	19.3 (ppmv)

Gasifier	
Top	-19 (mbar) 270 (°C)
Throat Top	651
Throat Bottom	677
Bottom	-

Air	
Into cyclones	50 (°C) *(2)*
Out cyclones	185 (°C) *(2)*
Into gasifier	98 (m^3/h) *(3)*

Water	
Into quench	28 (°C) *(2)*
Out quench	41 (°C) *(4)*
Into HESS	- 4 (°C)
Out HESS	44 (°C) *(2)*
Tank	30 (°C)

Chiller	
Fluid Out	18 (°C) *(4)*
Fluid In	20 (°C) *(2)*

Blower	
Speed	50 (%)

1. The producer gas leaves the base of the gasifier via two separate pipes (at 180º from each other), so two gas temperatures are reported (one for each pipe).
2. These values was read from in-line gauges
3. Air passing through the outer jacket of the cyclones and then into the gasifier, is measured at NTP. Air entering via the central shaft in the gasifier was not measured.
4. Values were measured using a hand held temperature probe.

Table A6-6 **Test Run 3**: Calculated parameters corresponding to snap-shots in time.

Test Run 3 - on Wednesday 12 October 2011						
Time	00:02:46	00:10:05	00:33:25	00:47:40	00:57:31	-
Blower Speed (%)	20	30	40	45	50	-
Air inlet flow (kg/h)	208	243	291	331	445	-
Char removal rate (kg/h)	19.44	19.44	19.44	19.44	19.44	-
Producer gas flow (kg/h)	243	346	416	474	620	-
Waste-wood feed rate (kg/h)	89	165	187	209	252	-
HHV (MJ/Nm^3)	2.45	5.27	5.23	5.35	4.53	-
LHV (MJ/Nm^3)	2.28	4.92	4.84	4.96	4.22	-
Heat flow (kW)	144	469	575	680	685	-
Equivalence ratio *1)*	0.38	0.27	0.29	0.29	0.34	-
Equivalence ratio *2)*	0.33	0.21	0.22	0.22	0.25	
Throat Top, ^oC	305	561	732	690	651	-
Throat Bottom, ^oC	545	524	768	847	677	-

1) Equivalence ratio was estimated by calculating total air required for complete combustion of producer gas and char received.
2) Equivalence ratio was estimated by assuming the composition of the waste-wood fed into the gasifier.